

Doctoral Dissertation

(Shinshu University)

**The provenance and the paleo-environment of  
the Siwalik Group along the Muksar Khola  
section, eastern Nepal Himalaya**

Rai Lalit Kumar

Student ID: 18HS407A



## ACKNOWLEDGEMENTS

I would like to extend my sincere thanks and gratitude to my academic supervisor Prof. Kohki Yoshida, Institute of Science, School of Science and Technology, Shinshu University for his precious supervision and guidance throughout this research.

I would also like to thank the people and government of Japan for awarding me with the Monbukagakusho scholarship (MEXT) throughout my study.

My deep gratitude goes to Prof. M. R. Dhital and Asst. Profs. K. K. Acharya of Central Department of Geology, Tribhuvan University. Prof. S. M. Rai and Assoc. Prof. A. P. Gajurel of Tri-Chandra Multiple Campus, Tribhuvan University for their continuous inspiration.

Special thanks to my friends Dr B. R. Gyawali, Mr C. B. Silwal, Mr D. Adhikari and students K. Timsina, Manish K.C. for their enormous help in the fieldwork and the people of the Gola and Magan village for their logistic support and help.

The author is grateful to the Department of Mines and Geology (DMG), the Government of Nepal for permitting the export of samples from Nepal to Japan and my friends Dr S. Bhandari, Mr M. Lamsal and Mr B.R. Silwal of the DMG for helping with the necessary documentation.

I would like to express my thanks to all the staff of the Department of Geology, Shinshu University for their assistance and support in numerous ways. Especially Dr K. Takahasi for guiding during the preparation of the thin section. Yukari Suzuki, Mayumi Sasaki, Yuko Terashita for sample preparation for heavy mineral analysis. I also acknowledge Emeritus Prof. H. Sakai, Kyoto University for his valuable suggestion and Prof. T. Kuritani, Hokkaido University for analyzing isotopes.

I would like to thank my friends in Japan Mr P. Maharjan and Mr B. Aryal for their unquestioning support during my stay in Japan.

My parents, my wife, my son and my brother have supported me throughout my study with patience, encouragement and love, which helped me to focus on research. This thesis is dedicated to all of them.

Lalit Kumar Rai

Matsumoto, Nagano, Japan

## Table of Contents

ACKNOWLEDGEMENTS.....	iii
Table of Contents.....	v
ABSTRACT.....	xi
ABBREVIATIONS.....	xiv
List of Figures.....	xvi
List of Tables.....	xxi
CHAPTER I	
INTRODUCTION.....	1
1.1 Introduction.....	1
1.2 Location and accessibility.....	2
1.3 Background and research objectives.....	3
1.4 Outline of the Thesis.....	5
CHAPTER II	
GEOLOGICAL SETTINGS AND LITERATURE REVIEW.....	7
2.1 Introduction.....	7
2.2 Geology of the Nepal Himalaya.....	8
2.2.1 Indo-Gangetic Plain (Terai).....	9
2.2.2 Sub-Himalaya (Siwaliks).....	9

2.2.3	Lesser Himalayan Sequence .....	10
2.2.4	Higher Himalayan Crystalline .....	10
2.2.5	Tibetan Tethys Himalaya .....	11
2.3	Geological setting.....	11
2.3.1	Eastern Nepal Himalaya .....	11
2.3.2	The Siwalik Group.....	13
2.4	Literature Review .....	15
2.4.1	Lithostratigraphy.....	15
2.4.2	Magnetostratigraphy .....	15
2.4.3	Depositional Environment .....	16
2.4.4	Provenance and tectonic Setting .....	17
2.4.5	Paleoclimate .....	17

### CHAPTER III

LITHOSTRATIGRAPHY .....	19
3.1 Introduction .....	19
3.2 Methods.....	20
3.3 Lithostratigraphy .....	20
3.3.1 Lower Siwaliks .....	23
3.3.2 Middle Siwaliks .....	27
3.3.3 Upper Siwaliks.....	36

## CHAPTER IV

PETROGRAPHY .....	39
4.1 Introduction .....	39
4.2 Methods .....	39
4.3 Results .....	41
4.4 Classification of Sandstone .....	43
4.5 Probable source rock .....	44

## CHAPTER V

HEAVY MINERAL ANALYSIS .....	46
5.1 Introduction .....	46
5.2 Methods .....	47
5.3 Results .....	47
5.4 Difference in heavy mineral assemblage under petrographic microscope and EDS	50
5.5 Probable source rock .....	51

## CHAPTER VI

CHEMICAL COMPOSITION OF .....	52
DETRITAL TOURMALINE AND GARNET .....	52
6.1 Introduction .....	52
6.2 Methods .....	53

6.3	Results .....	53
6.1.1	Chemical composition of detrital Tourmaline .....	53
6.1.2	Chemical composition of detrital Garnet.....	56
6.4	Probable source rock .....	58
CHAPTER VII		
	ISOTOPE ANALYSIS .....	61
7.1	Introduction .....	61
7.2	Methods.....	61
7.3	Results .....	62
7.3.1	Unleached method .....	62
7.3.2	Leached method .....	64
7.4	Probable Source Rock .....	65
CHAPTER VIII		
	FLUVIAL FACIES.....	67
8.1	Introduction .....	67
8.2	Methods.....	68
8.3	Facies associations .....	68
8.3.1	Facies Association, FA1 .....	73
8.3.2	Facies Association, FA2 .....	75



8.3.3	Facies Association, FA3 .....	78
8.3.4	Facies Association, FA4 .....	80
8.3.5	Facies Association, FA5 .....	82
8.4	Depositional Process .....	83
CHAPTER IX		
	DISCUSSION .....	85
9.1	Lithostratigraphic comparison of the Siwalik Group with previous work.....	85
9.2	Provenance .....	86
9.2.1	Denudation of Higher Himalayan Crystalline .....	86
9.2.2	Exposure of MCT zone.....	88
9.2.3	Re-supply of sediments from the Higher Himalayan Crystalline.....	90
9.2.4	Tibetan Tethys Himalaya and the Gangdise belt in southern Tibet.....	91
9.3	Exhumation history of the eastern Nepal Himalaya.....	92
9.4	Significance of the differences observed in isotopic values .....	95
9.5	Intensification of the monsoon in eastern Nepal Himalaya .....	97
9.6	Controlling factors for change in river system.....	100
9.7	Shifting of the foreland basin .....	109
9.8	Correlations .....	110
9.8.1	Lithostratigraphy.....	110
9.8.2	Fluvial environment.....	112

CHAPTER X

CONCLUSION.....116

REFERENCES .....119

APPENDIX.....133

## ABSTRACT

The Siwalik Group extending east to west co-linear with the main Himalayan range is considered as an important archive. It records the early Miocene–Pleistocene Himalaya exhumation history and consequent climate change due to this topographic change. This study deals with the Siwalik Group along the Muksar Khola section in eastern Nepal and mainly focuses on the lithostratigraphic classification, sediment provenance and hinterland phenomena, and interpretation of the fluvial environment. Results from the present study are further compared and discussed with the results of other Siwalik sections to understand the Himalaya.

In the present study, the Siwalik Group is divided into the Lower Siwaliks, the Middle Siwaliks, and the Upper Siwaliks based on lithology and grain size variation. In comparison with the preexisting depositional age, the Lower Siwaliks was deposited before 10 Ma and consists of grey to olive black mudstone to siltstone interbedded with light-grey, very fine- to fine-grained sandstone and a very thick succession of the intraformational conglomerate. Middle Siwaliks was deposited in between 10.0–3.5 Ma and is characterized by the domination of sandstone. In the present study, this sub-group is divided into the lower member and the upper member based on the variation on the lithology and their thickness, its composition, and sandstone induration degree. The lower member deposited before 5.9 Ma consists of fine- to medium-grained “salt and pepper” sandstone with greenish-grey to olive-grey mudstone. While the upper member is characterized by less indurated, light grey to white, medium- to very coarse-grained sandstone with an increased proportion of grey, dark grey to black mudstone. The Upper Siwaliks consists of a poorly sorted, clast supported conglomerate associated with very thickly bedded coarse- to very coarse-grained sandstone and very thickly bedded dull yellowish-grey to grey colour mudstone.

Study of the provenance, reveal continuous denudation of the eastern Nepal Himalaya and simultaneous shift of the provenance around middle Miocene–Pliocene. The sandstone petrography, heavy minerals assemblage, the chemical composition of detrital tourmaline and garnet, and Sr-Nd isotopes equivocally suggest provenance shifted from shallow to the deeper part of the Higher Himalayan Crystalline around 10.6 Ma. Lesser Himalaya Sequence supplied a considerable amount of sediments after 7.5 Ma and the Higher Himalayan Crystalline boosted the supply of sediments after 4.0 Ma. The occurrence of volcanic lithic fragments and the uniform occurrence of heavy minerals like titanite and the Zircon-Tourmaline-Rutile index reveals Tibetan Tethys Himalaya was a continuous source. The occurrence of detrital chromian spinel in the older section and extreme Ca-rich garnet ( $Grs+And>90$ ) in the younger section suggests Indus Tsangpo Suture Zone as a potential source. This change in the provenance was controlled by the exhumation of eastern Nepal Himalaya, which was observed at two stages: first around 11.0 Ma due to activation of the out-of-sequence thrust known as Sunkoshi Thrust and second due to the formation of the duplex structure in the underlying Lesser Himalaya Sequence after 4.0 Ma. This provenance study also reveals two important ideas: the chemical composition of detrital garnet is very suitable for determining the provenance in the Himalaya as it traces every change which is hardly defined by other proxies and the Sr-Nd isotopic values of the Siwalik sediments are dependent on the grain size.

Based on the facies analysis, five facies associations were discovered representing the fluvial environment. These are interpreted as the flood plain dominated fine-grained meandering river (FA1), flood dominated overbank environment (FA2), sandy meandering river (FA3), anastomosing river (FA4), and debris flow dominated braided river (FA6). These changes in the fluvial environments were controlled by the interplay between hinterland tectonics, climate and sea-level change. The absence of rapid exhumation of the hinterland, raised sea

level and comparative weak monsoon before 10.0 Ma resulted in the flood plain dominated fine-grained meandering river (FA1). High discharge due to intensified monsoon and rapid fall of the sea level around 10.5 Ma caused flood dominated overbank environment (FA2). Asymmetric subsidence of the foreland basin and less sediment supply due to the absence of duplex structure and activation of the out-of-sequence thrust resulted in the sandy meandering river (FA3) after 10.0 Ma. After the 5.9 Ma rise in the base level due to subsidence of the foreland basin and sea-level rise along with the strengthening of the monsoon gave rise to the anastomosing river (FA4). Debris flow dominated braided river (FA6) after 3.5 Ma was resulted due to the increase in the proximity of the basin close to the hinterland.

The genesis of the intraformational conglomerate of the FA2 suggests monsoon intensified at around 10.5 Ma in the eastern Nepal Himalaya. The present study also reveals continuous shifting of the foreland basin towards the hinterland. This change in the location of sediment deposition resulted in the coarsening upward succession in the sediments of Siwalik sediments. Further, this study shows a difference in the exhumation history of the eastern Nepal Himalaya compared to central and western Nepal Himalaya, subsequently, this brought a difference in the fluvial environment.

**Keywords:** Siwalik Group; Lithostratigraphy; Provenance; Facies analysis; Intraformational conglomerate; Fluvial; Sea-level change; Sandstone petrography; Heavy minerals; Detrital tourmaline; Detrital garnet; EDS analysis; Sr-Nd isotopes; Muksar Khola; Eastern Nepal; Miocene.

## ABBREVIATIONS

Al: Aluminium	Fe <sup>3+</sup> : Ferric ions
Al <sub>2</sub> O <sub>3</sub> : Aluminium oxide	FeO: Ferrous oxide
Alm: Almandite	Grs: Grossular
Aln: Allanite	Grt: Garnet
Ap: Apatite	HHC: Higher Himalayan Crystalline
And: Andradite	Ilm: Ilmenite
Amp: Amphibole	ITSZ: Indus-Tsangpo Suture Zone
B: Boron	K: Potassium
Ca: Calcium	K <sub>2</sub> O: Potassium oxide
CaO: Calcium oxide	Kf: Potassium feldspar
Cr: Chromium	KTT: Kamala-Tawa Thrust
Crd: Cordierite	Ky-Sil: Kyanite-Sillimanite
Cr <sub>2</sub> O <sub>3</sub> : Chromium oxide	L: Lithic fragments (Ls+Lm+Lv)
Cpx: Clino-pyroxene	Lm: Metamorphic lithic grain
Cspl: Chromian-spinal	Ls: Sedimentary lithic grain
Ep: Epidote	Lv: Volcanic lithic grain
F: Total feldspar grain	Lt: Total lithic fragments (L+Qp)
Fe: Iron (Ferrum)	LHS: Lesser Himalayan Sequence
Fe <sup>2+</sup> : Ferrous ions	MBT: Main Boundary Thrust

MCT: Mani Central Thrust	Qtz: Quartz
MDT: Main Dun Thrust	Rt: Rutile
MFT: Main Frontal Thrust	RT: Ramgarh Thrust
Ma: Million years ago	Si: Silicon
Mg: Magnesium	SKT: Sun Koshi Thrust
MgO: Magnesium oxide	Sps: Spessartine
Mn: Manganese	Sr: Strontium
MnO: Manganese oxide	St: Staurolite
Na: Sodium	Ti: Titanium
Na <sub>2</sub> O: Sodium oxide	Ttn: Titanite
Nd: Neodymium	TTH: Tibetan Tethys Himalaya
Pl: Plagioclase feldspar	TKT: Tamor Khola Thrust
Prp: Pyrope	Tur: Tourmaline
Qt: Quartz total (Qm+Qp)	Zo: Zoisite
Qm: Monocrystalline Quartz	Zr: Zircon
Qp: Polycrystalline Quartz	

## List of Figures

### Chapter I

- Figure 1.1:** Regional map showing the boundary of Nepal taken from Google Earth (left) and Map of Nepal showing the study area (right).....3

### Chapter II

- Figure 2.1:** Subdivision of the Himalaya from west to east. (modified after Gansser, 1964; Yin, 2006).....7
- Figure 2.2:** Geological map of Nepal showing the study area. (modified after Amatya and Jnawali, 1994).....8
- Figure 2.3:** (A) Index map showing eastern Nepal. (B) Simplified geological map of the eastern Nepal Himalaya (modified after Schelling, 1992; Rai et al., 2021).....12
- Figure 2.4:** Geological map of the Siwalik Group in eastern Nepal showing the study area (modified after Shrestha and Sharma, 1996).....14

### Chapter III

- Figure 3.1:** A) Geological Map of the Siwalik Group along the Muksar Khola section and B) Cross-section along A-B (modified after Rai and Yoshida, 2020).....21
- Figure 3.2:** Sedimentological column of the Siwalik Group along the Muksar Khola section showing lithostratigraphic division concerning the magnetostratigraphic age data of Ojha et al. (2009) (modified after Rai and Yoshida, 2020).....22
- Figure 3.3:** Detailed sedimentological column (representative) from the Lower Siwaliks (modified after Rai and Yoshida, 2020).....24
- Figure 3.4:** Field photographs of A) Inter-bedding of fine-grained sandstone and mudstone of the Lower Siwaliks; B) Intraformational conglomerate of the Lower Siwaliks (conglomerate member); C) Sandpipe observed in mudstone to siltstone of the Lower Siwaliks; D) Carbonized plant roots in siltstone of the Lower Siwaliks; E) Variegated mudstone of the Lower Siwaliks; F) Concretion observed in siltstone to fine-grained sandstone of the Lower Siwaliks..... 25
- Figure 3.5:** Sandstone bed thickness of the lower and the upper member of the Middle Siwaliks. (Amalgamated sandstone beds with thickness more than 6 m were excluded) (modified after Rai and Yoshida, 2020).....28
- Figure 3.6:** Proportion of different litho units in the Siwalik Group along the Muksar Khola (modified after Rai and Yoshida, 2020).....29



**Figure 3.7:** Detailed sedimentological column (continuous) of the lower member of the Middle Siwaliks (modified after Rai and Yoshida, 2020).....30–31

**Figure 3.8:** Field photographs of A) Amalgamated sandstone with multiple siltstone lag deposits at the base observed in the Middle Siwaliks (lower member); B) Bioturbated sandstone surface in the Middle Siwaliks; C) Bivalve shell in the sandstone of the Middle Siwaliks (lower member); D) Leaf imprints preserved in the siltstone of the Middle Siwaliks (lower member).....32

**Figure 3.9:** Detailed sedimentological column (continuous) of the upper member of the Middle Siwaliks (modified after Rai and Yoshida, 2020).....34–35

**Figure 3.10:** Field photographs of A) A typical fining upward sequence observed in very thickly bedded sandstone of the Middle Siwaliks (upper member); B) Pebbly sandstone of the Middle Siwaliks (upper member); C) Calcareous nodules observed in mudstone of the Middle Siwaliks (upper member); D) Convolute lamination observed in the sandstone of the Middle Siwaliks.....36

**Figure 3.11:** Detailed sedimentological column (representative) of the Upper Siwaliks (modified after Rai and Yoshida, 2020).....37

**Figure 3.12:** Conglomerate bed from Upper Siwaliks (left) and close up view of conglomerate (right).....38

## Chapter IV

**Figure 4.1:** Stratigraphic column and the sampling horizons. The examined analysis are shown as (M) sandstone modal composition, (Hm) heavy mineral analysis, (T) detrital tourmaline geochemistry, (G) detrital garnet geochemistry, (Sr-Nd) isotopic analysis. Sample MK-01, MK-27 and MK-28 are collected beyond the presented sedimentological log (modified after Rai et al., 2021).....40

**Figure 4.2:** Photomicrographs of the sandstone. A: Matrix of the intraformational conglomerate of the Lower Siwaliks (UCN), B: Sandstone of the Lower Siwaliks (UCN), C) Sandstone of the lower member of the Middle Siwaliks (UCN), D) sheared mudstone in the sandstone of the lower member of the Middle Siwaliks (UPPL) (After Rai et al., 2021). Abbreviations: Qm: Monocrystalline quartz, Qp: Polycrystalline quartz, Pl: Plagioclase feldspar, Kf: K-feldspar, Ls: Sedimentary lithics, Lm: Metamorphic lithics, Lv: Volcanic lithics, Cal cement: Calcareous cement.....43

**Figure 4.3:** Classification of the sandstone. A) Ternary diagram based on schemes proposed by Pettijohn et al., 1987); B) Ternary diagram based on schemes proposed by Folk (1980); C) Qt-F-L and D)Qm-F-Lt Ternary diagram for the framework modes of the sandstone, showing the different provenance fields defined by Dickinson (1985) (After Rai et al., 2021). Abbreviations as in Table. 4.1. Qt: Total quartz grains (Qm+Qp), F: Total feldspar grains (Pl+Kf), L: Lithic fragments (Ls+Lm+Lv), Lt: Total lithic fragments (L+Qp).....44

<b>Figure 4.4:</b> Vertical variation of feldspar content in the sandstone. Depositional ages of samples are based on preexisting age data of the Ojha et al. (2009).....	<b>45</b>
---	-----------

## Chapter V

<b>Figure 5.1:</b> Heavy mineral assemblage in the present study area identified under a petrographic microscope (point count). Depositional ages of samples are based on preexisting age data of the Ojha et al. (2009).....	<b>48</b>
---	-----------

<b>Figure 5.2:</b> Heavy mineral assemblage in the present study area identified under EDS (modified after Rai et al., 2021). Depositional ages of samples are based on preexisting age data of the Ojha et al. (2009).....	<b>49</b>
---	-----------

## Chapter VI

<b>Figure 6.1:</b> Photomicrographs (UPPL). A) Detrital dark green tourmaline, B) Detrital yellowish green tourmaline (after Rai et al., 2021), C) Detrital garnet with inclusion (after Rai et al., 2021).....	<b>53</b>
---	-----------

<b>Figure 6.2:</b> Detrital tourmaline composition plotted on Al-Fe-Mg and Ca-Fe-Mg diagrams. Discrimination fields for various rock types according to Henry and Guidotti (1985) are as follows: (a) Li-rich granitoids, pegmatites, and aplites; (b) Li-poor granitoids, pegmatites, and aplites; (c) hydrothermally altered granitic rocks; (d) aluminous pellites and psammites; (e) Al-poor pellites and psammites; (f) Fe <sup>3+</sup> -rich quartz-tourmaline rocks; (g) Low-Ca meta-ultramafics; (h) metacarbonates and metapyroxenites; (1) Li-rich granitoids, pegmatites, and aplites; (2) Li-poor granitoids, pegmatites, and aplites; (3) Ca-rich pellites, psammites, and calc-silicates; (4) Ca-poor pellites, psammites, and quartz-tourmaline rocks; (5) metacarbonates; (6) meta-ultramafic rocks. Depositional ages of samples are based on preexisting age data of the Ojha et al. (2009).....	<b>54</b>
---	-----------

<b>Figure 6.3:</b> Detrital garnet compositions plotted in Prp-Alm+Sps-Grs+And and Alm-Prp-Sps diagram (modified after Rai and Yoshida, 2021). Abbreviations, Prp: pyrope, Alm: almandine, Sps: spessartine, Grs: Grossular, And: andradite. Discrimination fields for various rock types for Prp-Alm+Sps-Grs+And diagram according to Mange and Morton (2007) are as follows: Type-A: mainly from high-grade granulite-facies metasediments or charnokites and intermediate felsic igneous rocks. Type-B: amphibolite-facies metasedimentary rocks and intermediate to felsic igneous rocks. Type-Bi: intermediate to felsic igneous rocks. Type-C: high-grade metabasic rocks. Type-D: metasomatic rocks, very low-grade metamafic rocks and ultrahigh temperature metamorphosed calc-silicate granulites. Depositional ages of samples are based on preexisting age data of the Ojha et al. (2009).....	<b>57</b>
--	-----------

<b>Figure 6.4:</b> Chemical composition of garnet from the parent rocks of the different lithostratigraphic units of the Himalaya based on the previous studies (modified after Rai et al., 2021).....	<b>59</b>
--	-----------

## Chapter VII

<b>Figure 7.1:</b> $\Sigma Nd(0)$ values of the Siwalik Group samples from the Muksar Khola section. Depositional ages of samples are based on preexisting age data of the Ojha et al. (2009).....	<b>63</b>
--	-----------

<b>Figure 7.2:</b> Nd-Sr isotopic data of the Siwalik Group samples from the Muksar Khola section compared with typical values for major Himalayan tectonic units (modified from Szulc et al., 2006); River sediments of the Brahmaputra River (Singh and France-Lanord, 2002); River sediments of Ganga basin (Singh et al., 2008) and middle Miocene to Holocene sediments recovered in OPD Leg 116 (France-Lanord et al., 1993).....	<b>65</b>
---	-----------

## Chapter VIII

<b>Figure 8.1:</b> Outcrop photographs of the lithofacies, A) Reddish-brown paleosols (P); B) Peaty mudstone (C); C) Laminated mudstone (Fl); D) Massive mudstone (Fm); E) Horizontal lamination (Sh); F) Planer cross-stratification (Sp); G) Ripple cross lamination (Sr); H) Trough cross-stratification (St); I) Massive sandstone (Sm); J) Stratified gravel (Gp); K) Matrix supported gravel with inverse grading (Gmg); L) Matrix supported poorly sorted pebble to cobble size massive gravel (Gmm).....	<b>70–71</b>
--	--------------

<b>Figure 8.2:</b> Representative sedimentological log of the facies associations identified on the Siwalik Group of the Muksar Khola section (modified after Rai and Yoshida, 2021, Location is given in Figure 8.3).....	<b>72</b>
--	-----------

<b>Figure 8.3:</b> Geological map showing the facies associations and paleo flow direction (left) and location of sedimentological log presented in Figure 8.2 (right) (modified after Rai and Yoshida, 2021).....	<b>73</b>
--	-----------

<b>Figure 8.4:</b> Outcrop photographs of, A) Laterally accreted sandstone bed (FA1); B) Intraformational conglomerate followed by parallel to ripple laminated very fine-grained sandstone representing levee deposits (FA2); C) Ripple lamination on the very fine-grained sandstone (FA2); D) Channel lag deposits with coal fragments (FA3); E) Parallel to ripple laminated very fine-grained sandstone intercalated with mudstone representing levee deposits (FA3); F) Matrix supported conglomerate associated with sandstone and mudstone (FA5).....	<b>76</b>
---	-----------

<b>Figure 8.5:</b> Evolution of the fluvial system in the present study area based on preexisting age data of the Ojha et al. (2009) (modified after Rai and Yoshida, 2021).....	<b>84</b>
--	-----------

## Chapter IX

- Figure 9.1:** Vertical variation of the heavy minerals in the present study (modified after Rai et al., 2021). Depositional ages of samples are based on preexisting age data of the Ojha et al. (2009).....87
- Figure 9.2:** A) Ca/(Mg+Fe+Mn+Ca) Compositional histogram of the detrital garnets. B) Mn/(Mg+Fe+Mn) Compositional histogram of the detrital garnets. Depositional age is based on the preexisting age data of Ojha et al. (2009) (modified after Rai et al., 2021). .....89
- Figure 9.3:** Schematic diagram showing two major exhumations of the eastern Nepal Himalaya. Abbreviations: STDS: South Tibetan Detachment system; MCT: Main Central Thrust; SKT: Sun Koshi Thrust; RT: Ramgarh Thrust; MBT: Main Boundary Thrust; Cspl: Chromian Spinal zone; Ep: Epidote zone; Crd: Cordierite zone; Ky+Sil: Al-silicate (Kyanite+sillimanite) zone; St: Staurolite zone.....94
- Figure 9.4:**  $\Sigma Nd(0)$  values of the Siwalik Group of the Muksar Khola section from the previous study of Robinson et al. (2001).....95
- Figure 9.5:** Schematic diagram showing A) Meandering river during normal flow condition and B) River during high discharge.....100
- Figure 9.6:** Schematic diagram showing a depositional model for FA1 and FA2 concerning climate and tectonics. Abbreviations: RT: Ramgarh Thrust; MCT: Main Central Thrust. ....101
- Figure 9.7:** Schematic diagram showing a depositional model for FA3 concerning asymmetric subsidence due to activation of the OST. Abbreviations: RT: Ramgarh Thrust; MCT: Main Central Thrust; OST: Out-of-sequence Thrust.....103
- Figure 9.8:** Schematic diagram showing a depositional model for FA4 concerning tectonics and climate. Abbreviations: MBT: Main Boundary Thrust; RT: Ramgarh Thrust; MCT: Main Central Thrust; SKT: Sun Koshi Thrust; TKT: Tamor Khola Thrust; OST: Out-of-sequence Thrust.....106
- Figure 9.9:** Schematic diagram showing a depositional model for FA5 concerning tectonics. Abbreviations: MBT: Main Boundary Thrust; RT: Ramgarh Thrust; MCT: Main Central Thrust; SKT: Sun Koshi Thrust; TKT: Tamor Khola Thrust; OST: Out-of-sequence Thrust.....108
- Figure 9.10:** Schematic diagram showing the existence of small and large rivers in an interfan area.....109
- Figure 9.11:** Map of Nepal showing the Siwalik Group (yellow belt) and the location of the Karnali River, the Surai Khola and the Muksar Khola section (modified after Rai and Yoshida, 2021).....113

## List of Tables

<b>Table 3.1:</b> Mudstone colour observed in the present study area based on the Munsell colour chart (modified after Rai and Yoshida, 2020).....	26
<b>Table 4.1:</b> Modal composition of the Siwalik Group sandstones from the Muksar Khola section. Qm: Monocrystalline quartz, Qp: Polycrystalline quartz, Pl: Plagioclase, Kf: K-feldspar, Ls: Sedimentary lithics, Lm: Metamorphic lithics, Lv: Volcanic lithics, Qt: Total quartz grains (Qm+Qp), F: Total feldspar grains (Pl+Kf), L: Lithic fragments (Ls+Lm+Lv), Lt: Total lithic fragments (L+Qp) (modified after Rai et al., 2021).....	42
<b>Table 5.1:</b> Heavy mineral assemblage of the Siwalik Group sandstones from the Muksar Khola section identified under a petrographic microscope (point count).....	50
<b>Table 5.2:</b> Heavy mineral assemblage of the Siwalik Group sandstones from the Muksar Khola section identified under EDS (modified after Rai et al., 2021).....	50
<b>Table 6.1:</b> Chemical composition of detrital tourmaline grains from the Siwalik Group sandstones of the Muksar Khola section.....	55
<b>Table 6.2:</b> Chemical composition of detrital garnet grains from the Siwalik Group sandstones of the Muksar Khola section.....	58
<b>Table 7.1:</b> Sr-Nd isotopic compositions of the Siwalik Group along the Muksar Khola section (Unleached samples).....	64
<b>Table 7.2:</b> Sr-Nd isotopic compositions of the Siwalik Group along the Muksar Khola section (Leached samples).....	64
<b>Table 8.1:</b> Description and interpretation of the depositional facies (modified after Rai and Yoshida, 2021).....	69
<b>Table 8.2:</b> Facies associations recognized in the Siwalik Group of the Muksar Khola section (interpretation based on Miall, 1977; 1985; 2000; 2006).....	70
<b>Table 9.1:</b> Lithostratigraphic classification and correlation of the present study with representing Siwalik Group of central and western Nepal (modified after Rai and Yoshida, 2020).....	112
<b>Table 9.2:</b> Comparison of the fluvial systems of the present study area with different Siwalik Group of Nepal (modified after Rai and Yoshida, 2021).....	113

# CHAPTER I

## INTRODUCTION

### 1.1 Introduction

Himalaya started to uplift as the northward drifting Indian sub-continent collided with the Eurasian plate at around 50 Ma (Le Fort, 1975). The continuity of this drifting force on the Indian sub-continent even after the collision of two landmasses resulted in various tectonic activities (Burchfiel et al., 1992) and gradual change in the paleogeography of this region. This in turn affected the atmospheric circulation (Raymo and Ruddiman, 1992) initiating the Asian monsoon (Kutzbach et al., 1989; Clift et al., 2008; Boos and Kuang, 2010; Armstrong and Allen, 2011). These changes in the paleogeography, as well as climate caused weathering and erosion of the newly formed mountain range producing enormous sediments. These sediments were transported by various transverse river systems and deposited on the foreland basin (Tandon, 1976; Parkash et al., 1980; Tokuoka et al., 1990; Hisatomi and Tanaka, 1994; Willis, 1993b, Nakayama and Ulak, 1999; Rai and Yoshida, 2021). The Siwalik Group is made up of these sediments (Gansser, 1964; Parkash et al., 1980; Corvinus, 1993). At present, it is observed as the southernmost hill range existing co-linear to the main Himalayan range with varying thickness (Dhital, 2015).

The Siwalik Groups is a natural archive, which records the Miocene–Pleistocene exhumation history of the Himalaya. Therefore, it has been the center of interest for many studies including stratigraphic classifications, sediment depositional environment and deciphering the Himalaya climate, exhumation, and its denudation etc. The lithostratigraphy of the Siwalik Group has been classified into 3-fold to 5-fold classification (Pilgrim, 1913, Auden, 1935; Yoshida and Arita, 1982; Tokuoka et al., 1990; Dhital et al., 1995; Ulak and Nakayama, 1998). Sedimentological studies suggest these sediments were mainly deposited in the fluvial

environment (Tandon, 1976; Parkash et al., 1980; Tokuoka et al., 1990; Hisatomi and Tanaka, 1994; Willis, 1993b, Nakayama and Ulak, 1999) during the middle Miocene to early Pleistocene time (Appel and Rosler, 1994; Gautam and Appel, 1994; Rosler et al., 1997; Gautam and Fujiwara, 2000; Ojha et al., 2009; Chirouze et al., 2012b). Whereas, in north-east India and Bhutan fluvial environment along with an open marine to the deltaic environment are reported (Coutand et al., 2016; Taral et al., 2018; 2019). Studies of the detrital sediments of the Siwalik Group including sandstone petrography (Garzanti et al., 1996; Sigdel and Sakai, 2013; Tamrakar et al., 2003), heavy mineral analysis (DeCelles et al., 1998b; Garzanti et al. 2007; Yoshida et al., 2019), isotropic fingerprints (Robinson et al., 2001; Huyghe et al., 2005; Chirouze et al., 2013), geochronology (DeCelles et al., 1998b; Chirouze et al., 2012a; Baral et al., 2016) and geochemistry (Lee et al., 2003) reveals these sediments were sourced by tectonically active Himalaya. This exhumation of the Himalayan range resulted in the onset of the Asian monsoon (Armstrong and Allen, 2011; Clift and Webb, 2018), whose intensification was recorded around 10.0 Ma based on facies analysis (Nakayama and Ulak, 1999). Carbon isotope data showed a major climatic shift occurred at around 7 Ma in the Himalaya (Harrison et al., 1993; Quade et al., 1995) due to the inception or a marked strengthening of the Asian monsoon system (Quade et al., 1989; Nakayama and Ulak, 1999).

## **1.2 Location and accessibility**

The present study deals with the Siwalik Group along the Muksar Khola section. This section covers the northern part of the Siraha district and a southern part of the Udayapur district in the eastern part of Nepal (Fig. 1.1). Geographically, the area lies between 86°22' to 86°23' East longitudes and 26°50' to 26°55' North latitudes and covers the part of the topographic map number 2686 02B and 2686 02D (Department of Survey, Government of Nepal) of 1:25000 scale.

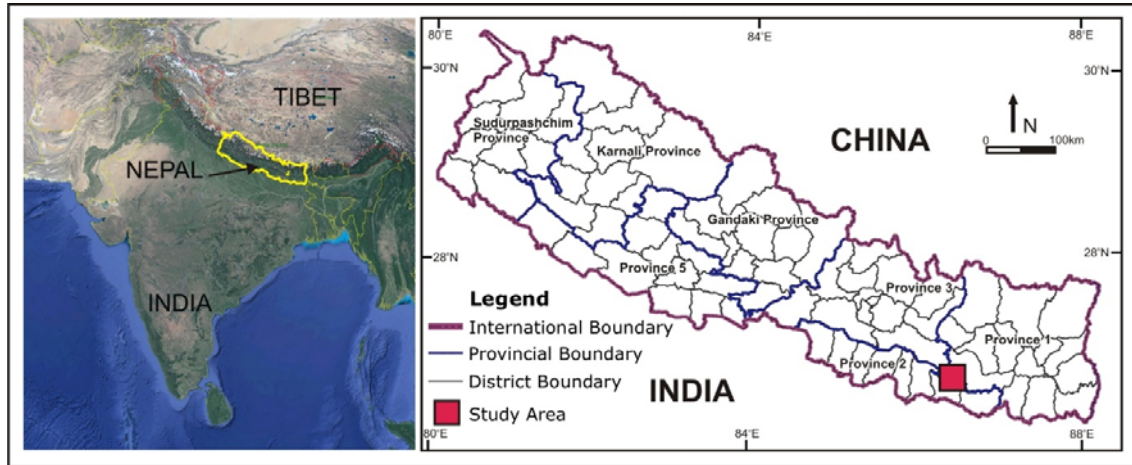


Figure 1.1: Regional map showing the boundary of Nepal taken from Google Earth (left) and Map of Nepal showing the study area (right).

The study area is accessible by road. The Mahendra Highway (East-west national highway) which connects Kathmandu a capital city passes about 10 km south of the study area. Golbazar is a town suited along this highway, from which a link road goes north and joins a small village named Golla, situated beside the Muksar Khola. The present study area lies north of this village within walking distance of about 10 minutes.

### 1.3 Background and research objectives

Various studies have been carried out along the different Siwalik sections of the Himalaya, which suggests major mountain building phenomena and climate change along the Himalaya was observed around Miocene to early Pleistocene (Harrison et al., 1993; Quade and Cerling, 1995; Quade et al., 1995; DeCelles et al., 1998b, 2001; Huyghe et al., 2001; Robinson et al., 2001; Najman et al., 2009; Chirouze et al., 2012a; 2013; Coutand et al., 2016; Vogeli et al., 2017). These studies also reveal exhumation and the climatic conditions of the Himalaya, was not laterally coeval, it was observed early in the western part in comparison to the eastern part (Robinson et al., 2001; Yin, 2006; Ojha et al., 2009; Vogeli et al., 2017).



Sedimentological studies of the Siwalik Group from Pakistan to the eastern Nepal Himalaya show change in the river system from meandering to braided which was controlled by the hinterland tectonics and climate (Tokuoka et al., 1990, 1994; Willis, 1993b; Hisatomi and Tanaka, 1994; Khan et al., 1997; Zaleha, 1997; Nakayama and Ulak, 1999; Huyghe et al., 2001; Ulak and Nakayama 2001; Kumar et al., 2003; Ulak, 2004; 2009; Sigdel and Sakai, 2016). Therefore, these differences in the hinterland exhumation and climate should have been traced in the coeval depositional environment of the foreland basin.

Similarly, Siwalik Groups along the Darjeeling-Sikkim, Bhutan and north-eastern Indian Himalaya, records deltaic to open marine deposits (Coutand et al., 2016; Taral et al., 2018; 2019). Considering the proximity of the eastern Nepal Himalaya to the Darjeeling-Sikkim area, the Siwalik Group of the eastern Nepal Himalaya should also be influenced by sea-level change, since the depositional environment of the foreland basin is also controlled by sea-level change (Zaitlin et al., 1994; Oldknow and Hooke, 2017) and the eustatic curve proposed by Haq et al. (1988) shows the frequent change in the sea level during the depositional time of the Siwalik sediments. Though Ulak (2004, 2009) carried out the sedimentological study in the Siwaliks of eastern Nepal along the Koshi and the Kankai River sections, his results are surprisingly similar and completely ruled by the Siwalik Group of central Nepal by Nakayama and Ulak (1999).

The hinterland tectonics has an influencing role in the foreland fluvial environment, however, the Miocene to early Pleistocene exhumation history of eastern Nepal Himalaya is little understood. In the previous studies of the Siwaliks along the Muksar Khola section, Robinson et al. (2001) and Chirouze et al. (2012a) tried to decipher the exhumation history of the eastern Nepal Himalaya based on provenance study, but their limited data set neither could explain the existence of different tectonics window of the eastern Nepal Himalaya whose rocks show relatively young zircon fission-track (ZFT) age of late Miocene to early Pliocene

(Sakai et al., 2013; Nakajima et al., 2020a), nor record any change in the provenance or contribution of sediments from these windows. Moreover, the tectonic models of the eastern Nepal Himalaya proposed by various researchers regarding the existence of the out-of-sequence thrust also lead to a contradiction (Schelling and Arita, 1991; Schelling, 1992; Imayama et al., 2008; Sakai et al., 2013). Therefore, a clear exhumation history of the hinterland is important for understanding the depositional environment of the foreland basin. A provenance study of detrital sediments is widely used to reconstruct the exhumation history of the hinterland (DeCelles et al., 1998, 2001; Huyghe et al., 2001; Robinson et al., 2001; Najman et al., 2009; Chirouze et al., 2012a; 2013), therefore, provenance study with multiple proxies could be more reliable to decipher the hinterland tectonics.

Therefore, the present study analyzes the Siwalik Group along the Muksar Khola section. The main objectives of the present study are as follows

- To establish a detailed lithostratigraphy of the area.
- Determination of the sediment provenance to decipher hinterland tectonics.
- To establish a fluvial environment and its controlling factors.
- Comparison of the fluvial environment of the present study with the other Siwalik section.

#### **1.4 Outline of the Thesis**

This thesis is organized into ten chapters.

**Chapter I** includes an introduction, location and accessibility, background and research objectives.

**Chapter II** reviews the general geology of the Himalaya, geological settings around eastern Nepal Himalaya, the Muksar Khola section and the brief literature review of the Siwalik

Group regarding lithostratigraphy, magnetostratigraphy, depositional environment and provenance.

**Chapter III** describes the lithology along the Muksar Khola section, its classification and its correlation to the other previously studied Siwalik succession.

**Chapter IV** describes the sandstone petrography and deals with the classification of sandstone and its provenance.

**Chapter V** deals with the heavy minerals and their assemblage for the determination of provenance.

**Chapter VI** deals with the EDS analysis of the detrital tourmaline and garnet. Chemical compositions of detrital tourmaline and garnet are calculated and assigned to the end-member composition for determination of provenance.

**Chapter VII** deals with the Sr-Nd isotopic analysis for the determination of probable provenance.

**Chapter VIII** deals with the sedimentary facies, facies association and interpretation to decipher the fluvial environment responsible for the deposition of the Siwalik sediments of the Muksar Khola section.

**Chapter IX** includes the discussion of results and inferences of the fluvial system and provenance.

**Chapter X** is the conclusion of the thesis.

**Appendix** includes the route map of the study area.

## CHAPTER II

### GEOLOGICAL SETTINGS AND LITERATURE REVIEW

#### 2.1 Introduction

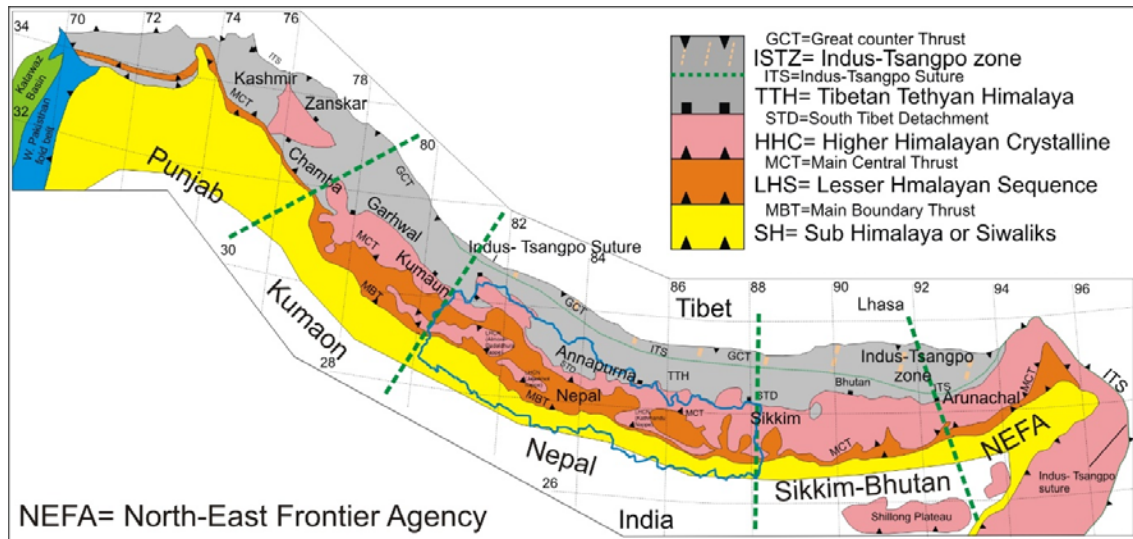


Figure 2.1: Subdivision of the Himalaya from west to east. (modified after Gansser, 1964; Yin, 2006).

The collision of the northward moving Indian sub-continent collided with the Eurasian plate led to a large crustal shortening, accomplished by the orogenic process of the Himalaya. The intense seismic activities occurring in the Himalaya at present-day gives evidence of its orogenic continuity and in present-day, the rate of the Indian Plate movement is about 5 cm per year (Pandey et al., 1995). This makes Himalaya the youngest mountain system in the world and is extended in an east-west trend from Namche Barwa in the east to Nanga Parbat in the west with an approximate length of 2400 km and width of 230 to 350 km (Le Fort, 1996). This mountain range includes Nepal, Bhutan and part of China, Pakistan and India. Geographically and geologically, it is divided into five sections (Bordet, 1961; Gansser, 1964). From west to east these are the Panjab Himalaya, Kumaon Himalaya, Nepal Himalaya,

Sikkim-Bhutan Himalaya, and the North-East Frontier Agency (NEFA) Himalaya (Fig. 2.1). The Nepal Himalaya extending from the Mechi River in the east to the Mahakali River in the west, running the entire length of Nepal is a part of this great Himalaya range.

## 2.2 Geology of the Nepal Himalaya

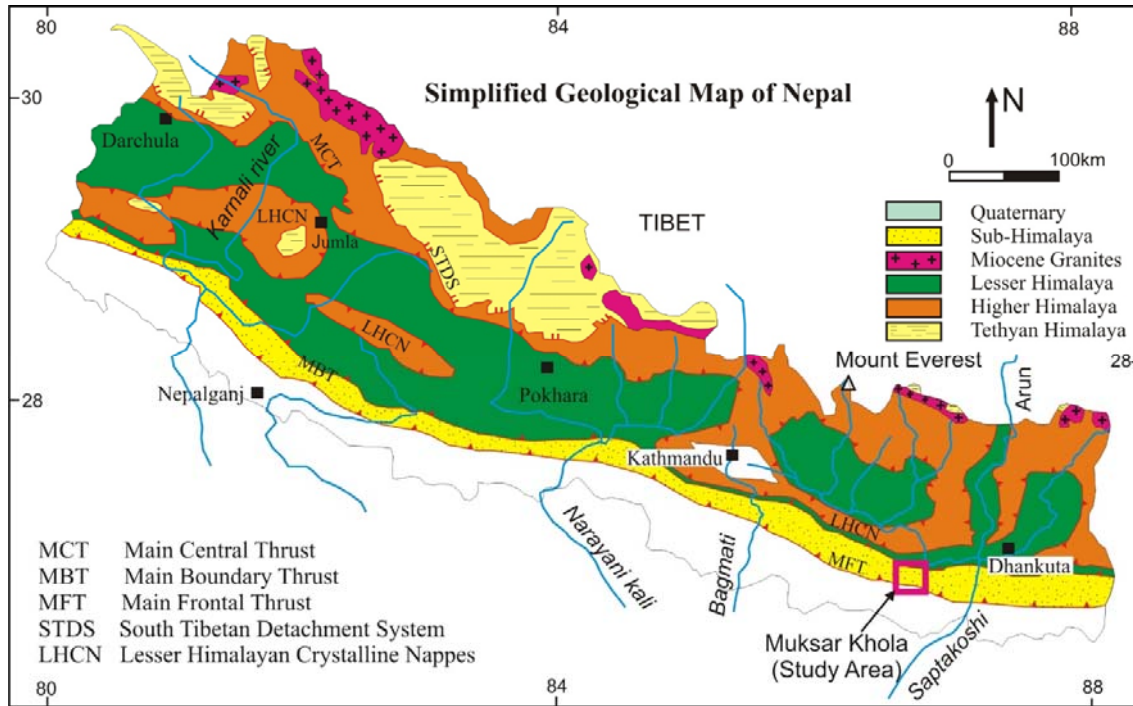


Figure 2.2: Geological map of Nepal showing the study area. (modified after Amatya and Jnawali, 1994).

The Nepal Himalaya occupies the central part of the Himalayan arc, which nearly covers one-third of the entire range. Geographically, the Nepal Himalaya lies within 80°11' to 88°27' East longitudes and 26°02' to 30°27' North latitudes. The Nepal Himalaya is tectonically and morphologically divided into five longitudinal units (Fig. 2.2), each having unique stratigraphic and evolutionary geological characters (Gansser, 1964; Le Fort, 1975; Valdiya, 1980). The units from south to north are briefly described in the following paragraphs.

### **2.2.1 Indo-Gangetic Plain (Terai)**

The Indo-Gangetic Plain, also known as the Terai plain is the Himalayan foreland basin. It consists of alluvial deposits from the Pleistocene to recent and rests over the Precambrian and Gondwana rocks of the Eocene-Oligocene age (Sharma, 1990). It forms the southernmost tectonic unit of the Nepal Himalaya and is separated by the Main Frontal Thrust (MFT) from the Sub-Himalaya (Fig. 2.2). The grain size gradually decreases towards the south and the average thickness of the deposit is considered as 1500 m. Geomorphologically, it is subdivided into the Northern (Bhabar), Middle and Southern zones.

### **2.2.2 Sub-Himalaya (Siwalik Group)**

The Sub-Himalaya or the Siwalik Group, occupy the Churia range forming the southern part of the Himalaya. It is bounded by the MFT to the south and the Main Boundary Thrust (MBT) to the north, which separates it from the Indo-Gangetic Plain and the Lesser Himalaya Sequence respectively (Fig. 2.2). The Siwalik Group is about 5–6 km in thickness and mainly composed of fluvial deposits of the middle Miocene to early Pleistocene age and contains vertebrate fossils (Parkash et al., 1980; Nakayama and Ulak, 1999). Based on the paleomagnetic studies, the age of the exposed Siwalik Group in Nepal ranges from ~14Ma to < 2Ma (Appel and Rosler, 1994; Gautam and Fujiwara, 2000; Ojha et al., 2009). This Group is mainly subdivided into three broad units: the Lower Siwaliks, the Middle Siwaliks and the Upper Siwaliks based on lithological variation and grain size (Auden, 1935; Hagen, 1969; Yoshida and Arita, 1982).

### **2.2.3 Lesser Himalayan Sequence**

The Lesser Himalayan Sequence (LHS) is unfossiliferous low-grade metasedimentary rocks. It mainly consists of rocks like slate, phyllite, quartzite, limestone, dolomite etc. of the Proterozoic (Gansser, 1964) to the Gondwana and post-Gondwana deposits of Mesozoic to Cenozoic age (Sakai, 1983). It lies in between the Siwalik Group to the south and the Higher Himalayan Crystalline to the north and is separated by MBT and the Main Central Thrust (MCT) respectively. The width of the LHS is not uniform throughout the Himalayan range due to the development of the crystalline thrust sheets. These crystalline thrust sheets comprise metamorphic rocks like Schist, gneiss, marble ranging from Precambrian to Eocene (Stocklin and Bhattarai, 1977; Stocklin, 1980).

### **2.2.4 Higher Himalayan Crystalline**

The Higher Himalayan Crystalline (HHC) consists of about 10 km thick succession of high-grade crystalline rocks including gneisses, schists, migmatites of the Precambrian age also known as Tibetan Slab (Le Fort, 1975) and extends continuously along with the entire Himalaya range. It lies in between the LHS and the Tibetan Tethys Himalaya separated by MCT to the South and the South Tibetan Detachment System (STDS) to the north respectively. This sequence consists of four main units: Kyanite-Sillimanite Gneiss, Pyroxene Marble and Gneiss, Banded Gneiss and Augen Gneiss (Bordet et al., 1972). Le Fort (1975) divided this zone into three formations: Formation I, Formation II and Formation III in ascending order. This HHC is frequently intruded by the Miocene granites in its northern boundary.

### **2.2.5 Tibetan Tethys Himalaya**

The Tibetan Tethys Himalaya (TTH) overlies the HHC and extends into Tibet in the north, where it is abruptly cut off by the Indus-Tsangpo Suture Zone (ITSZ). The width of the unit is approximately 40 km and is composed of highly fossiliferous sedimentary rocks including slate, sandstone and limestone of the Cambrian to Eocene age, deposited in the Tethys Sea (Upreti, 1999). In Nepal, the TTH has a very limited aerial extent with the best section being found in the Annapurna, Dhaulagiri and Dolpa region (Upreti, 1999). Most of the high peaks of Nepal, including Everest, Manaslu, Annapurna, Saipal and Dhaulagiri lie in this zone.

## **2.3 Geological setting**

### **2.3.1 Eastern Nepal Himalaya**

Eastern Nepal Himalaya comprises the Siwalik Group, LHS, HHC and TTH. Various studies have been carried out in the eastern Nepal Himalaya which resulted in diverse division and classifications of lithological units making the geology of the eastern Nepal Himalaya quite complicated (Schelling, 1992; Searle et al., 2003; Streule et al., 2010; Sakai et al., 2013). Among these, the lithostratigraphic division of Schelling (1992) illustrated in Figure 2.3 presents a regional geological map. In eastern Nepal Himalaya, LHS is exposed as a narrow belt due to the thrusting of overlying HHC along with the MCT (Sakai et al., 2013). This took place after the activation of the MCT around 22-16 Ma (Le Fort, 1986; Hodges et al., 1992). Besides this, large parts of the LHS are mainly exposed as tectonic windows like the Ramechhap window (also known as the Okhardhuaga Window), the Arun window and the Taplejung window (Fig. 2.3).



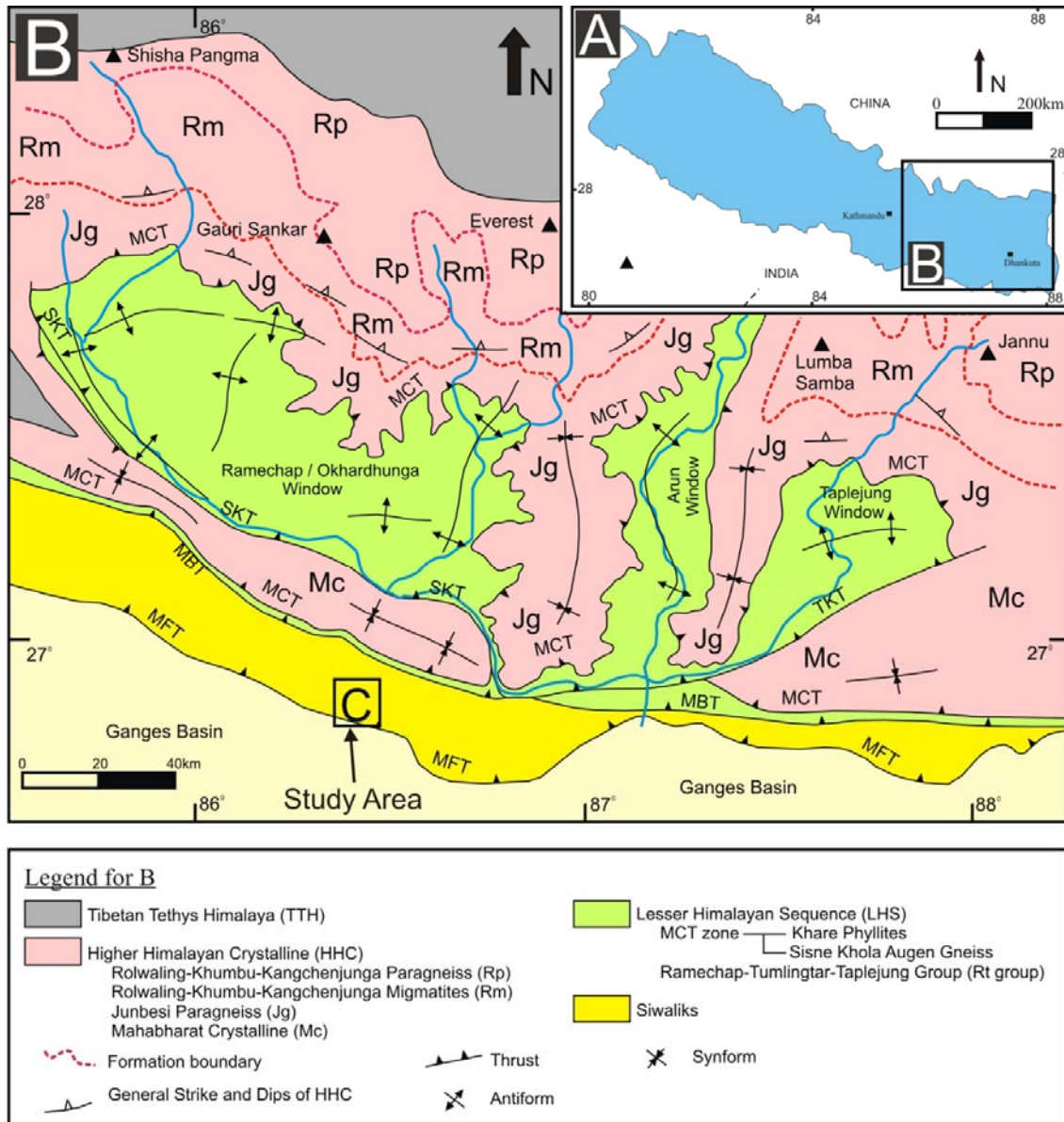


Figure 2.3: (A) Index map showing eastern Nepal. (B) Simplified geological map of the eastern Nepal Himalaya (modified after Schelling, 1992; Rai et al., 2021).

The LHS in the eastern Nepal Himalaya is divided into two units: the Ramechhap-Tumlingtar- Taplejung Group (RT Group) and the Main Central Thrust zone (MCT zone) (Schelling, 1992). The RT Group equivalent to the Nawakot complex of central Nepal (Schelling, 1992; Imayama and Arita, 2008) consists of metaquartzite, slate, phyllite, calcite- and dolomite-marble, rare conglomerate, and occasional bands of mylonitic augen gneiss. Similarly, the

MCT zone is further divided into the Sisne Khola Augen Gneiss and the Khare Phyllites (Schelling, 1992; Imayama et al., 2010). The Sisne Khola Augen Gneiss consists of augen gneiss and mylonitic augen gneiss with mylonitic metaquartzite, whereas the Khare Phyllites consists of graphite-rich phyllite, black slate, calcite marble, dolomite marble, talc schist, magnesite, and actinolite-epidote schist (Schelling, 1992; Imayama et al., 2010).

In eastern Nepal, HHC comprises of the Junbesi Paragneiss (Jp), the Rolwaling-Khumbu-Kangchenjunga Migmatites (Rm) and the Rolwaling-Khumbu-Kangchenjunga Paragneiss (Rp) from south to north (Schelling, 1992; Imayama et al., 2010). Strongly foliated garnet-biotite schist, feldspathic gneiss, calc-silicate schist, metaquartzite, augen gneiss with rare amphibolite are observed in Jp. Similarly, sillimanite-bearing migmatitic orthogneiss intercalated with paragneiss and sparse amphibolite are observed in Rm whereas the Rp consists of sillimanite-bearing, biotite rich paragneiss intercalated with metaquartzite, calc-silicate gneiss, marble, granitic gneiss and augen gneiss. The southern extinction of the HHC thrust sheet or Lesser Himalayan Crystalline belt is termed the Mahabharat Crystallines (Schelling, 1992) which is equivalent to the Jp (Imayama et al., 2010).

### **2.3.2 The Siwalik Group**

In the eastern Nepal Himalaya, the Siwalik Group is observed as three major belts, these are separated by the Main dune Thrust (MDT) and the Kamala-Tawa Thrust (KTT) (Shrestha and Sharma, 1996; DMG, 2011; Fig. 2.4). Shrestha and Sharma (1996) classified Siwalik successions into three litho units, namely the Lower Siwaliks, the Middle Siwaliks and the Upper Siwaliks. These three litho units are only observed in the southern belt, which is bounded by the MFT in the south and MDT in the north. The middle belt comprises only Lower Siwaliks. Whereas the northern belt which is bounded by the KTT in the south and the

MBT in the north consists of the Lower Siwaliks and the lower Middle Siwaliks. The present study lies on the southern belt (> 4 km thick) along the Muksar Khola section.

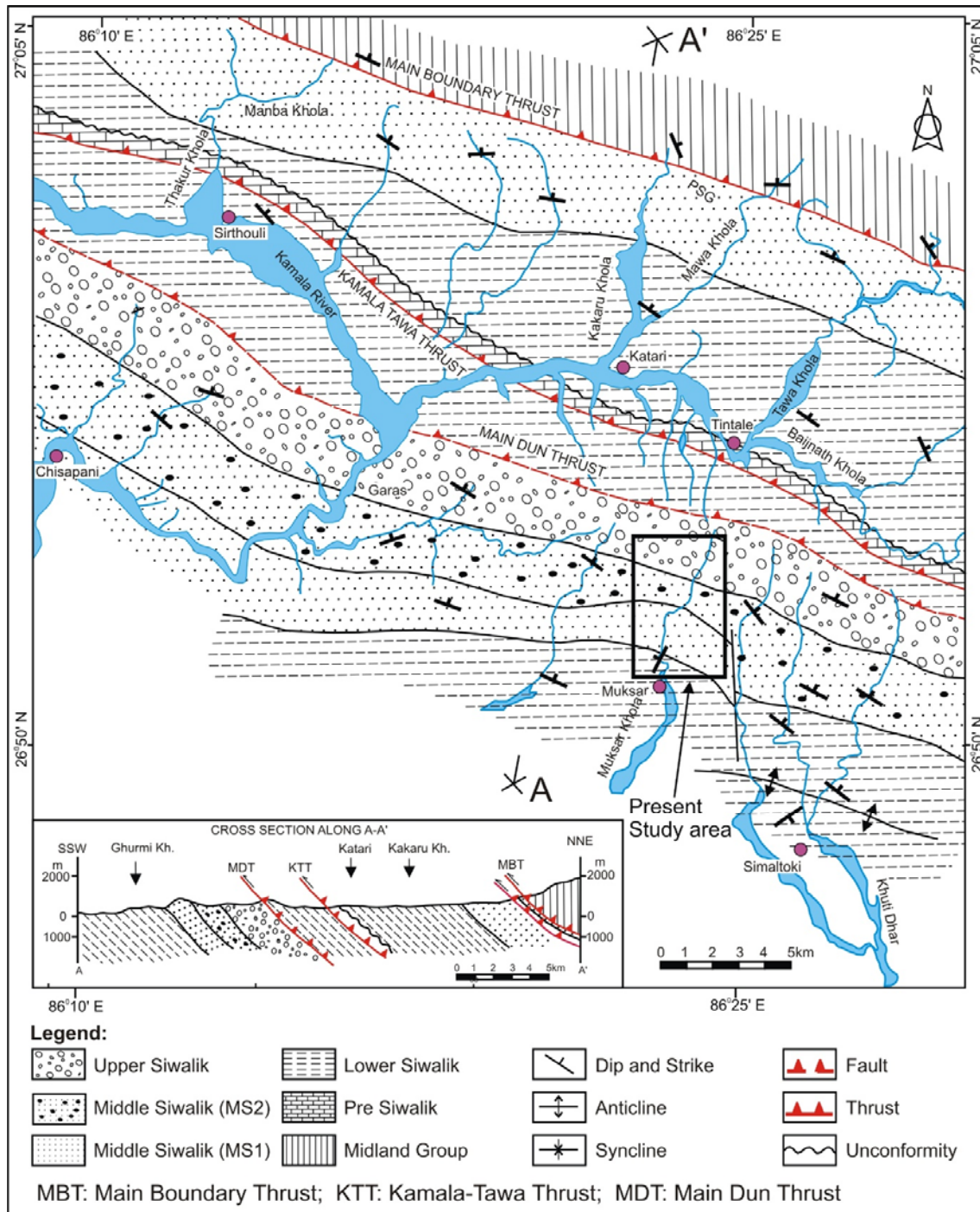


Figure 2.4: Geological map of the Siwalik Group in eastern Nepal showing the study area (modified after Shrestha and Sharma, 1996).

## **2.4 Literature Review**

The Siwalik Group is a natural archive that holds important information on the late Tertiary exhumation history of the Himalaya. Various studies have been carried out in the Siwalik successions in recent years which can be summarized in the following sub-headings.

### **2.4.1 Lithostratigraphy**

Lithostratigraphy of the Siwalik Group in the Himalaya has been established by various researchers (Pilgrim, 1913; Auden, 1935; Lewis, 1937; Hagen, 1969; Glennie and Ziggler, 1964; Tokuoka et al., 1990; Corvinus, 1993; Sah et al., 1994; Dhital et al., 1995; Ulak and Nakayama, 1998; Ulak, 2004; 2009; Sigdel et al., 2011; Adhikari and Sakai, 2015, Adhikari et al., 2018). Among these classifications the traditional three-fold classification based on grain-size i.e. Lower, Middle and Upper Siwaliks based on the lithology are broadly used for the classification of the Siwalik successions (Auden, 1935; Hagen 1969; Yoshida and Arita, 1982; Ulak, 2004; 2009; Adhikari et al., 2018). Dispute this other classification with local stratigraphic names are also widely used which classifies the Siwalik Group in four-fold to six-fold classifications (Tokuoka et al., 1986; Sah et al., 1994; Dhital et al., 1995; Sigdel et al., 2011; Adhikari and Sakai, 2015).

### **2.4.2 Magnetostratigraphy**

Paleomagnetic age data of the Siwalik Group is very important to understand the Himalayan phenomena recorded in Siwalik sediments concerning the geological timeframe. Magnetostratigraphic studies have been carried out in the various section of the Siwalik Group from Pakistan in the west (Johnson et al., 1985) to the Arunachal Pradesh of India in the east (Chirouze et al., 2012b). These studies suggest the Siwalik Group was deposited

around middle Miocene to early Pleistocene time. In Nepal, the paleomagnetic studies have been carried out in different Siwalik successions (Tokuoka et al., 1986; Appel et al., 1991; Harrison et al., 1993; Appel and Rosler, 1994; Gautam and Appel, 1994; Rosler et al., 1997; Gautam and Fujiwara, 2000; Ojha et al., 2009). In the Muksar Khola section, the paleomagnetic study was carried out by Ojha et al. (2009) and suggested the Middle Siwaliks of the Muksar Khola section was deposited within 10.0-3.5 Ma.

### **2.4.3 Depositional Environment**

Studies of the depositional facies of the Siwalik sediments in Nepal Himalaya and the north-western Indian Himalaya concluded these sediments were deposited by the fluvial system (Willis, 1993b; Khan et al., 1997; Zaleha, 1997; Kumar et al., 2003; Tokuoka et al. 1986, 1990, 1994; Hisatomi and Tanaka, 1994; Nakayama and Ulak, 1999; Ulak and Nakayama, 2001; Ulak, 2004, 2009; Huyghe et al., 2005). Meandering and braided channels were reported as the dominating fluvial system and the appearance of these fluvial systems is consistent among the Siwalik sections, but its timing differs. Dispute, some studies also revealed the existence of the anastomosing river system in a certain part of the paleo foreland basin (Nakayama and Ulak, 1999; Huyghe et al., 2005). Recent studies in north-eastern India and Bhutan reveal the influence of the marine deposition in the Siwalik Group (Coutand et al., 2016; Taral et al., 2018; 2019). Deltaic to open marine environments were reported in the Lower Siwaliks in these Siwalik sections. Moreover, few successions of the Middle Siwaliks and the lower Upper Siwaliks also record the near-coastal environments (Taral et al., 2018; 2019).

#### **2.4.4 Provenance and tectonic Setting**

Various studies based on detrital sediments has been carried out to reveal the provenance of the Siwalik sediments and the exhumation of the Himalaya. These include sandstone petrography (Garzanti et al., 1996; Sigdel and Sakai, 2013; Tamrakar et al., 2003), heavy mineral analysis (DeCelles et al., 1998; Garzanti et al. 2007; Yoshida et al., 2019), isotropic fingerprints (Robinson et al., 2001; Huyghe et al., 2005; Chirouze et al., 2013), geochronology (DeCelles et al., 1998; Chirouze et al., 2012a; Baral et al., 2016) and geochemistry (Lee et al., 2003; Nakajima et al., 2020b). These studies suggest, the sediments of the Siwalik Group were mainly supplied from the HHC along with TTH and the LHS. These studies also reveal the sediment compositions varies among the different Siwalik successions suggesting the diachronous uplift and erosional unroofing of the Himalaya east to west.

#### **2.4.5 Paleoclimate**

The stable carbon isotopes from the Siwalik sediments are widely used to interpret the paleoclimate of the Himalaya. The stable carbon isotopic signature of C3 vegetation has  $\delta^{13}\text{C}_{\text{org}}$  values between -22 and -30, whereas C4 plants  $\delta^{13}\text{C}_{\text{org}}$  values range from -10 to -14 (Cerling et al., 1997). Generally, C3 plants are supposed to represent cool and humid Climate whereas C4 plants represent warm and water-stressed climate (Ehleringer, 1988). Srivastava et al. (2018) suggested that during the middle and late Miocene the summer monsoon precipitation was almost the same, while in the late Miocene the winter season precipitation significantly decreased increasing the seasonality which caused C4 plants to take over C3. Therefore, a change in these plants suggests a change in the climatic condition (Cotton et al., 2016). The isotopic value from the Siwalik sediments across the Himalaya shows the significant variation in paleo-climatic conditions east to west. Quade and Cerling (1995)

noticed the gradual shift of C4 plants from C3 plants at 7.3 Ma and after 6.0 Ma C4 plant completely dominated in northern Pakistan. A similar shift was observed in north-western India at 7.0 Ma (Vogeli et al., 2017). This climatic shift has been recorded in central Nepal (Bakiya Khola and Surai Khola section) at around 7.0 Ma (Harrison et al., 1993; Quade et al., 1995; Srivastava et al., 2018). In the Muksar Khola section shift in the vegetation was observed around the stratigraphic thickness of 1700m (Quade et al., 1995). This stratigraphic thickness is roughly around 6.0 to 5.0 Ma based on the stratigraphic column of Ojha et al. (2009). Despite these results, some researchers suggested that the climate change occurred around 10 Ma in central Nepal revealed by isotopic analysis of the paleosols (Tanaka, 1997). But such a shift in the vegetation is not noticed in the Kameng River in the north-eastern Indian Himalaya which remain almost the same humid with low seasonality (Vogeli et al., 2017). Kundu et al. (2012) suggested that the Siwalik succession of Tista valley was deposited in a humid climate similar to the eastern Himalaya climate, though his interpretation was based on the mineral characteristics (alteration of feldspar grain in sandstone) rather than vegetation. Khan et al., (2018) suggested that over the past 15 million years the overall eastern Himalaya (Darjeeling and Arunachal Pradesh) climate appears to have been remarkably uniform.

## CHAPTER III

### LITHOSTRATIGRAPHY

#### **3.1 Introduction**

The Muksar Khola section in eastern Nepal has been a focus of various studies (Quade et al., 1995; Robinson et al., 2001; Ojha et al., 2009; Chirouze et al., 2012a). But these studies mainly focused on isotopes, magnetostratigraphy, geochronology etc. for the determination of climate, provenance, depositional age, and exhumation history of eastern Nepal. Further, these studies were carried out in the Middle Siwaliks and they did not examine the lithofacies in detail. Shrestha and Sharma (1996) and DMG (2011) prepared a broad scale geological map of this region and includes the Siwalik Group along the Muksar Khola section but, they only divided the Siwalik Group into the Lower, the Middle and the Upper Siwaliks. Shrestha and Sharma (1996) presented the table showing the lithology of these subgroups, but they did not mention the section they consider (Fig. 2.4). Similarly, Ojha et al. (2009) presented a sedimentological log for evaluating the depositional age but this log is on a large scale and also lack lithological descriptions. Chirouze et al. (2012a) briefly define the lithology, but they too lack detailed sedimentological logs and geological maps, further their classification was based on Ojha et al. (2009).

This study focuses on the stratigraphic classification of the Siwalik Group and their lithological description. Classifications are carried out based on classical threefold classification, previously used in the different Siwalik sections (Pilgrim, 1913, Hagen, 1951; Shrestha and Sharma, 1996; Ulak, 2004, 2009; Adhikari et al., 2018). This lithostratigraphic classification will establish a template for future research.



### **3.2 Methods**

This study is based on the field data acquired from the geological traverses along the Muksar Khola section. A route map (appendix) and detailed sedimentological log of the entire section was prepared to precisely divide the lithological units. Rocks were classified into mudstone, sandstone and conglomerate based on grain size. The colour of mudstones was determined using the Munsell colour chart. Variation in the lithological characteristics was taken as the basis for the classification of rock units into the member and litho units. The paleomagnetic age data by Ojha et al. (2009) was used to determine the specific age for each litho-unit and member, which was further used for regional correlation with the other sections of the Nepal Himalaya.

### **3.3 Lithostratigraphy**

In this study lithostratigraphy of the Siwalik Group along the Muksar Khola section located on the southern belt is established. Siwalik Group in this section is classified into three lithostratigraphic units i.e., Lower, Middle and Upper Siwaliks. The Lower Siwaliks consists of a conglomerate member and the Middle Siwaliks is further divided into two members: lower member and upper member. A geological map with cross-section is presented in Figure 3.1 and classification concerning the depositional age established by Ojha et al. (2009) is presented in Figure 3.2.

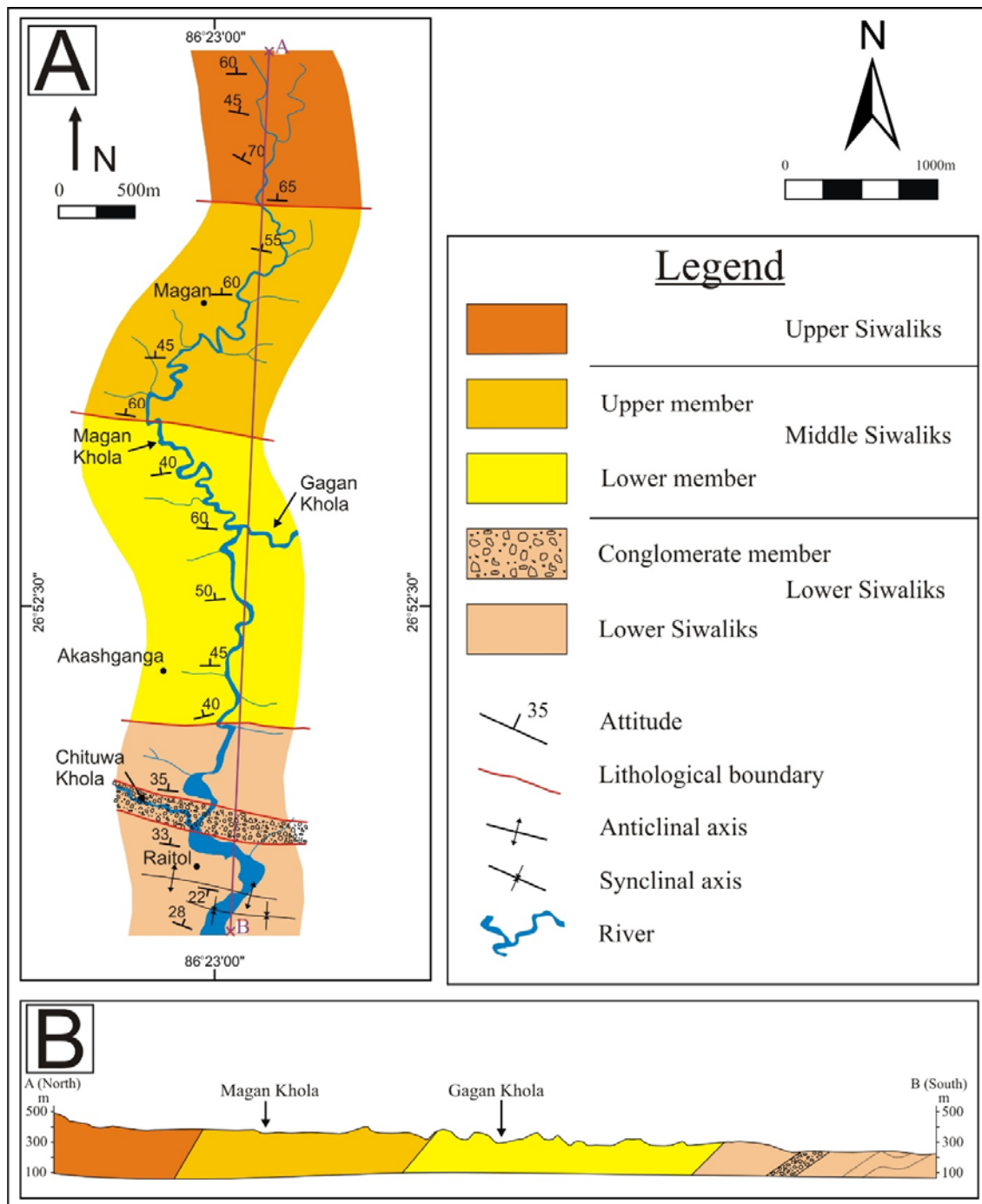


Figure 3.1: A) Geological Map of the Siwalik Group along the Muksar Khola section and B) Cross-section along A-B (modified after Rai and Yoshida, 2020).

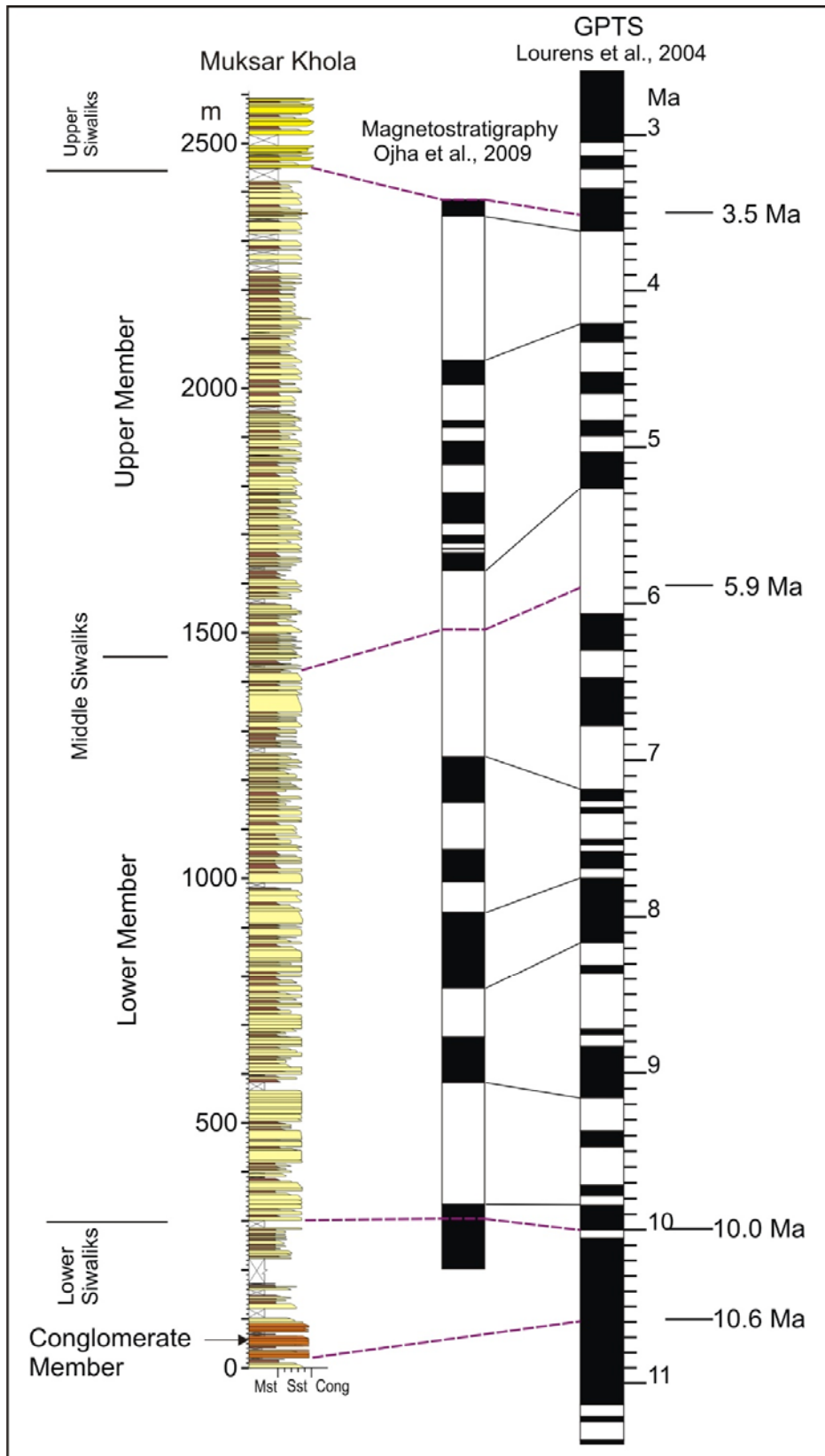


Figure 3.2: Sedimentological column of the Siwalik Group along the Muksar Khola section showing lithostratigraphic division concerning the magnetostratigraphic age data of Ojha et al. (2009) (modified after Rai and Yoshida, 2020).

### 3.3.1 Lower Siwaliks

This litho-unit is observed along both the banks of the Muksar Khola around the Gola and Raitol villages (Fig. 3.1). This unit attains a thickness of > 400 m, with an intraformational conglomerate member around the upper section. The detailed sedimentological log of this unit is presented in Figure 3.3. Mudstone and fine-grained sandstone (Fig. 3.4-A) are the dominating rock types with a remarkable succession of the intraformational conglomerate (Fig. 3.4-B). Based on the preexisting paleomagnetic age this unit was deposited before 10 Ma (Fig. 3.2; Ojha et al., 2009).

The Lower Siwaliks lithology consists of very fine- to fine-grained, light-grey coloured sandstone interbedded with dark grey to olive black mudstone to siltstone. The thickness of very fine-grained sandstone beds ranges from 0.30-0.80 m, whereas fine-grained sandstone beds have an average thickness of 1.0 m. Fine- to medium-grained sandstone beds thickness ranges from 1.0–1.5 m with occasional beds with thickness ~4.0 m. Fine-to medium-grained “salt and pepper” textured sandstone with thickness ranging 0.3–1.0 m are observed in the lower section, in the vicinity of the low angled anticline axis (Fig. 3.1). Planer cross-stratification and parallel to ripple lamination are the common sedimentary structures observed. Mudstone shows bioturbation with an average thickness of 0.4–1.5 m but occasionally 2.0–3.5 m thick mudstone beds are also observed. These mudstones are mostly olive-grey to dark-grey with a few yellowish- to reddish-grey colours (Table: 1). Sandpipes (Fig. 3.4-C) and carbonized roots (Fig. 3.4-D) are mainly preserved in siltstone. Towards the younger succession abundant mottled and variegated mudstone are preserved (Fig. 3.4-E). Both the mudstone and siltstone shows concretions (2–6 cm in diameter) whereas in fine- to medium-grained sandstone large layered concretions are developed (sometimes 30 cm in diameter, Fig. 3.4-F).

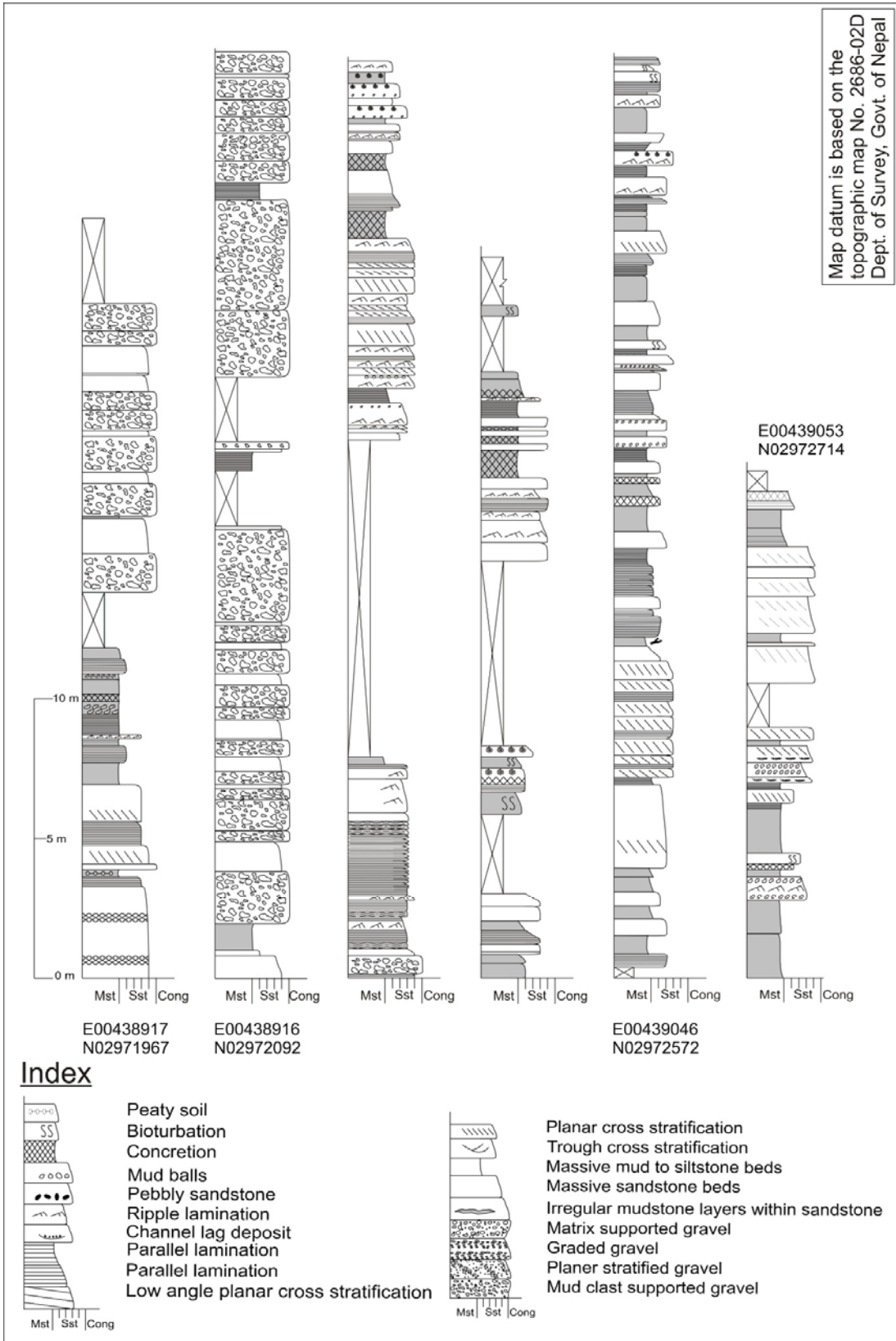


Figure 3.3: Detailed sedimentological column (representative) from the Lower Siwaliks (modified after Rai and Yoshida, 2020).

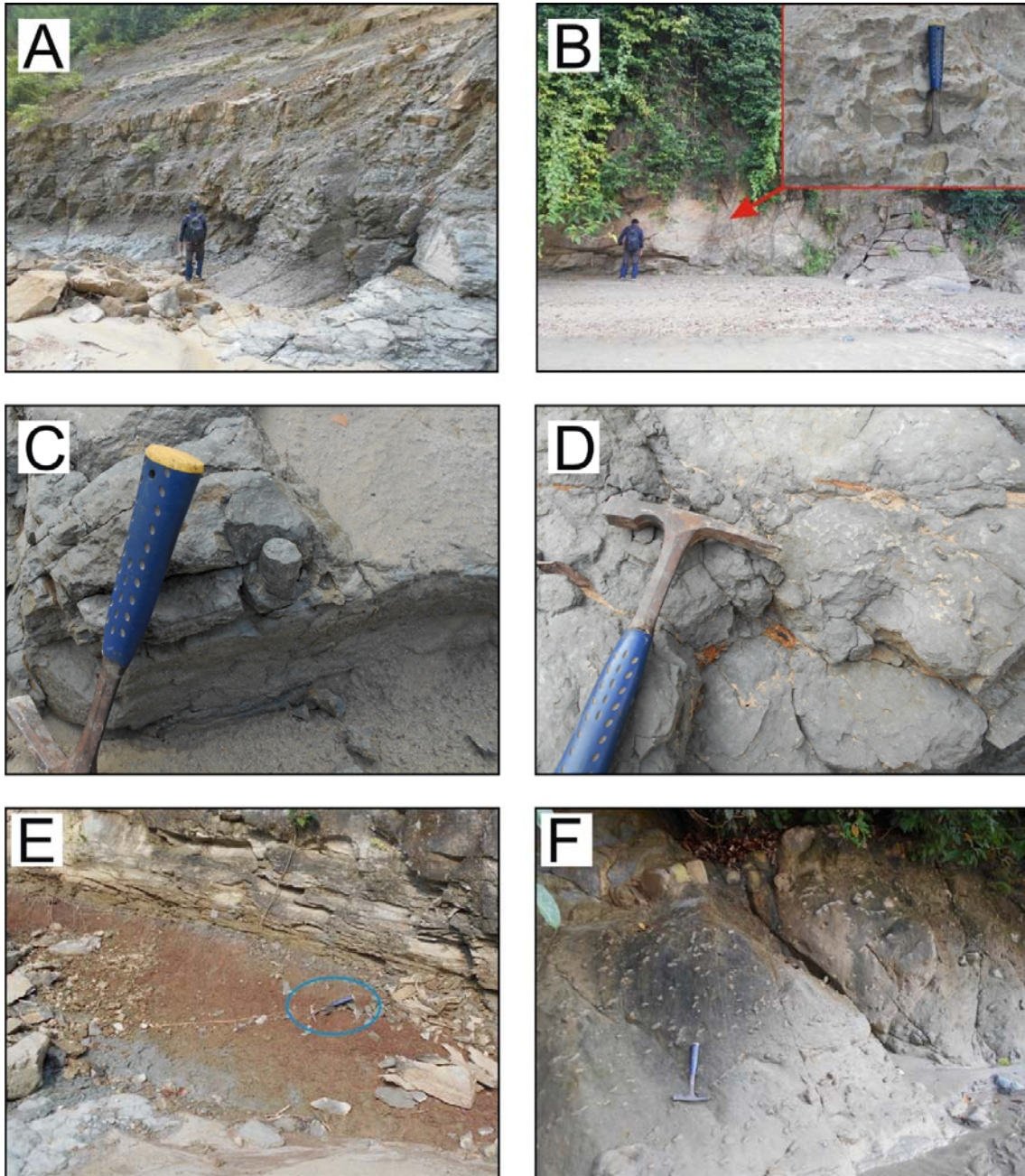


Figure 3.4: Field photographs of A) Inter-bedding of fine-grained sandstone and mudstone of the Lower Siwaliks; B) Intraformational conglomerate of the Lower Siwaliks (conglomerate member); C) Sandpipe observed in mudstone to siltstone of the Lower Siwaliks; D) Carbonized plant roots in siltstone of the Lower Siwaliks; E) Variegated mudstone of the Lower Siwaliks; F) Concretion observed in siltstone to fine-grained sandstone of the Lower Siwaliks.

Table 3.1: Mudstone colour observed in the present study area based on the Munsell colour chart (modified after Rai and Yoshida, 2020).

Formation	MUNSELL COLOUR CODE			Colour Interpretation
	Hue	Value/Chroma	%	
Upper Siwaliks	2.5Y	6/1; 6/4	43%	Yellowish grey and dull yellow
	N	4; 5	43%	Grey
	2.5GY	4/1	14%	Dark olive grey
Middle Siwaliks (upper member)	7.5Y	3/1; 4/1; 4/2; 6/1	14%	Grey, greyish olive to olive black
	N	1.5; 2; 3; 4; 5; 6	54.5%	Grey, dark grey to black
	2.5GY	2/1; 3/1; 4/1; 5/1	14.5%	Olive grey, dark olive grey to black
	5B	3/1; 4/1; 5/1; 6/1	6.5%	Bluish grey to dark bluish black
	5BP	2/1; 3/1; 4/1	8.5%	Dark bluish grey to bluish black
	5P	1.7/1; 5/1	2%	Purplish grey to purplish black
Middle Siwaliks (lower member)	5Y	4/2; 4/3	3.5%	Dark olive
	7.5Y	3/1; 3/2; 4/2; 4/3	9%	Greyish olive to olive black
	10Y	2/1; 3/1; 3/2; 4/2	6%	Olive grey to olive black
	N	1.5; 2; 3; 4; 5	18%	Grey to black
	2.5GY	2/1; 3/1; 4/1	32%	Dark olive grey to black
	5GY	3/1; 4/1; 5/1; 6/1	10%	Olive grey to dark olive grey
	7.5GY	2/1; 3/1; 4/1	10.5%	Dark greenish grey
	5G	3/1; 4/1	6.5%	Dark greenish grey
	10G	3/1; 4/1	4.5 %	Dark greenish grey
	10BG	3/1; 4/1	4.5%	Dark bluish grey
	5PB	2/1; 3/1	1.5%	Dark bluish grey to bluish black
5P	1.7/1; 2/1; 3/1	3%	Dark purplish grey to purplish black	
Lower Siwaliks	10R	3/1	6.5%	Dark reddish grey
	10YR	4/3	7%	Dull yellowish brown
	7.5Y	3/1; 4/1; 5/2; 5/3	33.5%	Grey, greyish olive to olive black
	10Y	5/1; 5/2	20%	Grey to dark grey
	N	3; 5	13%	Grey to dark grey
	2.5GY	4/1; 5/1	20%	Olive grey, dark olive grey

### **3.3.1.1 Lower Siwaliks (Conglomerate member)**

This member is well exposed around the confluence of the Muksar Khola and the Chituwa Khola with a thickness of ~90 m (Fig. 3.1). This member is dominated by poorly sorted clast supported intraformational conglomerate and medium- to coarse-grained massive sandstone with rare laminated olive-grey mudstone (Figs. 3.3, 3.4-B). The intraformational conglomerate is made up of mud clast and medium- to very coarse-grained sandstone matrix. Its thickness ranges from 0.4 to >4.0 m. Mudstone clasts are 1–4 cm average in diameter (some clasts are elongated up to 10 cm) and reddish-brown to grey coloured with angular to sub-angular shape (Fig. 3.4-B). Soft deformation in these mud clasts is also observed in considerable amounts. The proportion of clast and matrix is about 70% to 30% respectively. Sandstone thickness ranges from 0.1 to 0.8 m and is light-grey in colour with massive and uniform grain size base to top. Mudstones are very rare with thickness ranging from 0.4 to 0.5 m and are observed towards the upper section of this member. Its colour range from dark-olive to bluish-grey with a thickness of 0.4 to 0.5 m. This member has not been dated till this study but based on the oldest sedimentation rate of Ojha et al. (2009) and the thickness from the present sedimentological log a tentative age of 10.6 Ma is estimated.

### **3.3.2 Middle Siwaliks**

The Middle Siwaliks rocks are best observed along the Muksar Khola around Aakashganga Temple and Magan village (Fig. 3.1). Based on preexisting age data it was deposited between 10.0–3.5 Ma (Fig. 3.2) with an overall thickness of ~2150 m. In this study, the Middle Siwaliks is divided into two members: the lower and upper member. This division is based on the lithological variation and their thickness, induration of sandstone beds and proportion of biotite grain in sandstone. The upper member shows an increase in the mudstone proportion and thickness of the sandstone bed compared to the lower member (Fig. 3.5 and 3.6).



Similarly, the colour of mudstone also varies, the lower member shows greenish-grey to olive-grey colour, whereas the upper member shows dark-grey to black colour (Table 3.1).

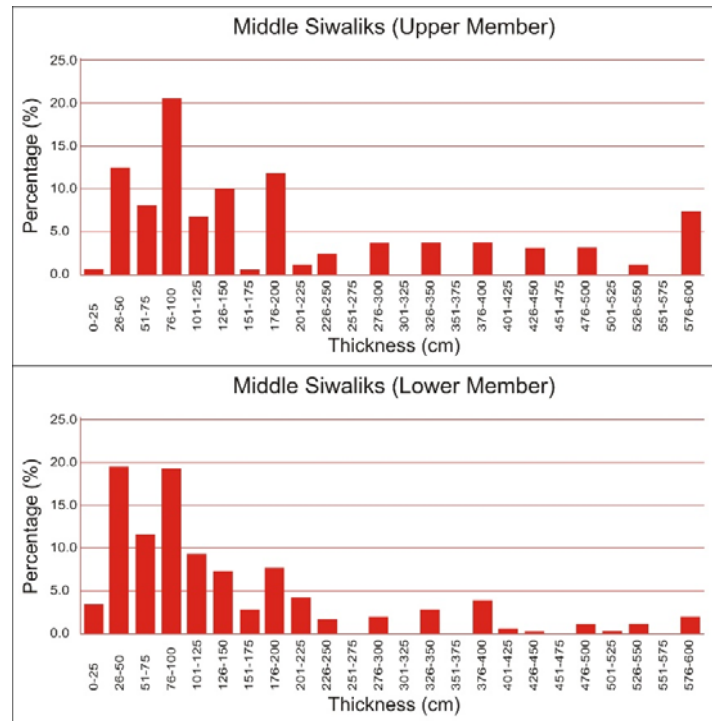


Figure 3.5: Sandstone bed thickness of the lower and the upper member of the Middle Siwaliks. (Amalgamated sandstone beds with thickness more than 6 m were excluded) (modified after Rai and Yoshida, 2020).

### 3.3.2.1 Lower Member

The lithology of this member is characterized by “salt and pepper” appearance sandstone, showing fining-upward succession and gleyed mudstone with dominating dark greenish-grey to olive-grey and black colour (Table 1). The detailed sedimentological log of this unit is presented in Figure 3.7. Mudstone thickness ranges from 0.3–1.0 m, occasionally very thick beds up to 8m are also observed. Dominating sandstone beds are medium-grained and medium- to thickly-bedded with thickness ranging from 26–100 cm (Fig. 3.5), occasionally medium- to coarse-grained sandstone are also observed (Fig. 3.7). In this member episodic occurrence of thick amalgamated sandstone beds (>10 m thick) are observed (Fig. 3.8-A). The frequency of such amalgamated sandstone beds decreases towards the upper section.

Planer cross-stratification, and parallel and ripple lamination are mostly observed in these sandstone beds. Trough cross-stratification with channel lag deposits is mainly observed in amalgamated sandstone beds. Bioturbation is observed in both mudstone and some very thick sandstone beds (Fig. 3.8-B). Bivalve shells (Fig. 3.8-C) and leaf fossils (Fig. 3.8-D) are observed in medium-grained sandstone and mudstone to fine-grained sandstone respectively. Both sandstone and mudstone possess concretions, their size is similar to the Lower Siwaliks, but density is comparatively less. The overall 1150 m thick lower member of the Middle Siwaliks was deposited around 10.0 to 5.9 Ma (Fig. 3.2; Ojha et al., 2009).

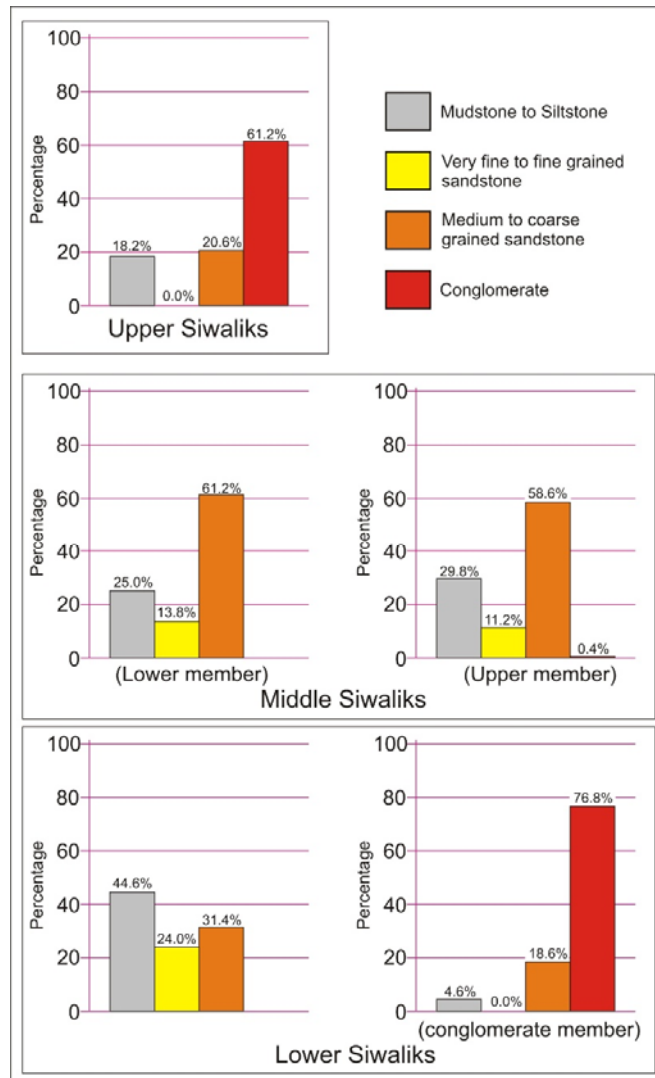
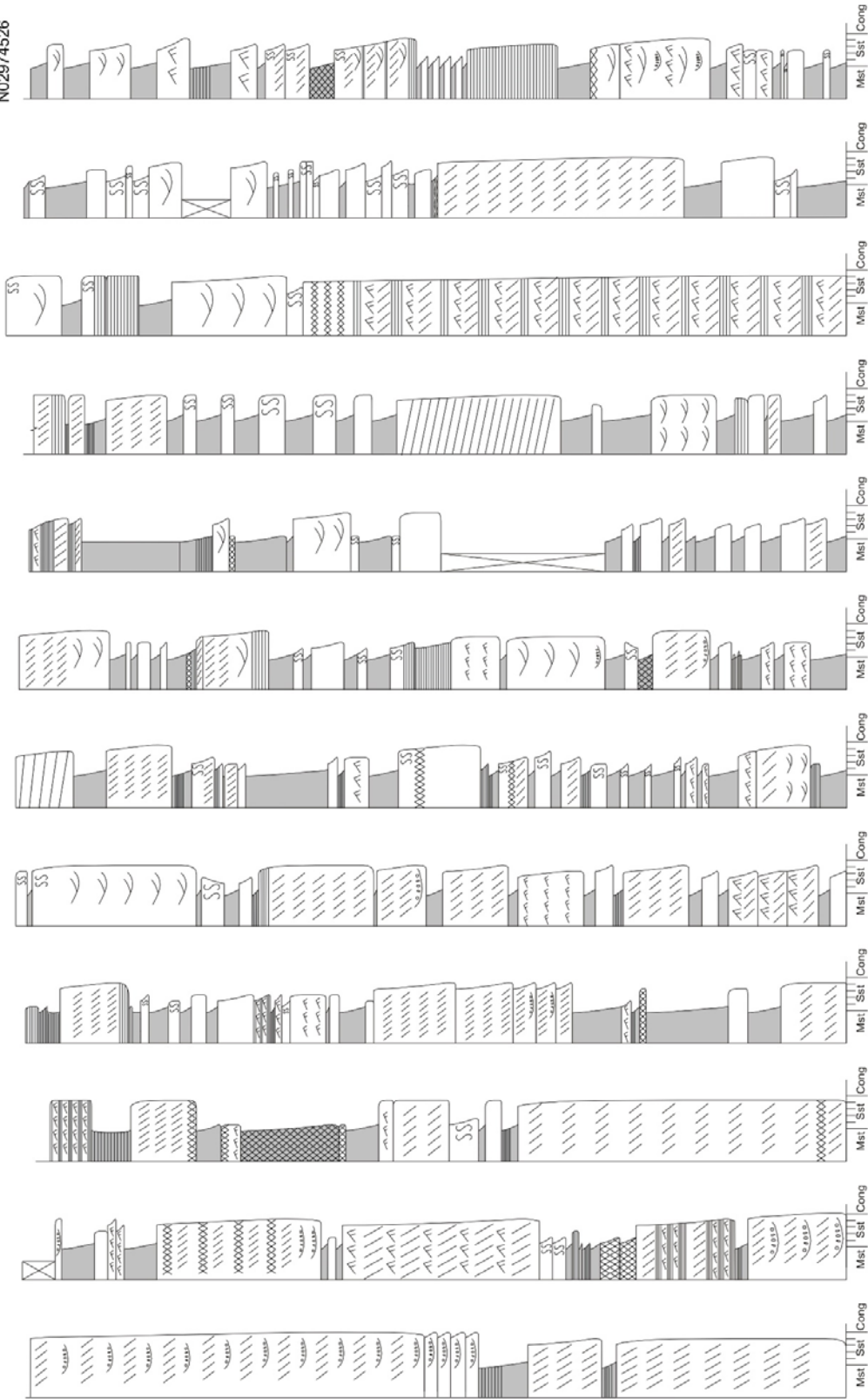


Figure 3.6: Proportion of different litho units in the Siwalik Group along the Muksar Khola (modified after Rai and Yoshida, 2020).



E00438583  
N02974526



Map datum is based on the topographic map No. 2686-02D Dept. of Survey, Govt. of Nepal

Figure 3.7: Continued.

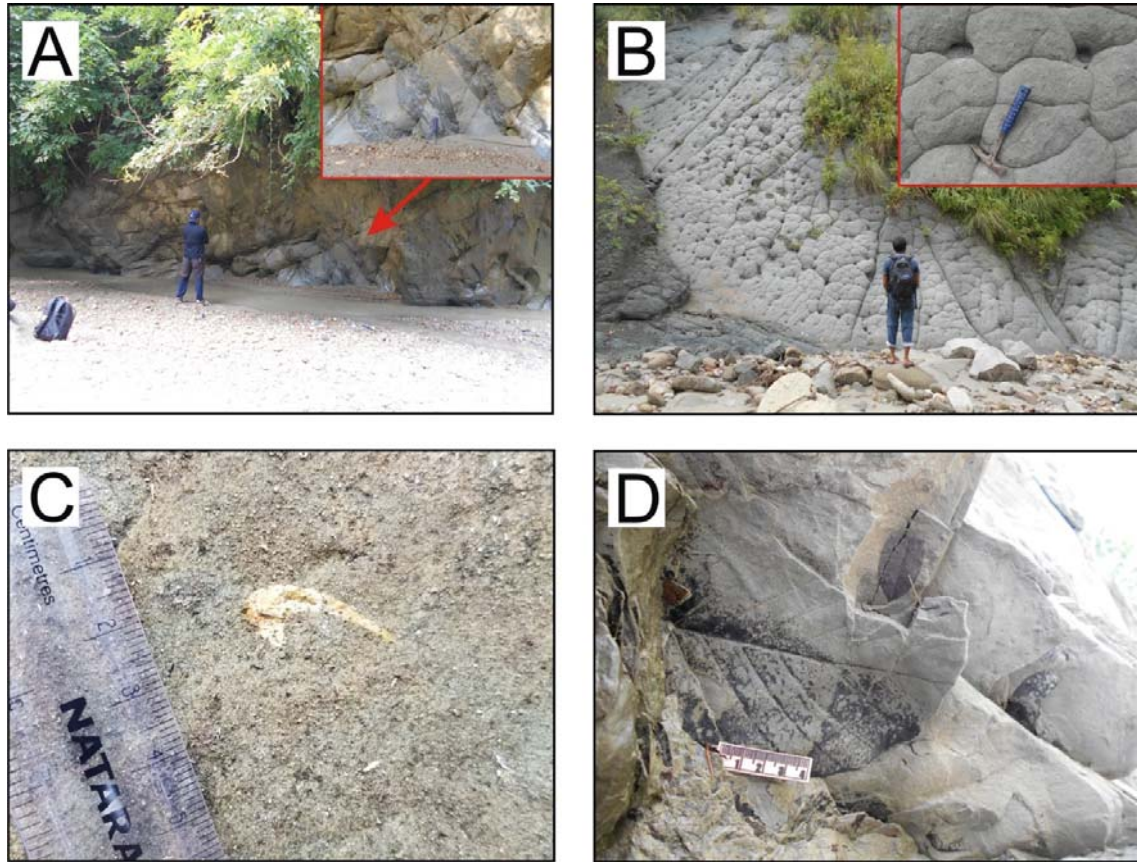


Figure 3.8: Field photographs of A) Amalgamated sandstone with multiple siltstone lag deposits at the base observed in the Middle Siwaliks (lower member); B) Bioturbated sandstone surface in the Middle Siwaliks; C) Bivalve shell in the sandstone of the Middle Siwaliks (lower member); D) Leaf imprints preserved in the siltstone of the Middle Siwaliks (lower member).

### 3.3.2.2 Upper Member

The upper member of the Middle Siwaliks consists of medium- to coarse-grained, light grey sandstone interbedded with dark-grey to black mudstone. The detailed sedimentological log of this unit is presented in Figure 3.9. Fining upward sequence is well observed in sandstone beds with the thickness ranging 1.0–2.0 m (Figs. 3.6; 3.10-A). The sandstone of this member almost lacks the “salt and pepper” texture as observed in the sandstone of the lower member. This “salt and pepper” texture are rarely observed in the beds around the lower section of this member. Moreover, in this member sandstones are less indurated, and the degree of induration decreases towards the upper section of this member with the increase in the

occurrence of pebbly sandstone beds. Dominating sedimentary structure is trough cross-stratification with channel lag deposits (Fig. 3.10-B). Planer cross-stratification and ripple laminations are also observed in a minor amount at the lower section of this member. The thickness of channel lag deposits is observed to increase drastically in the upper section (up to 30–50 cm) resembling conglomerate beds. Dominating mudstone is gleyed with grey, dark-grey to black colour, and the occasional occurrence of variegated to purple mudstone (Table 1). Bioturbated mudstones are 0.4–2.0 m in thickness, but frequently mudstone with thickness 2.0–6.0 m are also observed. Occasionally concretions are observed in siltstone to mudstone (Fig. 3.10-C). This member shows huge amounts of syn-tectonic deformation as well as convolute lamination in sandstone beds (Figs. 3.10-D). This member is preserved with an overall thickness of ca. 1000 m and its depositional age ranges between 5.9–3.5 Ma (Fig. 3; Ojha et al., 2009).

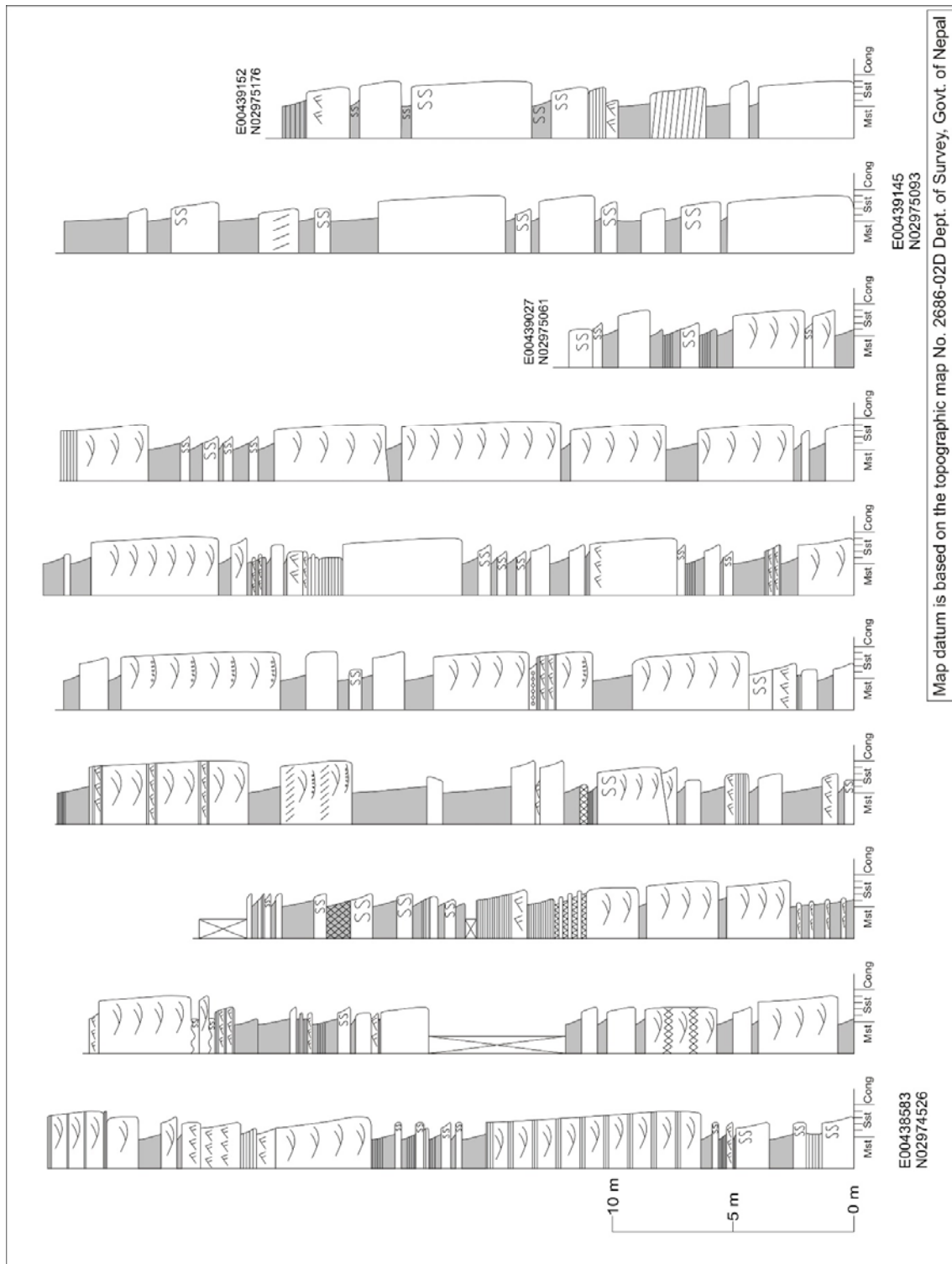


Figure 3.9: Detailed sedimentological column (continuous) of the upper member of the Middle Siwaliks (modified after Rai and Yoshida, 2020).

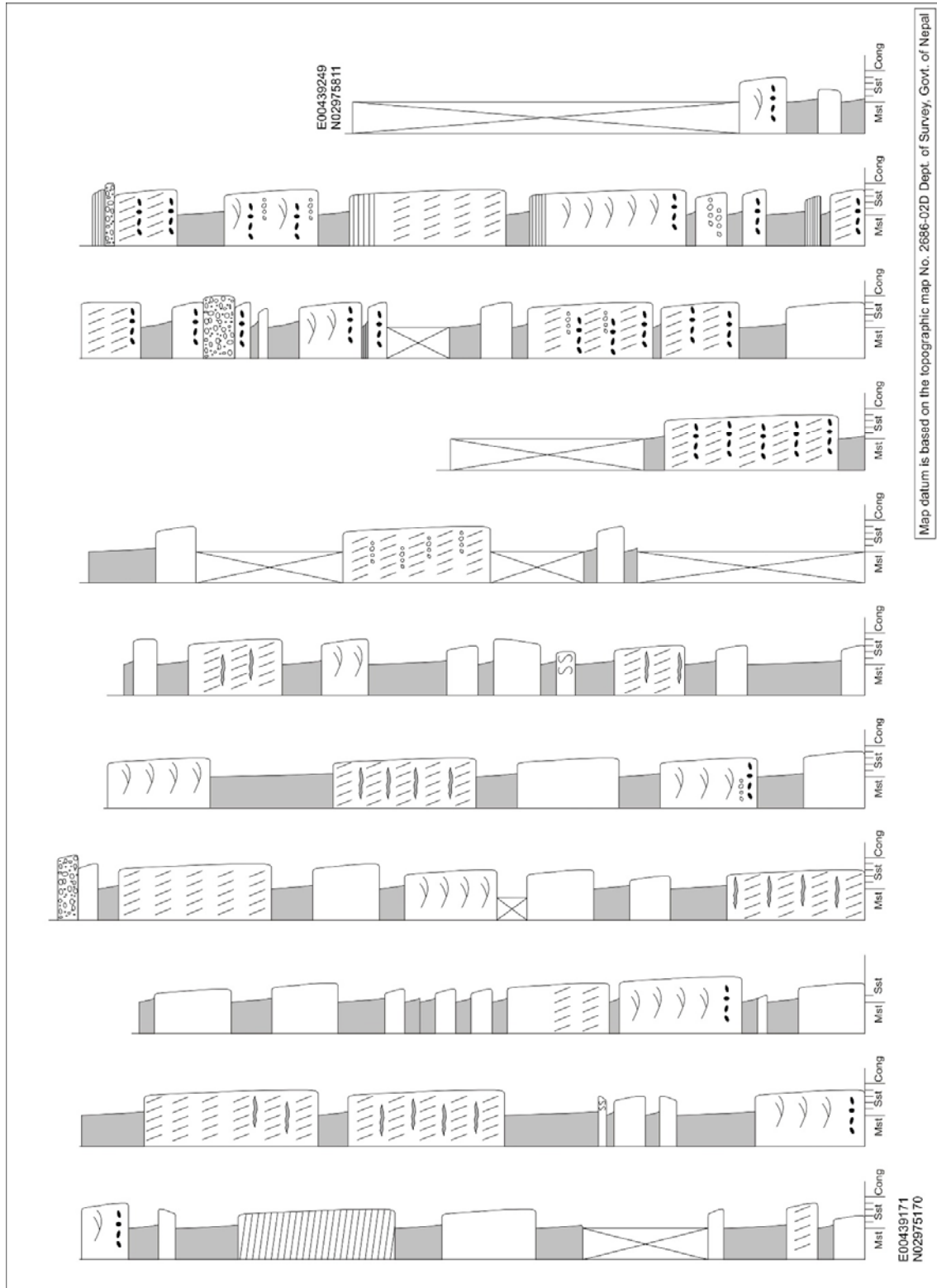


Figure 3.9: Continued



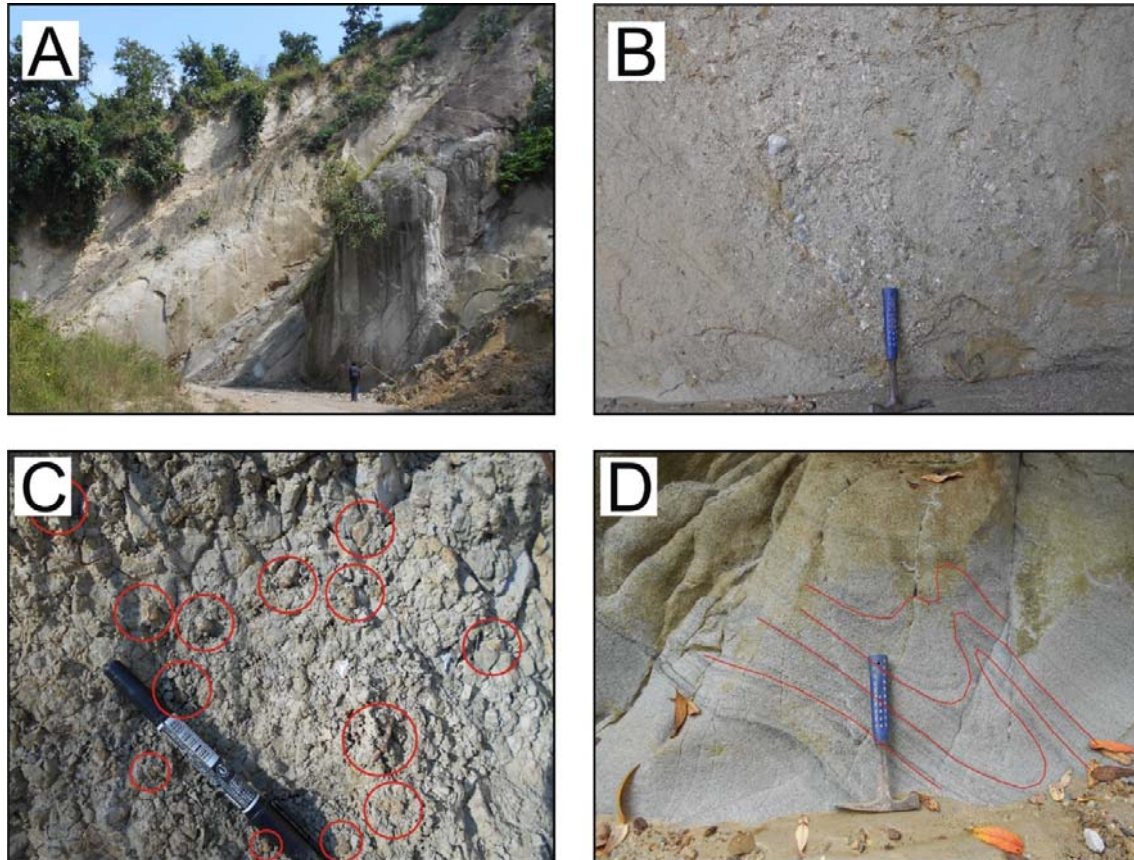


Figure 3.10: Field photographs of A) A typical fining upward sequence observed in very thickly bedded sandstone of the Middle Siwaliks (upper member); B) Pebbly sandstone of the Middle Siwaliks (upper member); C) Calcareous nodules observed in mudstone of the Middle Siwaliks (upper member); D) Convolute lamination observed in the sandstone of the Middle Siwaliks.

### 3.3.3 Upper Siwaliks

This unit is well observed along the Muksar Khola around the upper end of the Magan Village and the Chure dada (local name) (Fig. 3.1). The total thickness of this unit is more than 1000 m (MDT is not accessible along this section) and consists of very thickly-bedded clast supported conglomerate and very thick beds of sandstone and mudstone. The detailed sedimentological log of this unit is presented in Figure 3.11. Conglomerate beds are poorly sorted and consist of pebble to cobble sized clasts and very coarse-grained sand to granules matrix (Fig. 3.12). The clasts are randomly oriented with subrounded to subangular shapes. The clast is dominated by quartzite with few amounts of sandstones, mudstones and purple

meta-sandstones. In the lower section, this conglomerate shows poorly developed parallel cross-stratification whereas in the upper section inverse grading dominates. Sandstones in this unit are very thickly-bedded with coarse to very coarse-grain (1.0-3.0 m). These sandstone beds are mostly massive with occasional parallel cross-stratification (very rare) showing slight fining upward succession. Isolated pebbles in sandstone are abundant, occasionally resembling pebbly sandstones. Mudstones are very thickly-bedded (>4m) and bioturbated with dull yellowish-grey to grey colour (Table: 1). Ojha et al. (2009) paleomagnetic age suggest this unit was deposited after 3.5 Ma (Fig. 3.2).

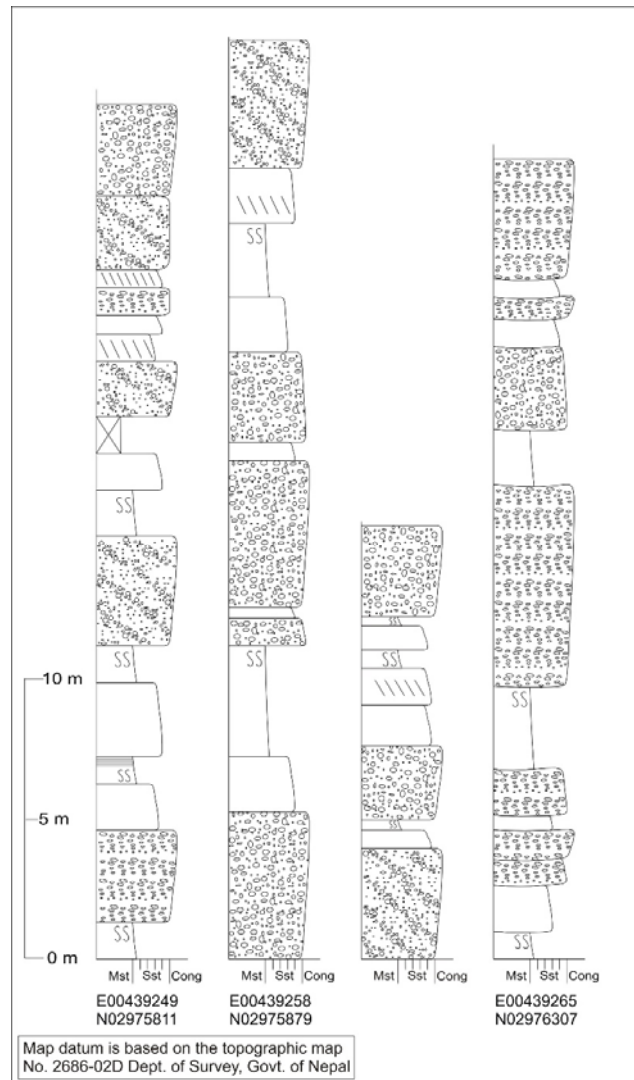


Figure 3.11: Detailed sedimentological column (representative) of the Upper Siwaliks (modified after Rai and Yoshida, 2020).



*Figure 3.12: Conglomerate bed from Upper Siwaliks (left) and close up view of conglomerate (right).*

## CHAPTER IV

### PETROGRAPHY

#### 4.1 Introduction

The character of the sediment provenance and the nature of the sedimentary processes within the depositional basin affects the sandstone composition (Dickinson and Suczek, 1979). Moreover, the variation in the composition of sedimentary rock is also controlled by the tectonic setting (Ingersoll and Suczek 1979, Dickinson 1985). Therefore, minerals occurring in the sedimentary rocks are general guides for the identification of the provenance and tectonic setting of an area. The most commonly used approach in provenance studies is to consider sandstone composition in the context of a tectonic framework. Standard methods for sandstone provenance analysis use modal analysis of detrital framework components (Dickinson and Suczek 1979, Dickinson 1985). Such methods have been used to determine the provenance of the fluvial succession of the Siwalik Group, which is an important repository recording the provenance and tectonic history of the Himalaya (Critelli and Ingersoll 1994). Crook (1974) and Schwab (1975) have observed composition of the sandstone reveals its associated source: quartz-rich rocks are associated with passive continental margins, quartz-poor rocks are associated with the volcanogenic derivation of magmatic island origin and intermediate quartz content are associated mainly with active continental margins or other orogenic belts.

#### 4.2 Methods

Sixteen samples including twelve sandstone and four conglomerate matrix were examined using standard thin-section petrography (denoted by 'M' in Fig. 4.1). Among these, five

samples were from the Lower Siwaliks, seven samples were from the Middle Siwaliks and four samples were from the Upper Siwaliks. The corresponding depositional age of each sample was estimated from preexisting age data of Ojha et al. (2009).

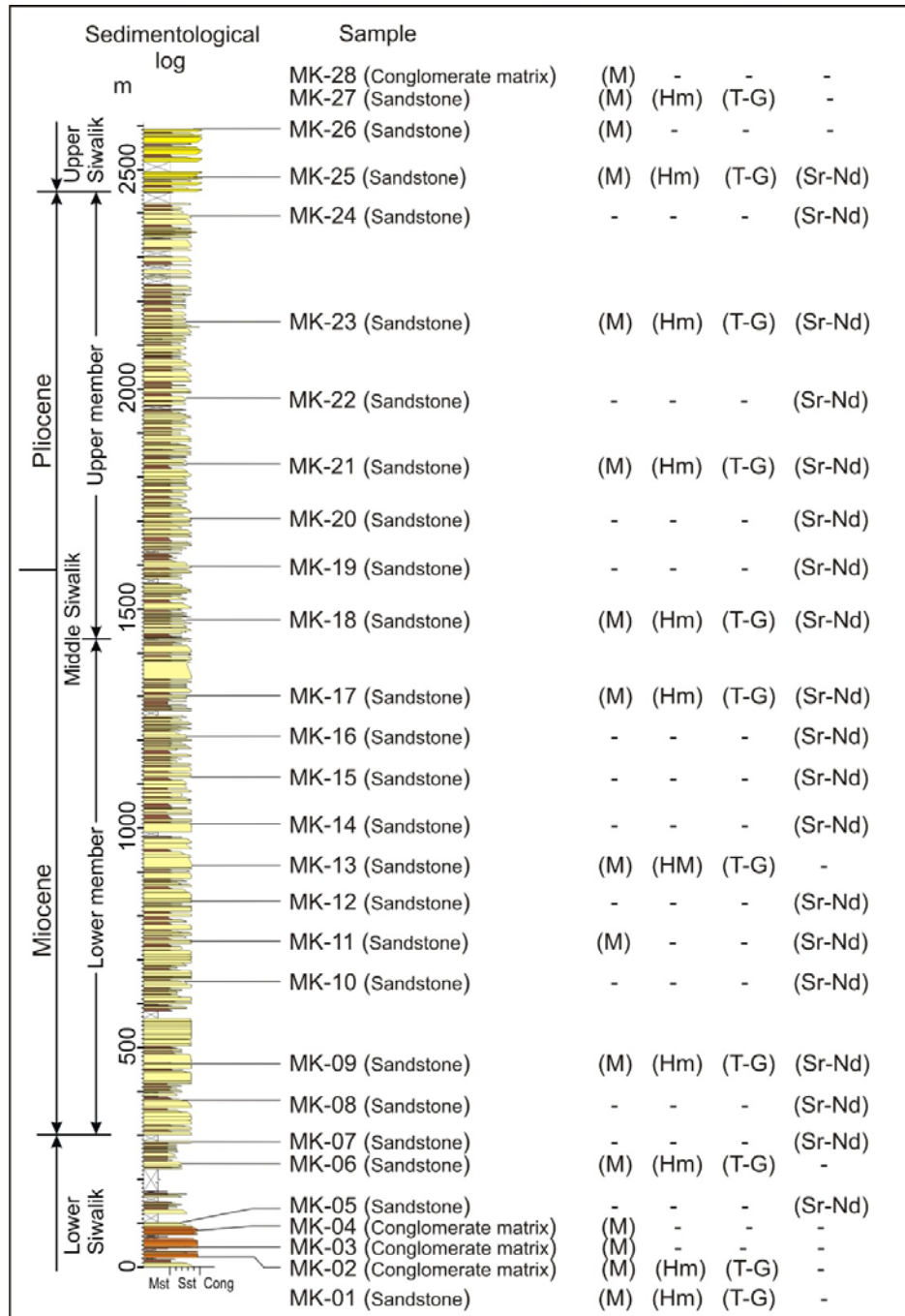


Figure 4.1: Stratigraphic column and the sampling horizons. The examined analysis are shown as (M) sandstone modal composition, (Hm) heavy mineral analysis, (T) detrital tourmaline geochemistry, (G) detrital garnet geochemistry and (Sr-Nd) isotopic analysis. Sample MK-01, MK-27 and MK-28 are collected beyond the presented sedimentological log (modified after Rai et al., 2021).

Point counting was carried out to identify individual grain or crystals larger than 0.0625 mm. A total of 500 points in each sample was counted for modal analysis using the Gazzi-Dickinson method (Ingersoll and Suczek, 1979; Dickinson, 1985). The grid spacing used in the point counting was maintained to exceed the grain size so that the individual grains were not counted more than once. The main categories of grains identified included monocrystalline quartz (Qm), polycrystalline quartz (Qp), plagioclase (P), K-feldspar (K), sedimentary lithics (Ls), metamorphic lithics (Lm) and volcanic lithics (Lv). Besides micas, chlorite, dolomite and heavy minerals were also included in point counts.

### **4.3 Results**

The results of point counting are summarized in Table 4.1. Conglomerate matrix from the Lower Siwaliks are rich in carbonate cement (up to 43%) with very less matrix (<4%) (Fig. 4.2-A). The sandstone from the Lower Siwaliks is considerably rich in both carbonate cement and matrix (Fig. 4.2-B). The sandstones from the Middle Siwaliks are poorly consolidated and readily disintegrated into the sand, therefore, lacking proper information regarding cement and matrix. Though few samples from the lower section of the Middle Siwaliks shows an increase in the proportion of matrix (up to 14%) and a decrease in the proportion of carbonate cement (<6%) compared to the Lower Siwaliks (Fig. 4.2-C).

Framework grains mostly contains quartz, feldspar, and lithic grains. Dominating grains are monocrystalline quartz, with very low feldspar grains in all samples. Lithic fragments contain sedimentary, metamorphic as well as volcanic lithic grains. Metamorphic lithic grains (phyllite, schist, gneiss) are considerably abundant in all samples (Fig. 4.2-D), whereas sedimentary lithic grains (mudstone) mainly dominate in the samples from the Lower Siwaliks and the lower member of the Middle Siwaliks. Some sample (MK-13) shows shared texture in these sedimentary lithic grains (Fig. 4.2-D). Similarly, volcanic lithic grains

(andesite, basalt, tuff, glassy volcanic rock) are also considerably observed in the samples of the Lower Siwaliks and the lower member of the Middle Siwaliks (Fig. 4.2-D).

Table 4.1: Modal composition of the Siwalik Group sandstones from the Muksar Khola section. Qm: Monocrystalline quartz, Qp: Polycrystalline quartz, Pl: Plagioclase, Kf: K-feldspar, Ls: Sedimentary lithics, Lm: Metamorphic lithics, Lv: Volcanic lithics, Qt: Total quartz grains (Qm+Qp), F: Total feldspar grains (Pl+Kf), L: Lithic fragments (Ls+Lm+Lv), Lt: Total lithic fragments (L+Qp) (modified after Rai et al., 2021).

Litho units	Lower Siwalik Group					Middle Siwalik Group						Upper Siwalik Group				
	MK-01	MK-02	Mk-03	MK-04	MK-06	MK-09	MK-11	MK-13	MK-17	MK-18	MM-21	MK-23	MK-25	MK-26	MK-27	MK-28
Sample No.	Sst.	Cong.	Cong.	Cong.	Sst.	Sst.	Sst.	Sst.	Sst.	Sst.	Sst.	Sst.	Sst.	Sst.	Sst.	Cong.
Grain size	M	C	C	C	M	M	M	C	C	M	M	M	C	C	M	C
Age		10.5	10.5	10.5	10	9.4	8.3	7.7	6.5	5.7	4.4	4	3.4			
Qm	420	356	360	312	391	379	413	216	394	439	439	407	413	405	408	411
Qp	52	58	64	98	62	32	44	108	54	21	26	36	32	60	52	39
Pl	5	4	0	1	10	14	10	7	7	3	2	2	3	0	1	2
Kf	2	4	3	1	6	0	1	14	5	2	4	2	2	1	0	2
Ls	1	29	45	48	6	8	0	41	0	0	0	0	1	0	0	3
Lm	20	37	27	32	23	61	28	78	37	33	29	52	49	34	39	42
Lv	0	12	1	8	2	6	4	36	3	2	0	1	0	0	0	1
Sub-total	500	500	500	500	500	500	500	500	500	500	500	500	500	500	500	500
Cement	-	402	184	116	173	-	-	37	-	-	-	-	-	-	-	-
Matrix	-	21	27	18	117	-	64	86	38	-	-	-	-	-	-	-
Heavy minerals	5	3	9	3	5	6	2	1	5	7	7	7	5	2	4	8
Mica	78	3	9	1	38	2	101	52	37	7	3	6	15	11	24	15
Chlorite	-	1	2	-	1	1	10	-	2	13	-	1	-	-	-	-
Carbonate grains	-	1	8	4	3	1	-	2	-	-	-	-	-	-	-	-
Sub-total	83	431	239	142	337	10	177	178	82	27	10	14	20	13	28	23
Total	583	931	739	642	837	510	677	678	582	527	510	514	520	513	528	523
Qt/QtFL	0.94	0.83	0.85	0.82	0.91	0.82	0.91	0.65	0.90	0.92	0.93	0.89	0.89	0.93	0.92	0.90
F/QtFL	0.01	0.02	0.01	0.00	0.03	0.03	0.02	0.04	0.02	0.01	0.01	0.01	0.01	0.00	0.00	0.01
L/QtFL	0.04	0.16	0.15	0.18	0.06	0.15	0.06	0.31	0.08	0.07	0.06	0.11	0.10	0.07	0.08	0.09
Qm/QmFLt	0.84	0.71	0.72	0.62	0.78	0.76	0.83	0.43	0.79	0.88	0.88	0.81	0.83	0.81	0.82	0.82
F/QmFLt	0.01	0.02	0.01	0.00	0.03	0.03	0.02	0.04	0.02	0.01	0.01	0.01	0.01	0.00	0.00	0.01
Lt/QmFLt	0.15	0.27	0.27	0.37	0.19	0.21	0.15	0.53	0.19	0.11	0.11	0.18	0.16	0.19	0.18	0.17

Sst.: Sample from sandstone; Cong.: Sample from conglomerate matrix; M: Medium grained; C: Coarse grained.

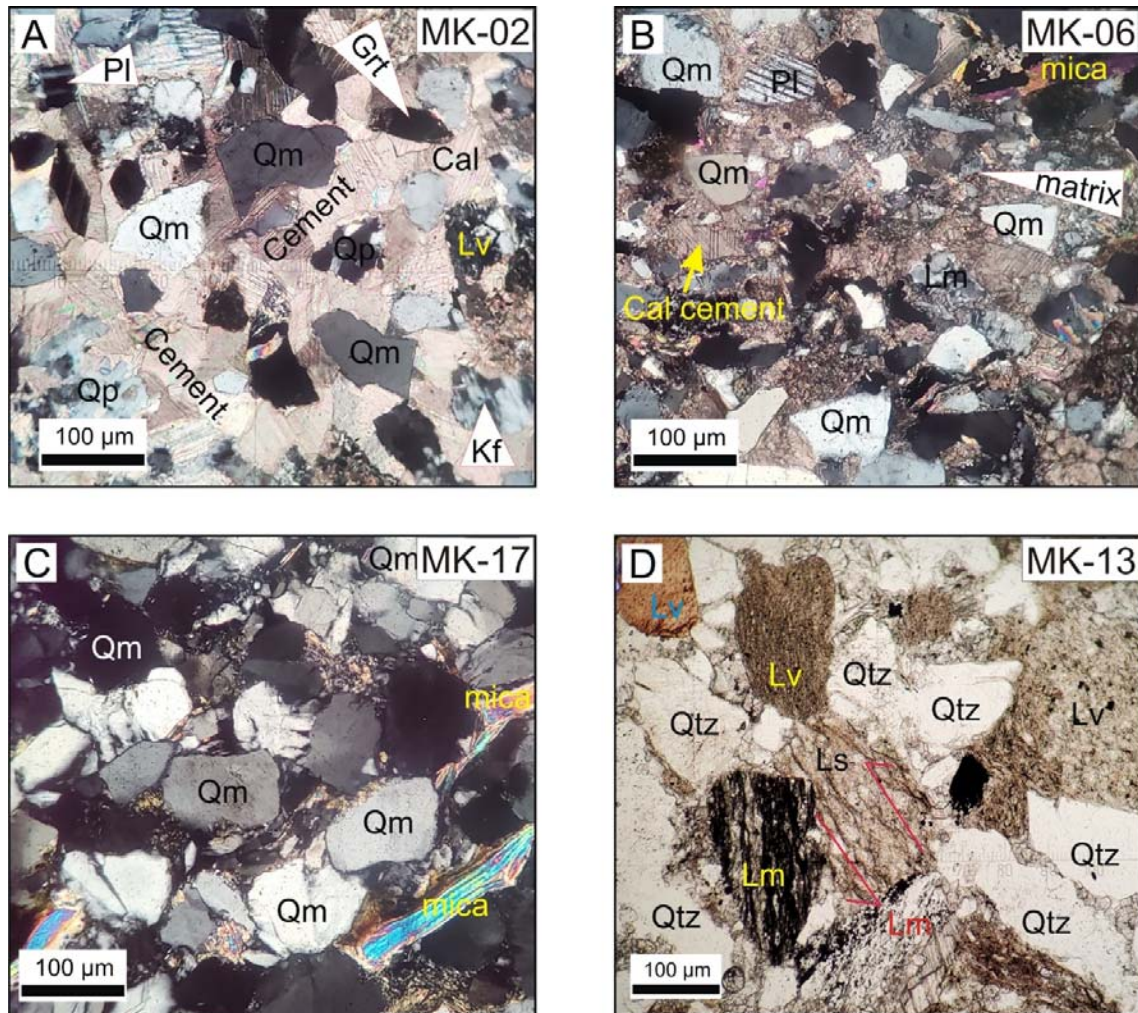


Figure 4.2: Photomicrographs of the sandstone. A: Matrix of the intraformational conglomerate of the Lower Siwaliks (UCN), B: Sandstone of the Lower Siwaliks (UCN), C) Sandstone of the lower member of the Middle Siwaliks (UCN), D) sheared mudstone in the sandstone of the lower member of the Middle Siwaliks (UPPL) (After Rai et al., 2021). Abbreviations: Qm: Monocrystalline quartz, Qp: Polycrystalline quartz, Pl: Plagioclase feldspar, Kf: K-feldspar, Ls: Sedimentary lithics, Lm: Metamorphic lithics, Lv: Volcanic lithics, Cal cement: Calcium carbonate cement.

#### 4.4 Classification of Sandstone

According to the classification scheme of the Pettijohn et al. (1987), most of the samples are sub-litharenite with one sample each from the Lower Siwaliks and the Middle Siwaliks is arenite and lithic arenite respectively (Fig. 4.3-A). The same result is observed in the Folk (1980) classification scheme (Fig. 4.3-B).



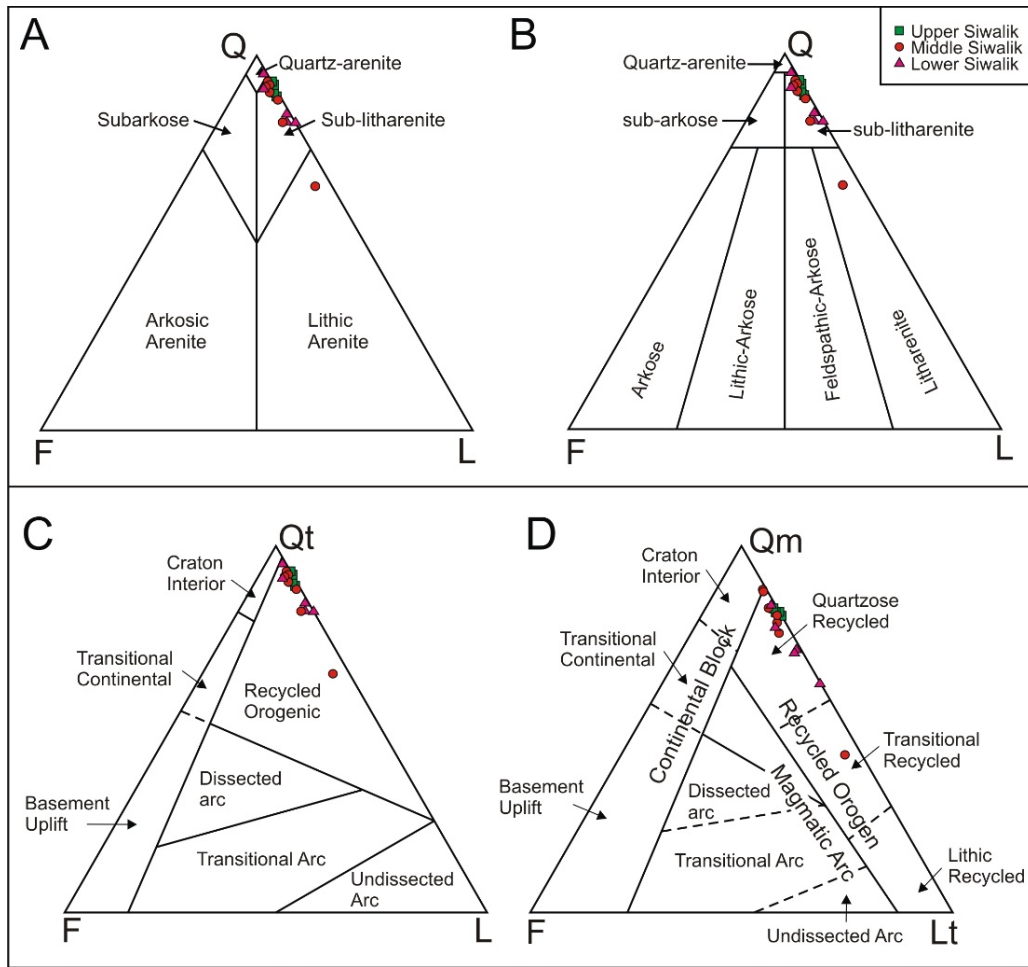


Figure 4.3: Classification of the sandstone. A) Ternary diagram based on schemes proposed by Pettijohn et al. (1987); B) Ternary diagram based on schemes proposed by Folk (1980); C) Qt-F-L and D) Qm-F-Lt Ternary diagram for the framework modes of the sandstone, showing the different provenance fields defined by Dickinson (1985) (After Rai et al., 2021). Abbreviations as in Table. 4.1. Qt; Total quartz grains ( $Q_m + Q_p$ ), F: Total feldspar grains ( $P_l + K_f$ ), L: Lithic fragments ( $L_s + L_m + L_v$ ), Lt: Total lithic fragments ( $L + Q_p$ ).

#### 4.5 Probable source rock

The Qt-F-L and Qm-F-Lt ternary diagrams of Dickinson (1985) suggests a recycled orogenic provenance (Fig. 4.3-C and D). This result is similar to the previously published results from different Siwalik successions (Garzanti et al., 1996; Tamrakar et al., 2003; Sigdel and Sakai, 2013). The occurrence of sedimentary lithic grains in the older succession with an increase in metamorphic grains towards the younger successions observed in the present study is similar to the previous result of Chirouze et al. (2012a). In the present study abundant metamorphic

grains like schist and gneiss (Fig. 4.2-D) reveal the MCT zone and the HHC as the source areas. Comparatively decrease in the feldspar content after 6.5 Ma (Fig. 4.4), indicates an increased supply of the LHS sediments. The occurrence of both the volcanic lithic grains and carbonate in the samples of the Lower Siwaliks indicates sediments contribution from TTH around the late Miocene. Moreover, volcanic rocks like andesite are characteristic of the island arc (Kemner et al., 2015). Mudstone fragments with shared texture in the lower member of the Middle Siwaliks sample are quite interesting, such unmetamorphosed mudstone showing shared texture are related to the thrusting in an accretionary complex (Ishiga and Ishiyama, 1987; Yamamoto et al., 2005; Raymond and Bero, 2015).

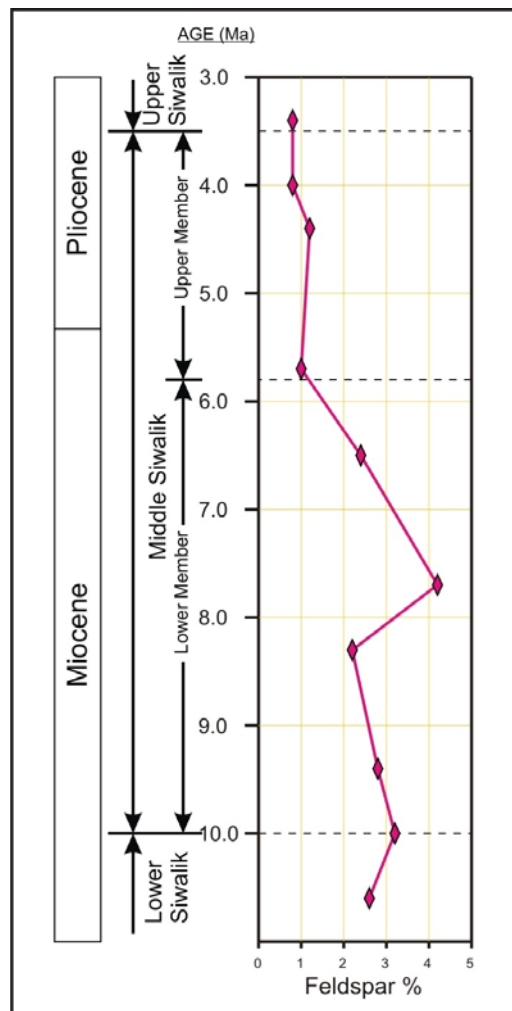


Figure 4.4: Vertical variation of feldspar content in the sandstone. Depositional ages of samples are based on preexisting age data of the Ojha et al. (2009).

## CHAPTER V

### HEAVY MINERAL ANALYSIS

#### 5.1 Introduction

Minerals having a density of more than 2.89 are designated as heavy minerals and both opaque and non-opaque minerals are found in nature. Heavy minerals have specific and restricted parageneses, these properties provide very useful information regarding the provenance and the nature of the source rock (Morton and Hallsworth, 1994; 1999; Garzanti et al., 2007; Yoshida et al., 2019). Therefore, heavy mineral analysis is one of the most sensitive and widely used techniques in the determination of the provenance of clastic deposits. The study of heavy minerals is particularly useful in studies of sedimentation related to the tectonic uplift of orogenic belts, as the evolution and unroofing episodes are reflected in their foreland sediments (Mange and Maurer, 1992). However, the composition of heavy mineral assemblages is modified by several other processes like physical sorting, mechanical abrasion and dissolution during the sedimentation cycle (Morton, 1984; Morton and Hallsworth, 1999). Though the original provenance signal of the heavy mineral is modified and do not solely reflect the composition of the parent rocks, still they bear the little resemblance of source rocks.

The geology of the Himalayan range is exposed in a linear fashion east to west. Each sequence of the Himalaya has a distinctive rock type and parageneses. Therefore, not all but some heavy minerals show characteristic relation to the distinct Himalayan sequence. The interplay between tectonics and climate give rise to the uplift of the Himalaya and its denudation. These denudated sediments were deposited in the Miocene-early Pleistocene foreland basin presently known as the Siwalik Group. The heavy mineral assemblage of the sandstone from the Siwalik Group can therefore be traced with the corresponding rock units

of the Himalaya. Further, it reveals the Eocene exhumation and denudation history of the Himalayas.

## **5.2 Methods**

For heavy minerals analysis, eleven samples were considered (denoted by 'Hm' in Fig. 4.1). Three samples were considered from the Lower Siwaliks, six from the Middle Siwaliks and two from the Upper Siwaliks. The heavy mineral grains were separated using a heavy liquid (sodium polytungstate) and glued onto a glass slide with epoxy resin. All thin sections were polished and carbon-coated for the EDS analysis. Firstly, representative six samples from the Lower Siwaliks and the Middle Siwaliks were identified under the petrographic microscope using the point-counting method (Table 5.1). The grid spacing used in the point counting was maintained to exceed the grain size so that the individual grains were not counted more than once. After that heavy minerals were identified using the microprobe analyzer (JEOL-5033) at the Faculty of Science, Shinshu University, Japan. Operating conditions included an acceleration voltage of 15 kV, probe current of 20 nA, a counting time of 60 s per grains, and a beam diameter of 15  $\mu\text{m}$ .

## **5.3 Results**

The non-opaque heavy minerals assemblage from the sandstones of the present study are summarized in Tables 5.1 and 5.2. Table 5.1 includes the result of point counting under the petrographic microscope. Recognized heavy minerals are apatite, zircon, tourmaline, rutile, garnet, titanite, amphibole, staurolite, epidote, zoisite, clinozoisite, sillimanite, kyanite, scapolite and spinel (Fig 5.1). Table 5.2 includes the heavy minerals recognized under the microprobe analyzer. These heavy minerals are recognized as apatite, zircon, tourmaline,

rutile, garnet, titanite, amphibole, staurolite, epidote, zoisite, kyanite, cordierite, chromian-spinel, clino-pyroxene, arenite, ilmenite, and pyrite (Fig. 5.2). Point-counting under the petrographic microscope shows abundant zircon, tourmaline, and garnet in all samples and a drastic difference in the heavy mineral assemblage between the samples of the Lower Siwaliks and the Middle Siwaliks (Fig. 5.1). The proportion of tourmaline and garnet decreases in the samples of the Middle Siwaliks with an increase in amphibole, staurolite, zoisite and kyanite (Fig. 5.1)

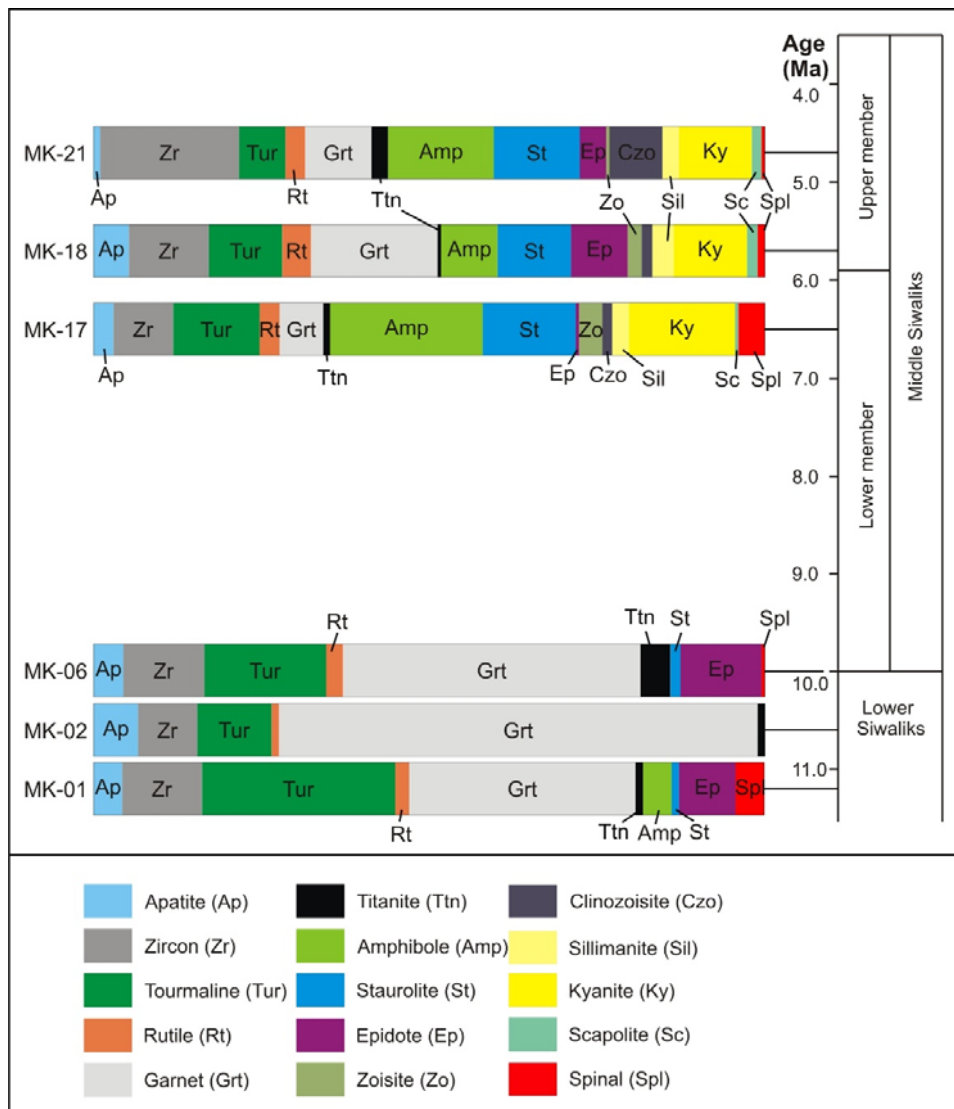


Figure 5.1: Heavy mineral assemblage in the present study area identified under a petrographic microscope (point count). Depositional ages of samples are based on preexisting age data of the Ojha et al. (2009).

Results from the EDS analysis shows abundant tourmaline and Garnet among heavy minerals. Heavy minerals like zircon, tourmaline, rutile (ZTR), garnet and ilmenite doesn't show a distinctive change in their occurrence concerning the succession age. Heavy minerals like apatite, titanite, cordierite, chromian-spinal, allanite and pyrite show a decreasing trend whereas, epidote, amphibole, staurolite, zoisite, Al-silicate (sillimanite+kyanite) and clinopyroxene show the increasing trend towards the younger succession.

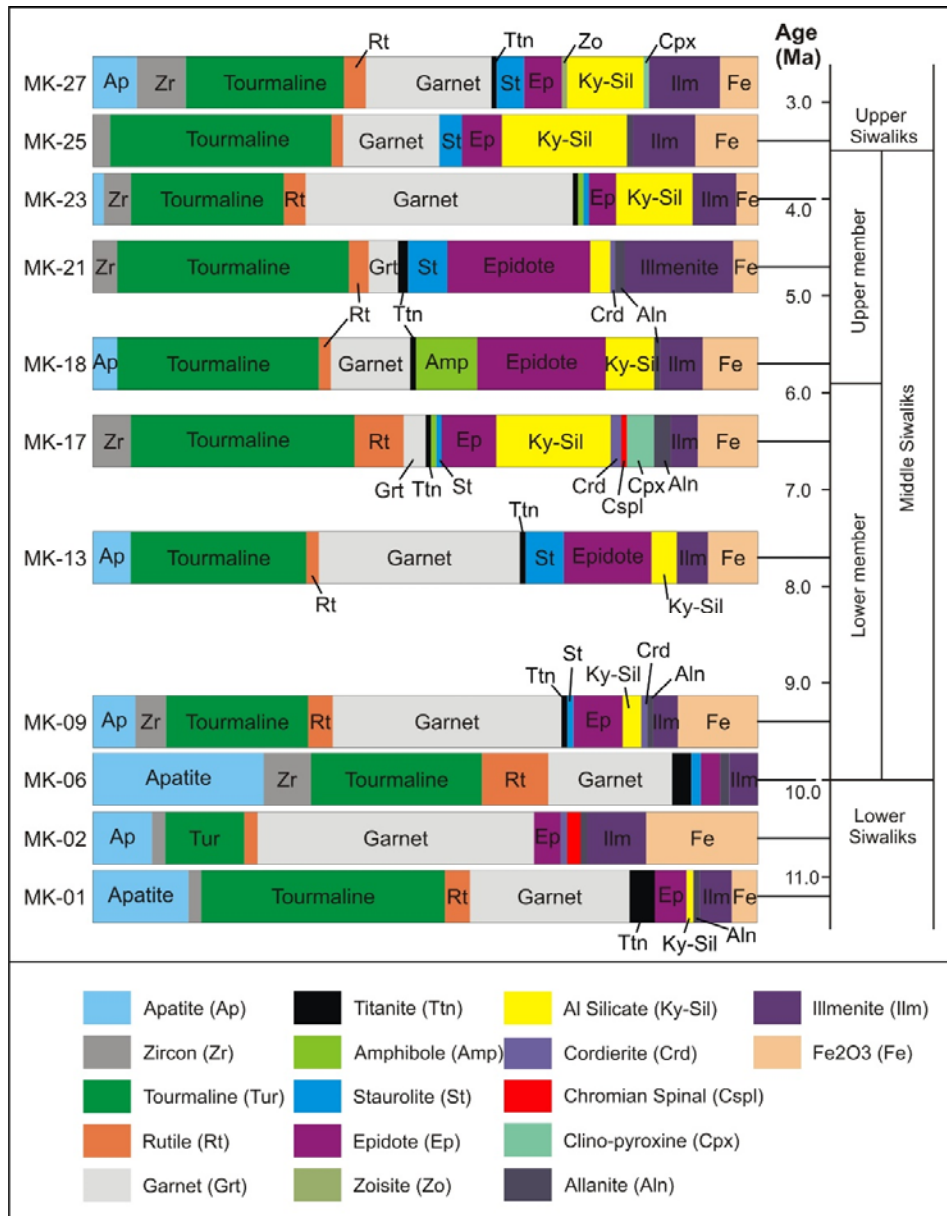


Figure 5.2: Heavy mineral assemblage in the present study area identified under EDS (modified after Rai et al., 2021). Depositional ages of samples are based on preexisting age data of the Ojha et al. (2009).

Table 5.1: Heavy mineral assemblage of the Siwalik Group sandstones from the Muksar Khola section identified under a petrographic microscope (point count).

Litho units	Sample No	Age	Apatite	Zircon	Tourmaline	Rutile	Garnet	Titanite	Amphibole	Staurolite	Epidote	Zoisite	Clinozoisite	Sillimanite	Kyanite	Scapolite	Spinal	Total
Middle Siwaliks	MK-21	4.7	2	41	14	6	20	5	31	25	8	1	16	5	22	3	1	200
	MK-18	5.7	10	23	20	8	35	1	16	21	16	4	3	6	20	3	2	188
	MK-17	6.5	6	18	26	6	13	2	45	28	1	7	3	5	31	1	8	200
Lower Siwaliks	MK-06	10.0	9	25	37	5	89	9	0	3	25	0	0	0	0	0	1	203
	MK-02	10.6	6	8	10	1	65	1	0	0	0	0	0	0	0	0	0	91
	MK-01	-	4	11	27	2	32	1	4	1	8	0	0	0	0	0	4	94

Table 5.2: Heavy mineral assemblage of the Siwalik Group sandstones from the Muksar Khola section identified under EDS (modified after Rai et al., 2021).

Litho units	Sample No	Age (Ma)	Apatite	Zircon	Tourmaline	Rutile	Garnet	Titanite	Amphibole	Staurolite	Epidote	Zoisite	Al-Silicate	Cordierite	Spinal	Clino-pyroxine	Allanite	Ilmenite	Fe oxide	Total
Upper Siwaliks	MK-28	-	8	9	29	4	23	1	0	5	7	1	14	0	0	1	0	13	7	122
	MK-25	3.4	0	3	39	2	17	0	0	4	7	0	22	0	0	0	1	11	11	117
Middle Siwaliks	MK-23	4.00	2	5	28	4	49	1	1	1	5	0	14	0	0	0	0	8	4	122
	MK-21	4.7	0	5	47	4	6	2	0	8	29	0	4	1	0	0	2	22	5	135
	MK-18	5.7	4	0	33	2	13	1	10	0	21	0	8	0	0	0	1	7	9	109
	MK-17	6.5	0	7	41	9	4	1	1	1	10	0	21	2	1	5	3	5	11	122
	MK-13	7.7	6	0	28	2	32	1	0	6	14	0	4	0	0	0	0	5	8	106
	MK-09	9.4	7	5	23	4	37	1	0	1	8	0	3	1	0	0	1	4	13	108
Lower Siwaliks	MK-06	10.0	18	5	18	7	13	2	0	1	2	0	0	0	0	0	1	3	0	70
	MK-02	10.6	9	2	12	2	42	0	0	0	4	0	0	1	2	0	1	9	17	101
	MK-01	-	15	2	38	4	25	4	0	0	5	0	1	0	0	0	1	5	4	104

#### 5.4 Difference in heavy mineral assemblage under petrographic microscope and EDS

The present study shows a difference between the heavy mineral assemblage identified under the petrographic microscope and microprobe analyzer (Figs. 5.1; 5.2). This observed difference should result from the difference in the process of mineral identification. Since, the EDS analysis measures the composition of the minerals (Ruiz-Vargas et al., 2014), it encounters a problem to identify different polymorphs (such as kyanite and sillimanite). But, since it uses a focused electron beam which is bombarded to the specimen, it has a very high resolution (Miller et al., 2009; Zhao et al., 2015). Therefore, under EDS small mineral

fragments can be identified which are otherwise very hard to identify under the petrographic microscope. In this study, more importance is given to the heavy minerals assemblages identified under EDS for the determination of the provenance and related discussion.

### **5.5 Probable source rock**

Heavy minerals provide useful information regarding the provenance and source rocks (Morton and Hallsworth, 1994; Garzanti et al., 2007). In the present study, most of the heavy minerals identified can be traced to the high-grade metamorphic rocks of the HHC (Schelling, 1992; Kaneko, 1995; Yoneshiro and Kizaki, 1996; Searle et al., 2003; Imayama et al., 2010; Streule et al., 2010; Dhital, 2015). The occurrence of amphibole is very sparse in the eastern Nepal Himalayan parent rocks, they are usually found in the HHC and MCT zone (Schelling, 1992; Searle et al., 2003; Imayama et al., 2010). In contrast, amphibolite is reported in LHS by some researchers (Paudel and Arita, 2002; Rai et al., 2016) suggesting LHS as the possible source of amphibole. Staurolite is characteristic of the upper part of the LHS around the MCT and Khare-Phyllite (Yoneshiro and Kizaki, 1996; Arita, 1983; Schelling, 1992; Imayama et al., 2010). Epidote is characteristic of the Rp, a shallow part of the HHC (Searle et al., 2003) and the Khare Phyllite (Schelling, 1992; Searle et al., 2003). Detrital zoisite observed in the Upper Siwaliks is limited to the LHS (Schelling, 1992; Searle et al., 2003; Garzanti et al., 2007; Imayama et al., 2010). Similarly, kyanite+sillimanite is reported in the Mahabharat Crystalline and Jp, a deeper part of the HHC (Schelling, 1992; Imayama et al., 2010; Rai et al., 2016). Various research points TTH as the source of titanite and high ZTR index (Garzanti et al., 2007, Nakajima et al., 2020b) and chromian-spinel suggests ophiolites of the ITSZ (Radhakrishna et al., 1987; Garzanti et al., 2005).



CHAPTER VI

**CHEMICAL COMPOSITION OF  
DETRITAL TOURMALINE AND GARNET**

**6.1 Introduction**

Heavy minerals like tourmaline and garnets are very resistant in clastic sedimentary environments and are strong tools for the provenance study (Henry and Dutrow, 1992; Morton, 1985). Therefore, the chemical composition of the detrital garnet and tourmaline is very useful for tracking the provenance of sediments (Nishio and Yoshida, 2014). The abundant occurrence of detrital tourmaline and garnet in all the samples of the present study (Fig. 5.1) is therefore used to determine the source rock and its denudation time.

Tourmaline is a common accessory mineral found in many rock types and terrains, it develops virtually in all grades of metamorphic rocks and granitoid intrusive rocks and their associated aplites, pegmatites and hydrothermal aureoles (Henry and Guidotti, 1985) which proves it as a useful provenance indicator. The occurrence of tourmaline is very wide in Himalayan rocks, it is found in almost all the formations of the LHS to the TTH and granites and the aplite pegmatitic veins (Rai, 2004). Similarly, garnets also exist in a wide range of rocks, they are common in metamorphic rocks but are also found in granites and pegmatites, peridotites (Suggate and Hall, 2014). Its chemical composition depends on the composition of the source rocks and pressure and temperature conditions during its formation (Wright, 1938; Morton, 1985; Deer et al., 1992). In Himalaya garnet from different complexes show a variation in the chemical composition of its endmember (Arita, 1983; Neogi et al., 1998; Imayama et al., 2010; Saha, 2013). In this study, the chemical composition of detrital tourmaline and garnet are calculated to reveal the provenance of the Siwalik sediments.

## 6.2 Methods

For chemical analysis of detrital tourmaline and garnet, ten samples were considered (denoted by ‘T-G’ in Fig. 4.1). The heavy mineral grains were separated using a heavy liquid (sodium polytungstate) and glued onto a glass slide with epoxy resin. All thin sections were polished and carbon-coated. Chemical analysis of the detrital garnet and tourmaline grains were analyzed with an EDS (JEOL-5033) microprobe analyzer at the Faculty of Science, Shinshu University, Japan. Operating conditions included an acceleration voltage of 15 kV, probe current of 20 nA, a counting time of 60 s per grains, and a beam diameter of 15  $\mu\text{m}$ . All analyses were performed at the core of the grains.

## 6.3 Results

### 6.1.1 Chemical composition of detrital Tourmaline

Under a petrographic microscope (UPPL) colour of the detrital tourmalines widely varies from yellow, yellowish-green and dark green and are mostly euhedral in shape (Fig. 6.1-A & B). The chemical composition of each sample is plotted in the Al–Fe–Mg–Ca discrimination diagrams of Henry and Guidotti (1985) (Fig. 6.2). Representative analysis of the detrital tourmaline is summarized in Table 6.1.

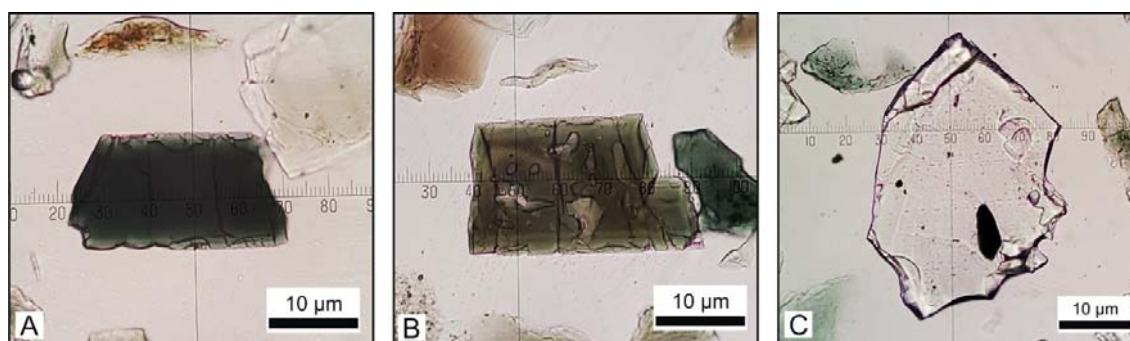


Figure 6.1: Photomicrographs (UPPL). A) Detrital dark green tourmaline, B) Detrital yellowish green tourmaline (after Rai et al., 2021), C) Detrital garnet with inclusion (after Rai et al., 2021).

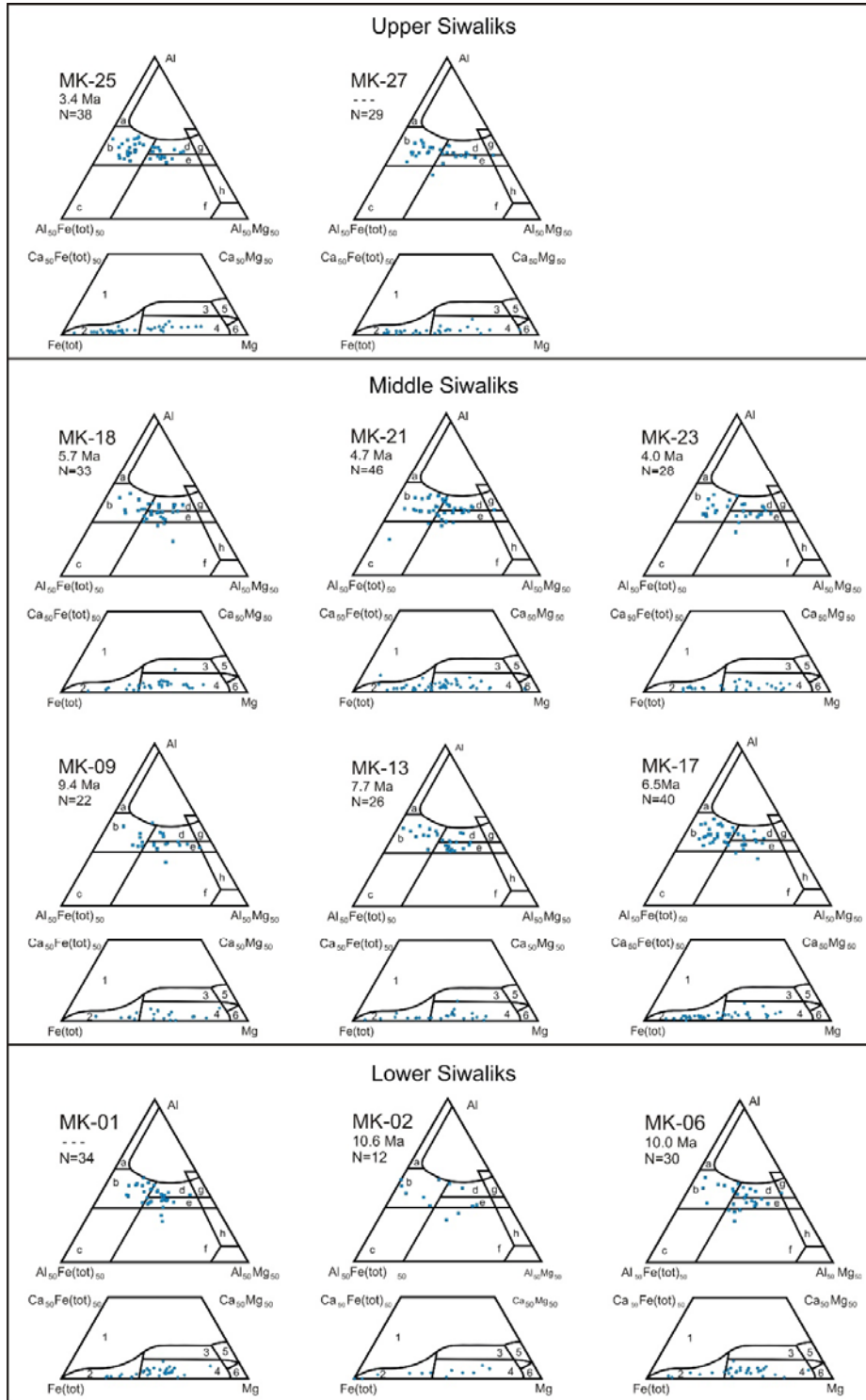


Figure 6.2: Detrital tourmaline composition plotted on Al-Fe-Mg and Ca-Fe-Mg diagrams. Discrimination fields for various rock types according to Henry and Guidotti (1985) are as follows: (a) Li-rich granitoids, pegmatites, and aplites; (b) Li-poor granitoids, pegmatites, and aplites; (c) hydrothermally altered granitic rocks; (d) aluminous pelrites and psammites; (e) Al-poor pelrites and psammites; (f) Fe<sup>3+</sup>-rich quartz-tourmaline rocks; (g) Low-Ca meta-ultramafics; (h) metacarbonates and metapyroxenites; (1) Li-rich granitoids, pegmatites, and aplites; (2) Li-poor granitoids, pegmatites, and aplites; (3) Ca-rich pelrites, psammites, and calc-silicates; (4) Ca-poor pelrites, psammites, and quartz-tourmaline rocks; (5) metacarbonates; (6) meta-ultramafic rocks. Depositional ages of samples are based on preexisting age data of the Ojha et al. (2009).

Table 6.1: Chemical composition of detrital tourmaline grains from the Siwalik Group sandstones of the Muksar Khola section.

Litho units	Lower Siwaliks			Middle Siwaliks						Upper Siwaliks	
Sample No.	MK-01	MK-02	MK-06	MK-09	MK-13	MK-17	MK-18	MK-21	MK-23	MK-25	MK-27
Memo	258	123	72	148	356	58	88	104	60	22	58
SiO <sub>2</sub>	35.92	34	34.81	34.05	36.14	34.25	35.59	35.04	34.56	34.91	34.26
TiO <sub>2</sub>	0.61	0.89	0.21	0.46	0.72	0.49	0.37	1.19	0.67	0.72	0.96
Al <sub>2</sub> O <sub>3</sub>	32.78	32.74	32.21	33.93	30.8	31.99	31.75	31.84	32.03	33.47	30.09
Cr <sub>2</sub> O <sub>3</sub>	0.00	0.01	0.00	0.07	0.09	0.09	0.04	0.11	0.02	0.02	0.05
FeO*	8.61	7.8	14.57	13.48	7.15	12.63	10.86	8.69	14.27	10.92	14.35
MnO	0.01	0.02	0.07	0.12	0	0.3	0.11	0.24	0.26	0.22	0.23
MgO	6.36	4.75	1.26	1.6	7.53	3.32	4.31	5.08	2.39	2.82	2.34
CaO	0.98	0.7	0.09	0.38	0.84	0.26	0.2	0.79	0.43	0.32	0.38
Na <sub>2</sub> O	1.83	1.69	1.89	1.9	2.18	2.24	2.51	2.03	2.36	1.89	2.42
K <sub>2</sub> O	0.04	0.04	0.08	0.08	0.02	0.05	0.01	0.09	0.07	0.07	0.06
<b>Total</b>	<b>87.14</b>	<b>82.64</b>	<b>85.19</b>	<b>86.07</b>	<b>85.47</b>	<b>85.62</b>	<b>85.75</b>	<b>85.10</b>	<b>87.06</b>	<b>85.36</b>	<b>85.14</b>
Si	5.88	5.87	6.00	5.79	6.01	5.83	6.00	5.93	5.85	5.92	5.96
Ti	0.08	0.12	0.03	0.06	0.09	0.06	0.05	0.15	0.09	0.09	0.13
Al	6.32	6.66	6.54	6.80	6.03	6.42	6.31	6.35	6.40	6.69	6.17
Cr	0.00	0.00	0.00	0.01	0.01	0.01	0.01	0.01	0.00	0.00	0.01
Fe	1.18	1.13	2.10	1.92	0.99	1.80	1.53	1.23	2.02	1.55	2.09
Mn	0.00	0.00	0.01	0.02	0.00	0.04	0.02	0.03	0.04	0.03	0.03
Mg	1.55	1.22	0.32	0.41	1.86	0.84	1.08	1.28	0.60	0.71	0.61
<b>Total</b>	<b>15.00</b>	<b>15.00</b>	<b>15.00</b>	<b>15.00</b>	<b>15.00</b>	<b>15.00</b>	<b>15.00</b>	<b>15.00</b>	<b>15.00</b>	<b>15.00</b>	<b>15.00</b>
Ca	0.17	0.13	0.02	0.07	0.15	0.05	0.04	0.14	0.08	0.06	0.07
Na	0.58	0.57	0.63	0.63	0.70	0.74	0.82	0.67	0.78	0.62	0.82
K	0.01	0.01	0.02	0.02	0.00	0.01	0.00	0.02	0.02	0.02	0.01
B*	3.00	3.00	3.00	3.00	3.00	3.00	3.00	3.00	3.00	3.00	3.00
<b>Total</b>	<b>18.76</b>	<b>18.70</b>	<b>18.67</b>	<b>18.71</b>	<b>18.86</b>	<b>18.80</b>	<b>18.86</b>	<b>18.83</b>	<b>18.87</b>	<b>18.69</b>	<b>18.90</b>

LS: Lower Siwaliks; MS: Middle Siwaliks; US: Upper Siwaliks, FeO\* is total. B\* is assuming 3 p.f.u.

The EDS analysis of the detrital tourmaline does not show much variation in the composition throughout the succession (Fig. 6.2). In the Al–Fe–Mg diagram most of the tourmaline grains are clustered within the magmatic source (granitoids and associated pegmatites) and meta-sedimentary source (Al-rich and Al-poor metapelites and metapsammites). A similar plot is observed in the Ca–Fe–Mg diagram, showing magmatic (Li-poor granitoids and associated pegmatites) and metasedimentary (Ca-poor composition of metapsammopelites) sources in all samples. Detrital tourmalines of the Lower Siwaliks and the lower member of the Middle Siwaliks (Miocene) shows slight domination of the tourmaline sourced by meta-sedimentary terrains over magmatic origin. Whereas samples from the upper member of the Middle Siwaliks and the Upper Siwaliks (Pleistocene) shows a slight increase in the detrital tourmaline from the magmatic origin. Few grains from the samples from the upper member

of the Middle Siwaliks and the Upper Siwaliks (Pleistocene) fall in the meta-ultra mafics (samples MK-21 & MK-27).

### **6.1.2 Chemical composition of detrital Garnet**

Under a petrographic microscope (UPPL), detrital garnets are colourless and angular in shape with inclusions (Fig. 6.1-C). The molecular end members of the detrital garnet were calculated using the methods of Deer et al. (1992) and plotted in the Prp–Alm+Sps–Grs+And ternary diagrams for provenance field after Mange and Morton (2007) (Figs. 6.3). Table 6.2 contains the summary of the representative analysis of the detrital garnets. The total calculated oxides were near 100%. Garnets are rich in FeO (14.12 – 39.86 wt%, average 28.73 wt%), and poor in Cr<sub>2</sub>O<sub>3</sub> (less than 0.36 wt %) and TiO<sub>2</sub> (less than 0.58 wt%). The MgO content ranges from 0.05-8.34 wt% (average 2.06 wt%). The MnO content is generally erratic and reaches a maximum of 26 wt%. The CaO content ranges from 0.22–37.26 wt% (8.09 wt% on average). The chemical composition of the garnet grains is dominated by almandine followed by pyrope, spessartine and grossular respectively. But some garnet grains shows relatively high grossular and moderate andradite contains, this increases towards the younger successions (Figs. 6.3). The detrital garnet chemistry on Prp–Alm+Sps–Grs+And diagram shows compositional variations. Most garnet grains in all samples are distributed in the Type-B areas. Sample from the Lower Siwaliks belonging to upper middle Miocene (MK-01) shows most of the garnet distribution in Type-Bi, with minor distribution in Type-A and Type-C. These garnets in Type-Bi are reduced from the sample MK-02 and reappear from sample Mk-23 of upper Middle Siwaliks (early Pliocene). Moderate and high Ca-rich garnet proportion increases from the sample (MK-17) of upper Middle Siwaliks (late Miocene). Similarly, Mn-rich garnet proportion increases from the upper Middle Siwaliks (early Pliocene) samples.

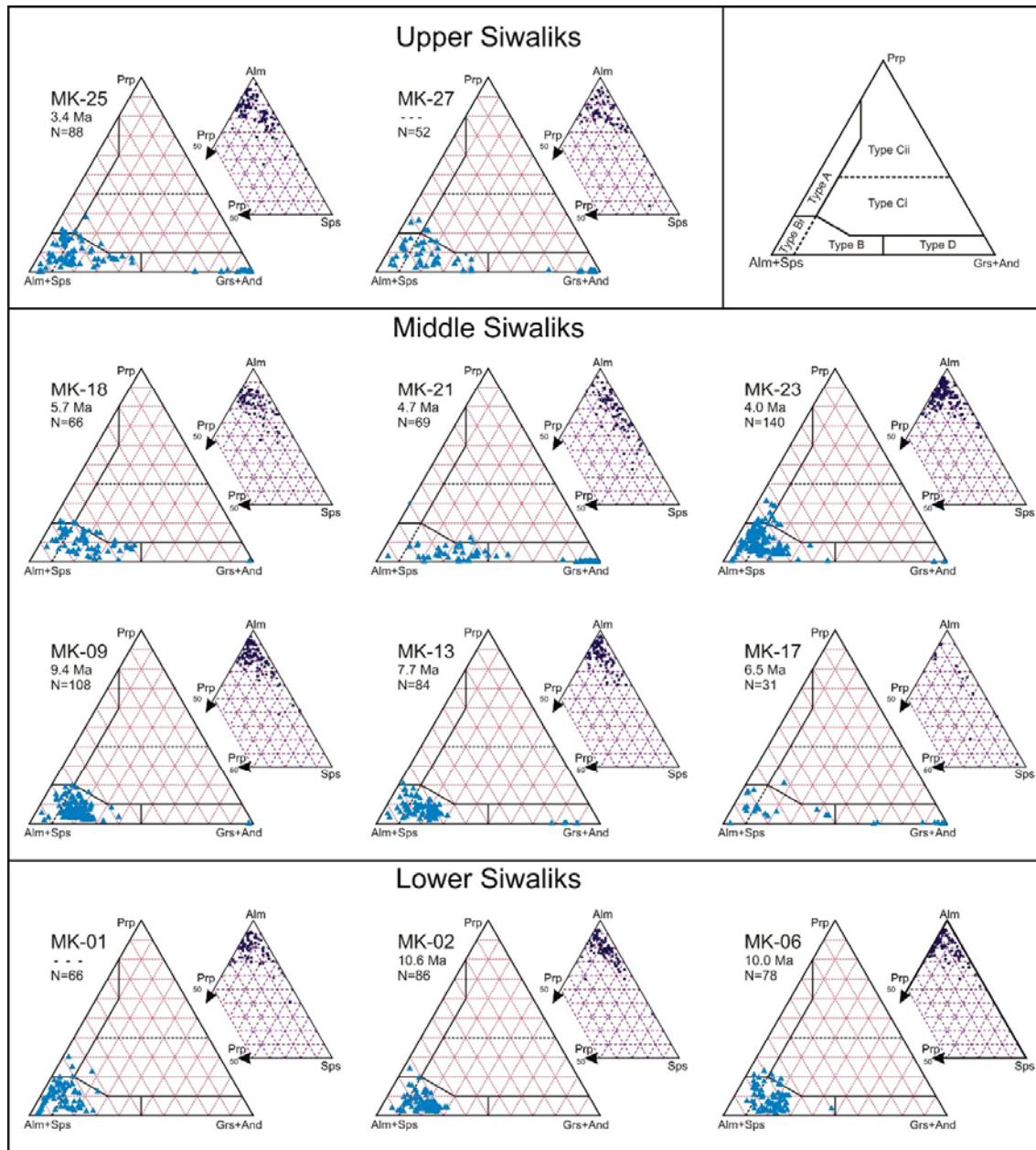


Figure 6.3: Detrital garnet compositions plotted in Prp-Alm+Sps-Grs+And and Alm-Prp-Sps diagram (modified after Rai and Yoshida, 2021). Abbreviations, Prp: pyrope, Alm: almandine, Sps: spessartine, Grs: Grossular, And: andradite. Discrimination fields for various rock types for Prp-Alm+Sps-Grs+And diagram according to Mange and Morton (2007) are as follows: Type-A: mainly from high-grade granulite-facies metasediments or charnokites and intermediate felsic igneous rocks. Type-B: amphibolite-facies metasedimentary rocks and intermediate to felsic igneous rocks. Type-Bi: intermediate to felsic igneous rocks. Type-C: high-grade metabasic rocks. Type-D: metasomatic rocks, very low-grade metamafic rocks and ultrahigh temperature metamorphosed calc-silicate granulites. Depositional ages of samples are based on preexisting age data of the Ojha et al. (2009)

Table 6.2: Chemical composition of detrital garnet grains from the Siwalik Group sandstones of the Muksar Khola section.

Litho units	Lower Siwaliks			Middle Siwaliks						Upper Siwaliks	
Samples	MK-01	MK-02	MK-06	MK-09	MK-13	MK-17	MK-18	MK-21	MK-23	MK-25	MK-27
memo	201	553	697	302	445	141	62	250	284	266	159
SiO <sub>2</sub>	36.9	36.69	37.84	37.47	36.90	37.30	37.50	36.96	37.63	37.31	36.77
TiO <sub>2</sub>	0.11	0.01	0.01	0.10	0.12	0.12	0.12	0.35	0.11	0.12	0.14
Al <sub>2</sub> O <sub>3</sub>	21.03	20.56	21.11	21.08	20.72	20.76	20.91	20.79	21.01	21.23	20.36
Cr <sub>2</sub> O <sub>3</sub>	0	0.02	0.03	0.00	0.11	0.00	0.00	0	0.04	0.02	0.05
FeO	31.67	29.61	28.71	31.88	28.53	33.35	30.63	16.8	30.58	33.50	29.18
MnO	3.12	4.46	1.15	0.67	3.88	0.26	2.44	11.19	2.54	3.97	6.10
MgO	4.13	1.76	4.83	4.98	1.38	1.56	5.11	0.46	3.03	1.53	2.16
CaO	2.61	6.47	5.81	3.28	8.22	7.25	3.35	12.49	5.84	4.26	4.77
Total (wt%)	99.57	99.58	99.49	99.46	99.86	100.6	100.06	99.04	100.78	101.94	99.53
Si	2.96	2.96	2.99	2.98	2.97	2.98	2.97	2.98	2.98	2.96	2.98
Ti	0.01	0.00	0.00	0.01	0.01	0.01	0.01	0.02	0.01	0.01	0.01
Al	1.99	1.96	1.97	1.98	1.96	1.96	1.95	1.97	1.96	1.99	1.94
Cr	0.00	0.00	0.00	0.00	0.01	0.00	0.00	0.00	0.00	0.00	0.00
Fe <sup>3+</sup>	0.09	0.11	0.04	0.05	0.08	0.07	0.10	0.03	0.06	0.07	0.08
Fe <sup>2+</sup>	2.03	1.89	1.85	2.07	1.84	2.16	1.92	1.10	1.96	2.16	1.89
Mn	0.21	0.31	0.08	0.05	0.26	0.02	0.16	0.76	0.17	0.27	0.42
Mg	0.49	0.21	0.57	0.59	0.17	0.19	0.60	0.06	0.36	0.18	0.26
Ca	0.22	0.56	0.49	0.28	0.71	0.62	0.28	1.08	0.50	0.36	0.41
Total	8.00	8.00	8.00	8.00	8.00	8.00	8.00	8.00	8.00	8.00	8.00
Almandine	68.71	63.67	61.96	69.41	61.80	72.48	64.75	36.83	65.78	72.77	63.46
Pyrope	16.57	7.14	19.01	19.71	5.47	6.13	20.19	1.58	11.90	6.01	8.63
Grossular	2.76	13.06	14.09	6.57	18.95	17.15	4.00	33.46	13.00	8.46	9.09
Spessartine	7.15	10.30	2.57	1.51	8.89	0.59	5.50	25.54	5.71	9.00	14.03
Uvarovite	0.00	0.06	0.09	0.00	0.35	0.00	0.00	0.00	0.13	0.06	0.16
Andradite	4.81	5.77	2.27	2.80	4.53	3.65	5.56	2.59	3.48	3.69	4.62

LS: Lower Siwaliks; MS: Middle Siwaliks; US: Upper Siwaliks.

## 6.4 Probable source rock

The possible source for the tourmaline grains suggesting magmatic source (granitoids or associated pegmatites) is more likely to be the Miocene leucogranites and the pegmatites of Rpye of the HHC (Schelling, 1992) and the Paleoproterozoic granite of the LHS (Tamor Khola granites) (Takigami et al., 2002; Sakai et al., 2013). Similarly, the tourmaline grains plotted in zone-d and zone-e are generally associated with the mica-schists and paragneisses (Kowal-Linka and Stawikowski, 2013) and are also associated with veins and altered aplites (Burianek et al., 2003; Jiang et al., 2003). These suggest tourmaline grain plotted in zone-d and zone-e are most probably sourced by the LHS, Jp of the HHC and the TTH. Few grains

which are plotted in the meta-ultramafic rocks (Samples MK-21 & MK-27), such meta-ultramafic rocks were reported on the ITSZ (Radhakrishna et al., 1987; O'Brien, 2019). Therefore, this points out the possibility of the ITSZ also a possible source.

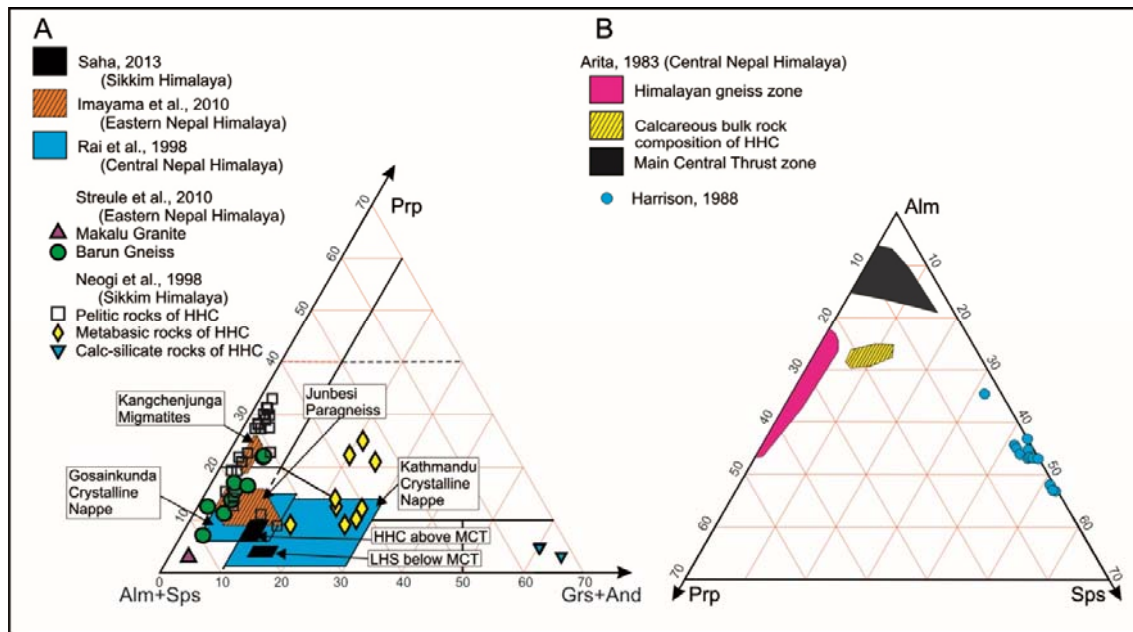


Figure 6.4: Chemical composition of garnet from the parent rocks of the different lithostratigraphic units of the Himalaya based on the previous studies (modified after Rai et al., 2021).

Previous studies in the eastern Nepal Himalaya show garnets from the MCT zone are rich in almandine (Fe-rich) and comparatively low in pyrope (Mg-rich). The proportion of garnet with pyrope composition increases towards the HHC with the decrease in grossular composition (Ca-rich) (Arita, 1983; Neogi et al., 1998; Imayama et al., 2010; Saha, 2013). Figure 6.4 show the results from the previous studies, which suggest garnets plotted in Type-A and Type-C zones are characteristic of a shallow part of the HHC, such Mg-rich garnets were reported in pelitic and metabasic rocks of the HHC in the Sikkim Himalaya (Neogi et al., 1998) and the Rm in the Taplejung area (Imayama et al., 2010). Relatively low-Ca garnets ( $Prp_{6-25}Grs_{<10}$ ) plotted in Type-Bi zone are reported in the leucogranites and Barun gneiss of the Everest-Makalu area and pelitic rocks of the HHC in the Sikkim Himalaya which are



comparable to the Rp (Neogi et al., 1998; Streule et al., 2010). Garnets of magmatic (felsic) origins, i.e., granites are characteristics of Alm+Sps end-member composition of Type-Bi (Brouand 1989; Mange and Morton, 2007; Suggate and Hall, 2014), Streule et al. (2010) reported such composition in the granite of the Everest-Makalu area. Type-B garnets are associated with amphibolite-facies of metasedimentary rocks and intermediate to felsic igneous rocks (Mange and Morton, 2007). Garnet with the composition of (Alm<sub>60-77</sub>Sps<sub>3-13</sub>Prp<sub>3-5</sub>Grs+And<sub>13-17</sub>) and (Alm<sub>60-85</sub>Sps<sub>2-15</sub>Prp<sub>6-10</sub>Grs+And<sub>10-13</sub>) was reported in the LHS and the HHC in the vicinity of the MCT of the Sikkim Himalaya (Saha, 2013). Nakajima et al. (2020b) concluded low pyrope and low to moderate grossular (Prp<sub><10</sub>Grs<sub>15-25</sub>) garnet were supplied by the Bhimphedi Group of the Kathmandu Crystalline Nappe in western Nepal. The Mahabharat Crystalline in the eastern Nepal Himalaya is equivalent to the Bhimphedi Group (Schelling, 1992) but the garnet composition of this unit has not been studied yet. Therefore, the Mahabharat Crystalline and LHS in the vicinity of the MCT is considered as the probable source of low pyrope and low to moderate grossular (Prp<sub><10</sub>Grs<sub>15-25</sub>) garnet. Contact and thermally metamorphosed calcareous sediments, calc-silicate gneiss or skarn are the sources of extremely high Ca-rich garnet (Grs<sub>>90%</sub>) (Deer et al., 1997; Mange and Morton, 2007; Suggate and Hall, 2014). The occurrence of such Ca-rich garnet (Grs<sub>79</sub>And<sub>13</sub>Prp<sub>8</sub>) is reported in the calc-silicate rocks of the HHC in the Sikkim Himalaya (Neogi et al., 1998). Also, the occurrence of such extreme Ca-rich garnets (And<sub>100</sub>Grs<sub>0</sub> to And<sub>10</sub>Grs<sub>90</sub>) are reported in the skarn formation of the Gangdese belt of southern Tibet (Xu et al., 2016). Similarly, Mn-rich garnets occur in the inner or replacement zone of complex granitic pegmatites and aplites (Baldwin and Knorring, 1983; Harrison, 1988) (Fig. 6.4-B).

## CHAPTER VII

### ISOTOPE ANALYSIS

#### 7.1 Introduction

Radioactive decay affects certain isotopes at a steady rate, including the decay of radioactive elements into stable isotopes of other elements. This has led to the development of techniques for the dating of rocks and minerals using the radioactive isotopes of parent elements and their corresponding daughter elements (Nakano, 2016). These geochemical fingerprints can be used for the identification or characterization of specific geological reservoirs on earth and further applied to reveal the provenance of clastic sediments from those reservoirs (Hoefs, 2009). Strontium and neodymium isotopes are very useful tools to distinguish the rocks between different units of the Himalaya (France-Lanord et al., 1993; Parrish and Hodges, 1996; Galy et al. 1998; Robinson et al., 2001; Szulc et al., 2006; Imayama and Arita, 2008). Therefore, this difference in the isotopic values of Strontium and Neodymium in the different units of the Himalaya is widely used for the determination of the Siwalik Group provenance (Robinson et al., 2001; Huyghe et al., 2005; Szulc et al., 2006; France-Lanord et al., 1993).

#### 7.2 Methods

Nineteen samples were selected for strontium and neodymium isotope analysis (indicated by 'Sr-Nd' in Fig. 4.1). These samples were powdered at Shinshu University and  $^{143}\text{Nd}/^{144}\text{Nd}$  and  $^{87}\text{Sr}/^{86}\text{Sr}$  ratios of samples were determined by a multi-collector inductively coupled plasma mass spectrometer (Thermo Fisher Scientific, Neptune plus) at the Graduate School of Science, Hokkaido University. Both the unleached and the leached methods were carried out in this study. For the leached method, 10g of rock powder was leached with 5% HCl at

85°C of room temperature for 1 hour. For Sr isotope, the NIST987 standard determined during this study gave a mean  $^{87}\text{Sr}/^{86}\text{Sr}$  ratio of  $0.710214 \pm 0.000024$  ( $2\sigma$ ,  $n=32$ ). For Nd isotope, the analytical procedures for chemical separation followed the methods used in Pin et al. (1994) and Pin and Zalduegui (1997). Mass fractionation factors was internally corrected using  $^{146}\text{Nd}/^{144}\text{Nd} = 0.7219$ . Additional corrections were performed by applying a standard bracketing method using JNdi-1. The normalized values of the Nd standard JNdi-1 was  $^{143}\text{Nd}/^{144}\text{Nd} = 0.512117$  ( $2\sigma$ ,  $n=23$ ). The constants used for the  $\Sigma\text{Nd}(0)$  values were  $^{143}\text{Nd}/^{144}\text{Nd} = 0.5126380$  for the present-day chondritic uniform reservoir (CHUR) (Bouvier et al., 2008)

### **7.3 Results**

The Strontium and neodymium isotopic values from the sediments of the present study are presented in Figure 7.1 and summarized in Tables 7.1 and 7.2 with their corresponding deposition time. Under the unleached method, the  $^{87}\text{Sr}/^{86}\text{Sr}$  ratio ranges from 0.753191 to 0.823343, whereas values of  $\Sigma\text{Nd}(0)$  range from -15.3 to -21.2. Under the leached method, the  $^{87}\text{Sr}/^{86}\text{Sr}$  ratio ranges from 0.740111 to 0.819740, whereas values of  $\Sigma\text{Nd}(0)$  range from -15.3 to -20.6. In both techniques, the  $\Sigma\text{Nd}(0)$  values show a decrease in  $\Sigma\text{Nd}(0)$  values towards younger succession (Fig. 7.1).

#### **7.3.1 Unleached method**

The  $\Sigma\text{Nd}(0)$  values determined by unleached method are clustered mainly in three ranges i.e., -16.7 to -17.7; -18.6 to -19.9 and -20.8 to -21.2. The Lower Siwaliks and the lower member of the Middle Siwaliks (10.6–7.5 Ma) samples show  $\Sigma\text{Nd}(0)$  values within the range of -16.7 to -17.7 with exception of two samples showing the value of -19.5 and -15.3. Similarly,

samples belonging to the upper member of the Middle Siwaliks (7.5–3.4 Ma) lie within -18.6 to -19.9. Samples from the Upper Siwaliks shows  $\Sigma Nd(0)$  values in the range of -20.8 to -21.2.

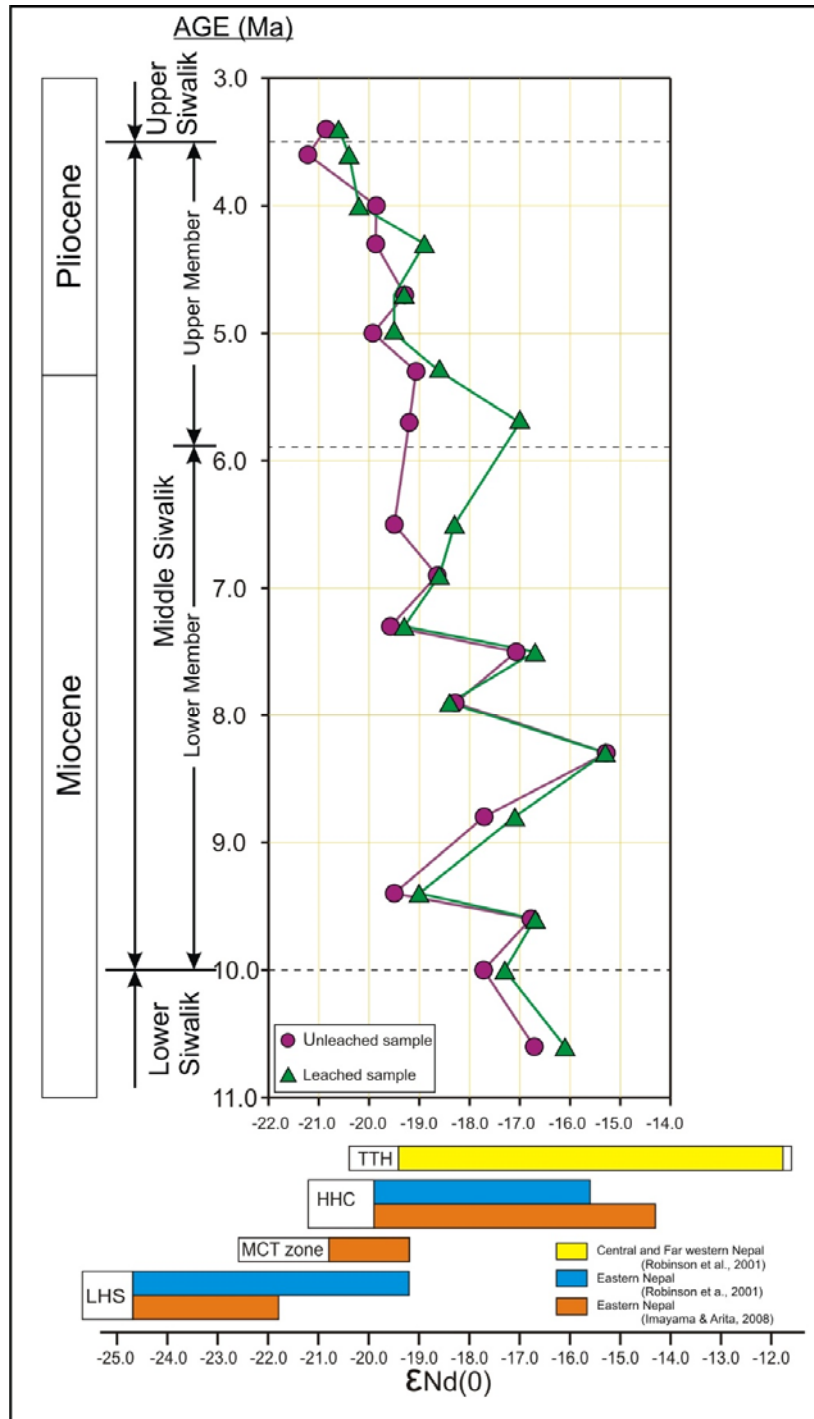


Figure 7.1:  $\Sigma Nd(0)$  values of the Siwalik Group samples from the Muksar Khola section.. Depositional ages of samples are based on preexisting age data of the Ojha et al. (2009)

### 7.3.2 Leached method

The  $\Sigma Nd(0)$  values determined by the leached method are quite similar to the results of unleached methods (Fig. 7.1) with slightly less negative value compared to the unleached method for all samples. The trend of change in the  $\Sigma Nd(0)$  values is also almost the same, dispute two samples of 5.7 and 6.5 Ma which shows comparatively less negative value.

Table 7.1: Sr-Nd isotopic compositions of Siwalik Group along the Muksar Khola section (Unleached samples).

Litho units	Sample	Rock Type	Grain size	Primary structures	Age	87Sr/86Sr	2 $\sigma$	143Nd/144Nd	2 $\sigma$	$\epsilon Nd(0)$
U. Siwaliks	MK-25	Sandstone	Coarse to medium	Massive	3.4	0.800666	0.000011	0.511567	0.0000044	-20.9
M. Siwaliks	MK-24	Sandstone	Coarse grain	Planer crossbed	3.6	0.809174	0.000010	0.511552	0.0000040	-21.2
	MK-23	Sandstone	Medium to fine	Massive	4	0.785360	0.000013	0.511621	0.0000041	-19.8
	MK-22	Sandstone	Medium to fine	Massive	4.3	0.776175	0.000006	0.511622	0.0000066	-19.8
	MK-21	Sandstone	Medium to fine	Massive	4.7	0.794290	0.000012	0.511649	0.0000070	-19.3
	MK-20	Sandstone	Coarse to medium	Trough crossbed	5	0.823343	0.000015	0.511618	0.0000048	-19.9
	MK-19	Sandstone	Medium to fine	Trough crossbed	5.3	0.800969	0.000010	0.511661	0.0000064	-19.1
	MK-18	Sandstone	Medium to fine	Trough crossbed	5.7	0.782379	0.000010	0.511652	0.0000039	-19.2
	MK-17	Sandstone	Coarse to medium	Trough crossbed	6.5	0.786756	0.000010	0.511637	0.0000057	-19.5
	MK-16	Sandstone	Very fine	Planer crossbed	6.9	0.796014	0.000011	0.511683	0.0000049	-18.6
	MK-15	Sandstone	Medium to fine	Planer crossbed	7.3	0.791336	0.000015	0.511635	0.0000056	-19.6
	MK-14	Sandstone	Coarse to medium	Planer crossbed	7.5	0.753191	0.000013	0.511763	0.0000043	-17.1
	MK-12	Sandstone	Medium to fine	Planer crossbed	7.9	0.787439	0.000011	0.511701	0.0000039	-18.3
	MK-11	Sandstone	Medium to fine	Planer crossbed	8.3	0.771066	0.000019	0.511854	0.0000050	-15.3
	MK-10	Sandstone	Medium to fine	Ripple lamination	8.8	0.786838	0.000011	0.511730	0.0000051	-17.7
L. Siwaliks	MK-09	Sandstone	Medium to fine	Planer crossbed	9.4	0.786838	0.000009	0.511638	0.0000047	-19.5
	MK-08	Sandstone	Very fine	Ripple lamination	9.6	0.753861	0.000016	0.511776	0.0000051	-16.8
	MK-07	Sandstone	Very fine	Ripple lamination	10	0.784027	0.000023	0.511730	0.0000034	-17.7
	MK-05	Sandstone	Fine grain	Ripple lamination	10.6	0.760848	0.000014	0.511779	0.0000044	-16.7

Table 7.2: Sr-Nd isotopic compositions of Siwalik Group along the Muksar Khola section (Leached samples).

Litho units	Sample	Rock Type	Grain size	Primary structures	Age	87Sr/86Sr	2 $\sigma$	143Nd/144Nd	2 $\sigma$	$\epsilon Nd(0)$
U. Siwaliks	MK-25	Sandstone	Coarse to medium	Massive	3.4	0.799851	0.000012	0.511584	0.000006	-20.6
M. Siwaliks	MK-24	Sandstone	Coarse grain	Planer crossbed	3.6	0.807452	0.000019	0.511595	0.000005	-20.4
	MK-23	Sandstone	Medium to fine	Massive	4	0.785330	0.000018	0.511603	0.000004	-20.2
	MK-22	Sandstone	Medium to fine	Massive	4.3	0.776705	0.000009	0.511670	0.000004	-18.9
	MK-21	Sandstone	Medium to fine	Massive	4.7	0.793271	0.000015	0.511647	0.000005	-19.3
	MK-20	Sandstone	Coarse to medium	Trough crossbed	5	0.819740	0.000014	0.511636	0.000005	-19.5
	MK-19	Sandstone	Medium to fine	Trough crossbed	5.3	0.796976	0.000012	0.511684	0.000005	-18.6
	MK-18	Sandstone	Medium to fine	Trough crossbed	5.7	0.781199	0.000015	0.511766	0.000005	-17.0
	MK-17	Sandstone	Coarse to medium	Trough crossbed	6.5	0.783079	0.000012	0.511700	0.000003	-18.3
	MK-16	Sandstone	Very fine	Planer crossbed	6.9	0.792308	0.000012	0.511681	0.000003	-18.7
	MK-15	Sandstone	Medium to fine	Planer crossbed	7.3	0.789324	0.000012	0.511648	0.000003	-19.3
	MK-14	Sandstone	Coarse to medium	Planer crossbed	7.5	0.752906	0.000011	0.511781	0.000007	-16.7
	MK-12	Sandstone	Medium to fine	Planer crossbed	7.9	0.757829	0.000014	0.511696	0.000005	-18.4
	MK-11	Sandstone	Medium to fine	Planer crossbed	8.3	0.766676	0.000011	0.511852	0.000004	-15.3
	MK-10	Sandstone	Medium to fine	Ripple lamination	8.8	0.763719	0.000006	0.511763	0.000004	-17.1
L. Siwaliks	MK-09	Sandstone	Medium to fine	Planer crossbed	9.4	0.795526	0.000012	0.511665	0.000005	-19.0
	MK-08	Sandstone	Very fine	Ripple lamination	9.6	0.753706	0.000017	0.511780	0.000006	-16.7
	MK-07	Sandstone	Very fine	Ripple lamination	10	0.772683	0.000014	0.511753	0.000005	-17.3
	MK-05	Sandstone	Fine grain	Ripple lamination	10.6	0.740111	0.000009	0.511812	0.000004	-16.1

## 7.4 Probable Source Rock

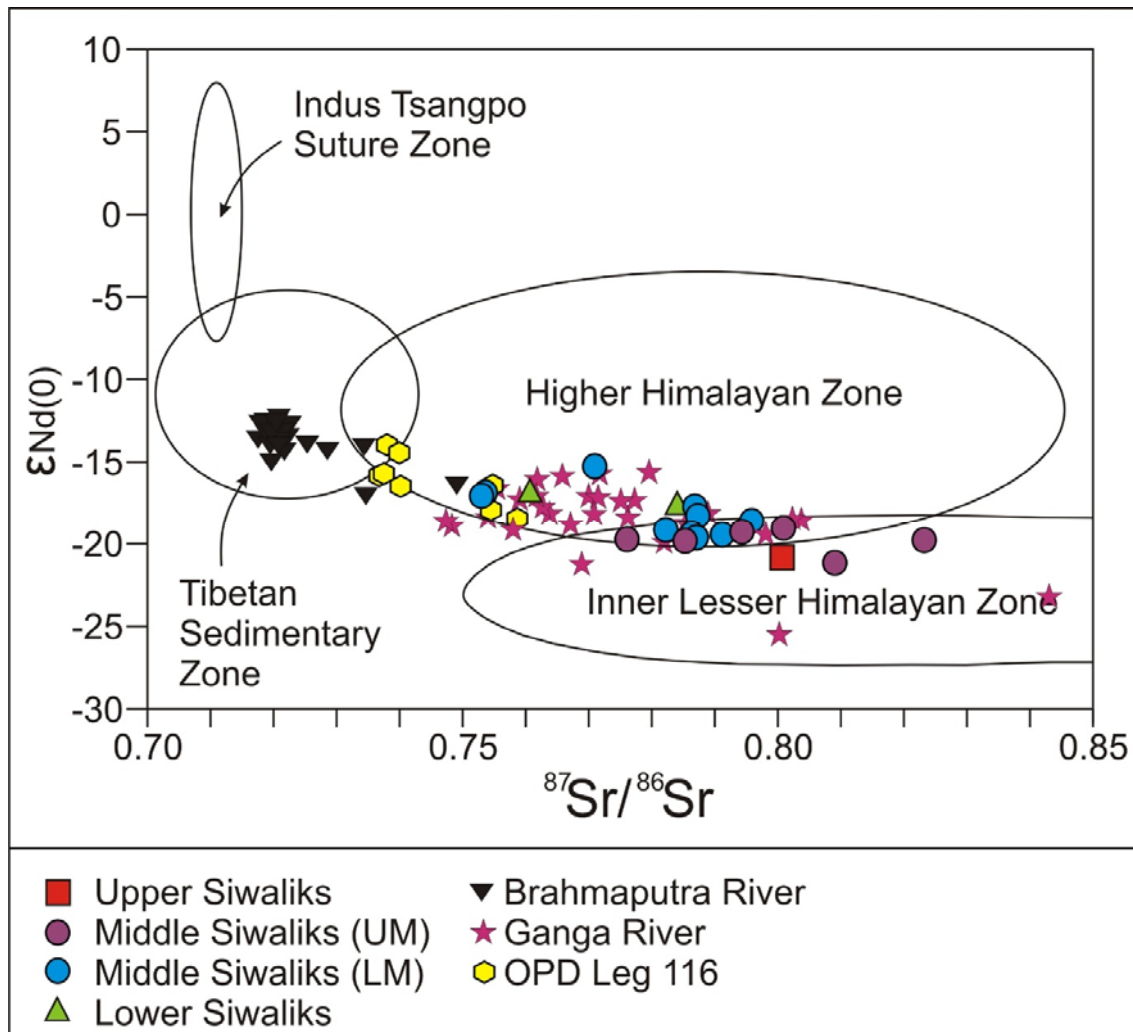


Figure 7.2: Nd-Sr isotopic data of the Siwalik Group samples from the Muksar Khola section compared with typical values for major Himalayan tectonic units (modified from Szulc et al., 2006); River sediments of the Brahmaputra River (Singh and France-Lanord, 2002); River sediments of Ganga basin (Singh et al., 2008) and middle Miocene to Holocene sediments recovered in OPD Leg 116 (France-Lanord et al., 1993).

Various research has shown that Nd isotopes do not significantly fractionate during the process of diagenesis, therefore sediments directly resemble the isotopic characteristics of the source rocks (Goldstein and Jacobsen, 1988; Meyer et al., 2011; Jonell et al., 2018). Moreover, the difference of  $\Sigma Nd(0)$  values of more than 1 directly reflect a provenance change (Jonell et al., 2018). Therefore, a decreasing trend of  $\Sigma Nd(0)$  values in the present study towards the younger successions reveal a significant change in the provenance. Before

7.3 Ma,  $\Sigma\text{Nd}(0)$  show less negative values (Fig. 7.1) suggesting the probability of the HHC and TTH as source areas (Galy et al. 1998; Robinson et al., 2001). Between 7.3 to 4.0 Ma increase in  $\Sigma\text{Nd}(0)$  values are observed revealing the possibility of the MCT zone (Parrish and Hodges, 1996; Imayama and Arita, 2008) or significant addition of the detritus from the LHS (Robinson et al., 2001). After 3.6 Ma highly negative  $\Sigma\text{Nd}(0)$  values are observed suggesting more sediments were derived from the LHS (Parrish and Hodges, 1996; Galy et al. 1998; Robinson et al., 2001; Imayama and Arita, 2008). Very radiogenic Sr isotopic composition suggests LHS as a source, which has a comparatively higher  $^{87}\text{Sr}/^{86}\text{Sr}$  ratio than the HHC (France-Lanord et al., 1993). The Nd-Sr isotopic data of the sediments (Fig. 7.2) suggests LHS and HHC as possible sources. This figure also clearly shows the shift of the provenance from the HHC to the LHS with young depositional age. The  $^{87}\text{Sr}/^{86}\text{Sr}$  ratio from the present study is comparable with those of other Himalayan rivers from central and western Himalaya (Singh et al., 2008). Comparison of the present result with the results of river sediments of the Ganga River and the Brahmaputra River and the Bangal fan sediments show close resemblance with the Ganga River sediments (Fig. 7.2).

## CHAPTER VIII

### FLUVIAL FACIES

#### 8.1 Introduction

Facies refers to the grouping of rock types having similar features. Sedimentary facies is a synthesis of sedimentary rocks and sedimentary environments that reflects a particular process or environment and form under certain conditions of sedimentation (Feng, 2019). These sediment bodies are related to a particular combination of compositional, physical and biological structures which makes them different from adjacent sediments that are deposited in different environments. Sediments are deposited by various processes under different environments. Moreover, several local environments may exist side by side within a basin, and the sedimentary rocks that are ultimately produced can be related to these depositional environments.

Most of the clastic fluvial deposits can be subdivided into gravel, sand and fines (mud, silt). Siwalik sediment represents this fluvial deposit, derived from the tectonically active Himalaya and deposited in the paleo-Gangetic basin (Tandon, 1976; Parkash et al., 1980; Tokuoka et al., 1990; Hisatomi and Tanaka, 1994; Willis 1993b). The fluvial environments of the Siwaliks were interpreted based on the facies study of these sediments, which revealed mainly the existence of the meandering and the braided river system (Hisatomi and Tanaka, 1994; Zaleha, 1997; Ulak and Nakayama, 2001; Ulak, 2009; Sigdel and Sakai, 2016), though in few sections anastomosed river system has also been reported (Huyghe et al., 2005; Nakayama and Ulak, 1999). The appearance of these fluvial systems is observed almost consistent throughout the Siwalik Group along the Himalaya with a slight difference in timing. Autocyclic and allocyclic processes such as hinterland tectonics and climate are considered to be the factor affecting the change in the fluvial system (Willis 1993a; Zaleha



1997). Therefore, facies study not only determines the types of fluvial environment responsible for the deposition but also helps to understand the coeval hinterland tectonics and climate. Therefore, this study deals with the facies analysis to decipher the fluvial environment and its controlling factors responsible for the deposition of the sediments of the Siwaliks succession of the Muksar Khola section of eastern Nepal Himalaya.

## **8.2 Methods**

In this study field data were acquired based on the topographic map of scale 1:25000. Lithofacies were identified based on the grain size and texture of the beds and associated sedimentary structures. Architectural elements were classified based on the nature of the internal and external geometry of the beds and the bounding surfaces. Mainly foresets of the cross-stratifications were measured for the paleocurrent analysis. The paleo-flow direction was estimated using standard methods (Tucker, 2003). Based on these lithofacies, architectural elements and paleocurrent directions, facies associations were classified following the code of Miall (1977, 1985, 2000 and 2006). Route map and detailed sedimentological logs were made to evaluate the precise boundary of the facies associations. The paleomagnetic data by Ojha et al. (2009) was used to determine the specific age for each facies association. Based on this facies association, river systems were interpreted.

## **8.3 Facies associations**

Based on the ratio of sandstone and mudstone, its grain size along with the sedimentary structure and the nature of the bed geometry, 12 sedimentary lithofacies and six facies associations have been identified. These are summarized in Table 8.1 and 8.2 and

representing photographs are displayed in Figure 8.1. Sedimentological logs representing each facies association are shown in Figure 8.2 and their location in Figure 8.3.

Table 8.1: Description and interpretation of the depositional facies (modified after Rai and Yoshida, 2021).

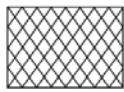







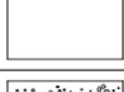
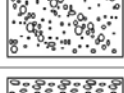
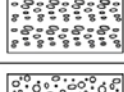
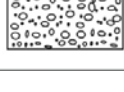
Facies Code	Symbol	Facies Characteristics	Sedimentary Structures	Interpretation	Remarks
P		Variegated with nodules and concretions Thickness upto 2 m	Pedogenic features	Soil with chemical precipitation (Miall, 2000; 2006)	Fig: 8.2(A)
C		Peaty mudstones Thickness upto 0.15 m	Plant, mud films	Vegetated swamp deposits (Miall, 2000; 2006)	Fig: 8.2(B)
Fl		Inter-lamination of mud, silt and very fine grain sand with occasional very small ripples Thickness upto 1 m	Fine lamination	Overbank or waning flood deposits (Miall, 1977; 2000; 2006)	Fig: 8.2(C)
Fm		Mudstones to very fine grain sandstones, Thickness upto 0.3 m	Massive	Overbank, abandoned channel, or drape deposits (Miall, 1977; 2000; 2006)	Fig: 8.2(D)
Sh		Fine to medium grain sandstones, occasionally concreted, Thickness upto 0.4 m	Horizontal lamination with parting or streaming lineation	Planer bed flow (intermediate to upper flow regime or lower flow regime) (Miall, 1977; 2000; 2006)	Fig: 8.2(E)
Sp		Fine to coarse grain sandstones, mudclast are occasionally present, Thickness upto 1 m	Solitary or grouped planar cross beds	Migration transverse and linguoid 2D dunes (lower flow regime) (Miall, 1977; 2000; 2006)	Fig: 8.2(F)
Sr		Fine to medium grain sandstones, occasionally concreted, Thickness upto 0.4 m	Ripple lamination	Ripples (lower flow regime) (Miall, 1977; 2000; 2006)	Fig: 8.2(G)
St		Medium to coarse grain sandstones, occasionally pebbly, Thickness upto 2 m	Solitary or grouped trough crossbeds	Migration of linguoid 3D dunes (lower flow regime) (Miall, 1977; 2000; 2006)	Fig: 8.2(H)
Sm		Medium to coarse grain sandstones, Thickness upto 1.5 m	Massive or faint lamination	Sediment gravity flow deposits, resulting from high concentration of sediment / water mixture (Martin and Turner, 1998; Miall, 2000; 2006)	Fig: 8.2(I)
Gp		Pebble sized clast stratified in matrix of medium to coarse grain sandstones. Thickness upto 2 m	Planar crossbeds	Transverse bedforms, Linguoid bars or deltaic growths from older bar remnants (Miall, 1977; 2000; 2006)	Fig: 8.2(J)
Gmg		Matrix supported gravel. Thickness 2 to 8 m	Inverse to normal grading Grading clast and/or matrix	Pseudoplastic debris flow (Low strength, viscous) Longitudinal bars, channel lag deposits (Miall, 1977; 2000; 2006)	Fig: 8.2(K)
Gmm		Matrix supported, poorly sorted massive gravel. Thickness 2 to 8 m	Structureless or weak grading	Plastic debris flow (High strength, viscous) Longitudinal bars, channel lag deposits (Miall, 1977; 2000; 2006)	Fig: 8.2(L)

Table 8.2: Facies associations recognized in the Siwalik Group of the Muksar Khola section (interpretation based on Miall, 1977; 1985; 2000; 2006).

Facies Association	Dominant lithofacies type	Minor lithofacies type	Characteristics architectural elements	Lithostratigraphic Unit	Interpretation
FA1	Sr, Fl, Fm, P	Sp, Sh, C	CH, SB, CS, LV, FF, LA	Lower Siwalik	Flood plain dominated fine-grained Meandering river
FA2	Gmm, Sm	Sr, Fl, Fm	GB, SB, LV, FF	Lower Siwalik	Flood dominated overbank environment
FA3	Sp, S, Sh, Fm	Gmm, St, Sm, Fl, P	CH, SB, CS, LV, FF, LA	Middle Siwalik	Sandy meandering river
FA4	St, Sp, Sm, Fm, Fl	Gmm, Sh, Sr, P	CH, SB, CS, LV, FF, DA	Middle Siwalik	Anastomosing river
FA5	Gmm, Gmg, Sm, Fm	Gp, Sp	CH, GB, SB, FF	Upper Siwalik	Debris flow dominated gravelly braided river

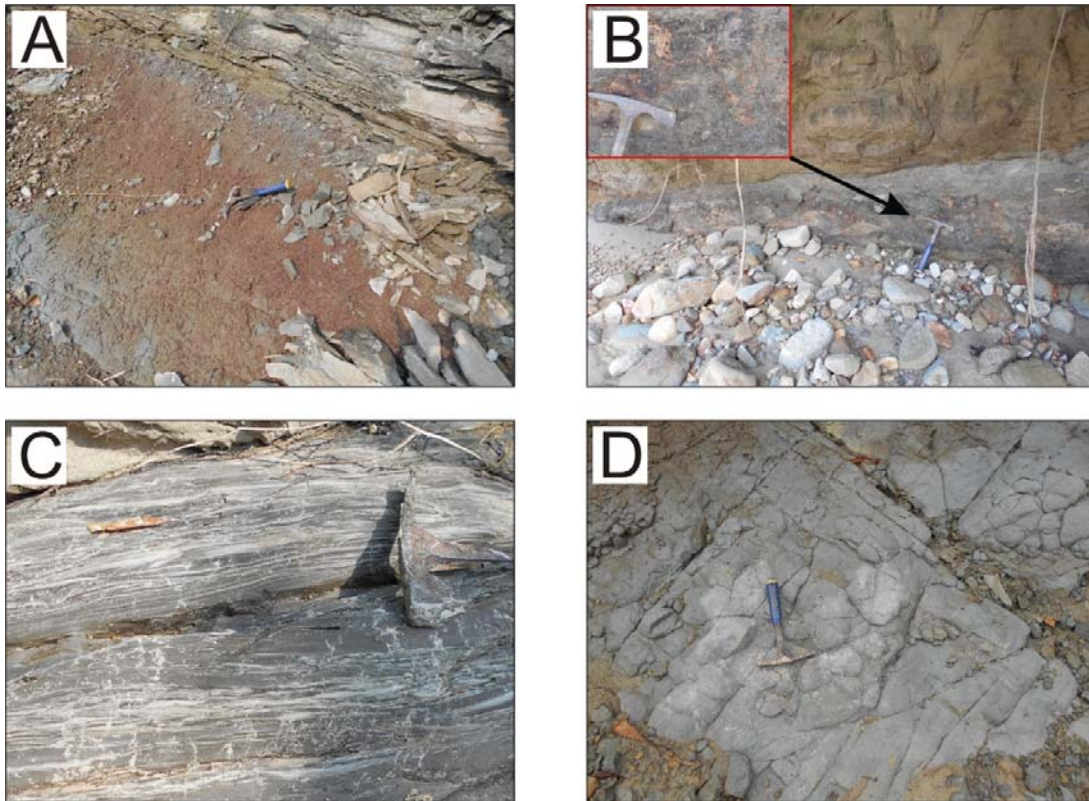


Figure 8.1: Outcrop photographs of the lithofacies, A) Reddish-brown paleosols (P); B) Peaty mudstone (C); C) Laminated mudstone (Fl); D) Massive mudstone (Fm).

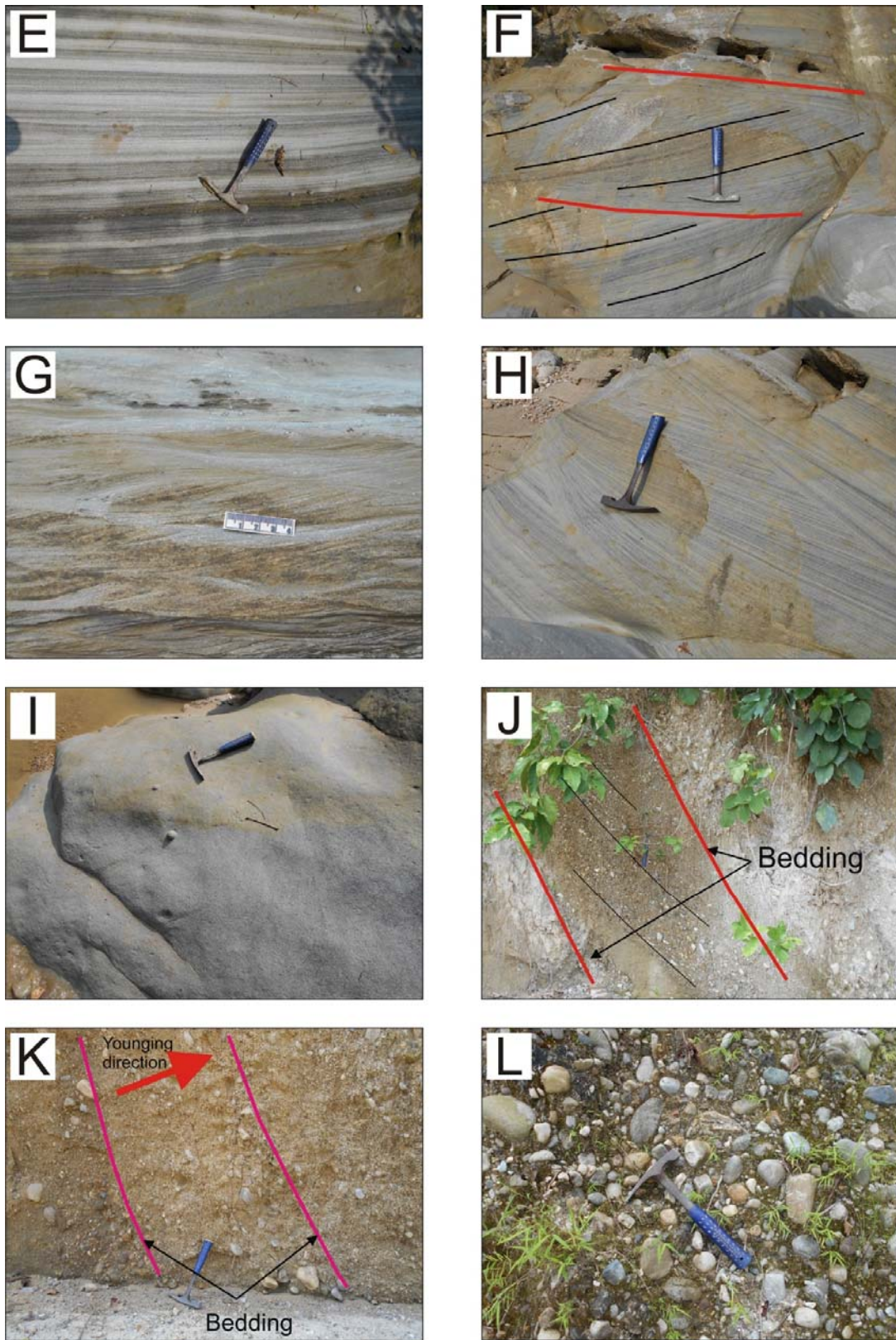


Figure 8.1: Continued, E) Horizontal lamination (Sh); F) Planer cross-stratification (Sp); G) Ripple cross lamination (Sr); H) Trough cross-stratification (St); I) Massive sandstone (Sm); J) Stratified gravel (Gp); K) Matrix supported gravel with inverse grading (Gmg); L) Matrix supported poorly sorted pebble to cobble size massive gravel (Gmm).

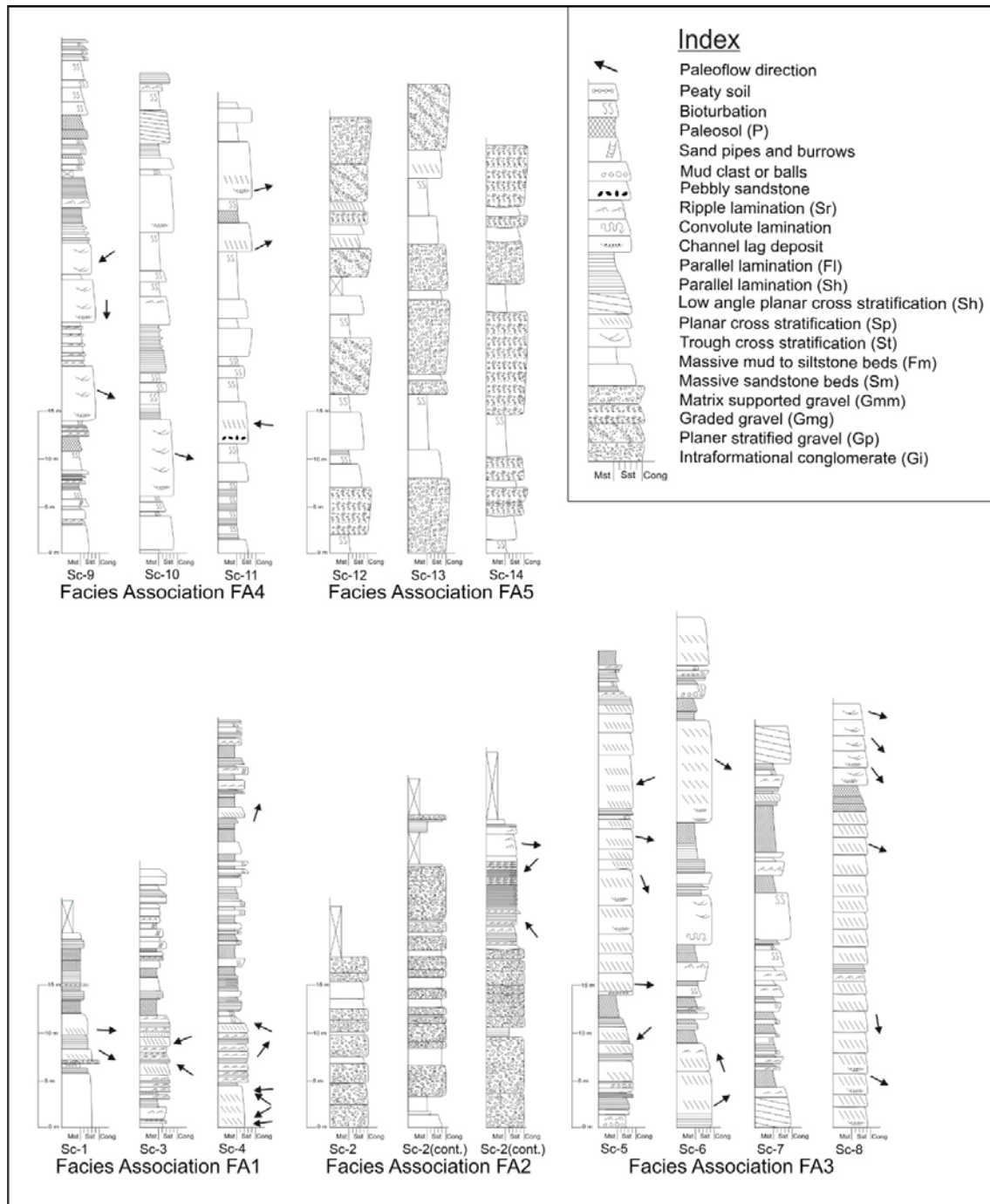


Figure 8.2: Representative sedimentological log of the facies associations identified on the Siwalik Group of the Muksar Khola section (modified after Rai and Yoshida, 2021, Location is given in Figure 8.3).

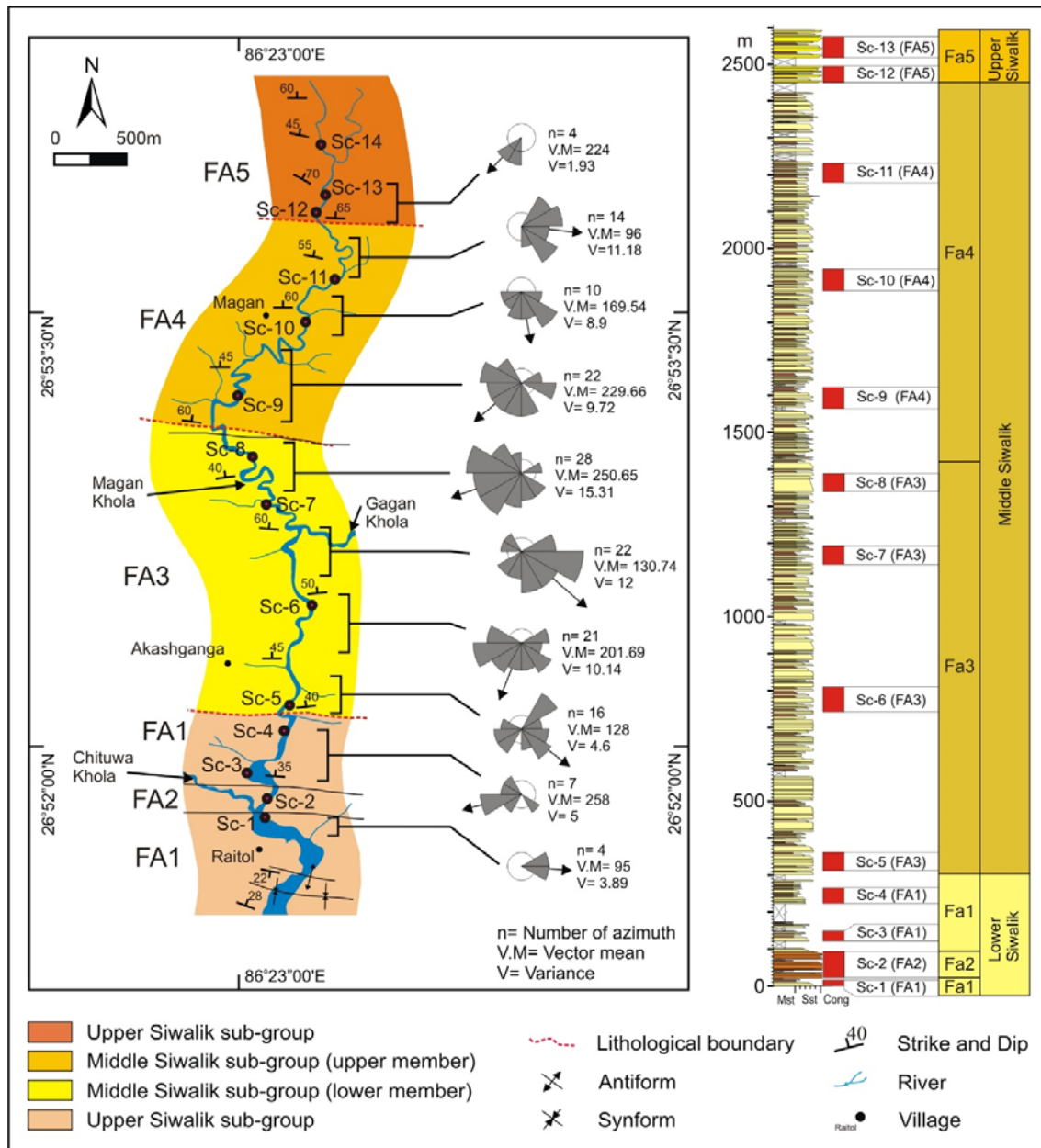


Figure 8.3: Geological map showing the facies associations and paleo flow direction (left), and location of sedimentological log presented in Figure 8.2 (right) (modified after Rai and Yoshida, 2021).

### 8.3.1 Facies Association, FA1

#### 8.3.1.1 Description

This facies association is dominated by thickly-bedded mudstone and very fine- to medium-grained sandstone. Fining-upward succession ranges from fine-grained sandstone to

mudstone. Mudstones are 0.4 to 2.0 m thick and show olive to dark-grey and reddish-brown colour and are mostly bioturbated, mottled or variegated (Fig. 8.1-A) with occasional facies C (Fig. 8.1-B). Facies Fl and Fm are also dominantly observed in mudstone (Fig. 8.1-C, D). The average thickness of sandstone beds ranges from 0.15–1.5 m, with few beds with more than 4 m in thickness (Fig. 8.2, Sc-1&4). Facies Sp with the erosional basal surface is observed in thick to very thickly bedded fine- to medium-grained sandstone (>70 cm), whereas facies Sh and Sr dominate in the thick beds (30-60 cm). Lateral accretionary structures are associated with these beds (Fig. 8.4-A). Fine-grained sandstones are medium to thickly bedded and are massive but occasionally facies Sh or Sr are also observed. In very fine- to fine-grained sandstones both fining- and coarsening-upward succession are observed and show facies Fm and P. The basal surface of fine- to fine-grained sandstones are non-erosive and occurs interbedded with very thick beds of mudstone (Fig. 8.2, Sc-4). Very fine-grained sandstones with thin to medium beds are mostly bioturbated with occasional occurrence of facies Sr or Fl. On the upper 15–25 cm thick portion of the fine-grained sandstone and mudstone beds calcareous nodules are often observed. Perpendicular sandpipes with a diameter of ca. 3 cm, roots and rootlets are often observed in massive mudstone and very fine-grained sandstone (Figs. 3.4-C, D). The paleocurrent data show a dispersive flow pattern but these are limited in this facies association (Fig. 8.3). This facies association FA1 is preserved in the Lower Siwaliks.

### **8.3.1.2 Interpretation**

Thick to very thickly bedded fine- to medium-grained sandstone with erosive basal surface and planar cross-stratification and ripple lamination suggests channel deposits (Miall, 2006). Massive fine-grained sandstone with medium to thick beds and occasional ripple or parallel lamination represents sheet flow (Miall, 2006). Bioturbated very fine- to fine-grained sandstone with medium beds showing either of fining- or coarsening-upward succession

occurring interbedded with flood plain deposits represents crevasse deposits (Nakayama and Ulak, 1999; Miall, 2006). Thin to medium bedded very fine-grained sandstones with parallel to ripple laminations with paleo flow direction normal to channel represents levee deposits (Singh, 1972). Bioturbated and variegated mudstone preserving sandpipes and rootlets represent flood plains and calcareous nodules suggest its long-term exposure (Nakayama and Ulak, 1999). Laminated mudstone suggests the waning stage of river flood and peaty mudstone represents some kind of swamp deposits indicating the overbank deposits (Miall, 2000; 2006). Lateral accretionary structures on sandstone along with frequent crevasse splay and dispersive paleo flow pattern indicates a high sinuous river. Therefore, FA1 is interpreted as the deposits of a flood plain dominated fine-grained meandering river system.

### **8.3.2 Facies Association, FA2**

#### **8.3.2.1 Description**

This facies association consists of thick to very thickly-bedded (0.4- >4.0 m), poorly-sorted, clast-supported intraformational conglomerate (Fig. 3.4-B), with occasional occurrence of thickly bedded coarse-grained sandstone and mudstone. The intraformational conglomerate is characterized by greenish-grey coloured siltstone to mudstone clast and matrix of medium- to very coarse-grained sand showing facies Gmm with planer basal surface. These clasts are angular to sub-angular in shape with an average diameter of 1–4 cm (some clasts show elongation up to 10 cm). Clast and matrix in these conglomerates exhibit an average ratio of about 70% and 30% respectively. Massive coarse-grained sandstone beds with a thickness of 0.1 to 0.8 m are observed in between these intraformational conglomerate beds around the lower part of this facies association. It disappears in the upper part, with an occasional occurrence of the parallel laminated mudstones with a thickness of 0.4 to 0.5 m (Fig. 8.2, Sc-2). Thin to medium beds of fine-grained sandstone with facies Sr and Fl is observed at the top



of this facies association (Figs. 8.4-B, C) with an overall vertical thickness of around 10 m. This facies association FA2 is preserved in the Lower Siwaliks with a thickness of about 80 to 90m within facies association FA1.

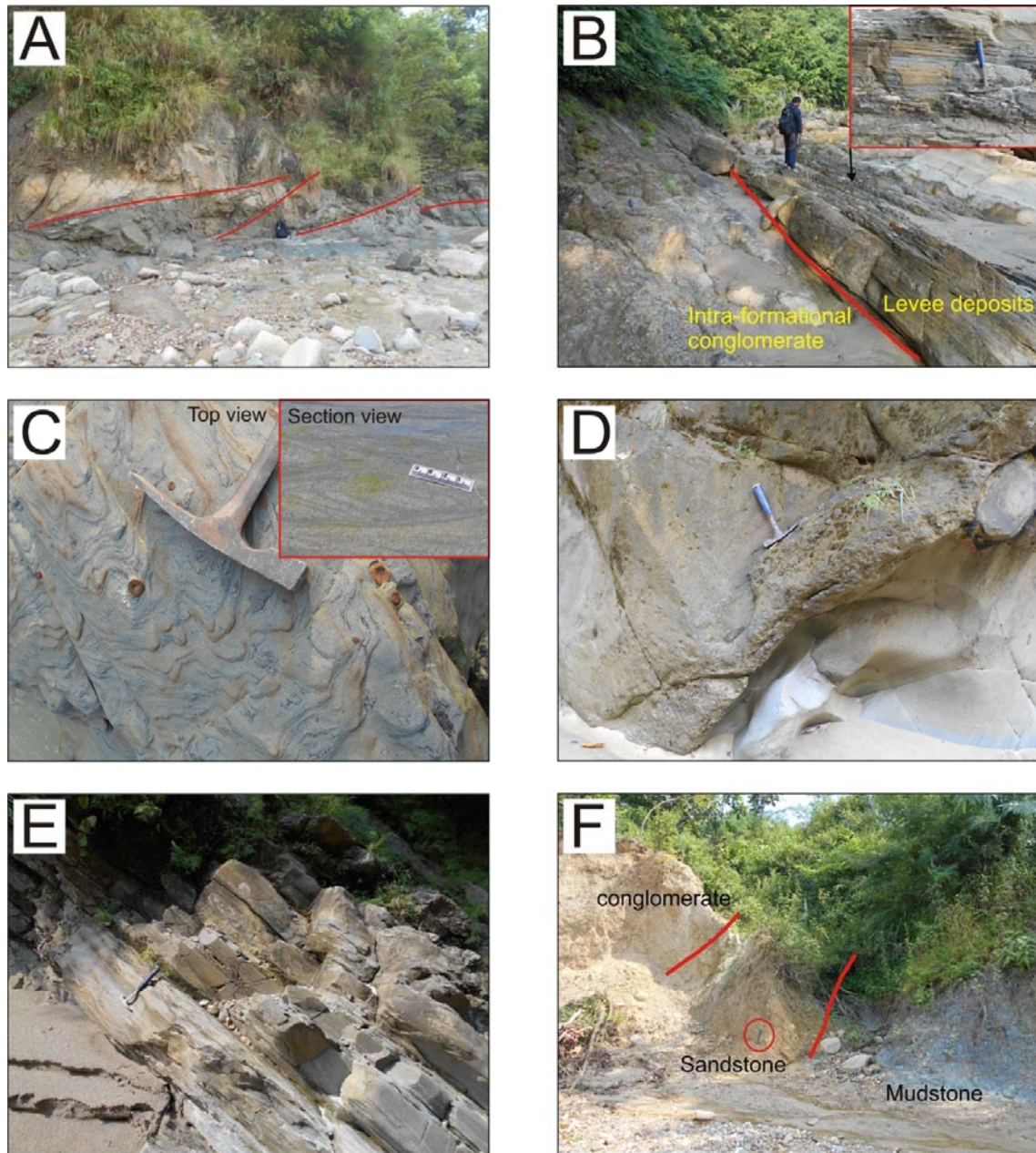


Figure 8.4: Outcrop photographs of, A) Laterally accreted sandstone bed (FA1); B) Intraformational conglomerate followed by parallel to ripple laminated very fine-grained sandstone representing levee deposits (FA2); C) Ripple lamination on the very fine-grained sandstone (FA2); D) Channel lag deposits with coal fragments (FA3); E) Parallel to ripple laminated very fine-grained sandstone intercalated with mudstone representing levee deposits (FA3); F) Matrix supported conglomerate associated with sandstone and mudstone (FA5).

### **8.3.2.2 Interpretation**

The intraformational conglomerate is resulted from the bank failure due to rapid lowering of water level during the waning stage of a flood (Gohain and Parkash, 1990; Singh et al., 1993; Plink-Bjorklund, 2015). This lowered water level of the channel undercuts the adjacent bank triggering bank slumping, if the bank is composed of cohesive mud, they break into large blocks (Singh et al., 1993). Such collapse of fluvial banks initiates sediment-laden currents movement across and along the fluvial channel (Martin and Turner, 1998). As this block rolls along the channel floor, it changes its size and shape from angular to rounded with a decrease in size as they travel long distances. Therefore, an angular to the sub-angular shape of mud clast suggests immature sediments which are not transported for a longer distance (Reineck and Singh 1980). This suggests these clasts were not deposited by the main channel undercutting overbank deposit, because in that case, these clasts would be disintegrated resulting in muddy sand due to longer transportation within the channel. Moreover, structureless massive beds with planer basal surfaces indicate debris-flow deposits (Miall, 2006). Therefore, this massive intraformational conglomerate with angular to sub-angular mud clast should be deposited away from the main channel, probably as a result of a large flood that covered the entire flood plain and undercut the distal alluvial terraces. The collapse of the alluvial terrace and its deposition in overbank settings caused an increase in the distance from the main channel therefore these collapsed sediments blocks were not much reworked. The massive sandstone bed with a flat basal surface observed in the lower section of this facies association associated in between conglomerate beds represents sheet flow deposits (Martin and Turner, 1998; Miall, 2006). Similarly, occasional laminated mudstone in the upper section of this facies association suggests a sudden decrease in the velocity and depth of water indicating the termination of the flood. Thin to medium bedded fine-grained sandstone showing facies Sr and Fl at the top intraformational conglomerate indicates a levee

deposit (Miall, 2006). The dominance of the overbank architectural elements and absence of channel deposits suggests this facies association FA2 as the deposits of the flood dominated overbank environment.

### **8.3.3 Facies Association, FA3**

#### **8.3.3.1 Description**

This facies association is characterized by the domination of sandstone facies with subordinate mudstone facies (Table. 8.2). It consists of very thickly bedded medium- to coarse-grained sandstone showing “salt and pepper” texture associated with very fine- to fine-grained sandstones and greenish-grey to dark coloured mudstone. Both amalgamated and non-amalgamated sandstone beds are observed in this facies association. Amalgamated sandstone thickness ranges from 4 to >20 m (Fig. 3.8-A) and occurs intermittently. These amalgamated sandstone beds are made up of 1.0 to 3.0 m thick individual sedimentary succession with erosive amalgamation surface and are dominated by facies Sp. Individual succession in the lower portion of amalgamated sandstone beds shows weakly developed fining-upward succession. It is characterized by coarse-grain at the base which decreases to medium- to coarse-grained sandstone at the top (Fig. 8.2, Sc-5) (sometimes identical grain size is observed making unclear amalgamation surface). At the base of these amalgamated beds sub-angular to angular mud clasts (up to 20-30 cm in length, Fig. 3.8-A) are sporadically observed. In contrast, individual fining upward succession ranges from coarse- to fine-grained sandstone towards the upper portion, making distinct amalgamation surface. Facies Sh is often observed at the top of the individual succession (Fig. 8.1-E) with an occasional thin lens of mudstone. Non-amalgamated sandstone beds thickness ranges from 0.2 to >3.0 m and is fine- to coarse-grained. Thick to very thick sandstone beds show dominating facies Sp (Fig. 8.1-F) with a slightly erosive basal surface. Lateral accretionary structures and channel

lags with a considerable amount of mud clast and coal fragments are also occasionally observed at the base (Fig. 8.4-D). Fine- to medium-grained sandstone beds are thickly bedded (50-90 cm) and display sheet-like geometry with planar basal surfaces. It is characterized by both fining and coarsening upward succession with dominating facies Sr (Fig. 8.1-G) and sometimes associated with mud clast. Very fine- to fine-grained sandstones with medium to thick beds (25-50 cm) show intercalation with mudstones. These sandstones occasionally show facies Sh or Sr but are mostly bioturbated (Fig. 8.4-E). Mudstones thickness ranges from 0.2 to 2.0 m and is mostly bioturbated or mottled, in a few beds facies Fl is occasionally observed. On the upper portion of both very fine- to fine-grained sandstone and mudstone beds, calcareous nodules are observed. Perpendicular sandpipes (ca. 12 cm long with diameter ca. 3 cm) are observed in these beds. In this facies association, high dispersion with frequent change in flow direction is revealed by the paleocurrent analysis (Fig. 8.3). The FA3 facies association is preserved in the lower member of the Middle Siwaliks.

### **8.3.3.2 Interpretation**

Amalgamated sandstone beds are deposited by channel with a high deposition rate, high flow energy with a high erosive capacity (Zhang et al., 2017). Unclear amalgamation surface indicates erosive features which frequently occurs within channel deposits, in contrast as the distance increase from the main channel deposition results with more distinct amalgamation surface with occasional occurrence of mudstone barriers (Walker 1966). Therefore, weakly developed fining upward succession with occasional unclear amalgamation surface in the lower section which changes to distinct amalgamation surface in the upper section suggests a shifting of the channel. Thick to very thick sandstone beds with planer cross-stratification and channel lags, showing fining upward succession indicates channel deposits (Miall, 2006). Thickly bedded fine- to medium-grained sandstone showing sheet-like geometry with both fining- and coarsening-upward succession and ripple lamination (Fig. 8.2, Sc-6 & 7) suggests

crevasse splay. Very fine-grained sandstones showing parallel to ripple laminations interbedded with mudstone represents levee deposits (Miall, 2006). Thick bioturbated mudstone indicates overbank deposits. Laminated mudstone suggests the waning stage of floods or swamp deposits. Laterally accreted fining upward succession of sandstone with high dispersive paleo-flow direction and intermittent crevasse deposits within thick flood plain deposits suggests the meandering nature of the river (Miall, 2006). On these bases, FA3 is interpreted as the deposits of the sandy meandering river system.

### **8.3.4 Facies Association, FA4**

#### **8.3.4.1 Description**

This facies association is characterized by very thickly bedded coarse-to very coarse-grained sandstone with subordinate pebbly sandstone associated with thickly bedded fine- to medium-grained sandstone and dark grey mudstone. Sandstones of this facies association lacks a “salt and pepper” texture and are less indurated compared to sandstones of FA3 and shows well-developed fining-upward succession (Fig. 3.10-A). The sandstone bed thickness ranges from 1.0 to > 5.0 m with the lenses of pebbly sandstone made up of sub-rounded quartzite at the base. Facies St (Fig. 8.1-H) dominates with the minor occurrence of facies Sp. Fine- to coarse-grained sandstones are very thickly bedded (>1 m) and massive with faint traces of cross-stratification. Downstream accretion is observed at the upper portion of these facies association, in these sandstone beds. Medium- to coarse-grained sandstones are thickly bedded and show coarsening upward succession. These sandstones are either massive or bioturbated (Fig. 8.1-I). Similarly, medium to thickly bedded (30–70 cm) fine-grained sandstones are also mostly bioturbated with occasional occurrence of facies Sr or Sp. These sandstones are interbedded with mudstone beds. This facies association records an increase in both proportion and the thickness of mudstones. The thickness of individual mudstone beds

ranges from 0.3 to 3.0 m with an overall thickness of >20 m. Most of the mudstones are gleyed or bioturbated, with occasional occurrence of facies Fl. At the upper section of this facies association, carbonaceous layers and variegated mudstones are sporadically observed. Paleocurrent shows high dispersion with the flow direction changing from southwest to the southeast (Fig. 8.3). This facies association FA4 is preserved along the upper section of the upper member of the Middle Siwaliks.

#### **8.3.4.2 Interpretation**

Coarse- to very coarse-grained sandstone consisting of pebbly lags deposits at the base represents channel deposits. Bioturbated massive sandstone beds showing coarsening-upward succession and interlayered with mudstone are overbank deposits representing crevasse or sheet flow deposits (Martin and Turner, 1998). Fine-grained sandstone with bioturbation and occasional ripple lamination interlayered with bioturbated or laminated mudstone suggests levee deposits. The occurrence of thick levee deposits suggests a stable channel. Gleyed mudstone indicates the influence of a shallow or fluctuating groundwater table in the overbank deposits (Tabor et al., 2017). Therefore, thick to very thick gleyed mudstone suggests frequent overbank flood resulting in continuous accumulation of fine sediments which rarely dry out completely (Sinha et al., 2005). Likewise, the rare occurrence of carbonaceous and variegated layers in the upper section of this facies association indicates flood plain was rarely exposed for a long time. High dispersion and repeated change in the paleo flow direction (Fig. 8.3) along with crevasse deposits suggests the sinuous nature of the channel. The well-developed fining-upward succession in sandstone beds, along with an increased proportion of flood plain with sheet flow deposits suggests a meandering river. The absence of lateral accretion and increased downstream accretion indicates bar deposits of the braided river system (Almeida et al., 2016). The presence of a large succession of overbank deposits bounding the sandstone beds and evidence of both the meandering and the braided

river system suggests an anastomosing river system (Bridge and Demicco, 2008; Makaske, 2001). Makaske (2001) suggested it is hard to demonstrate an anastomosing river system in the stratigraphic log, but normally anastomosing rivers show large flood plain deposits bounding the channel deposits (Miall, 2006). Sinha et al. (2005) also remarked in modern fluvial environment anastomosing rivers shows frequent and widespread overbank flooding with variable discharge. Therefore, FA4 is interpreted as deposits of an anastomosing river system.

### **8.3.5 Facies Association, FA5**

#### **8.3.5.1 Description**

This facies association is characterized by very thickly bedded poorly-sorted pebble to cobble conglomerate, coarse- to very coarse-grained sandstones and dull-yellowish-grey to purple-grey mudstones (Fig. 8.4-F). The thickness of individual conglomerate beds ranges from 0.8 to 2.0 m, which amalgamates to form >5.0 m thick succession. It consists of sub-rounded clast dominated by quartzite with moderate purple meta-sandstone and a few sandstone, mudstone and gneiss with very coarse-grained sand to granules matrix and dominantly shows non-erosional basal surface (Fig. 3.12). Stratified conglomerates (Fig. 8.1-J) are very rare and are limited at the lower section of this facies association. Dominating conglomerates are either inversely graded (Fig. 8.1-K) or structureless (Fig. 8.1-L). The thickness of sandstone ranges from 1.0 to 3.0 m with occasional >3.0 m. Sandstone beds are dominantly massive but few beds with slight fining-upward succession show faint planar cross-stratification. This sandstone consists of abundant pebbles (isolated), occasionally resembling pebbly sandstone. Mudstones are bioturbated without any pedogenic features with an average thickness of >4 m. This facies association FA5 is found in the Upper Siwaliks.

### **8.3.5.2 Interpretation**

Inversely graded and poorly sorted conglomerate suggests debris-flow deposits (Blair and McPherson, 1994; Miall, 2006, Nakayama and Ulak, 1999). Pebbly coarse- to very coarse-grained sandstones lacking well-developed fining-upward succession indicates a braided river system (Nakayama and Ulak, 1999). Thickly bedded mudstone with bioturbation suggests flood plain deposits (Miall, 2006). Thus, domination of inversely graded and poorly sorted conglomerate in this facies association helps to interpret FA5 as a deposit of debris flow dominated gravelly braided river system.

## **8.4 Depositional Process**

The study of the sedimentary facies in the present study reveals, three major fluvial systems: the meandering river, the anastomosing river and the braided river responsible for the deposition of the Siwalik succession of the Muksar Khola section (Fig. 8.5). Flood plain dominated fine-grained meandering river system (FA1) was recognized in the oldest succession. Around 10.5 Ma this overbank environment was dominated by large floods resulting in the flood dominated overbank environment (FA2). The actual time when this event occurred has been estimated using the oldest sedimentation rate of 0.33 mm/yr of Ojha et al. (2009) and the thickness of 210 m from the present study. These data give the tentative age of 10.6 Ma, comparing this age with the evidence from the other studies (discussed later), this age was estimated to be around 10.5 Ma. After 10.0 Ma increase in the domination of the sandy beds in the meandering river system (FA3) was observed. This river system intermittently encountered the deposition of the amalgamated sandstone succession for a limited period, which was mainly observed around 10.0 Ma, 9.4 Ma, 7.7 Ma and 6.2 Ma (Fig. 8.5). Deposition by the anastomosing river system (FA4) was observed after 5.9 Ma. After 3.5 Ma debris flow dominated gravelly braided river system (FA5) was observed.



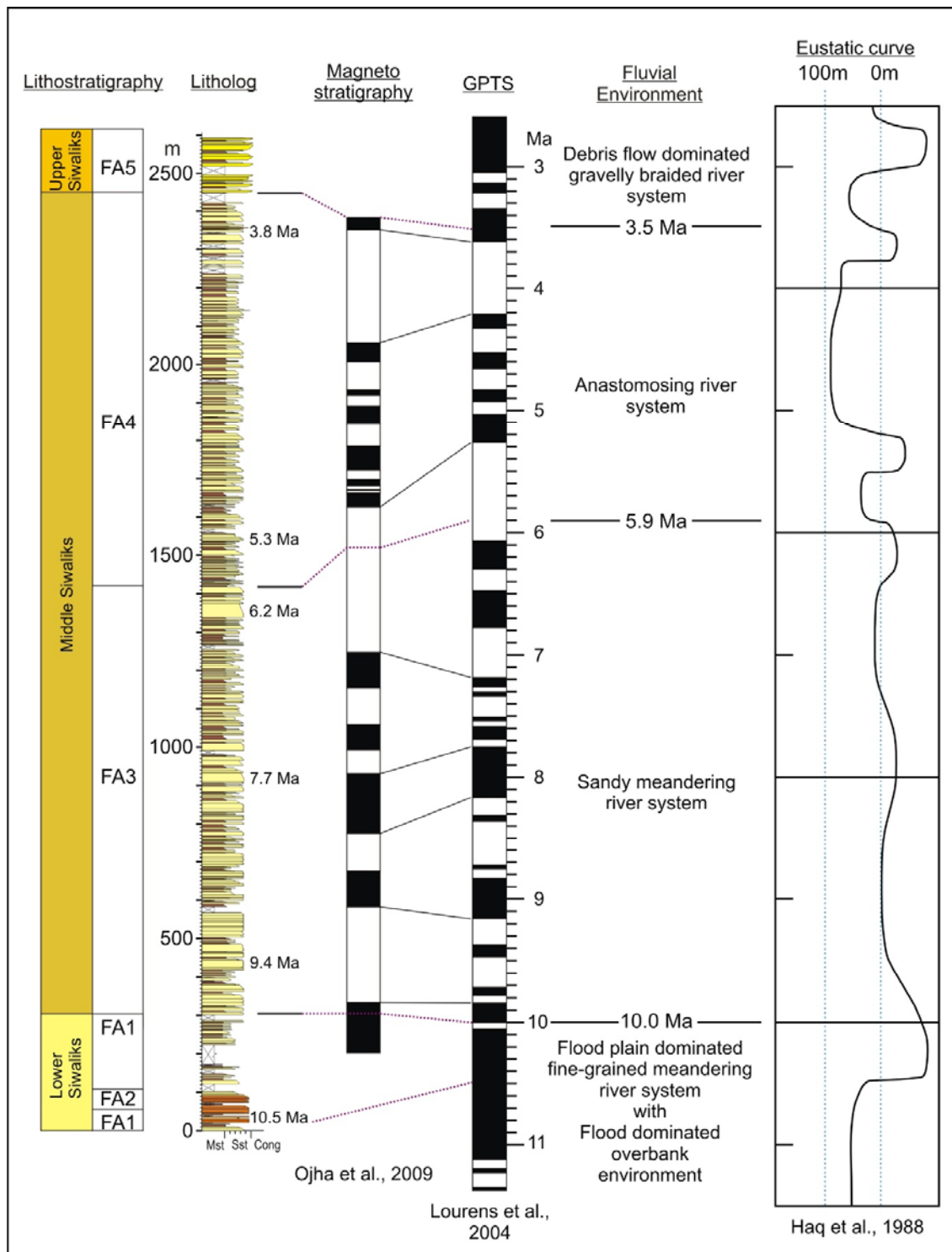


Figure 8.5: Evolution of the fluvial system in the present study area based on preexisting age data of the Ojha et al. (2009) (modified after Rai and Yoshida, 2021).

## CHAPTER IX

### DISCUSSION

#### **9.1 Lithostratigraphic comparison of the Siwalik Group with previous work**

Among the previous studies, Shrestha and Sharma (1996) and DMG (2011) geological map incorporates the Muksar Khola section. In their map, the Siwalik Group along the Muksar Khola section is classified as the Lower Siwaliks, lower member and the upper member of the Middle Siwaliks and the Upper Siwaliks but their geological maps are in large scale, therefore the location of the boundary is problematic, as well as their study lacks lithostratigraphic details. In this study, detailed lithostratigraphic classification is carried out adopting the previous classification of Shrestha and Sharma (1996). The present study reveals the litho boundaries differ from the previous studies: the thickness of the lower member of the Middle Siwaliks is more than that of the upper member, which is shown just opposite in the geological map of the previous study. Other than this their study does not report the occurrence of the intraformational conglomerate in the Lower Siwaliks. Shrestha and Sharma (1996) mention the occurrence of the conglomerate in the Lower Siwaliks of the northern belt bounded by the KTT and MBT (Fig. 2.4). This conglomerate was observed at the confluence of the Tawa Khola and the Baijnath Khola, south of the Tintale Village. In their stratigraphic column, they kept it at the base of the Lower Siwaliks as a basal conglomerate, separating it from the underlying Tintale Formation (Pre-Siwaliks) by an unconformity. Their basal conglomerate consists of sub-rounded to rounded pebbles of grey to white dolomites, banded white grey quartzites, dark-grey to black chert, purple and grey shale (Shrestha and Sharma, 1996). But, the present intraformational conglomerate differs from this basal conglomerate based on texture and composition and the position in the stratigraphic column. Additionally, the existence of a couple of folds in the Lower Siwaliks (Fig. 3.1) observed in the present

study is not mentioned in the previous study. Shrestha and Sharma (1996) mainly focused on this basal conglomerate, whereas DMG (2011) mapping was on a regional scale resulting in the scarcity of the details that was observed in this study. This fact suggests neither of the previous studies by Shrestha and Sharma (1996) and DMG (2011) considered the Siwalik Group along the Muksar Khola section in their study. Therefore, the present study is the first to investigate the detailed lithostratigraphy of the Siwalik Group along the Muksar Khola section.

## **9.2 Provenance**

In the present study, various proxies such as sandstone petrography, heavy mineral assemblage, the chemical composition of detrital tourmaline and garnet and Sr-Nd isotopes are used. These all proxies suggest the sediments were supplied from the TTH, the HHC and the LHS. Moreover, these proxies also clearly show the time when major changes occurred in the provenance. Therefore, provenance and its major change are interpreted based on these proxies.

### **9.2.1 Denudation of Higher Himalayan Crystalline**

The chemical composition of the garnet in five samples from the sandstone deposited before 7.7 Ma (MK-01 to MK-13) are comparatively rich in Mg (Figs. 6.3). Such Mg-rich garnet compositions are recorded in the rocks of the HHC (Arita, 1983; Neogi et al., 1998; Imayama et al., 2010; Saha, 2013). The heavy mineral assemblage and the Nd-Sr isotopic data from these samples also point to the HHC as the source area (Figs. 5.2, 5.2, 7.2). Precise observation of Figure 6.3 further reveals some changes in the garnet chemical composition. Among these samples, sample MK-01 shows low-Ca ( $\text{Prp}_{6-25}\text{GrS}_{<10}$ ) and Alm+Sps end

member (Type-Bi) garnet composition. This is slightly changed from sample MK-02 where most of the garnet composition falls in Type-B garnet composition ( $\text{Prp}_{<10}\text{Grs}_{15-25}$ ). In the eastern Nepal Himalaya occurrence of Type-Bi garnet with low-Ca and Alm-end member composition is recorded in a shallow part of the HHC such as the Barun gneiss and Makalu leucogranite (Fig. 6.4-A), whereas the above discussion suggests a deeper part of the HHC and LHS are the source of Type-B garnet composition ( $\text{Prp}_{<10}\text{Grs}_{15-25}$ ). The heavy mineral assemblage particularly detrital kyanite+sillimanite also show a similar trend. Kyanite and sillimanite are characteristics of the deeper part of the HHC and are observed to increase in the samples of younger age (Fig. 9.1). Therefore, this should be the result of a change in the provenance from the shallow to the deeper part of the HHC.

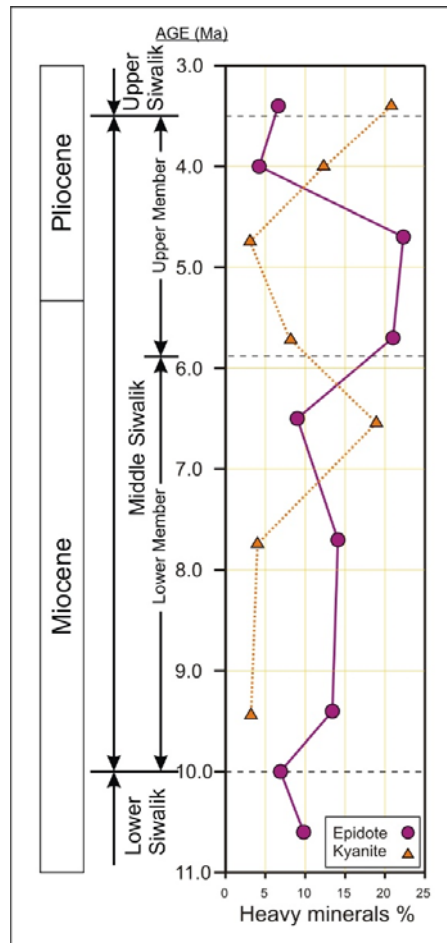


Figure 9.1: Vertical variation of the heavy minerals in the present study (modified after Rai et al., 2021). Depositional ages of samples are based on preexisting age data of the Ojha et al. (2009).

### 9.2.2 Exposure of MCT zone

After 6.5 Ma a decrease in detrital kyanite+sillimanite suggests a deeper part of the HHC was no longer the major source (Fig. 9.1). An increase in detrital epidote indicates either the provenance was shifted towards the shallow part of the HHC or the MCT zone (Fig. 9.1). Moreover, the chemical composition of garnet from the samples MK-17, MK-18 and MK-19 deposited after 6.5 Ma show a distinct increase in the proportion of Ca-rich garnet with an apparent absence of relative Mg-rich garnets ( $\text{Prp}_{>20}$ ) (Figs. 6.3, 9.2-A). The observed Ca-rich garnet composition ( $\text{Grs}+\text{And}_{35-50}$ ) in the present study has not been reported in the eastern Nepal Himalaya. Though in the previous study Ca-rich garnets were reported in the metabasic and calc-silicate rocks of the HHC in the Sikkim Himalaya (Fig. 6.4-A), the HHC of eastern Nepal Himalaya lacks such records. Moreover, if it was supplied by the HHC then it should appear in the samples from older succession which was sourced from the HHC. The absence of the Mg-rich garnets suggests LHS or a deeper part of the HHC as a source (Fig. 6.4-A). Heavy mineral assemblage identified under a petrographic microscope also clearly shows the difference in the Lower and Middle Siwaliks samples. Samples after 6.5 Ma shows a considerable increase in the heavy minerals characteristics of the LHS (Fig. 5.1). This result is also synchronous to the decrease in the feldspar content after 6.5 Ma (Fig. 4.4) and more negative  $\Sigma\text{Nd}(0)$  values after 7.5 Ma indicating an increase in the sediments from the LHS and MCT zone (Fig. 7.1). Similarly, Nd-Sr isotopic data also shows a cluster of samples from the upper member of the Middle Siwaliks in the zone of LHS (Fig. 7.2). In this account, the Ca-rich garnet composition ( $\text{Grs}+\text{And}_{35-50}$ ) observed in the present study should be related to the MCT zone, the calcareous rocks of the MCT zone in eastern Nepal which is thermally metamorphosed as reported by many researchers (Schelling, 1992; Imayama and Arita, 2008; Rai et al., 2016) could be the probable source.

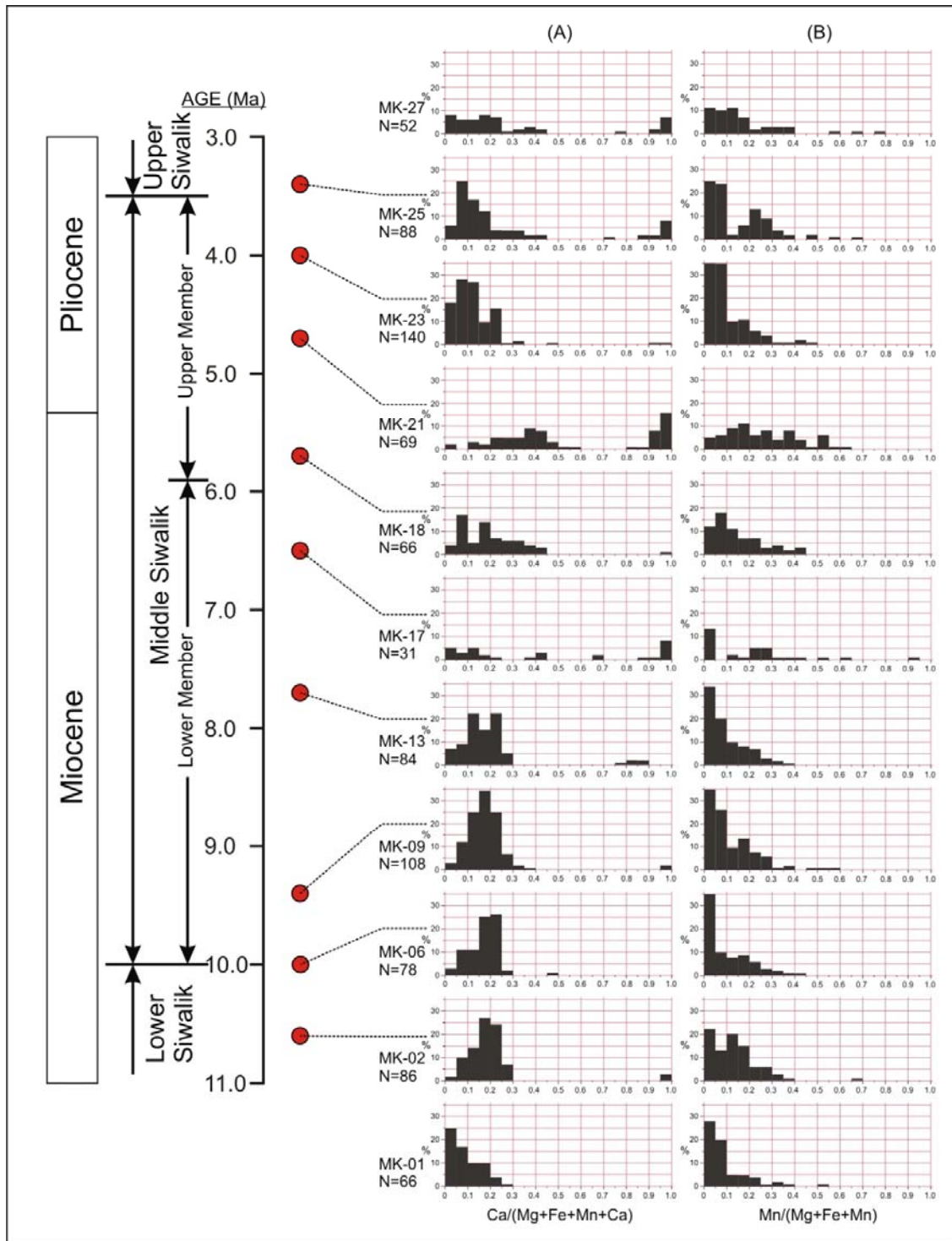


Figure 9.2: A)  $\text{Ca}/(\text{Mg}+\text{Fe}+\text{Mn}+\text{Ca})$  Compositional histogram of the detrital garnets. B)  $\text{Mn}/(\text{Mg}+\text{Fe}+\text{Mn})$  Compositional histogram of the detrital garnets. Depositional age is based on the preexisting age data of Ojha et al. (2009) (modified after Rai et al., 2021).

These assumptions also satisfy the result of the hinterland, Nakajima et al. (2020a) reported MCT zone of the Okhaldhunga window records the ZTF age of  $7.3 \pm 0.7$  Ma, suggesting by this time some part of the MCT zone was already exhumed. Therefore, probably MCT zone started to be exposed after 7.5 Ma. But the very negative  $\Sigma\text{Nd}(0)$  values (-20.9 to -21.2) and occurrence of detrital zoisite only in the sample from the younger succession in the present study (Figs. 5.1, 9.1) suggests a deeper part of the LHS was exposed only in the late Pliocene to Pleistocene.

### **9.2.3 Re-supply of sediments from the Higher Himalayan Crystalline**

The garnet chemical composition from sample MK-23 onwards reveals shallow part of the HHC increased the supply of sediments after 4.0 Ma. This is observed in Figure 6.3, which shows Type-A and Type-Bi garnet composition drastically increased with low-Ca ( $\text{Prp}_{6-25}\text{Grs}_{<10}$ ) and Alm-end member composition. This is similar to sample MK-01 which was supplied from the shallow part of the HHC. Moreover, an increase in the proportion of Mn-rich garnet composition is also observed after 4.7 Ma (Figs. 6.3, 9.2-B). Such Mn-rich garnets are characteristics of the inner or replacement zone of complex granitic pegmatites and aplites. In eastern Nepal Himalaya such pegmatites and aplites of several meters are observed around the Rp as a result of the intrusion of the Miocene leucogranites around Mt. Shinsha Pangma, the Mt. Everest-Makalu and the Mt. Jannu-Kangchenjunga region (Schelling, 1992; Imayama et al., 2010; Streule et al., 2010). Therefore, such Mn-rich garnets should be supplied from the Rp, a shallow part of the HHC. Similarly, Figure 9.1 shows after 4.0 Ma the proportion of detrital kyanite+sillimanite drastically increased suggesting the addition of the sediments from the deeper part of the HHC. In contrast, the continuous occurrence of the moderate Ca-rich garnet composition (Fig. 6.3) and the  $\Sigma\text{Nd}(0)$  values (Fig. 7.1) suggests the

MCT zone was still supplying the sediments. This concludes both the shallow and the deeper part of the HHC started to contribute sediment volume along with the MCT zone after 4.0 Ma.

#### **9.2.4 Tibetan Tethys Himalaya and the Gangdise belt in southern Tibet**

The result of sandstone petrography reveals a recycled orogeny as the provenance (Fig. 4.3). Such orogenic recycling occurs in various tectonic settings including suture belts, where sediments are sourced by the structurally juxtaposed continental sequence (Dickinson, 1985). The abundant volcanic lithic grains and unmetamorphosed mudstone grain with shared texture observed in the older succession should be supplied by such settings. The dominance of quartz grain and very low feldspar counts in the sandstone along with the subhedral shaped multi-cycled tourmaline (Fig. 6.1-B) formed due to authigenic growth during the diageneses process (Henry and Guidotti, 1985) suggests a continental source. Both the LHS and TTH are the candidates for such continental source but the uniform occurrence of titanite and ZTR index throughout the succession (Fig. 5.1) suggests TTH as the probable continental source.

Moreover, after 6.5 Ma of extreme Ca-rich garnets ( $\text{Grs}+\text{And}>90$ ) are observed (Figs. 6.3, 9.2-A). Such garnets could be sourced from either the calc-silicate rocks of the HHC or the skarn formation of the Gangdese belt north of the ITSZ. But none of any research in eastern, as well as central Nepal Himalaya, has reported such extreme calc-silicate rocks in the HHC (Arita, 1983; Imayama et al., 2010) (Fig. 7.9). Moreover, if the HHC was the source of such garnet it would have appeared in the younger samples discussed previously. Therefore, probably these extreme Ca-rich garnets ( $\text{Grs}>90$ ) should have been supplied by the Gangdese belt of southern Tibet suggesting paleo river depositing the Siwalik Group of the present study area had extended its catchment at the South Lasha Subterranean, north to the ITSZ probably around the late Miocene and was established after the Pliocene.



### **9.3 Exhumation history of the eastern Nepal Himalaya**

The change in the provenance discussed above should be a result of some hinterland tectonic phenomenon. Therefore, in this section, the exhumation history of the eastern Nepal Himalaya is discussed based on these observed provenance changes.

In the previous section, the chemical composition of detrital garnet in the sample MK-01 was characteristic of the shallow part of the HHC. Such garnets is observed to decrease from sample MK-02 (Fig. 6.3) with a marked increase in the proportion of detrital kyanite+sillimanite (Fig. 9.1). This change in the provenance should reflect the hinterland tectonics. Chirouze et al. (2012a) reported the signal of fast exhumation in their oldest studied samples (8.1 Ma – 6.6 Ma). Such late Miocene exhumation was regarded as a result of the LHS duplex structure in the western Nepal Himalaya (DeCelles et al., 1998, 2001; Robinson et al., 2001). But in the case of eastern Nepal Himalaya, the linear pattern of ZFT cooling age without any apparent age gap along the Okhaldhunga window (Nakajima et al., 2020a) suggests an absence of such a duplex structure. In eastern Nepal, an out-of-sequence thrust known as the Sun Koshi Thrust and the Tamor Khola Thrust is demarked by some researchers (Schelling and Arita, 1991; Schelling, 1992; Imayama and Arita, 2008). These thrusts exist in the southern border of the Ramechhap and Taplejung windows (Fig. 2.3) and are each other's extension and are considered as breaching thrusts (Schelling and Arita, 1991; Schelling, 1992; Imayama and Arita, 2008). The activation age of the Sun Koshi Thrust is not clear, but Arita et al. (1997) suggested such out-of-sequence thrust should be activated around 14.0–5.0 Ma. Moreover, the ZTF age of  $11.1 \pm 0.9$  Ma on the youngest rock of the RT Group reported by Nakajima et al. (2020a) from the southern part of the Okhaldhunga window just above the Sun Koshi Thrust suggests RT Group was already uplifted to the upper crust by this time. Therefore, this change in the provenance from the shallow to the deeper part of the HHC should be subjected to the activation of Sun Koshi Thrust. Based on

Nakajima et al. (2020a) ZTF age of  $11.1 \pm 0.9$  Ma from the sample just above the Sun Koshi Thrust and the provenance change observed around 10.6 Ma in the present study suggests probably Sun Koshi Thrust was activated around 11.0 Ma. Similarly, the provenance study revealed MCT zone supplied considerable sediment around 7.5-6.5 Ma. This suggests the Sun Koshi Thrust was still active during this time and at least exposed part of the MCT zone. In the previous study, Chirouze et al. (2012a) revealed fast exhumation of the eastern Nepal Himalaya was absent after 4.7 Ma. Also, Ojha et al., (2009) reported an increase in the sedimentation rate in the foreland basin of eastern Nepal Himalaya around 5.3 Ma due to the subsidence of the foreland basin resulting from MBT thrust loading. Probably around this time frame, the movement along the Sun Koshi Thrust was stopped due to the activation of the MBT. Therefore, the Sun Koshi Thrust in the eastern Nepal Himalaya was active from 11.0 Ma to 5.5 Ma (Fig. 9.3-A). Apart from this, the occurrence garnet with the chemical composition of low to moderate grossular and low pyrope ( $\text{Prp}_{<10}\text{Grs}_{15-25}$ ) (Fig. 6.3) suggests sediments were also supplied from the LHS and deeper part of the HCC. This could be a result of early exposure of some part of the LHS due to the activation of the Ramgarh Thrust. This thrust is believed to be active after  $\sim 15.0$  Ma until  $\sim 5.0$  Ma (DeCelles et al., 1998) and its occurrence is reported near the confluence of the Sunkoshi and the Arun River in eastern Nepal Himalaya (Pearson and DeCelles, 2005).

The observed increase in the sediment's characteristic of both the shallow as well as a deeper part of the HHC after 4.0 Ma must be subjected to the renewed exhumation of the HHC. One consideration for this later stage of exhumation may be the reactivation of the MCT (Copeland et al., 1991; Macfarlane, 1993), but the thermochronological studies of eastern Nepal Himalaya by Haviv et al. (2009) deny such possibility. This leads to the other consideration of the LHS duplex as presumed by various researchers (Schelling and Arita, 1991; Robinson et al., 2001; Haviv et al., 2009; Chirouze et al., 2012a). Therefore, the

formation of such duplex structure in the underlying LHS after 4.0 Ma could be the reason for the overall exhumation of the HHC, resulting in the supply of detritus from both the shallow and the deeper part of the HHC (Fig. 9.3-B).

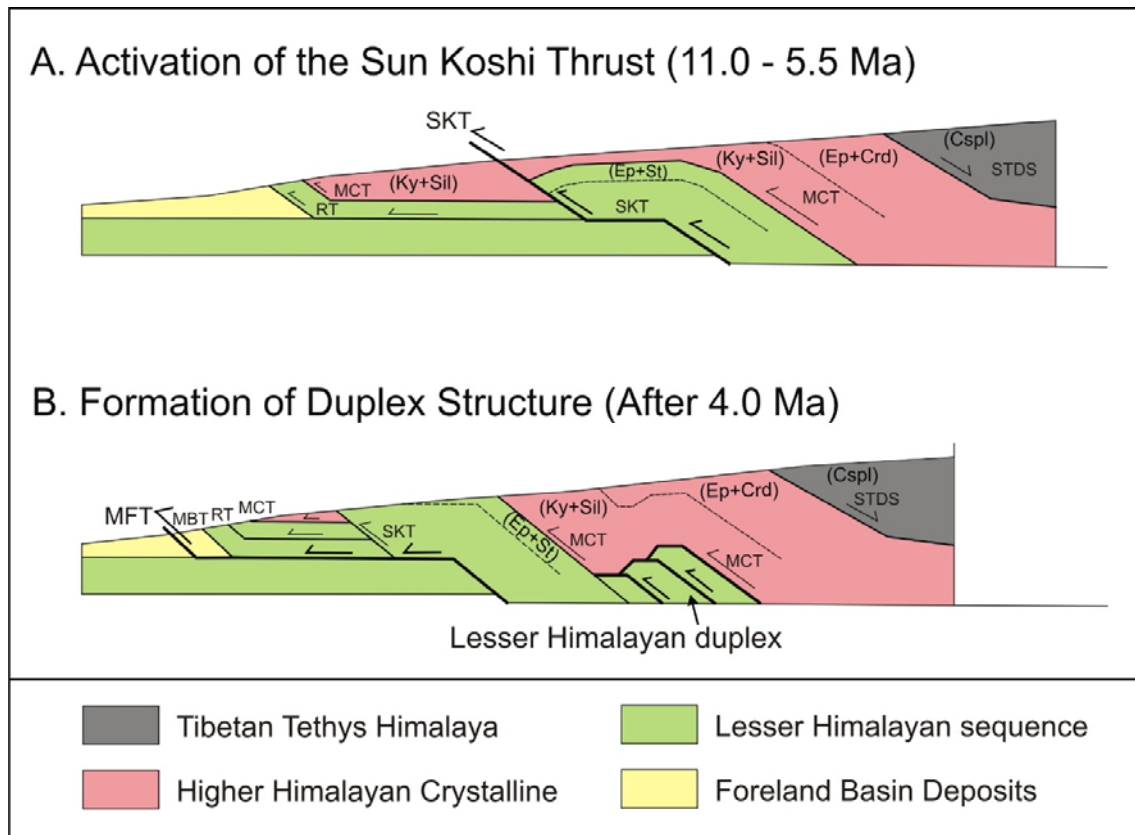


Figure 9.3: Schematic diagram showing two major exhumations of the eastern Nepal Himalaya. Abbreviations: STDS: South Tibetan Detachment system; MCT: Main Central Thrust; SKT: Sun Koshi Thrust; RT: Ramgarh Thrust; MBT: Main Boundary Thrust; Cspl: Chromian Spinal zone; Ep: Epidote zone; Crd: Cordierite zone; Ky+Sil: Al-silicate (Kyanite+sillimanite) zone; St: Staurolite zone.

In the western Nepal Himalaya, the formation of the duplex structure is reported around 12-10 Ma (Huyghe et al., 2001; Robinson et al., 2003; Bernet et al., 2006), in the central Nepal Himalaya at around 9.8 Ma (Herman et al., 2010) and in the Sikkim Himalaya at around 12-10 Ma (Landry et al., 2016), but in eastern Nepal, the out-of-sequence thrust was activated around this time. The timing of the duplex formation in other parts of the Himalaya and the out-of-sequence thrust in the eastern Nepal Himalaya is quite coeval. This reveals thrusting

was generated along the Himalaya around the mid-Miocene. In other parts of the Himalaya such thrust was imbricated to form a duplex structure, whereas in the eastern Nepal Himalaya it breached to surface developing out-of-sequence thrust.

#### 9.4 Significance of the differences observed in isotopic values

The trend of change in the  $\Sigma Nd(0)$  value in the present study is also quite similar to the results of the central and the western Nepal Himalaya (Robinson et al., 2001; Huyghe et al., 2005), with a slight difference in the  $\Sigma Nd(0)$  values and timing of this change. The isotope analysis in the present study reveals mainly two differences in the results: the slight difference in the  $\Sigma Nd(0)$  values between leached and unleached samples, and the difference between the result of the present with the previous result of Robinson et al. (2001) (Figs. 7.1 and 9.4).

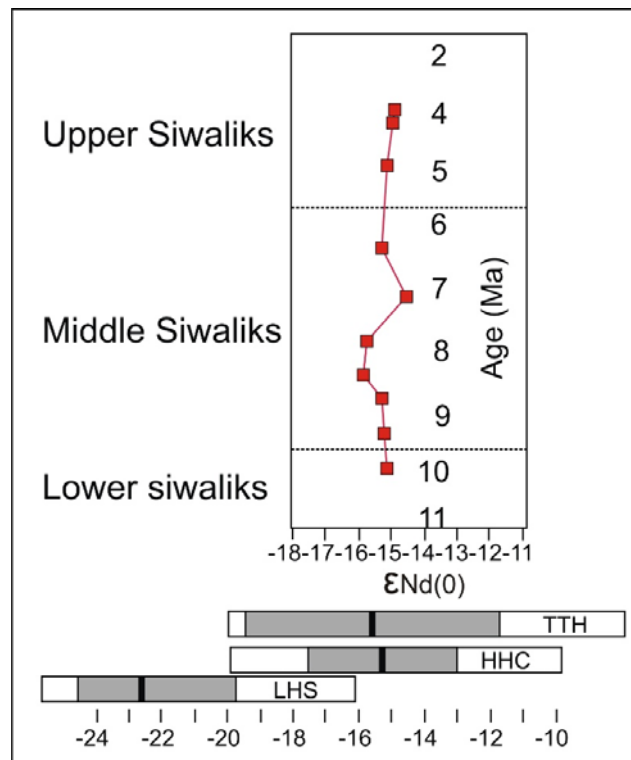


Figure 9.4:  $\Sigma Nd(0)$  values of the Siwalik Group samples of the Muksar Khola section from the previous study of Robinson et al. (2001).

During the acid leaching, minerals like garnet, amphibole, epidote, biotite are minimized or eliminated (Zhang et al., 2019). The slight difference observed in the result of the unleached and leached samples in the present study may be due to the elimination of such minerals or the contamination of samples in the process of sample collection, storage and preparation. Despite the small difference in all samples, the  $\Sigma\text{Nd}(0)$  values from samples MK-17 and MK-18 deposited around 6.5 and 5.7 Ma shows considerable variation in the  $\Sigma\text{Nd}(0)$  values. Unleached samples show the  $\Sigma\text{Nd}(0)$  value characteristic of the MCT zone or the LHS whereas leached samples  $\Sigma\text{Nd}(0)$  values suggest HHC. Various studies have shown rare earth minerals is highly compatible with epidote (Giere and Sorensen, 2004). The present study shows an increase in the garnet with chemical composition characteristic of the MCT zone as well as epidote sourced from the MCT zone around this time. Therefore, removal of such minerals during the acid leaching should have destroyed the neodymium with the signature of the MCT zone enriching the HHC signature.

The difference of the present isotopic result with the previous result of Robinson et al. (2001) along the same section is quite interesting. But the other provenance indicator in the present study supports the  $\Sigma\text{Nd}(0)$  values of the present study. Another important fact is that most of the Upper Siwaliks along the Himalaya and the present study consists of conglomerates supplied by the LHS rocks (Nakayama and Ulak, 1999; Sigdel and Sakai, 2016). In the present study more negative  $\Sigma\text{Nd}(0)$  values (-20.9 to -21.2) observed in the samples from Upper Siwaliks justifies this result (Fig. 7.1). But Robinson et al. (2001)  $\Sigma\text{Nd}(0)$  values suggest the HHC and the TTH as the source for the Upper Siwaliks (Fig. 9.4). The main difference in the Robinson et al. (2001) and present studies is the samples that were taken into consideration. Their samples were taken from the siltstone whereas in the present study we considered sandstone. Difference in the  $\Sigma\text{Nd}(0)$  value due to the variation in the grain size was also reported in the Siwalik Group of the Jawalamukhi section in northwestern India,

where  $\Sigma\text{Nd}(0)$  value of the conglomerate matrix was more negative compared to siltstone (Najman et al., 2009). Various studies have shown grain size variation has some effects on the Nd isotopic composition (Goldstein et al., 1984; Grousset et al., 1992; Yokoo et al., 2004; Kanayama et al., 2005; Feng et al., 2009). Even if the difference in the grain size is considered as a factor for difference in the  $\Sigma\text{Nd}(0)$  values, there should be a similarity in the trend of  $\Sigma\text{Nd}(0)$  change in the present and previous study. Therefore, this difference should not be controlled only by grain size. Another possibility is the fluid dynamics of the flowing water. Various experiments demonstrated fine-grained sediments are transported for a longer distance compared to coarse-grained sediments (Church and Hassan, 1992; Parsons and Stromberg, 1998). Since data from the present study suggest sediments were continuously supplied by the TTH as well as the HHC. These sediments supplied from the TTH and the HHC comparatively travelled for a longer distance resulting in more disintegration compared to the LHS sediments. These resulting grains were clustered in different grain-sized beds due to the hydraulic sorting. Hence, fine-grained sediments like mudstone and siltstone were dominated by the TTH and the HHC sediments, whereas coarse-grained sediments like sandstone were dominated by the LHS sediments. Moreover, such sediment sorting processes also lead to chemical variability between bedload and suspended load (Garzanti et al., 2010; 2011). Therefore, the difference in the present and the previous study results must be subjected to the difference in provenance.

### **9.5 Intensification of the monsoon in eastern Nepal Himalaya**

The present study records a unique occurrence of a large succession of the intraformational conglomerate in the Lower Siwaliks, which has not been reported in any of the other Siwalik sections. Interestingly, it has been excluded in the previous studies along the Muksar Khola section (Quade et al., 1995; Robinson et al., 2001; Chirouze et al., 2012a). As discussed in

the previous section such intraformational conglomerates are developed due to the collapse of the distal alluvial terraces. Alluvial terraces are developed as a result of cyclic deposition of alluvial sediments and incision of alluvial plain (Oldknow and Hooke, 2017). The reason for river incision is considered a complex mixture of various processes like climate, tectonics, eustatic fluctuations (Mukerji, 1990; Miall, 2006; Tandon et al., 2006; Oldknow and Hooke, 2017). The deposition time of this intraformational conglomerate (10.5 Ma) dramatically matches with the timing of rapid sea-level fall at 10.5 Ma (Haq et al., 1988), exhumation of the eastern Nepal Himalaya around 11.0 Ma and monsoon intensification in the central Nepal Himalaya at 10.5 Ma (Nakayama and Ulak, 1999).

Zaitlin et al. (1994) suggested in the region proximal to the coastal areas rivers undergo incision during sea-level fall and accommodation during its rise. Since an open marine to the deltaic environment has been reported in the Siwalik Group of northeast India, this fall of sea level can be taken into consideration. If this was the case in which Lower Siwaliks of the present study was deposited near the coast and was subsequently affected by the change in the sea level, then the Lower Siwaliks sediments should have preserved some effects of tides (Simms et al., 2006; Guliotta et al. 2016). But the absence of such tide-influenced deposits in the present study does not strongly support this idea. Moreover, Simms et al. (2006) mentioned if rapid sea-level fall is the reason for river incision as observed in the eustatic curve of Haq et al. (1988) then it results in a narrow and V-shaped valley rather than the formation of terraces (Fig. 8.5).

Similarly, Climate cause variations in the discharge which affects the transport capacity of the rivers resulting in the incision. River incisions are initiated when the discharge in the river increases more than that needed for transporting the available sediment (Bogaart et al., 2003). Such high discharge is initiated during strengthened or abnormal monsoon season (Plink-Bjorklund, 2015). The event of river incision due to intensified monsoon resulting in

increased precipitation was also recorded in the western Ganga plains around 10.0 ka to 5.0 ka (Tandon et al., 2006). The depositional age of this intraformational conglomerate member also shows coeval timing to the exhumation of eastern Nepal Himalaya as discussed above. Present provenance study shows exhumation of the hinterland started around 11.0 Ma due to the activation of the Sun Koshi Thrust. Also, various studies show exhumation of the hinterland was observed throughout the Himalaya range around this period (Huyghe et al., 2001; Robinson et al., 2003; Bernet et al., 2006; Herman et al., 2010; Landry et al., 2016). Such change in the paleogeography due to hinterland exhumation affects the atmospheric circulation (Raymo and Ruddiman, 1992) by creating the barrier which blocks the moisture-laden winds, triggering a strong monsoon (Kutzbach et al., 1989; Clift and Webb, 2018). Studies show the rapid rise of the Himalaya range resulted in either the onset of the South Asian monsoon or its intensification (Clift et al., 2008; Webb et al., 2017). Therefore, the alluvial terrace should have resulted from the river incision on the foreland basin favoured by the increased discharge during the starting phase of monsoon intensification. The massive coarse-grained sheet flow deposits observed within the beds of the intraformational conglomerate (Fig. 8.2, Sc-1) also give evidence of such increased discharge. Since the Lower Siwaliks is characterized by very fine- to fine-grained sediments, the occurrence of such coarse grain sediments is quite unusual. These coarse-grained sediments should be deposited upstream during the normal flow conditions because sediments particle size and their transportation distance are inversely proportional (Church and Hassan, 1992; Parsons and Stromberg, 1998). Though the present study lacks evidence related to tide-influenced deposits, such a drastic decrease in the sea level should have affected the regional base level of the foreland basin which favoured this climatically controlled incision. During normal flow conditions, flood plains were exposed in the incised valley (Fig. 9.5-A). As the monsoon intensification got stronger the water volume in the river channel also increased and could not



be accommodated on the pre-existing channel, these cause the water level to increase and submerge the overbank scoring and undercutting the distal alluvial terrace (Fig. 9.5-B). The increase in distance from the main channel, as well as the sudden increase in sediment load from collapsing terrace, resulted in a slowdown of the transport capacity. This might be the reason for the aggradation of thick intraformational conglomerate with angular to sub-angular mud clast.

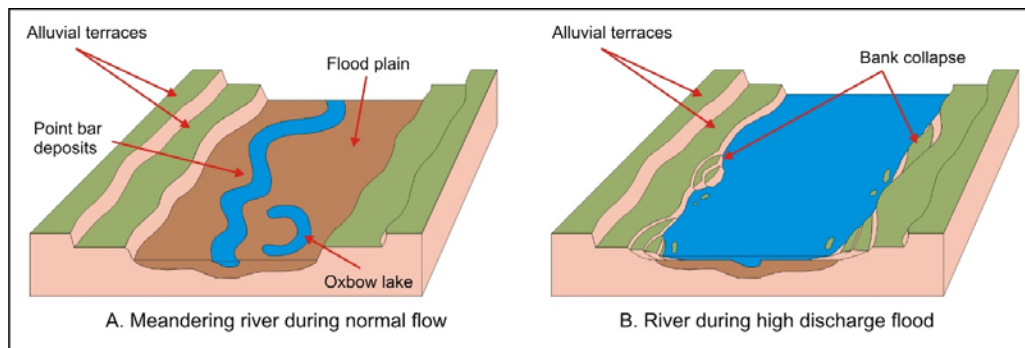


Figure 9.5: Schematic diagram showing A) Meandering river during normal flow condition and B) River during high discharge.

Therefore, the occurrence of intraformational conglomerate at around 10.5 Ma in the present study should be the result of high-magnitude floods, suggesting the intensification of monsoon in the eastern Nepal Himalaya. This monsoon intensification should be related to the exhumation of the eastern Nepal Himalaya after 11.0 Ma due to the activation of the Sun Koshi Thrust.

## 9.6 Controlling factors for change in river system

The nature of the channel is determined by the channel gradient and the discharge of fluid (Leopold and Wolman, 1957). Whereas the gradient of the channel is controlled by the sea-level change and tectonics (Smith and Smith, 1980; Smith, 1986; Burbank, 1992). Similarly, tectonics and climate control the discharge (Goodbred and Kuehl, 2000; Clift and Giosan,

2014; Clift, 2017). Therefore, tectonics, climate and sea-level change are the main factors that control the fluvial system in the foreland basin. As discussed above the fast exhumation of the hinterland in the eastern Nepal Himalaya started only after 11.0 Ma which intensified the monsoon in this region. Moreover, the eustatic curve proposed by Haq et al. (1988) show raised sea level before 10.5 Ma (Fig. 8.5). This raised sea level and absence of rapid exhumation of the hinterland should probably result in the low gradient of the foreland basin and also monsoon should have been comparatively weak. In the modern fluvial environment of the Himalayan foreland basin, flood events with bankfull discharge are observed during the period of the summer monsoon (June–September) when the precipitation is very high (Bhatta and Nakamura, 2005; Burbank et al., 2012). In contrast, during the monsoon depressions, rivers lack such bankfull discharge and large flood plains are exposed. Therefore, a low gradient of the foreland basin should have favoured the meandering river system and this meandering river continuously changed its channel creating a large flood plain. Moreover, since monsoon was comparatively weak during this period therefore bankfull discharge should have been rare, resulting in the domination of the flood plain (Fig. 9.6).

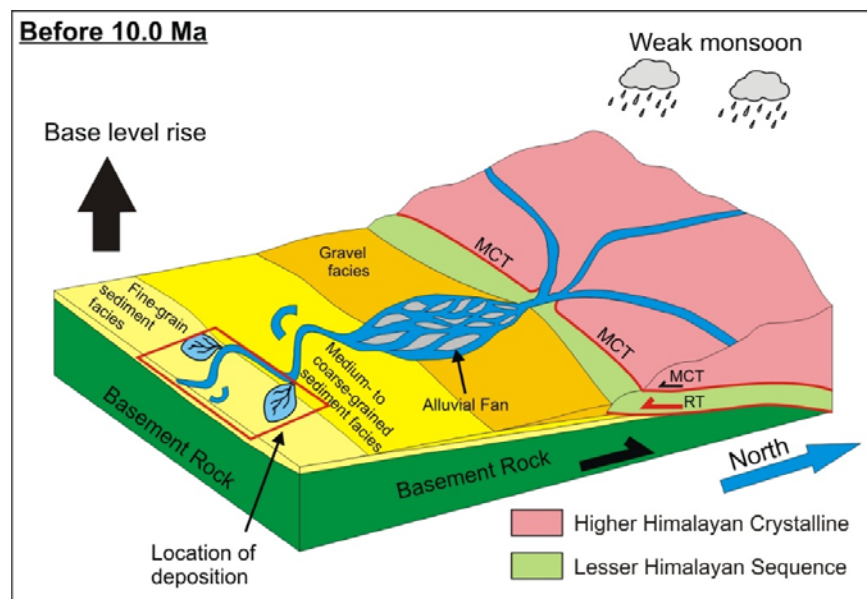


Figure 9.6: Schematic diagram showing a depositional model for FA1 and FA2 concerning climate and tectonics. Abbreviations: RT: Ramgarh Thrust; MCT: Main Central Thrust.

After 11.0 Ma, the braided river system should have dominated the river system. The fast exhumation of the hinterland and monsoon intensification in this region as discussed above should have resulted in an increase in the slope angle as well as sediment supply. In the central and western Nepal Himalaya, the evolution of the braided river was nearly coeval to such fast hinterland exhumation. These fast hinterland exhumations were observed around 12.0–10.0 Ma in the western and 9.8 Ma in the central Nepal Himalaya due to the formation of duplex structure (DeCelles et al., 1998; Robinson et al., 2001). These resulted in the evolution of the braided river system around 9.5 Ma in the Karnali River section and 6.5 Ma in the Surai Khola section (Table: 3). However, the present study area lacks a braided river system and is dominated by the meandering river system. This should be resulted due to the difference in the exhumation history of the eastern Nepal Himalaya to its central and western counterparts. The formation of duplex structure results in the imbrication of multiple thrusts exposing a large proportion of the underlying LHS. This regional uplift results in enhanced erosion of the hinterland increasing the sediment supply. In the eastern Nepal Himalaya, the observed fast exhumation was due to the out-of-sequence thrust known as the Sun Koshi Thrust. Such single breaching thrust results in hinterland uplift, but a large area is not exposed due to which the rate of erosion is comparatively less than the duplex structure. Robinson et al. (2001) also suggested less erosional unroofing due to the absence of such duplex structure in eastern Nepal Himalaya. The provenance data from the present study also suggests most of the sediments were supplied from the HHC, a significant amount of the sediments from the LHS was supplied only after 7.5 Ma. To build the relationship between the river system and the exhumation history of the hinterland, Burbank (1992) explanation about the fan growth in the foreland basin as a result of hinterland uplift seems significant. He suggested if mountain uplift is due to the thrusting, more subsidence and deposition take place in the proximal parts of the foreland basin restricting the fan growth due to the resultant

crustal thickening. Similarly, if enhanced erosion is the cause of such uplift, then due to the isostatic adjustment flexural uplift occurs which promotes the growth of the fan to a more distal part of the basin. Therefore, the possible explanation for domination of the meandering river system during the deposition of the lower member of the Middle Siwaliks may be the asymmetric subsidence of the foreland basin and less sediment supply due to the absence of duplex structure and activation of the out-of-sequence thrust in the eastern Nepal Himalaya. This resulted in the accommodation of maximum sediments in the proximal part of the foreland basin causing sediment starvation in the distal part where the present lower member of the Middle Siwaliks was being deposited (Fig. 9.7).

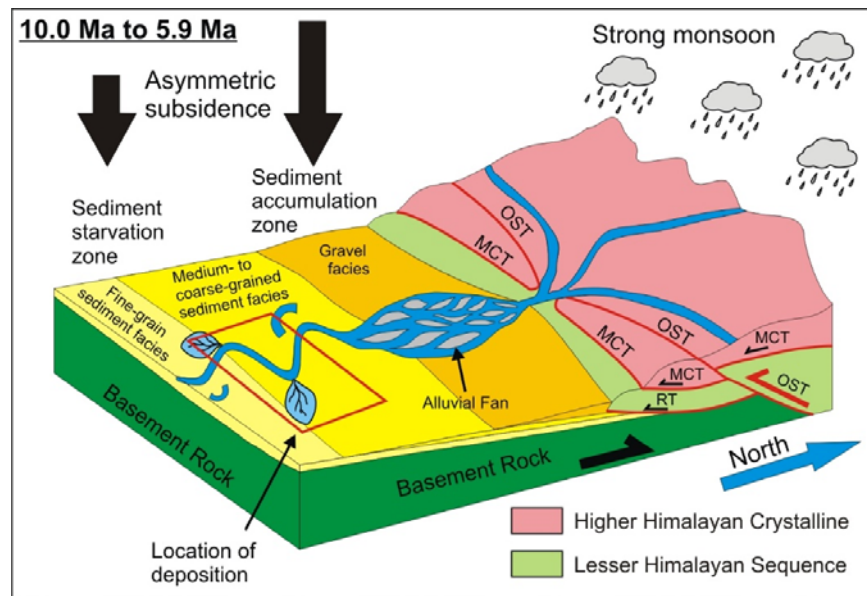


Figure 9.7: Schematic diagram showing a depositional model for FA3 concerning asymmetric subsidence due to activation of the OST. Abbreviations: RT: Ramgarh Thrust; MCT: Main Central Thrust; OST: Out-of-sequence Thrust.

Despite this, the periodic occurrence of amalgamated sandstone beds in limited thickness around 9.4 Ma, 7.7 Ma and 6.2 Ma within the sandy meandering river system (FA3) indicates some potentiality of the river to change its condition. As mentioned previously, amalgamated sandstone beds are the results of deposition in the central part of the channel with a high

deposition rate, high flow energy with a high erosive capacity. This cause erosion of the upper fine sediments of the underlying succession or beds and deposition of another succession (Zhang et al., 2017). Such character of the rivers occurs during the increased precipitation triggering landslides or slope failure in the hinterland resulting in the flood with high sediment supply. Researchers of the Quaternary evolution of the Indus and Ganges deltas suggested that sediment supply increased during times of strong monsoon (Goodbred and Kuehl, 2000; Clift and Giosan, 2014; Clift, 2017). The sub-angular to angular elongated mud clasts (up to 20-30 cm in length) observed at the bottom of these amalgamated sandstones (Fig. 3.8-A) also give evidence of high discharge. Therefore, this episodic occurrence of a very thick succession of amalgamated sandstone could be the result of high discharge due to the frequent fluctuation in the rate of precipitation for a certain time frame suggesting the episodic nature of high precipitation. Such episodic intensification of monsoon is also observed in the Ramnagar sub-basin of NW India which resulted in significant changes in fluvial sedimentology (Singh et al., 2012). But in the present study area, it is hard to justify as the climatic condition of eastern and central Nepal was quite similar and no such episodic nature of monsoon intensification was observed in central Nepal. Autogenetic effects such as lateral migration, sinuosity change, accretion, erosion could also cause such sandstone amalgamation. The amalgamated sandstone also shows evidence of lateral shifting of the channel, but such autogenetic effect is controlled by seasonal fluctuations in discharge (Slingerland and Smith, 2004; Durkin et al., 2017).

On the other hand, surprisingly the periodic occurrence of these amalgamated sandstone successions in the present study is synchronous to the timing of sea-level change (Fig. 8.5). Moreover, the Siwaliks along the eastern Himalaya sections records the open marine and deltaic environment till 5.0 Ma at Bhutan and 7.5 Ma at the Kameng River section of Arunachal Pradesh (Coutand et al., 2016; Taral et al., 2019). But as mentioned above any

evidence related to open marine or deltaic environment is absent in the present study area. Since the sea-level change has a regional effect and considering the proximity of the Sikkim-Darjeeling area to the present study area the effect of the sea-level change cannot be ignored. Though the foreland basin of eastern Nepal was not close to the coastal area, still its geometry should have been influenced by this change in sea level which cause the synchronization of lithological variation to the sea-level fluctuation. Therefore, this occasional occurrence of this very thick succession of the amalgamated sandstone must be the result of the interplay between high discharge and sea-level change in an asymmetrically subsidized foreland basin.

Climate and geological conditions are the factors that control anastomosing rivers (Nanson and Kington, 1996). In anastomosing rivers, anabranching of new channels is facilitated by the avulsion process (Makaske, 2001). The rate of avulsion is determined by the rate of sedimentation (Bridge and Leeder, 1979; Bryant et al., 1995) and rise in base level (Tornqvist, 1994; Makaske, 2001). An increase in these factors increases the frequency of avulsion. The base-level rise is further controlled by sea-level rise (Smith and Smith, 1980) and the subsidence of the foreland basin (Smith 1986). Anastomosing rivers are also observed in the modern fluvial environment: parts of the Koshi and the Baghmata Rivers in the Himalaya foreland basin (Gohain and Parkash, 1990; Jain and Sinha, 2004). The tectonic subsidence of the foreland basin and sedimentological readjustment are considered as the factors controlling anabranching on parts of these rivers (Jain and Sinha, 2004; Sinha et al., 2005). The subsidence of the foreland basin (Ojha et al., 2009) and sea-level rise (Fig. 8.5) fulfil the condition needed for the rise in the base level of the foreland basin. Regarding the sedimentological readjustment, a previous study along the Muksar Khola section reports a change of the C3 plants to C4 plants around this time (Quade et al., 1995). Such change indicates an increase in the seasonality suggesting strengthening of monsoon (Quade et al.,

1989; 1995) and an arid to a semi-arid climatic condition where bankfull discharge rarely exceeds more than once a year (Gibling et al., 1998). Under such conditions, sediments are deposited in the channel during the normal period, this makes the channel lose the accommodation capacity during the next flood favouring avulsion (Makaske, 2001). Such avulsion initiating anabranching of the new channel due to climatic conditions are reported by various researchers (Brizga and Finlayson, 1990; Mack and Leeder, 1998). Therefore, a rise in the base level due to subsidence of the foreland basin and sea-level rise and strengthening of the monsoon could also have favoured the anastomosing river during the deposition of the upper member of the Middle Siwaliks (Fig. 9.8).

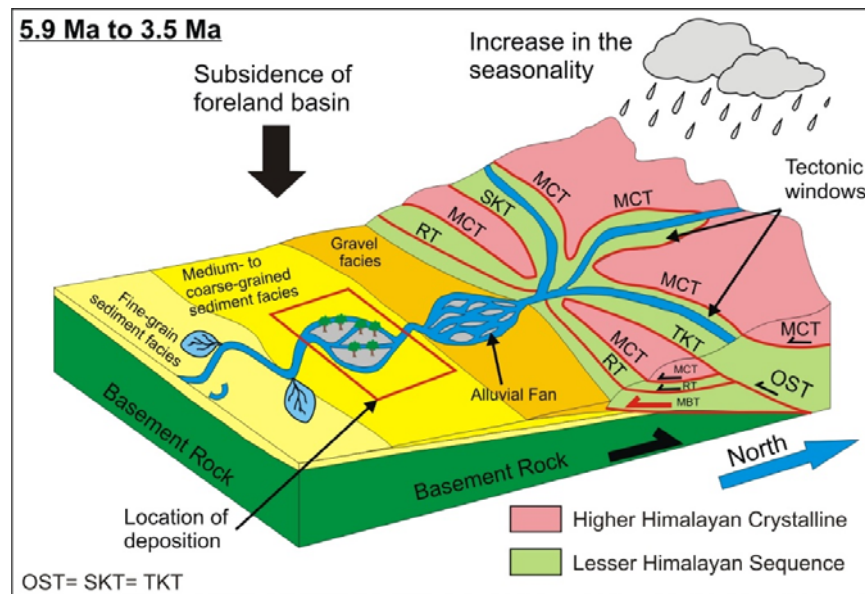


Figure 9.8: Schematic diagram showing a depositional model for FA4 concerning tectonics and climate. Abbreviations: MBT: Main Boundary Thrust; RT: Ramgarh Thrust; MCT: Main Central Thrust; SKT: Sun Koshi Thrust; TKT: Tamor Khola Thrust; OST: Out-of-sequence Thrust.

Debris-flow deposits are characteristics of inner alluvial fan (Blair and McPherson, 1994; Miall, 2006). In both, the paleo and modern fluvial systems boulder conglomerates are reported on such deposits (Singh et al., 1993; Nakayama and Ulak, 1999; Ulak and Nakayama, 2001; Miall, 2006; Sigdel and Sakai, 2016). In the present study, the observed

conglomerate lacks such boulder size clast and is interbedded with very thick beds of sandstone and mudstone. Most of the Siwalik sections rarely mentioned the occurrence of such thick beds of mudstone and sandstone, in some sections where it is observed are also in limited thickness (Nakayama and Ulak, 1999; Ulak and Nakayama, 2001; Sigdel and Sakai, 2016). Therefore, the absence of such boulder conglomerate with the presence of very thick beds of mudstone and sandstone suggests the present study area has a different depositional setting.

The occurrence of such thick sandstone and mudstone beds within conglomerate beds are also reported in the Nalad Khad and Jawalamukhi sections of the Himachal Pradesh (Brozovic and Burbank, 2000). Brozovic and Burbank (2000) suggested this as the result of long-distance gravel flow and presented three hypotheses that could explain this gravel progradation: (1) Increase in the discharge and sediment flux of rivers due to climate change, (2) Initiation of the MBT led to significant erosional relief developing above it and (3) Decrease in the subsidence rates of the foreland basin due to gradual hinterland erosion without major tectonism. The first consideration regarding climate change is quite obtuse in the present scenario since eastern and central Nepal Himalaya shares a similar climate but the Siwalik Group in the central Nepal Himalaya lacks such lithology. The second consideration suggests the development of erosional relief initiated by the MBT. But in eastern Nepal, the activation of the MBT started around 5.5 Ma (Rai et al., 2021) before the deposition of conglomerate and duplex structure started to develop at the rear part of the Himalaya after 4.0 Ma (Fig. 9.3). This leads to the third consideration; the formation of the duplex structure caused a gradual hinterland erosion. Moreover, crustal thickening at the rear of the Himalaya probably reduced the MBT thrusting. Both gradual hinterland erosion and reduction in the thrusting of the MBT caused a decrease in the subsidence rate of the foreland basin, resulting in the gravel progradation (Fig. 9.9).



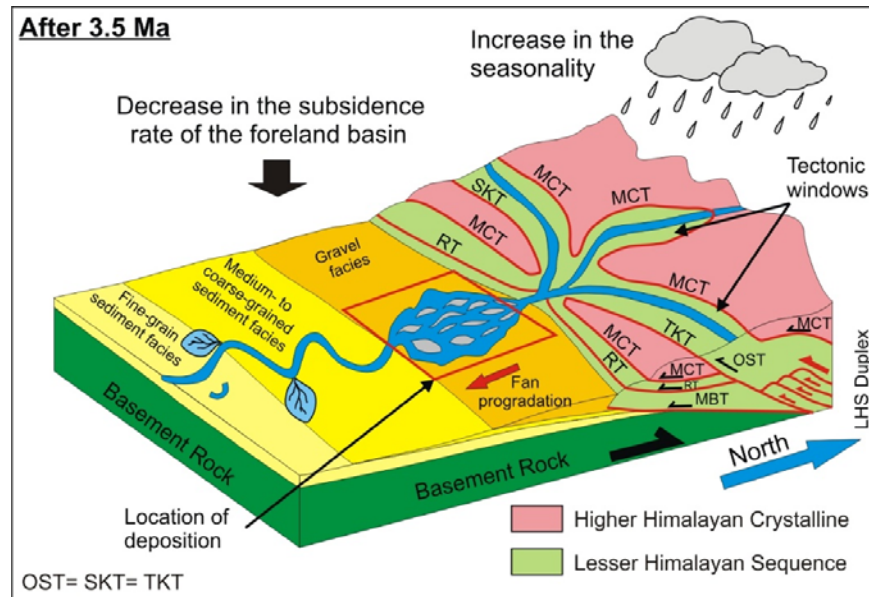


Figure 9.9: Schematic diagram showing a depositional model for FA5 concerning tectonics. Abbreviations: MBT: Main Boundary Thrust; RT: Ramgarh Thrust; MCT: Main Central Thrust; SKT: Sun Koshi Thrust; TKT: Tamar Khola Thrust; OST: Out-of-sequence Thrust.

Another possible reason may be the sharing of a depositional basin by two or more rivers. In the modern foreland basin of the Himalaya, numerous small rivers exist in between the large river throughout the Himalaya. These small rivers drain local catchment area which is isolated by the catchment area of the big river system (Willis, 1993b). The mudstone facies are generally deposits of an overbank environment (Miall, 2006). The presence of such very thick overbank deposits is quite rare in the braided river environment. On the other hand, conglomerate clast composition is characteristic of LHS rock, which is confined in a narrow belt in the eastern Nepal Himalaya and different tectonic windows of eastern Nepal (Schelling, 1992; Pearson and DeCelles, 2005). If conglomerate was supplied by the big rivers, then there should be a considerable amount of gravel characteristic of HHC rock. Therefore, the existence of such small river systems draining local areas into the common or proximal basin with the large river (Fig. 9.10) could be another possibility. Therefore, either a decrease in the subsidence rate of the foreland basin due to the formation of duplex structure at the rare part

of the Himalaya or the existence of the small alluvial fans may be the reason for the occurrence of thick sandstone and mudstone within the conglomerate beds.

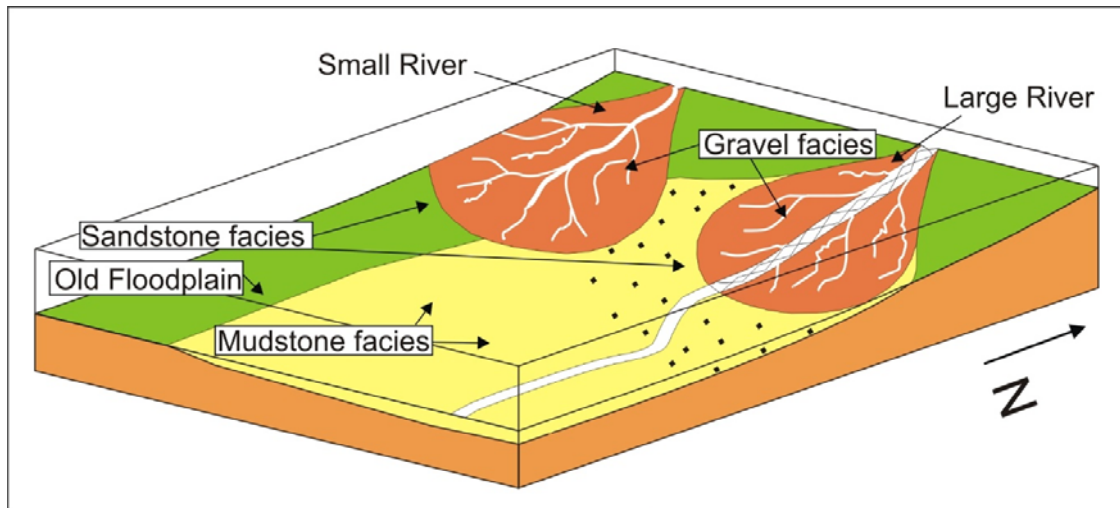


Figure 9.10: Schematic diagram showing the existence of small and large rivers in an interfan area.

### 9.7 Shifting of the foreland basin

In the previous sections, the effects of sea-level change which was synchronous to the appearance of intraformational conglomerate and thick amalgamated sandstone before 5.9 Ma was discussed. The sea-level fall was quite sudden at 10.5 Ma, this was coeval to the event of river incision and formation of the thick intraformational conglomerate in the present study. Between 10.0–5.9 Ma this change in the sea level was moderate but still it had some effects on the lithological variation (Fig. 8.5). Meanwhile, the eustatic curve also shows several fluctuations in the sea level after 5.9 Ma (Fig. 8.5). During the deposition of FA4, the sea level was comparatively raised (Fig. 8.5), this regionally affected the foreland basin rising its base level and favoured anastomosing river environment. But sedimentological log of the present does not show any drastic variation in the lithology during this sea-level fall (Figs. 3.9 & 8.5). Considering the lithology, it shows an increasing trend of grain size. FA1 is dominated by fine-grained sediments whereas in FA4 coarse-grained sediments dominate. If

the basin was stationary, then all the facies associations identified in this study should have been dominated by similar grain size. Therefore, this could be the result of the continuous shifting of the depositional basin towards the hinterland. FA1 and FA2 were deposited away from the hinterland resulting in the domination of fine sediments and more proximal to the coast which favoured the foreland geometry for river incision during the sea-level fall. During the deposition of FA3, the location of the deposition on the basin was shifted closer to the hinterland resulting in an increase in fine- to medium-grained sediments. This increase in the distance from the coastal area was still influenced by the fluctuation in the sea level resulting in variation in the lithology. Whereas, during the deposition of FA4, medium- to coarse-grained sediments suggests this facies association was deposited even close to the hinterland. The rise in the sea level affected the regional geometry of the foreland basin rising its base level, but the effects of short-term changes observed in the sea-level changes were overprinted by other factors like hinterland tectonics and climate as discussed above. Deposition of the FA5 is characterized by an abrupt increase in the grain size, suggesting the location of the deposition proximal to the hinterland. This argument suggests the Miocene foreland basin of the Himalaya was continuously shifting towards the hinterland resulting in coarsening upward succession in the fluvial deposits of the Siwalik Group as illustrated in Figures 9.6, 9.7, 9.8 and 9.9.

## **9.8 Correlations**

### **9.8.1 Lithostratigraphy**

The erosion of the uprising Himalaya in the north produced enormous sediments which were deposited in a foreland basin by the fluvial system. These sediments extend collinear south of the Himalaya from east to west. The fluvial system which is regarded as the depositing agent is controlled by the tectonics, climate and geomorphology of the hinterland. The present

study shows, change in this hinterland phenomena and proximity of basin to the hinterland through time resulted in vertical variation of lithology in the Siwalik group i.e., the Lower, Middle and Upper Siwaliks. Similarly, numerous fluvial systems were responsible for the deposition of these sediments along the Himalaya foreland basin. Each river and its depositional environment were independent to each other and had their own characteristic hinterland phenomena and climate (Nakayama and Ulak, 1999; Robinson et al., 2001; Ulak and Nakayama, 2001; Yin, 2006; Ojha et al., 2009; Vogeli et al., 2017). Moreover, the modern fluvial system shows the continuous shift of its course throughout time (Singh et al., 1993). This must be the reason for the differences observed in the lateral variation in the Siwalik succession, which lead to three-fold to five-fold lithological classifications of the Siwalik Group in various studies.

Four-fold to five-fold classification system (Tokuoka et al., 1986; Willis 1993b; Dhital et al., 1995; Sah et al., 1994; Zaleha 1997; Sigdel et al., 2011) uses various parameters such as grain size, sandstone and mudstone ratio, sandstone composition, fossils content etc. These parameters are dependent on the hinterland phenomena and the local depositional settings. Hence it differs from each river depositional basin and catchment area, and obviously, it is complicated to find the similarities in the Siwalik Group of different sections. Therefore, the correlation of the Siwalik Group based on four to five-fold classification with local stratigraphic names is quite complicated. On the other hand, three-fold classification of the Siwalik Group which is based on the grain size i.e., the Lower, Middle and Upper Siwaliks (Pilgrim, 1913; Auden 1935; Ulak, 2004, 2009; Adhikari et al., 2018) is quite similar throughout the Siwalik succession of the Himalaya. The present study also adopted this classification (Table 9.1) and correlation with other sections of the Siwalik Group is carried out based on a three-fold classification (Table 9.1).

Table 9.1: Lithostratigraphic classification and correlation of the present study with representing Siwalik Group of central and western Nepal (modified after Rai and Yoshida, 2020).

Age (Ma)	Karnali River Sigdel et al., 2011	Surai Khola Dhital et al., 1995	Tinau Khola Tokuoka et al., 1986	Hetauda-Amlekhganj -Bakia Khola Sah et al., 1994; Ulak and Nakayama' 1998	Muksar Khola Present Study		
1	Pani Khola Formation	Dhan Khola Formation	Deorali Formation	Churia Mai Formation	Upper Siwaliks		
2	Kuine Formation	Dobata Formation	Chitwan Formation	Churia Khola Formation			
3	Baka Formation Upper member Middle member Lower member	Surai Khola Formation Upper member Middle member Lower member	Binai Khola Formation Upper member Middle member Lower member	Amlekhganj Formation Upper member Middle member Lower member	3.5 Ma		
4					Chor Khola Formation Shivagarhi member Jungli Khola member	Arung Khola formation Upper member Middle member Lower member	Middle Siwaliks (Upper member)
5							
6		Chisapani Formation Upper member Middle member Lower member			Rapti Formation Upper member Middle member Lower member	5.9 Ma	
7	Lower member		Lower member	Lower member			
8						Lower member	Lower member
9	Lower member	Lower member	Lower member				
10				Lower member	Lower member	Lower member	10.0 Ma
11	Lower member	Lower member	Lower member				Lower member
12				Lower member	Lower member	Lower member	
13	Lower member	Lower member	Lower member				Lower member
14				Lower member	Lower member	Lower member	
15	Lower member	Lower member	Lower member				Lower member

### 9.8.2 Fluvial environment

This study was started, whether an asynchronous exhumation of the Himalaya west to east affected the fluvial system and its environment. For this, the Surai Khola and the Karnali River section in the central and western Nepal Himalaya respectively were considered for comparison and discussion (Fig. 9.11) and the results are presented in Table: 9.2. In this comparison, the hinterland climate and tectonics, and the probable catchment of the paleo river system are considered.

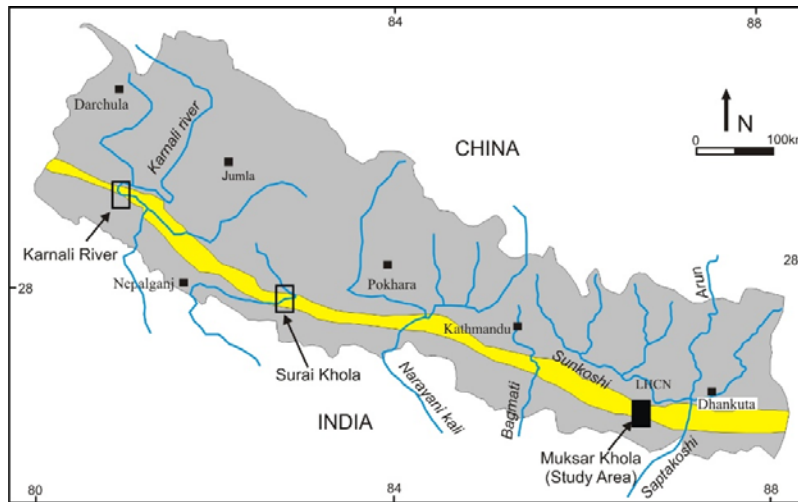


Figure 9.11: Map of Nepal showing the Siwalik Group (yellow belt) and the location of the Karnali River, the Surai Khola and the Muksar Khola section (modified after Rai and Yoshida, 2021).

Table 9.2: Comparison of the fluvial systems of the present study area with different Siwalik Group of Nepal (modified after Rai and Yoshida, 2021).

Age (Ma)	Karnali River		Surai Khola	Muksar Khola
	Huyghe et al. (2005)	Sigdel and Sakai (2016)	Nakayama and Ulak (1999)	Present Study
1		Debris flow dominated braided river system	Debris flow dominated braided river system 1.0 Ma	
2	Gravelly braided fluvial system	~2.0 Ma	Gravelly braided river system 2.5 Ma	Debris flow dominated gravelly braided river system 3.5 Ma
3		Gravelly braided river system	Anastomosed river system 4.0 Ma	
4	~3.9 Ma	~3.9 Ma	Shallow sandy braided river system	Anastomosing river system
5	5.5-5.6Ma	Shallow sandy braided river system	Deep sandy braided river system 6.5 Ma	5.9 Ma
6	SSBFS *	6.0 Ma	Flood flow dominated meandering river system 9.5 Ma	Sandy meandering river system 10.0 Ma
7	6.4 Ma	Deep sandy braided river system	Fine grained meandering river system	
8	Deep sandy braided fluvial system			
9	9.5 Ma	9.6 Ma		
10	Sandy flood flow-dominated meandering fluvial system	Flood flow dominated meandering river system		
11	12.6-12.7 Ma			
12	FFDMFS **			
13	13.1 Ma	13.5 Ma		
14	Fine grained meandering river system with low discharge and relief	Fine grained meandering river system		
15				

\*Shallow sandy braided fluvial system  
 \*\*Flood flow-dominated meandering fluvial system  
 \*\*\*Flood dominated overbank environment

The climatic condition of the Muksar Khola section and the Surai Khola section in eastern and central Nepal was almost similar (Quade et al., 1995) and the intensification of monsoon was also observed at the same time 10.5 Ma in eastern Nepal (present study), 10.5 Ma in central Nepal (Nakayama and Ulak, 1999). Similarly, the tectonic history of the central and western Nepal Himalaya was quite similar (Robinson et al., 2001; Bernet et al., 2006). This is also reflected in the fluvial environment which shows a similar trend of change in the river system (Table: 9.2). In both sections, the change from the meandering river to the braided river was subjected to the regional tectonics of the hinterland and climate was regarded as the factor for the change from the deep braided to the shallow braided river (Nakayama and Ulak, 1999; Huyghe et al., 2005; Sigdel and Sakai, 2016). These changes appeared much earlier in the Karnali River section due to the large catchment basin of the paleo Karnali River (Huyghe et al., 2005). Though the Muksar Khola section was also reported to be deposited by a river with a large catchment area (Chirouze et al., 2012a), the fluvial environment of the present study in eastern Nepal Himalaya is much different.

Regardless of the different similarities of the present study area with the Surai Khola and the Karnali River section, the only difference between the present study area with these two sections is the hinterland tectonics and the proximity to the sea. Therefore, this difference in the fluvial system must be due to the difference in the tectonics history of the hinterland and the proximity to the sea. The thrust loading subjected to duplex formation in central and western Nepal must have developed sufficient relief, triggering a significant amount of erosion (Huyghe et al., 2001). This cause flexural uplift across the foreland basin (Burbank, 1992) causing a significant increase in channel slope and sediment supply. Probably this causes the braided river system to dominate in the Siwalik Group of central and western Nepal. In the present study, the absence of such early duplex structure in the hinterland and rise in the base level of the foreland basin (as discussed above) caused the starvation of

sediment supply and low gradient resulting in domination of meandering river systems. Therefore, the major difference of fluvial environment observed in the present study concerning the Surai Khola and Karnali River section must be subjected to the difference in hinterland tectonics. Though, the change in sea level also has some role in the deposition of the Siwalik sediments in the present study.



## CHAPTER X

### CONCLUSION

Following conclusions are drawn from the present study of the Siwalik Group along the Muksar Khola section.

- The Siwalik succession along the Muksar Khola section is classified into the Lower Siwaliks, the lower member of the Middle Siwaliks, the upper member of the Middle Siwaliks and the Upper Siwaliks.
- Based on the pre-existing age data, the Lower Siwaliks was deposited before 10 Ma and consists of light-grey, very fine- to fine-grained sandstone interbedded with grey to olive black mudstone to siltstone. This study also records the occurrence of a very thick succession of the intraformational conglomerate in the Lower Siwaliks.
- Middle Siwaliks was deposited in between 10.0–3.5 Ma. It is characterized by the domination of sandstone and is divided into the lower member and the upper member based on the lithology, composition, thickness, and induration of sandstone. The lower member deposited before 5.9 Ma consists of fine- to medium-grained “salt and pepper” sandstone with greenish-grey to olive-grey mudstone. While the upper member is characterized by less indurated, light grey to white, medium- to very coarse-grained sandstone with an increased proportion of grey, dark grey to black mudstone.
- The Upper Siwaliks consists of a poorly sorted, clast supported conglomerate associated with very thickly bedded coarse- to very coarse-grained sandstone and very thickly bedded dull yellowish-grey to grey colour mudstone.
- The analysis of sandstone petrography, heavy minerals assemblage, detrital tourmaline and garnet chemical composition, and Sr-Nd isotope reveals TTH, HHC and LHS as the provenance of the Siwalik Group in the eastern Nepal Himalaya. This study also reveals a frequent change in provenance which was observed around 10.6 Ma, 7.5 Ma and 4.0 Ma.

Around 10.6 Ma provenance was shifted from shallow to the deeper part of the HHC. LHS supplied a considerable amount of sediments after 7.5 Ma and the HHC enhanced the sediment supply after 4.0 Ma.

- The occurrence of volcanic lithic fragments and the uniform occurrence of titanite and ZTR index suggests sediments were continuously supplied from TTH. Moreover, the occurrence of detrital chromian spinel and extreme Ca-rich garnet (Grs+And>90) suggests the Siwalik group in the Muksar Khola section was also supplied from the ITSZ.
- The eastern Nepal Himalaya experienced two-stage of exhumations due to activation of the Sun Koshi Thrust at around 11.0 Ma and the formation of the LHS duplex structure after 4.0 Ma.
- Facies analysis reveals twelve depositional facies and five facies associations. These facies associations are interpreted as the flood plain dominated fine-grained meandering river (FA1), flood dominated overbank environment (FA2), Sandy meandering river (FA3), anastomosing river (FA4), and debris flow dominated braided river (FA6). The interplay between hinterland tectonics, climate and sea-level change is considered as the controlling factors for these changes in the fluvial environment. The absence of rapid exhumation of the hinterland, raised sea level and comparative weak monsoon before 10.0 Ma resulted in the flood plain dominated fine-grained meandering river (FA1). High discharge due to intensified monsoon and rapid fall of the sea level around 10.5 Ma caused flood dominated overbank environment (FA2). Asymmetric subsidence of the foreland basin and less sediment supply due to the absence of duplex structure and activation of the out-of-sequence thrust resulted in the sandy meandering river (FA3) after 10.0 Ma. After the 5.9 Ma rise in the base level due to subsidence of the foreland basin and sea-level rise along with the strengthening of the monsoon gave rise to the

anastomosing river (FA4). Debris flow dominated braided river (FA6) after 3.5 Ma was resulted due to the increase in the proximity of the basin close to the hinterland.

- The genesis of an intraformational conglomerate reveals intensification of the monsoon started around 10.5 Ma in the eastern Nepal Himalaya as a result of hinterland exhumation.
- The Sr-Nd Isotopic values used for the determination of the provenance of the Siwalik Group sediments are dependent on the size of the sediment grains.
- Change in the location of deposition due to continuous shifting of the foreland basin towards hinterland resulted in the coarsening upward succession in the sediments of Siwalik Group.
- This study reveals the difference in the exhumation of the eastern Nepal Himalaya from its central and western Nepal counterparts. This significantly brought a difference in the fluvial environment in the Himalaya.

## REFERENCES

- Adhikari, S.K., Sakai, T., 2015. Lithostratigraphy of the Siwalik Group, Khutia Khola section, Far Western Nepal Himalaya. *Journal of Geological Society* 49, 29–39.
- Adhikari, D., Shrestha, K., Adhikari, P., Paudyal, K.N., Paudel, L., 2018. Geological study of Chatara–Barahakshetra section, Sunsari-Udayapur District, eastern Nepal. *Bulletin of Department of Geology, Tribhuvan University* 20-21, 49–58.
- Almeida, R.P., Freitas, B.T., Turra, B.B., Figueiredo, F.T., Marconato, A., Janikian, L., 2016. Reconstructing fluvial bar surfaces from compound cross-strata and the interpretation of bar accretion direction in large river deposits. *Sedimentology* 63, 609–628.
- Amatya, K.M., Jnawali, B.M., 1994. Geological map of Nepal: Kathmandu, Nepal. Department of Mines and Geology, scale 1:1 000 000.
- Appel, E., Rosler, W., Cornivus, G., 1991. Magnetostratigraphy of the Miocene-Pleistocene Surai Khola, Siwaliks in west Nepal. *Geophysical Journal of International* 105, 423–426.
- Appel, E., Rosler, W., 1994. Magnetic polarity stratigraphy of the Neogene Surai Khola section (Siwaliks, SW Nepal). *Himalayan Geology* 15, 63–68.
- Arita, K., 1983. Origin of the inverted metamorphism of the Lower Himalayas, central Nepal. *Tectonophysics* 95, 43–60.
- Arita, K., Dallmeyer, R.D., Takasu, A., 1997. Tectonothermal evolution of the Lesser Himalaya, Nepal: constraints from  $^{40}\text{Ar}/^{39}\text{Ar}$  ages from the Kathmandu Nappe. *Island Arc* 6, 372–385.
- Armstrong, H.A., Allen, M.B., 2011. Shifts in the Intertropical Convergence Zone, Himalayan exhumation and late Cenozoic climate. *Geological Society of America* 39, 11–14.
- Auden, J.B., 1935. Traverses in the Himalaya. *Records of Geological Survey of India* 69, 123–167.
- Baldwin, J.R., Knorring, O.V., 1983. Compositional range of Mn-garnet in zoned granitic pegmatites. *Canadian Mineralogist* 21, 683–688.
- Baral, U., Lin, D., Chamlagain, D., 2016. Detrital zircon U-Pb geochronology of the Siwalik Group of the Nepal Himalaya: implications for provenance analysis. *International Journal of Earth Sciences* 105, 921–936.
- Bernet, M., Van Der Beek, P.A., Pik, R., Huyghe, P., Mugnier, J.L., Labrin, E., Szulc, A., 2006. Miocene to Recent exhumation of the central Himalaya determined from combined detrital zircon fission-track and U/Pb analysis of Siwalik sediments, western Nepal. *Basin Research* 18, 393–412.
- Bhatt, B.C., Nakamura, K., 2005. Characteristics of Monsoon Rainfall around the Himalaya Revealed by TRMM Precipitation Radar. *American Meteorological Society* 133, 149–165.
- Blair, T.C., McPherson, J.G., 1994. Alluvial fans and their natural distinction from rivers based on morphology, hydraulic processes, sedimentary processes, and facies assemblages. *Journal of Sedimentary Research* 64, 450–489.
- Bordet, P., 1961. In: *Recherches géologiques dans l'Himalaya du Népal région du Makalu*. Paris Editions du Centre National de la Recherche Scientifique, Paris.
- Bordet, P., Colchen, M., Le Fort, P., 1972. Some features of the geology of the Annapurna range Nepal Himalaya. *Himalayan Geology* 2, 537–563.
- Bouvier, A., Vervoort, J.D., Patchett, P.J., 2008. The Lu-Hf and Sm-Nd isotopic composition of CHUR: constraints from unequilibrated chondrites and implications for the bulk composition of terrestrial planets. *Earth and Planetary Science Letters* 273, 48v57.

- Bogaart, P.W., Van Balen, R.T., Kasse, C., Vandenberghe, J., 2003. Process-based modelling of fluvial system response to rapid climate change I. Model formulation and generic applications: *Quaternary Science Reviews* 22, 2077–2095.
- Boos, W.R., Kuang, Z., 2010. Dominant control of the South Asian monsoon by orographic insulation versus plateau heating. *Nature* 463, 218–222.
- Bridge, J.S., Leeder, M.R., 1979. A simulation model of alluvial stratigraphy. *Sedimentology* 26, 617–644.
- Bridge, J.S., Demicco, R.V., 2008. *Earth surface processes, landforms and sediment deposits*. Cambridge University Press, UK.
- Brizga, S.O., Finlayson, B.L., 1990. Channel avulsion and river metamorphosis: the case of the Thomson river, Victoria, Australia. *Earth Surface Processes and Landforms* 15, 391–404.
- Brouand, M., 1989. *Petrogenese des migmatites de la Dalle du Tibet (Himalaya du Nepal)*. (Thesis). Institute National Polytechnique de Lorraine, Nancy, 217pp.
- Brozovic, N., Burbank, D.W., 2000. Dynamic fluvial systems and gravel progradation in the Himalayan foreland. *Geological Society of America Bulletin* 112, 394–412.
- Bryant, M., Falk, P., Paola, C., 1995. Experimental study of avulsion frequency and rate of deposition. *Geology* 23, 365–368.
- Burbank, D.W., 1992. Causes of recent Himalayan Uplift deduced from deposited patterns in the Ganges basin. *Nature* 357, 680–683.
- Burbank, D.W., Bookhagen, B., Gabet, E.J., Putkonen, J., 2012. Modern climate and erosion in the Himalaya. *Comptes Rendus Geoscience* 344, 610–626.
- Burchfiel, B.C., Chen, Z., Hodges, K.V., Liu, Y., Royden, L.H., Deng, C., Xu, J., 1992. The South Tibetan Detachment System, Himalayan orogen: extension contemporaneous with and parallel to shortening in a collisional mountain belt. *Geological Society of America Special Papers* 269, 1–41.
- Burianek, D., Filip, J., Novak, M., 2003. Tourmalines of the Metabasite Zone, Brno Batholith. *Geolines* 16, 19.
- Cerling, T.E., Harris, J.M., MacFadden, B.J., Leakey, M.G., Quade, J., Eisenmann, V., Ehleringer, J.R., 1997. Global vegetation change through the Miocene/Pliocene boundary. *Nature* 389, 153–158.
- Chirouze, F., Bernet, M., Huyghe, P., Erens, V., Dupont-Nivet, G., Senebier, F., 2012a. Detrital thermochronology and sediment petrology of the middle Siwaliks along the Muksar Khola section in eastern Nepal. *Journal of Asian Earth Sciences* 44, 94–106.
- Chirouze, F., Dupont-Nivet, G., Huyghe, P., Van der Beek, P., Chakraborty, T., Bernet, M., Erens, V., 2012b. Magnetostratigraphy of the Neogene Siwalik Group in the far eastern Himalaya: Kameng section, Arunachal Pradesh, India. *Journal of Asian Earth Sciences* 44, 117–135.
- Chirouze, F., Huyghe, P., Van der Beek, P., Chauvel, C., Chakraborty, T., Dupont-Nivet, G., Bernet, M., 2013. Tectonics, exhumation, and drainage evolution of the eastern Himalaya since 13 Ma from detrital geochemistry and thermochronology, Kameng River Section, Arunachal Pradesh. *Geological Society of America Bulletin* 125, 523–538.
- Church, M., Hassan, M.A., 1992. Size and distance of travel of unconstrained clasts on a streambed. *Water Resources Research* 28, 299–303.
- Clift, P.D., 2017. Cenozoic sedimentary records of climate-tectonic coupling in the Western Himalaya. *Progress in Earth and Planetary Science* 4, 1–22.
- Clift, P.D., Hodges, K.V., Heslop, D., Hannigan, R., Van Long, H., 2008. Calves G. Correlation of Himalayan exhumation rates and Asian monsoon intensity: *Nature Geoscience* 1, 875–880

- Clift, P.D., Giosan, L., 2014. Sediment fluxes and buffering in the post-glacial Indus Basin. *Basin Research* 26, 369–386.
- Clift, P.D., Webb, A.G., 2018. A history of the Asian monsoon and its interactions with solid Earth tectonics in Cenozoic South Asia. In: Treloar, P.J., Searle, M.P., (eds.), *Himalayan Tectonics: A Modern Synthesis*. Geological Society of London, Special Publications 483, 631–652.
- Copeland, P., Harrison, T.M., Hodges, K.V., Maruélol, P., Le Fort, P., Pecher, A., 1991. An early Pliocene thermal disturbance of the Main Central Thrust, central Nepal: Implications for Himalayan tectonics. *Journal of Geophysical Research: Solid Earth* 96, 8475–8500.
- Corvinus, G., 1993. The Siwalik group of sediments at Surai Khola in western Nepal and its palaeontological record. *Journal of Nepal Geological Society* 9, 21–35.
- Cotton, J.M., Cerling, T.E., Hoppe, K.A., Mosier, T.M., Still, C.J., 2016. Climate, CO<sub>2</sub>, and the history of North American grasses since the Last Glacial Maximum. *Science Advance* 2, e1501346.
- Coutand, I., Barrier, L., Govin, G., Grujic, D., Hoorn, C., Dupont-Nivet, G., Najman, Y., 2016 Late Miocene-Pleistocene evolution of India-Eurasia convergence partitioning between the Bhutan Himalaya and the Shillong Plateau: New evidences from foreland basin deposits along the Dungsam Chu section, eastern Bhutan. *Tectonics* 35, 2963–2994.
- Critelli, S., Ingersoll, R.V., 1994. Sandstone Petrography and Provenance of the Siwalik Group (northwestern Pakistan and western-southeastern Nepal). *Journal of Sedimentary research* 64, 815–823.
- Crook, K.A.W., 1974. Lithogenesis and geotectonics: the significance of compositional variation in flysch arenites (graywackes), in modern and ancient geosynclinal sedimentation. *SEPM, Special publication* 19, 304–310.
- DeCelles, P. G., Gehrels, G. E., Quade, J., Ojha, T. P., Kapp, P. A., Upreti, B. N., 1998. Neogene foreland basin deposits, erosional unroofing, and the kinematic history of the Himalayan fold-thrust belt, western Nepal. *Geological Society of America Bulletin* 110, 2–21.
- DeCelles, P.G., Robinson, D.M., Quade, J., Ojha, T.P., Garzzone, C.N., Copeland, P., Upreti, B.N., 2001. Stratigraphy, structure, and tectonic evolution of the Himalayan fold-thrust belt in western Nepal. *Tectonics* 20, 487–509.
- Deer, W.A., Howie, R.A., Zussman, J., 1992. *An Introduction to the Rock-Forming Minerals*. Longman, Hongkong.
- Deer, W.A., Howie, R.A., Zussman, J., 1997. *Rock-forming minerals, volume 1A: Orthosilicates*, (2nd Ed.). Geological Society, London.
- Dhital, M.R., Gajurel, A. P., Pathak, D., Paudel, L. P., Kizaki, K., 1995. Geology and structure of the Siwaliks and Lesser Himalaya in the Surai Khola-Bardanda area, mid-western Nepal. *Bulletin of Department of Geology, Tribhuvan University* 4, 1–70.
- Dhital, M.R., 2015. *Geology of Nepal Himalaya Regional Perspective of the Classic Collided Orogen*. Springer, Switzerland.
- Dickinson, W.R. and Suczek, C., 1979. Plate tectonics and sandstone compositions. *American Association of Petroleum Geologists Bulletin* 63, 2164–2182.
- Dickinson, W.R., 1985. Interpreting detrital modes of greywacke and arkose. *Journal of Sedimentary Petrology* 40, 695–707.
- DMG, 2011, *Geological Map of Eastern Nepal*, 1:250,000.
- Durkin, P.R., Boyd, R.L., Hubbard, S.M., Shultz, A.W., Blum, M.D., 2017. Three-Dimensional Reconstruction of Meander-Belt Evolution, Cretaceous McMurray Formation, Alberta Foreland Basin, Canada. *Journal of Sedimentary Research* 87, 1075–1099.

- Ehleringer, J.R., 1988. Carbon isotope ratios and physiological processes in aridland plants. In: Ehleringer, J.R., Nagy, K.A., (eds.), *stable isotope in ecological research*. Springer, New York, 41–54.
- Feng, J.L., Zhu, L.P., Zhen, X.L., Hu, Z.G., 2009. Grain size effect on Sr and Nd isotopic compositions in eolian dust: Implications for tracing dust provenience and Nd model age. *Geochemical Journal* 43, 123–131.
- Feng, Z.Z., 2019. A review on the definitions of terms of sedimentary facies. *Journal of Palaeogeography* 8, 1–11.
- Folk, R.L., 1980. *Petrology of Sedimentary Rocks*. Hemphill Publishing Company, Austin.
- France-Lanord, C., Derry, L., Michard, A., 1993. Evolution of the Himalaya since Miocene time: Isotopic and sedimentological evidence from the Bengal Fan. In: Treloar, P.J., Searle, M.P., (eds.), *Himalayan Tectonics*. Geological Society of London Special Publication 74, 603–622.
- Galy, A., France-Lanord, C., Hurtrez, J. E., 1998. Distribution of physical erosion in Himalaya from river particle geochemistry. *Mineralogical Magazine* 62, 493–494.
- Gansser, A., 1964. *Geology of the Himalayas*. Wiley InterScience, London.
- Garzanti, E., Critelli, S., Ingersoll, R.V., 1996. Paleogeographic and paleotectonic evolution of the Himalayan Range as reflected by detrital modes of Tertiary sandstones and modern sands (Indus transect, India and Pakistan). *Geological Society of America Bulletin* 108, 631–642.
- Garzanti, E., Vezzoli, G., Andò, S., Paparella, P., Clift, P.D., 2005. Petrology of Indus River sands: a key to interpret erosion history of the Western Himalayan Syntaxis. *Earth and Planetary Science Letters* 229, 287–302.
- Garzanti, E., Vezzoli, G., Andò, S., Lavé, J., Attal, M., France-Lanord, C., DeCelles, P., 2007. Quantifying sand provenance and erosion (Marsyandi River, Nepal Himalaya). *Earth and Planetary Science Letters* 258, 500–515.
- Garzanti, E., Ando, S., France-Lanord, C., Vezzoli, G., Censi, P., Galy, V., Najman, Y., 2010. Mineralogical and chemical variability of fluvial sediments 1. Bedload sand (Ganga–Brahmaputra, Bangladesh). *Earth and Planetary Science Letters* 299, 368–381.
- Garzanti, E., Andò, S., France-Lanord, C., Censi, P., Vignola, Pietro, Galy, V., Lupker, M., 2011. Mineralogical and chemical variability of fluvial sediments 2. Suspended-load silt (Ganga–Brahmaputra, Bangladesh). *Earth and Planetary Science Letters* 302, 107–120.
- Gautam, P., Appel, E., 1994. Magnetic-polarity stratigraphy of Siwalik Group sediments of Tinau Khola section in west central Nepal, revisited. *Geophysical Journal International* 117, 223–34.
- Gautam, P., Fujiwara, Y., 2000. Magnetic polarity stratigraphy of Siwalik Group of Karnali River section in Western Central Nepal. *Geophysical Journal International* 142, 812–24.
- Gibling, M.R., Nanson, G.R., Maroulis, J.C., 1998. Anastomosing river sedimentation in the Channel Country of central Australia. *Sedimentology* 45, 595–619.
- Giere, R., Sorensen, S.S., 2004. Allanite and other REE-rich epidote-group minerals. *Reviews in Mineralogy and Geochemistry* 56, 431–493.
- Glennie, K. W., Ziegler, M. A., 1964. The Siwalik Formations of Nepal. XXII International Geological Congress, Delhi, 15, 82–95.
- Gohain, K., Parkash, B., 1990. Morphology of the Kosi megafan. In: Rachocki, A.H., Church, M., (eds.), *Alluvial Fans: A Field Approach*. John Wiley and Son Ltd, Chichester, UK.
- Goldstein, S.L., O’Nions, R.K., Hamilton, P.J., 1984. A Sm-Nd isotopic study of atmospheric dusts and particulates from major river systems. *Earth and Planetary Science Letters* 70, 221–236.
- Goldstein, S.J., Jacobsen, S.B., 1988. Nd and Sr isotopic systematics of river water suspended material: implications for crustal evolution. *Earth and Planetary Science Letters* 87, 249–265.

- Goodbred, S.L., Kuehl, S.A., 2000. Enormous Ganges-Brahmaputra sediment discharge during strengthened early Holocene monsoon. *Geology* 28, 1083–1086.
- Grousset, F.E., Biscaye, P.E., Revel, M., Petit, J.R., Pye, K., Joussaume, S., Jouzel, J., 1992. Antarctic (Dome C) ice core dusts at 18 ky B.P.: Isotopic constraints on origins and atmospheric circulation. *Earth and Planetary Science Letters* 111, 175–182.
- Guliotta, M., Flint, S.S., Hodgson, D.M., Veiga, G.D., 2016. Recognition criteria, characteristics and implications of the fluvial to marine transition zone in ancient deltaic deposits (Lajas Formation, Argentina). *Sedimentology* 63, 1971–2001.
- Hagen, T., 1951. Preliminary note on the geological structure of Central Nepal. *Verhandlungen der Schweizerischen Naturforschenden Gesellschaft, Luzern*, 133–134.
- Hagen, T., 1969. Report on the Geological Survey of Nepal: Preliminary Reconnaissance. *Denkschriften der Medicinisch-Naturwissenschaftlichen Gesellschaft zu Jena* 86, 185.
- Harrison, T.N., 1988. Magmatic Garnets in the Cairngorm Granite, Scotland. *Mineralogical Magazine* 52, 659–667.
- Harrison, T.M., Copeland, P., Hall, S.A., Quade, J., Burner, S., Ojha, T.P., Kidd, W.S.F., 1993. Isotopic preservation of Himalayan–Tibetan uplift, denudation, and climatic histories in two molasse deposits. *The Journal of Geology* 101, 157–175.
- Haq, B.U., Hardenbol, J., Vial, P.R., 1988. Mesozoic and Cenozoic chronostratigraphy and cycles of sea-level change. In: Wilgus, C.K., Hastings, B.S., Kendall, C.G.St.C., Posamentier, H.W., Ross, C.A., Van Wagoner, J.C. (eds.), *Sea-Level Changes: An Integrated Approach*. Soc Econ Paleontol Mineral Spec Publ 42: 71–108.
- Haviv, I., Avouac, J., Farley, K.A., Harrison, M.T., Heizler, M.T., Prabhat, N.C., Mahéo, G., 2009. Uplift and exhumation along the Arun River (Eastern Nepal): implications for the mechanism of uplift of the High Himalaya and the coupling between erosion and tectonics. *AGU Fall Meeting 2009*, Abstract # T31E-07.
- Henry, D.J., Guidotti, C.V., 1985. Tourmaline as a petrogenetic indicator mineral: and example from the staurolite-grade metapelites of NW Maine. *American Mineralogist* 70, 1–15.
- Henry, D.J., Dutrow, B.L., 1992. Tourmaline in a low grade clastic metasedimentary rock: an example of the petrogenetic potential of tourmaline. *Contributions to Mineralogy and Petrology* 112, 203–218.
- Herman, F., Copeland, P., Avouac, J.P., Bollinger, L., Mahéo, G., Le Fort, P., Rai, S., Foster, D., Pêcher, A., Stüwe, K., Henry, P., 2010. Exhumation, crustal deformation, and thermal structure of the Nepal Himalaya derived from the inversion of thermochronological and thermobarometric data and modeling of the topography. *Journal of Geophysical Research* 115, B06407. <https://doi.org/10.1029/2008JB006126>.
- Hisatomi, K., Tanaka, S., 1994. Climatic and environmental changes at 9 and 7.5 Ma in the Churia (Sivalik) Group, west-central Nepal. *Himalayan Geology* 15, 161–180.
- Hodges, K.V., Parrish, R.R., Housch, T.B., Lux, D.R., Burchfiel, B.C., Royden, L.H., Chen, Z., 1992. Simultaneous Miocene extension and shortening in the Himalayan Orogen. *Science* 258, 1466–1470.
- Hoefs, J., 2009. Geochemical fingerprints: a critical appraisal. *European Journal of Mineralogy* 22, 3–15.
- Huyghe, P., Galy, A., Mugnier, J. L., France-Lanord, C., 2001. Propagation of the thrust system and erosion in the Lesser Himalaya: Geochemical and sedimentological evidences. *Geology* 29, 1007–1010.



- Huyghe, P., Mugnier, J.L., Gajurel, A.P., Delcaillau, B., 2005. Tectonic and climatic control of the changes in the sedimentary record of the Karnali River section (Siwaliks of western Nepal). *The Island Arc* 14, 311–327.
- Imayama, T., Arita, K., 2008. Nd isotopic data reveal the material and tectonic nature of the Main Central Thrust zone in Nepal Himalaya. *Tectonophysics* 451, 265–281.
- Imayama, T., Takeshita, T., Arita, K., 2010. Metamorphic P-T profile and P-T path discontinuity across the far-eastern Nepal Himalaya: investigation of channel flow models. *Journal of metamorphic Geology* 28, 527–549.
- Ingersoll, R. V., Suczek C.A., 1979. Petrology and Provenance Neogene sand from Nicobar and Bengal fans. DSDP site 211 and 218. *Journal of Sedimentary Petrology* 49, 1217–1228.
- Ishiga, H., Ishiyama, D., 1987. Jurassic accretionary complex in Kaminokuni terrane, southwestern Hokkaido, Japan. *Mining Geology* 37, 381–394.
- Jain, V., Sinha, R., 2004. Fluvial dynamics of an anabranching river system in Himalayan foreland basin, Bagmati river, north Bihar plains, India. *Geomorphology* 60, 147–170.
- Jiang, S.Y., Yanf, J.H., Novak, M., Selway, J., 2003. Chemical and boron isotopic compositions of tourmaline from the Lavicky leucogranite, Czech Republic. *Geochemical Journal* 37, 545–556.
- Johnson, N.M., Stix, J., Tauxe, L., Cervený, P.F., Tahirkheli, R.A.K., 1985. Palaeomagnetic chronology, fluvial processes and tectonic implications of the Siwalik deposits near Chinji Village, Pakistan. *Journal of Geology* 93, 27–40.
- Jonell, T.N., Li, Y., Blusztajn, J., Giosan, L., Clift, P.D., 2018. Signal or noise? Isolating grain size effects on Nd and Sr isotope variability in Indus delta sediment provenance. *Chemical Geology* 485, 56–73.
- Kanayama, S., Yabuki, S., zeng, F., Liu, M., Shen, Z., Liu, L., Yanagisawa, F., Abe, O., 2005. Size-dependent geochemical characteristics of Asian dust-Sr and Nd Isotope composition as tracers for source identification. *Journal of Meteorological Society of Japan* 83, 107–120.
- Kaneko, Y., 1995. Thermal structure in the Annapurna region, central Nepal Himalaya: Implication for the inverted metamorphism. *Journal of Mineralogical and Petrological Sciences* 90, 143–154.
- Kemner, F., Haase, K.M., Beier, C., Krumm, S., Brandi, P.A., 2015. Formation of andesite melts and Ca-rich plagioclase in the submarine Monowai volcanic system, Kermadec arc. *Geochemistry Geophysics geosystems* 16, 4130–4152.
- Khan, I.A., Bridge, J.S., Kappelman, J., Wilson, R., 1997. Evolution of Miocene fluvial environments, eastern Potwar plateau, Northern Pakistan. *Sedimentology* 44, 221–251.
- Khan, M.A., Bera, M., Spicer, R.A., Spicer, T.E.V., Bera, S., 2018. Palaeoclimatic estimates for a latest Miocene-Pliocene flora from the Siwalik Group of Bhutan: Evidence for the development of the South Asian Monsoon in the eastern Himalaya. *Palaeogeography, Palaeoclimatology, Palaeoecology* 514, 326–335.
- Kowal-Linka, M., Stawikowski, W., 2013. Garnet and tourmaline as provenance indicators of terrigenous material in epicontinental carbonates (Middle Triassic, S Poland). *Sedimentary Geology* 291, 27–47.
- Kumar, R., Ghosh, S. K., Sangode, S. J., 2003. Mio-Pliocene sedimentation history in the northwestern part of the Himalayan foreland basin, India. *Current Science* 84, 1006–1013.
- Kundu, A., Matin, A., and 654 Mukul, M., 2012. Depositional environment and provenance of Middle Siwalik sediments in Tista valley, Darjiling District, Eastern Himalaya, India. *Journal of Earth System Science* 121, 73–89.

- Kutzbach, J.E., Guetter, P.J., Ruddiman, W.F., Prell, W.L., 1989. Sensitivity of climate to late Cenozoic uplift in southern Asia and the American west—numerical experiments. *Journal of Geophysical Research* 94, 18393–18407.
- Landry, K.R., Coutand, I., Whipp, D.M., Jr., Grujic, D., Hourigan, J.K., 2016. Late Neogene tectonically driven crustal exhumation of the Sikkim Himalaya: Insights from inversion of multithermochronologic data. *Tectonics* 35, 833–859.
- Lee, J.I., Clift, P.D., Layne, G., Blum, J., Khan, A.A., 2003. Sediment flux in the modern Indus River inferred from the trace element composition of detrital amphibole grains. *Sedimentary Geology* 160, 243–257.
- Le Fort, P., 1975. Himalayas; The Collided Range: Present Knowledge of the Continental Arc. *American Journal of Science* 275, 1–44.
- Le Fort, P., 1986. Metamorphism and magmatism during the Himalayan collision. In: Cowards, M.P., Ries, A.C., (eds.), *Collision Tectonics*. Geological Society Special Publication 19, 159–172.
- Le Fort, P., 1996. Evolution of the Himalaya. In: Yin, A., Harrison, T.M., (eds), *The tectonics of Asia*. Cambridge University Press, New York.
- Leopold, L. B., Wolman, M.G., 1957. River channel patterns: braided, meandering and straight. U.S. Geological Survey Professional Paper 282, 39–85.
- Lewis, G.E., 1937. A new Siwalik correlation. *American Journal of Science* 33, 191–204.
- Lourens, L.J., Hilgen, F.J., Laskar, J., Shackleton, N.J., Wilson, D., 2004. The Neogene Period. In: Gradstein, F.M., Ogg, J.G., Smith, A.G., (eds), *A Geologic Time Scale 2004*, Cambridge Univ Press, Cambridge, 409–440.
- Macfarlane, A.M., 1993. Chronology of tectonic events in the crystalline core of the Himalaya, Langtang National Park, central Nepal. *Tectonics* 12, 1004–1025.
- Mack, G.H., Leeder, M.R., 1998. Channel shifting of the Rio Grande, southern Rio Grande rift: implications for alluvial stratigraphic models. *Sedimentary Geology* 117, 207–219.
- Makaske, B., 2001. Anastomosing rivers: a review of their classification, origin and sedimentary products: *Earth-Science Reviews* 53, 149–196.
- Mange, M.A., Maurer, H.F.W., 1992. *Heavy minerals in colour*. Chapman and Hill, London.
- Mange, M.A., Morton, A.C., 2007. Geochemistry of Heavy Minerals. In: Mange, M.A., Wright, D.T., (eds), *Heavy Minerals in use*. *Developments in Sedimentology* 58, Elsevier Science, 345–391.
- Martin, C.A.L., Turner, B.R., 1998. Origins of massive-type sandstones in braided river systems. *Earth-Science Reviews* 44, 15–38.
- Meyer, I., Davies, G.R., Stuut, J.B.W., 2011. Grain size control on Sr-Nd isotope provenance studies and impact on paleoclimate reconstructions: an example from deep-sea sediments offshore NW Africa. *Geochemistry Geophysics Geosystems* 12, Q03005.
- Miall, A. D., 1977. A Review of the Braided River Depositional Environment. *Earth Science Reviews* 13, 1–62.
- Miall, A. D., 1985. Architectural-element analysis: A new method of facies analysis applied to fluvial deposits. *Earth Science Reviews* 22, 261–308.
- Miall, A. D., 2000. *Principles of sedimentary basin analysis*, (3rd Ed.). Springer, Verlag Berlin Heidelberg.
- Miall, A. D., 2006. *The Geology of Fluvial Deposits, Sedimentary Facies, Basin Analysis, and Petroleum Geology*. Springer.
- Miller, M., Curk, U., Mirtic, B., 2009. The use of SEM/EDS method in mineralogical analysis of ordinary chondritic meteorite. *Geologija* 52. 183–192.

- Morton, A.C., 1984. Stability of detrital heavy minerals in Tertiary sandstones from the North Sea basin. *Clay Mineralogy* 19, 287–308.
- Morton, A.C., 1985. A new approach to provenance studies: electron microprobe analysis of detrital garnets from Middle Jurassic sandstones of the northern North Sea. *Sedimentology* 32, 553–566
- Morton, A.C., Hallsworth, C.R., 1994. Identifying provenance-specific features of detrital heavy mineral assemblages in sandstones. *Sedimentary Geology* 90, 241–256.
- Morton, A.C., Hallsworth, C.R., 1999. Processes controlling the composition of heavy mineral assemblages in sandstones. *Sedimentary Geology* 124, 3–29.
- Mukerji, A.B., 1990. The Chandigarh Dun alluvial fans: An analysis of the process-form relationship. In: Rachocki, A.H., Church, M., (eds), *Alluvial Fans: A Field Approach*, John Wiley and Son Ltd, Chichester, UK, 131–149.
- Najman, Y., Bickle, M., Garzanti, E., Pringle, M., Barfod, D., Brozovic, N., Burbank, D., Ando, S., 2009. Reconstructing the exhumation history of the Lesser Himalaya, NW India. From a multitechnique provenance study of the foreland basin Siwalik Group. *Tectonics* 28, TC5018.
- Nakajima, T., Sakai, H., Iwano, H., Danhara, T., Hirata, T., 2020a. Northward younging zircon fission-track ages from 13 to 2 Ma in the eastern extension of the Kathmandu nappe and underlying Lesser Himalayan sediments distributed to the south of Mt. Everest. *Island Arc* 29, e12352.
- Nakajima, T., Matsumoto, Y., Rai, L.K., Yoshida, K., 2020b. Middle Miocene denudation of the Higher Himalayan Crystallines revealed by chemical composition of detrital garnets from the Siwalik foreland basin sediments, western and central Nepal. *Journal of Asian Earth Sciences* 200, 104473.
- Nakano, T., 2016. Potential uses of stable isotope ratios of Sr, Nd, and Pb in geological materials for environmental studies. *Proceedings of the Japan Academy* 92, 167–184.
- Nakayama, K., Ulak, P. D., 1999. Evolution of fluvial style in the Siwalik Group in the foothills of the Nepal Himalaya. *Sedimentary Geology* 125, 205–24.
- Nanson, G.C., Knighton, A.D., 1996. Anabranching Rivers: their cause, character and classification. *Earth Surface Processes and Landforms* 21, 217–239.
- Neogi, S., Dasgupta, S., Fukuoka, M., 1998. High P–T Polymetamorphism, Dehydration Melting, and Generation of Migmatites and Granites in the Higher Himalayan Crystalline Complex, Sikkim, India. *Journal of Petrology* 39, 61–99.
- Nishio, M., Yoshida, K., 2014. Tectonic constraints to Cretaceous magmatic arc deduced from detrital heavy minerals in northeastern Japan - evidence from detrital garnets, tourmalines and chromian spinels. *Cretaceous Research* 48, 39–53.
- O'Brien, P.J., 2019. Eclogites and other high-pressure rocks in the Himalaya: a review. In: Treloar, P.J., Searle, M.P., (eds.), *Himalayan Tectonics: A Modern Synthesis* 483, 183–213.
- Ojha, T.P., Butler, R.F., Decelles, P.G., Quade, J., 2009. Magnetic polarity stratigraphy of the Neogene foreland basin deposits of Nepal. *Basin Research* 21, 61–90.
- Oldknow, C.J., Hooke, J.M., 2017. Alluvial terrace development and changing landscape connectivity in the Great Karoo, South Africa. Insights from the Wilgerbosch River catchment, Sneeuberg. *Geomorphology* 288, 12–18.
- Pandey, M.R., Tandukar, R.P., Avouac, J.P., Lave, J., Massot, J.P., 1995. Interseismic Strain Accumulation on the Himalayan Crustal Ramp (Nepal). *Geophysical Research Letters* 22, 751–754.
- Parrish, R.R., Hodges, K.V., 1996. Isotopic constraints on the age and provenance of the Lesser and Greater Himalayan sequences, Nepalese Himalaya. *Geological Society of America Bulletin* 108, 904–911.

- Parsons, A.J., Stromberg, S.G., 1998. Experiment analysis of size and distance of travel of unconstrained particles in interrill flow. *Water Resources Research* 34, 2377–2381
- Paudel, L.P., Arita, K., 2002. Locating the Main Central Thrust in central Nepal using lithologic, microstructural and metamorphic criteria. *Journal of Nepal Geological Society* 26, 29–42.
- Pearson, O.N., DeCelles, P.G., 2005. Structural geology and regional tectonic significance of the Ramgarh thrust, Himalayan fold-thrust belt of Nepal. *Tectonics* 24, TC4008.
- Pettijohn, F.J., Siever, R., Potter, P.E., 1987. *Sand and Sandstone*, (2nd Ed.). Springer, Verlag.
- Pilgrim, G.E., 1913. The correlation of the Siwaliks with mammal horizons of Europe. *Records of Geological Survey of India* 43, 264–326.
- Pin, C., Briot, D., Bassin, C., Poitrasson, F., 1994. Concomitant separation of strontium and samarium-neodymium for isotopic analysis in silicate samples, based on specific extraction chromatography. *Analytica Chimica Acta* 298, 209–217.
- Pin, C., Zalduegui, J.S., 1997. Sequential separation of light 692 rare-earth elements, thorium and uranium by miniaturized extraction chromatography: application to isotopic analyses of silicate rocks. *Analytica Chimica Acta* 339, 79–89.
- Plink-Bjorklund, P., 2015. Morphodynamics of rivers strongly affected by monsoon precipitation: Review of depositional style and forcing factors. *Sedimentary Geology* 323, 110–147.
- Parkash, B., Sharma, R.P., Roy, A.K., 1980. The Siwalik Group (molasse) - sediments shed by collision of continental plates. *Sedimentary Geology* 25, 127–159.
- Quade, J., Cerling, T., Bowman, J., 1989. Development of Asian monsoon revealed by marked ecological shift during the latest Miocene in northern Pakistan. *Nature* 342, 163–166.
- Quade, J., Cater, J.M.L., Ojha, T.P., Adam, J., Harrison, T.M., 1995. Late Miocene environmental change in Nepal and the Northern Indian subcontinent: Stable isotopic evidence from paleosols. *Geological Society of America Bulletin* 107, 1381–1397.
- Quade, J., Cerling, T.E., 1995. Expansion of C4 grasses in the late Miocene of northern Pakistan: evidence from stable isotopes in paleosols. *Palaeogeography, Palaeoclimatology, Palaeoecology* 115, 91–116.
- Radhakrishna, T., Rao, V.D., Murali, A.V., 1987. Geochemistry and petrogenesis of ultramafic and mafic plutonic rocks of the Dras ophiolitic melange, Indus suture (northwest Himalaya). *Earth and Planetary Science Letters* 82, 136–144.
- Rai, S.M., Guillot, S., Le Fort, P., Upreti, B.N., 1998. Pressure–temperature evolution in the Kathmandu and Gosainkund regions, central Nepal. *Journal of Asian Earth Sciences* 16, 283–298.
- Rai, S.M., 2004. Tourmaline chemistry in the Miocene and Paleozoic granites, Central Nepal. *Journal of Nepal Geological Society* 29, 23–34.
- Rai, L.K., Acharya, K.K., Dhital, M.R., 2016. Lithostratigraphy and structure of the Dharan–Mulghat area, Lesser Himalayan sequence, eastern Nepal Himalaya. *Journal of Nepal Geological Society* 51, 77–88.
- Rai, L.K., Yoshida, K., 2020. Lithostratigraphy of the Siwalik Group along the Muksar Kholasection, Siraha-Udayapur districts, eastern Nepal Himalaya. *Journal of Nepal Geological Society* 60, 207–224.
- Rai, L.K., Yoshida, K., Kuritani, T., 2021. Reconstruction of the exhumation history of the eastern Nepal Himalaya based on provenance changes. *Sedimentary Geology* 420, 105920.
- Rai, L.K., Yoshida, K., 2021. Sedimentary facies analysis of the fluvial environment in the Siwalik Group of eastern Nepal: deciphering its relation to contemporary Himalayan tectonics, climate and sea-level change. *Progress in earth and Planetary Science* 8, 49.

- Raymo, M.E., Ruddiman, W.F., 1992. Tectonic forcing of late Cenozoic climate. *Nature* 359, 117–122.
- Raymond, L.A., Bero, D.A., 2015. Sandstone-matrix mélanges, architectural subdivision, and geologic history of accretionary complexes: A sedimentological and structural perspective from the Franciscan Complex of Sonoma and Marin counties, California, USA. *Geosphere* 11, 1077–1110.
- Reineck, H.E., Singh, I.B., 1980. *Depositional Sedimentary Environments: with reference to terrigenous clastics*. Springer, Berlin.
- Robinson, D.M., Decelles, P.G., Patchett, P.J., Garzzone, C.N., 2001. The kinematic history of the Nepalese Himalaya interpreted from Nd isotopes. *Earth and Planetary Science Letters* 192, 507–521.
- Robinson, D.M., DeCelles, P.G., Garzzone, C.N., Pearson, O.N., Harrison, T.M., Catlos, E.J., 2003. Kinematic model for the Main Central Thrust in Nepal. *Geology* 31, 359–362.
- Rosler, W., Metzler, W., Appel, E., 1997. Neogene magnetic polarity stratigraphy of some fluvial Siwalik sections, Nepal. *Geophysical Journal International* 130, 89–111.
- Ruiz-Vargas, J., Siredey-Schwaller, N., Noyrez, P., Mathieu, S., Bocher, P., Gey, N., 2014. Potential and limitations of microanalysis SEM techniques to characterize borides in brazed Ni-based superalloys. *Materials Characterization* 94, 46–57.
- Sah, R.B., Ulak, P.D., Gajurel, A.P., Rimal, L.N., 1994. Lithostratigraphy of Siwaliks sediments of Amlekhganj-Hetauda area, sub-Himalaya of Nepal. *Himalayan geology* 15, 37–48.
- Saha, D., 2013. Lesser Himalayan sequences in Eastern Himalaya and their deformation: Implications for Paleoproterozoic tectonic activity along the northern margin of India. *Geoscience Frontiers* 4, 289–304.
- Sakai, H., 1983. Geology of the Tansen Group of the Lesser Himalaya in Nepal. *Memoirs of the Faculty of Science, Kyushu University, Series D, Geology* 25, 27–74.
- Sakai, H., Iwano, H., Danhara, T., Takigami, Y., Rai, S.M., Upreti, B.N., Hirata, T., 2013. Rift-related origin of the Paleoproterozoic Kuncha Formation, and cooling history of the Kuncha nappe and Taplejung granites, eastern Nepal Lesser Himalaya: a multichronological approach. *Island Arc* 22, 338–360.
- Schelling, D., Arita, K., 1991. Thrust tectonics, central shortening, and the structure of the far-eastern Nepal Himalaya. *Tectonics* 10, 851–862.
- Schelling, D., 1992. The tectonostratigraphy and structure of the eastern Nepal Himalaya. *Tectonics* 11, 925–943.
- Schwab, F.L., 1975. Framework mineralogy and chemical composition of continental margin-type sandstone. *Geology* 3, 487–490.
- Searle, M.P., Simpson, R.L., Law, R.D., Parrish, R.R., Waters, D.J., 2003. The structural geometry, metamorphic and magmatic evolution of the Everest massif, High Himalaya of Nepal-South Tibet. *Journal of Geological Society, London* 160, 345–366.
- Sharma, C.K., 1990. *Geology of Nepal and adjoining countries*. Sangeeta Sharma, Kathmandu.
- Shrestha, R.B., Sharma, S.R., 1996. The lower Siwalik-basement unconformity in the sub-Himalaya of eastern Nepal and its significance. *Journal of Nepal Geological Society* 13, 29–36.
- Sigdel, A., Sakai, T., Ulak, P.D., Gajurel, A. P., Upreti, B.N., 2011. Lithostratigraphy of the Siwalik Group, Karnali River section, far-west Nepal Himalaya. *Journal of Nepal Geological Society* 43, 83–101.

- Sigdel, A., Sakai, T., 2013, Petrography of Miocene Siwalik Group sandstones, Karnali River section, Nepal Himalaya: Implications for source lithology and tectonic setting. *Journal of Nepal Geological Society* 46, 95–110.
- Sigdel, A., Sakai, T., 2016. Sedimentary facies analysis on the fluvial systems in the Siwalik Group, Karnali River section, Nepal Himalaya, and their significance for understanding the paleoclimate and Himalayan tectonics. *Journal of Nepal Geological Society* 51, 11–26.
- Simms, A.R., Anderson, J.B., Taha, Z.P., Rodriguez, A.B., 2006. Overfilled versus underfilled incised valleys: examples from the Quaternary Gulf of Mexico. *SEPM, Special publication* 85, 117–139.
- Singh, A.B., 1972. On the bedding in the natural-levee and point bar deposits of the Gomti River, Uttar Pradesh, India. *Sedimentary Geology* 7, 309–317.
- Singh, H., Parkash, B., Gohain, K., 1993. Facies analysis of the Kosi megafan deposits. *Sedimentary Geology* 85, 87–113.
- Singh, S.K., France-Lanord, C., 2002. Tracing the distribution of erosion in the Brahmaputra watershed from isotopic compositions of stream sediments. *Earth and Planetary Science Letters* 202, 645–662.
- Singh, S.K., Rai, S.K., Krishnaswami S., 2008. Sr and Nd isotopes in river sediments from the Ganga Basin: Sediment provenance and spatial variability in physical erosion. *Journal of Geophysical Research* 113, F03006.
- Singh, S., Prakash, B., Awasthi, A. K., Singh, T., 2012. Palaeoprecipitation record using O-isotope studies of the Himalayan Foreland Basin sediments. *Palaeogeography, Palaeoclimatology, Palaeoecology* 331-332, 39–49.
- Sinha, R., Gibling, M.R., Jain, V., Tandon, S.K., 2005. Sedimentology and avulsion patterns of the anabranching Bagmati River in the Himalayan foreland basin, India. In: Blum, M.D., Marriott, S.B., Leclair, S.F., (eds), *Fluvial Sedimentology VII*, Special Publications of the International Association of Sedimentologists 35, 181–196.
- Slingerland, R., Smith, N.D., 2004. River avulsions and their deposits. *Annual Review of Earth and Planetary Sciences* 32, 257–285.
- Smith, D.G., 1986. Anastomosing river deposits, sedimentation rates and basin subsidence, Magdalena River, northwestern Colombia, South America. *Sedimentary Geology* 46, 177–196.
- Smith, D.G., Smith, N.D., 1980. Sedimentation in anastomosed river systems: examples from alluvial valleys near Banff, Alberta. *Journal of Sedimentary Petrology* 50, 157–164.
- Srivastava, G., Paudyal, K.N., Utescher, T., Mehrotra, R.C., 2018. Miocene vegetation shift and climate change: Evidence from the Siwalik of Nepal. *Global and Planetary Change* 161, 108–120.
- Stocklin, J., Bhattarai, K.D., 1977, *Geology of the Kathmandu area and central Mahabharat range, Nepal Himalaya*. Report of Department of Mines and Geology/UNDP (unpublished).
- Stocklin, J., 1980, *Geology of Nepal and its regional frame*. *Journal of Geological Society of London* 137, 1–34.
- Streule, M.J., Searle, M.P., Waters, D.J., Horstwood, M.S.A., 2010. Metamorphism, melting, and channel flow in the Greater Himalayan Sequence and Makalu leucogranite: Constraints from thermobarometry, metamorphic modeling, and U-Pb geochronology. *Tectonics* 29, TC5011.
- Suggate, S.M., Hall, R., 2014. Using detrital garnet compositions to determine provenance: A new compositional database and procedure. *Geological Society, London, Special Publication* 386, 373–393.
- Szulc, A.G., Najman, Y., Sinclair, H., Pringle, M., Bickle, M., Chapman, H., Garzanti, E., Ando, S., Huyghe, P., Mugnier, J.L., Ojha, T.P., DeCelles, P.G., 2006, *Tectonic evolution of the*

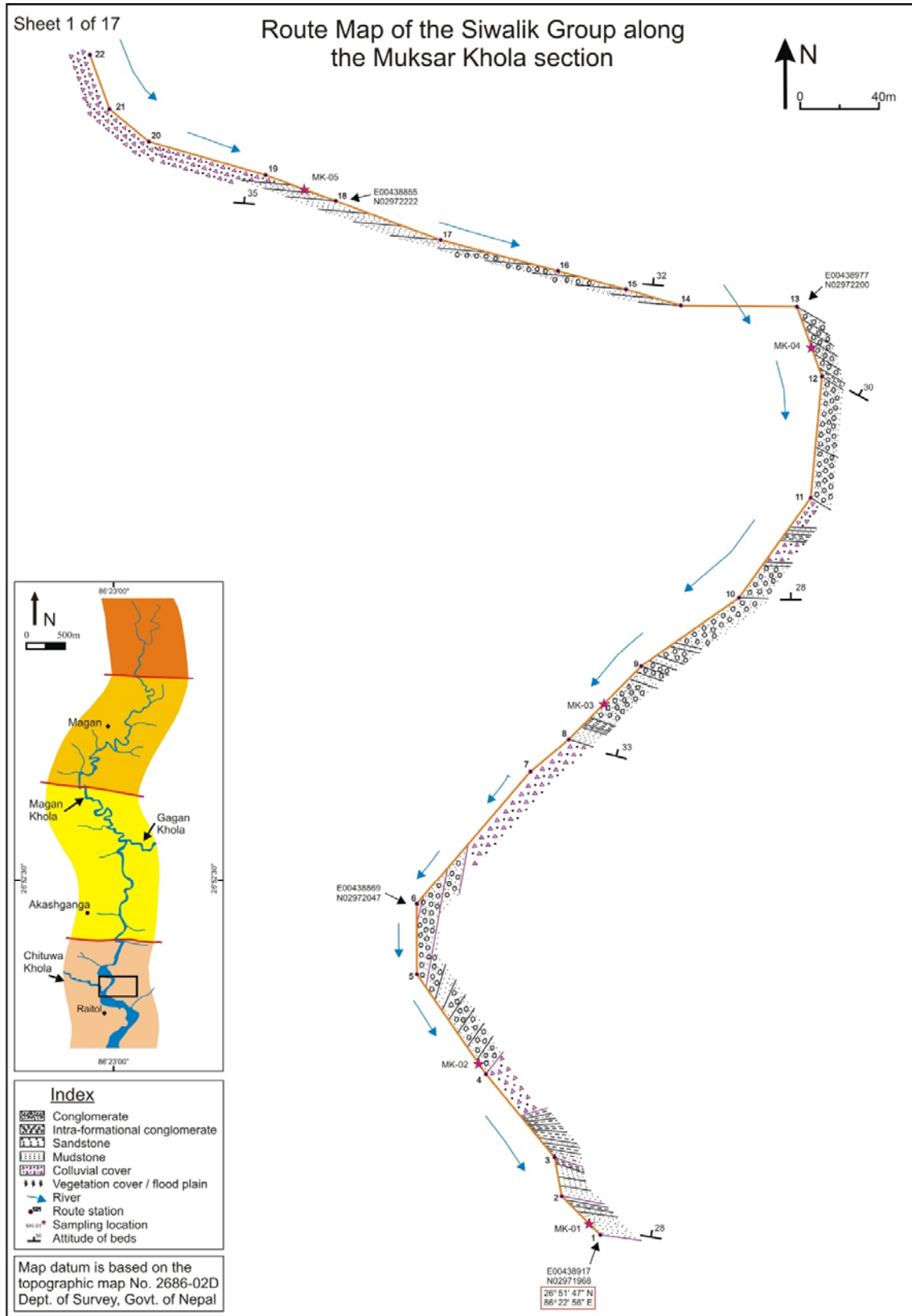
- Himalaya constrained by detrital  $^{40}\text{Ar}$ - $^{39}\text{Ar}$ , Sm-Nd and petrographic data from the Siwalik foreland basin succession, SW Nepal. *Basin Research* 18, 375–391.
- Tabor, N.J., Myres, T., Michel, L.A., 2017, Sedimentologist's guide for recognition, description, and classification of paleosols. In: Ziegler, K., Parker, W., (eds), *Terrestrial Depositional Systems*, Elsevier, 165–208.
- Takigami, Y., Sakai, H., Orihashi, Y., 2002. 1.5–1.7 Ga rocks discovered from the Lesser Himalaya and Siwalik belt:  $^{40}\text{Ar}$ - $^{39}\text{Ar}$  ages and their significances in the evolution of the Himalayan orogen. *Geochimica et Cosmochimica Acta* 66, A762.
- Tamrakar, N.K., Yokota, S., Shrestha, S.D., 2003. Petrography of the Siwalik sandstones, Amlekhganj-Suparitar area, central Nepal Himalaya. *Journal of Nepal Geological Society* 28, 41–56.
- Tandon, S.K., 1976. Siwalik sedimentation in a part of the Kumaun Himalaya, India. *Sedimentary Geology* 16, 131–154.
- Tandon, S.K., Gibling, M.R., Sinha, S., Singh, V., Ghazanfari, P., Dasgupta, A., Jain, M., Jaim, V., 2006. Alluvial valleys of the Ganga plains, India: Timing and causes of Incision. *SEPM, Special publication* 85, 15–35.
- Tanaka, S., 1997. Uplift of the Himalaya and climate changes at 10.0 Ma evidence from records of the carbon stable isotopes and fluvial sediments in the Churia Group Nepal. *Journal of Geological Society of Japan* 103, 253–264.
- Taral, S., Sarkar, S., Chakraborty, T., 2018. An ichnological model for a deltaic depositional system: New insights from the Neogene Siwalik Foreland Basin of Darjeeling-Sikkim Himalaya. *Palaeogeography, Palaeoclimatology, Palaeoecology* 511, 188–207.
- Taral, S., Chakraborty, T., Huyghe, P., Van der Beek, P., Vogeli, N., Dupont-Nivet, G., 2019. Shallow marine to fluvial transition in the Siwalik succession of the Kameng River section, Arunachal Himalaya and its implication for foreland basin evolution. *Journal of Asian Earth Sciences* 184, 103908.
- Tokuoka, T., Takayasu, K., Yoshida, M., Hisatomi, K., 1986. The Churia (Siwalik) Group of Arung Khola area, west-central Nepal. *Memoirs of Faculty of Science, Shimane University* 22, 135–210.
- Tokuoka, T., Takayasu, K., Hisatomi, K., Yamasaki, H., Tanaka, S., Konomatu, M., Sah, R.B., Roy, S.M., 1990. The Churia (Siwalik) Group of Tinau Khola-Binai Khola area, west-central Nepal. *Memoirs of Faculty of Science, Shimane University* 24, 71–88.
- Tokuoka, T., Takayasu, K., Hisatomi, K., Tanaka, S., Yamasaki, H., Konomatsu, M., 1994, The Churia Siwalik Group in West Central Nepal. *Himalayan Geology* 15, 23–35.
- Tornqvist, T.E., 1994. Middle and late Holocene avulsion history of the River Rhine ŽRhine–Meuse delta Netherlands. *Geology* 22, 711–714.
- Tucker, M.E., 2003. *Sedimentary rocks in the Field* (3rd Ed.). John Wiley and Sons Ltd, England.
- Ulak, P.D., Nakayama, K., 1998. Lithostratigraphy and evolution of the fluvial style in the Siwalik Group in the Hetauda-Bakiya Khola area, Central Nepal. *Bulletin of Department of Geology, Tribhuvan University* 6, 1–14.
- Ulak, P.D., Nakayama, K., 2001, Neogene fluvial systems in the Siwalik Group along the Tinau Khola section, west central Nepal Himalaya. *Journal of Nepal Geological Society* 25, 111–122.
- Ulak, P.D., 2004. Evolution of fluvial system in Siwalik Group of Chatara-Barahakshetra area, east Nepal Himalaya. *Journal of Nepal Geological Society* 30, 67–74.
- Ulak, P.D., 2009. Lithostratigraphy and late Cenozoic fluvial styles of Siwalik Group along Kankai River section, East Nepal Himalaya: *Bulletin of Department of Geology, Tribhuvan University* 12, 63–74.

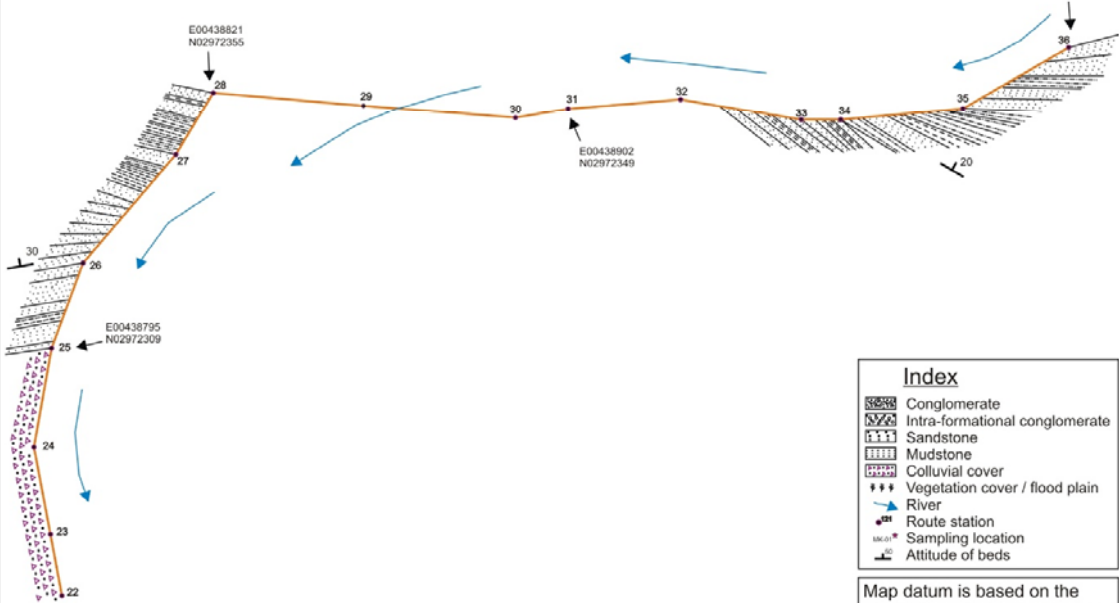
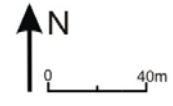
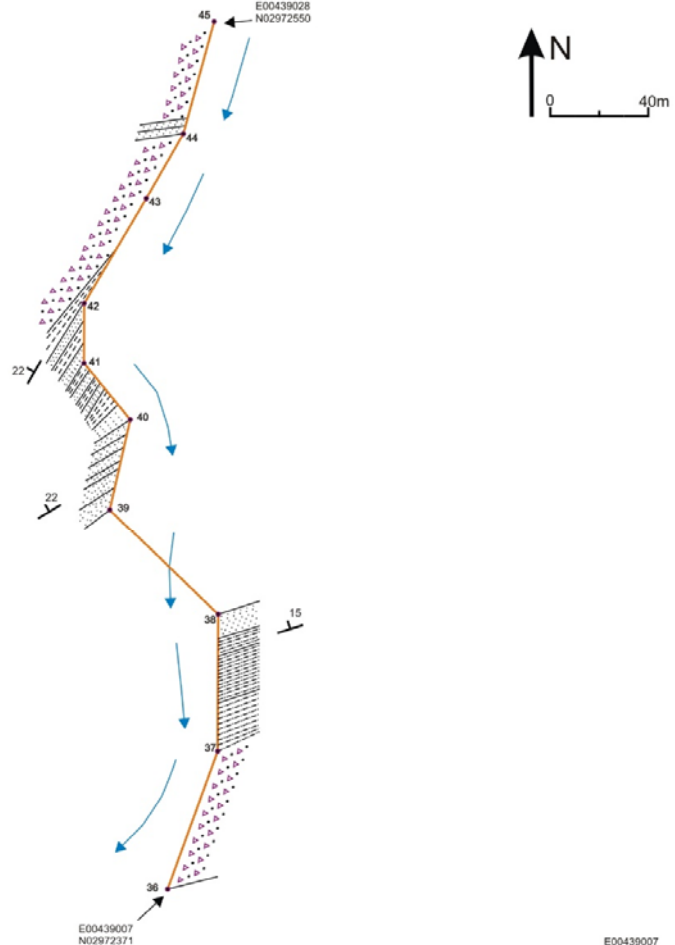
- Upreti, B.N., 1999. An overview of the stratigraphy and tectonics of the Nepal Himalaya. *Journal of Asian Earth Sciences* 17, 577–606.
- Valdiya, K.S., 1980. The two Intracrustal Boundary Thrusts of the Himalaya. *Tectonophysics* 66, 323–348.
- Vogeli, N., Najman, Y., Van der Beek, P., Huyghe, P., Wynn, P.M., Govin, G., Van der Veen, I., Sachse, D., 2017. Lateral variations in vegetation in the Himalaya since the Miocene and implications for climate evolution. *Earth and Planetary Science Letters* 471, 1–9.
- Walker, R.G., 1966. Shale grit and Grindslow shales: Transition from turbidite to shallow water sediments in the upper Carboniferous of northern England. *Journal of Sedimentary Research* 1, 90–114.
- Webb, A.A.G., Guo, H., Clift, P.D., Husson, L., Muller, T., Costantino, D., Yin, A., Xu, Z., Cao, H., Wand, Q., 2017. The Himalaya in 3D: Slab dynamics controlled mountain building and monsoon intensification. *Lithosphere* 9, 637–651.
- Willis, B.J., 1993a. Ancient river systems in the Himalayan foredeep, Chinji village area, northern Pakistan. *Sedimentary Geology* 88, 1–76.
- Willis, B.J., 1993b. Evolution of Miocene fluvial systems in the Himalayan foredeep through a two kilometer-thick succession in northern Pakistan. *Sedimentary Geology* 88, 77–121.
- Wright, W.I., 1938. The composition and occurrence of garnets. *American Mineralogist* 23, 436–449
- Xu, J., Ciobanu, C.L., Cook, N.J., Zheng, Y., Sun, X., Wade, B.P., 2016. Skarn formation and trace elements in garnet and associated minerals from Zhibula copper deposit, Gangdese Belt, southern Tibet. *Lithos* 262, 213–231.
- Yamamoto, Y., Mukoyoshi, H., Ogawa, Y., 2005. Structural characteristics of shallowly buried accretionary prism: Rapidly uplifted Neogene accreted sediments on the Miura-Boso Peninsula, central Japan. *Tectonics* 24, TC5008.
- Yin, A., 2006. Cenozoic tectonic evolution of the Himalayan orogen as constrained by along strike variation of structural geometry, exhumation history, and foreland sedimentation. *Earth-Science Reviews* 76, 1–131.
- Yokoo, Y., Nakano, T., Nishikawa, M., Hao, Q., 2004. Mineralogical variation of Sr-Nd isotopic and elemental compositions in loess and desert sand from the central Loess Plateau in China as a provenance tracer of wet and dry deposition in the northwestern Pacific. *Chemical Geology* 204, 45–62.
- Yoneshiro, T., Kizaki, K., 1996. Metamorphism and thermal structure of the Karnali Krippe, western Nepal Himalaya. *Bulletin of Department of Geology, Tribhuvan University* 5, 1–22.
- Yoshida, M. and Arita, K., 1982, On the Siwaliks observed along some routes in Central Nepal. *Journal of Nepal Geological Society* 2, 51–58.
- Yoshida, K., Rai, L.K., Manoj, M.C., 2019. Heavy mineral assemblage in the Himalayan river tributaries and correlation to Bengal Fan deposits. American Geophysical Union, Fall Meeting 2019, abstract #T13F-0260.
- Zaitlin, B.A., Dalrymple, R.W., Boyd, R., 1994. The stratigraphic organization of incised-valley systems associated with relative sealevel change, in Dalrymple, R.W., Boyd, R., and Zaitlin, B.A. (Eds.), *Incised-Valley Systems: Origin and Sedimentary Sequences: SEPM, Special publication* 51, 45–60.
- Zaleha, M.J., 1997. Intra-and extrabasinal controls on fluvial deposition in the Miocene Indo Gangatic foreland basin, northern Pakistan. *Sedimentology* 44, 369–390.
- Zhang, L., Wanf, H., Li, Y., Pan, M., 2017. Quantitative characterization of sandstone amalgamation and its impact on reservoir connectivity. *Petroleum Exploration and Development* 44, 226–233.



- Zhang, Y., Wei, X., Shi, X., Xu, Y., Ren, Z., Yan, Q., Guan, Y., 2019. Evaluating the effect of leaching on trace element and Nd-Pb isotopic systematics in continental basalts. *Solid Earth Science* 4, 1–11.
- Zhao, D., Shang, Y., Essene, E.J., 2015. Electron probe microanalysis and microscopy: Principles and applications in characterization of mineral inclusions in chromite from diamond deposit. *Ore Geology Reviews* 65, 733–748.

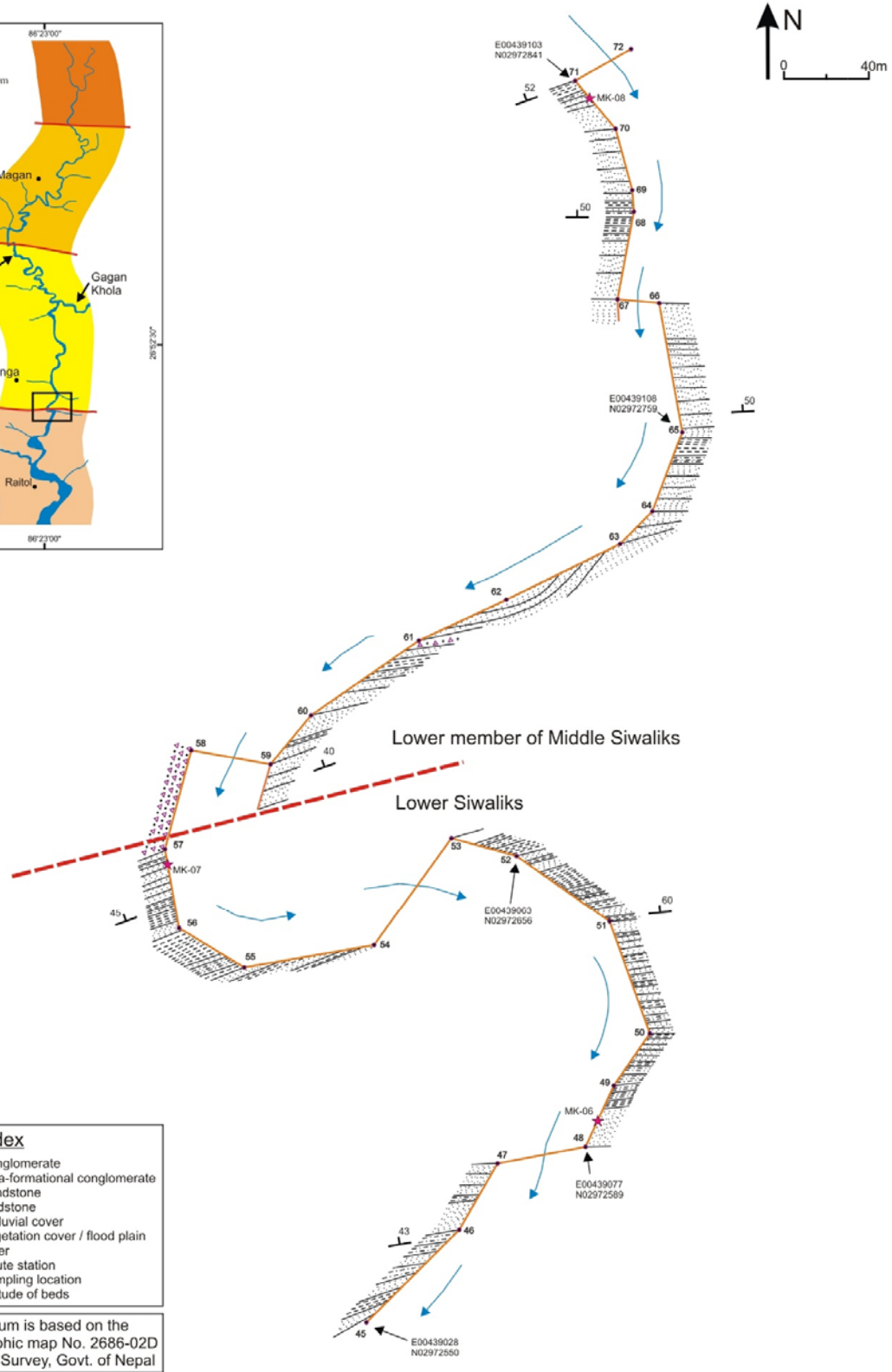
# APPENDIX





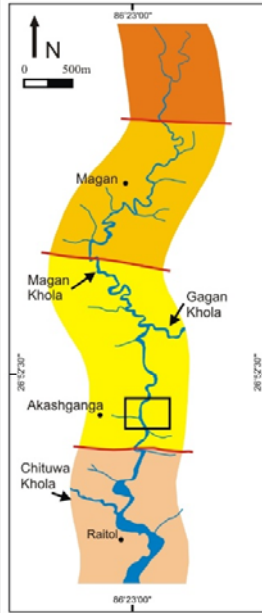
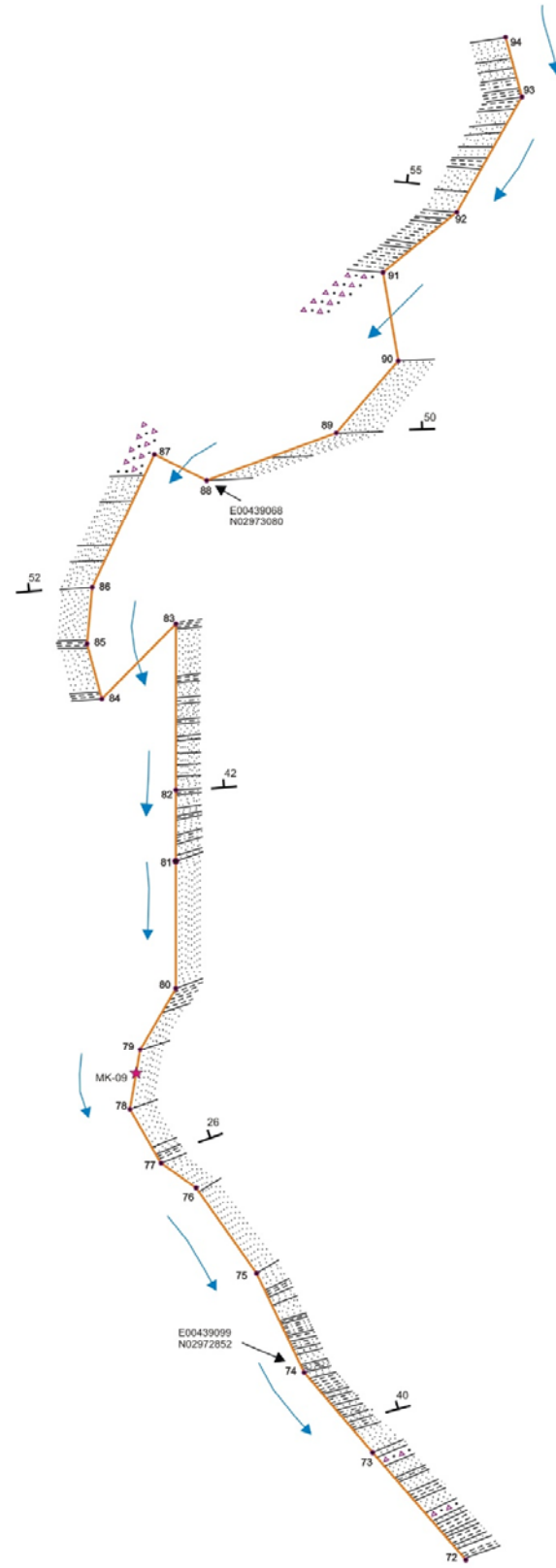
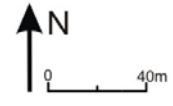
Index	
	Conglomerate
	Intra-formational conglomerate
	Sandstone
	Mudstone
	Colluvial cover
	River
	Route station
	Sampling location
	Altitude of beds

Map datum is based on the topographic map No. 2686-02D Dept. of Survey, Govt. of Nepal



Index	
	Conglomerate
	Intra-formational conglomerate
	Sandstone
	Mudstone
	Colluvial cover
	Vegetation cover / flood plain
	River
	Route station
	Sampling location
	Attitude of beds

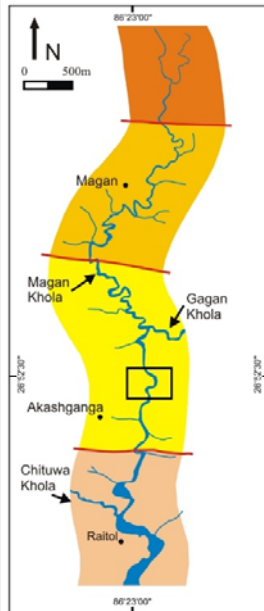
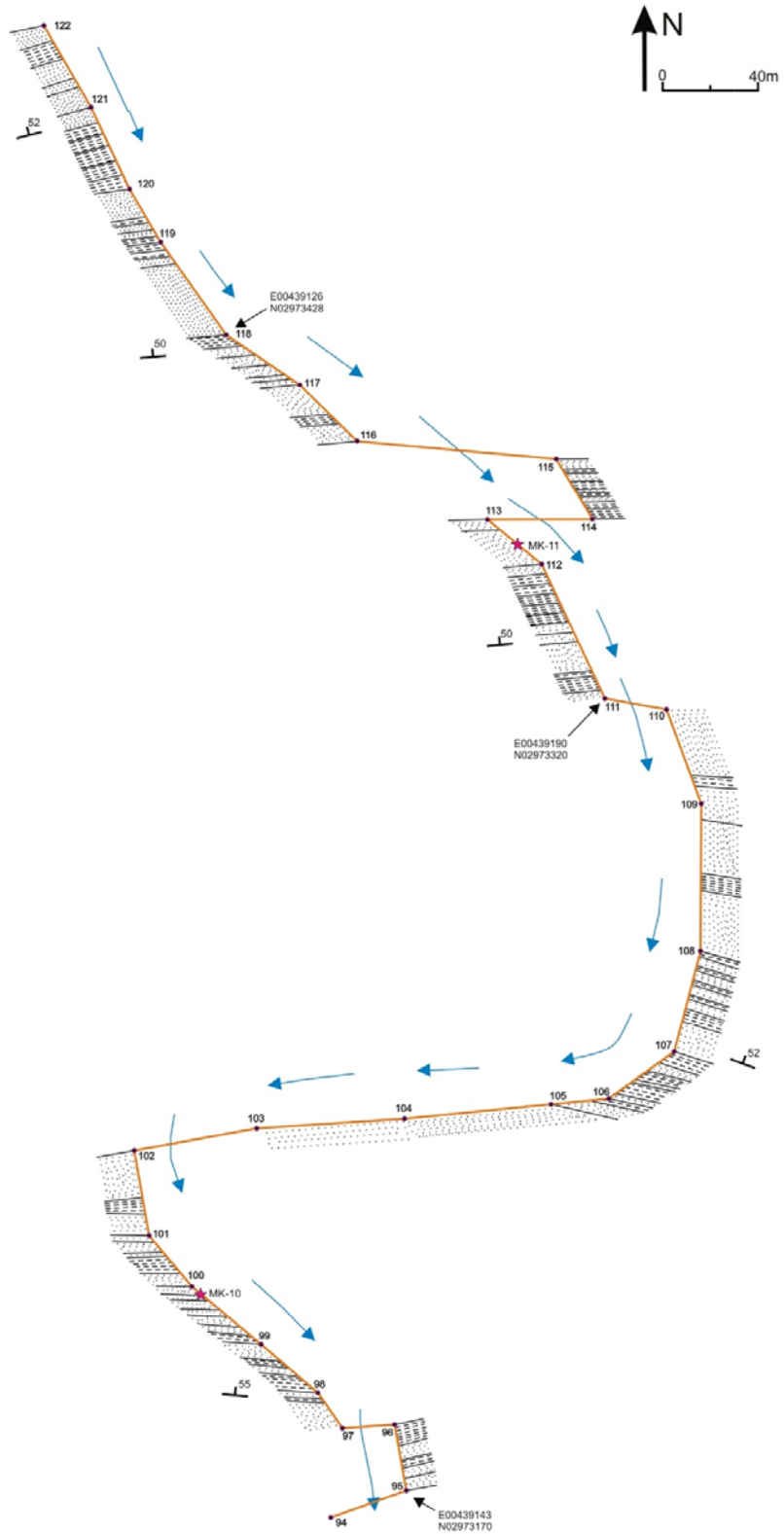
Map datum is based on the topographic map No. 2686-02D Dept. of Survey, Govt. of Nepal



**Index**

	Conglomerate
	Intra-formational conglomerate
	Sandstone
	Mudstone
	Colluvial cover
	Vegetation cover / flood plain
	River
	Route station
	Sampling location
	Attitude of beds

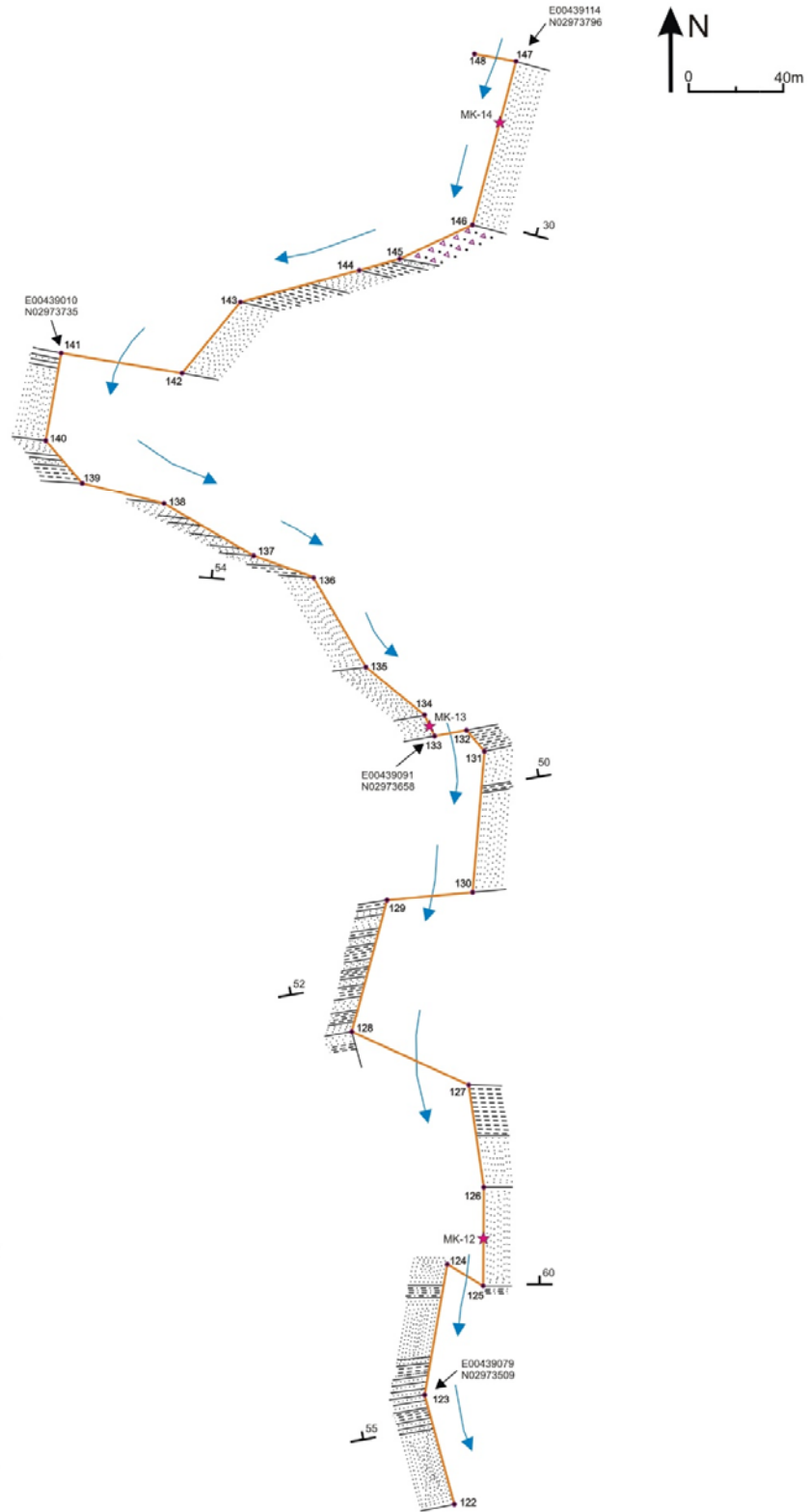
Map datum is based on the topographic map No. 2686-02D Dept. of Survey, Govt. of Nepal



**Index**

	Conglomerate
	Intra-formational conglomerate
	Sandstone
	Mudstone
	Colluvial cover
	Vegetation cover / flood plain
	River
	Route station
	Sampling location
	Attitude of beds

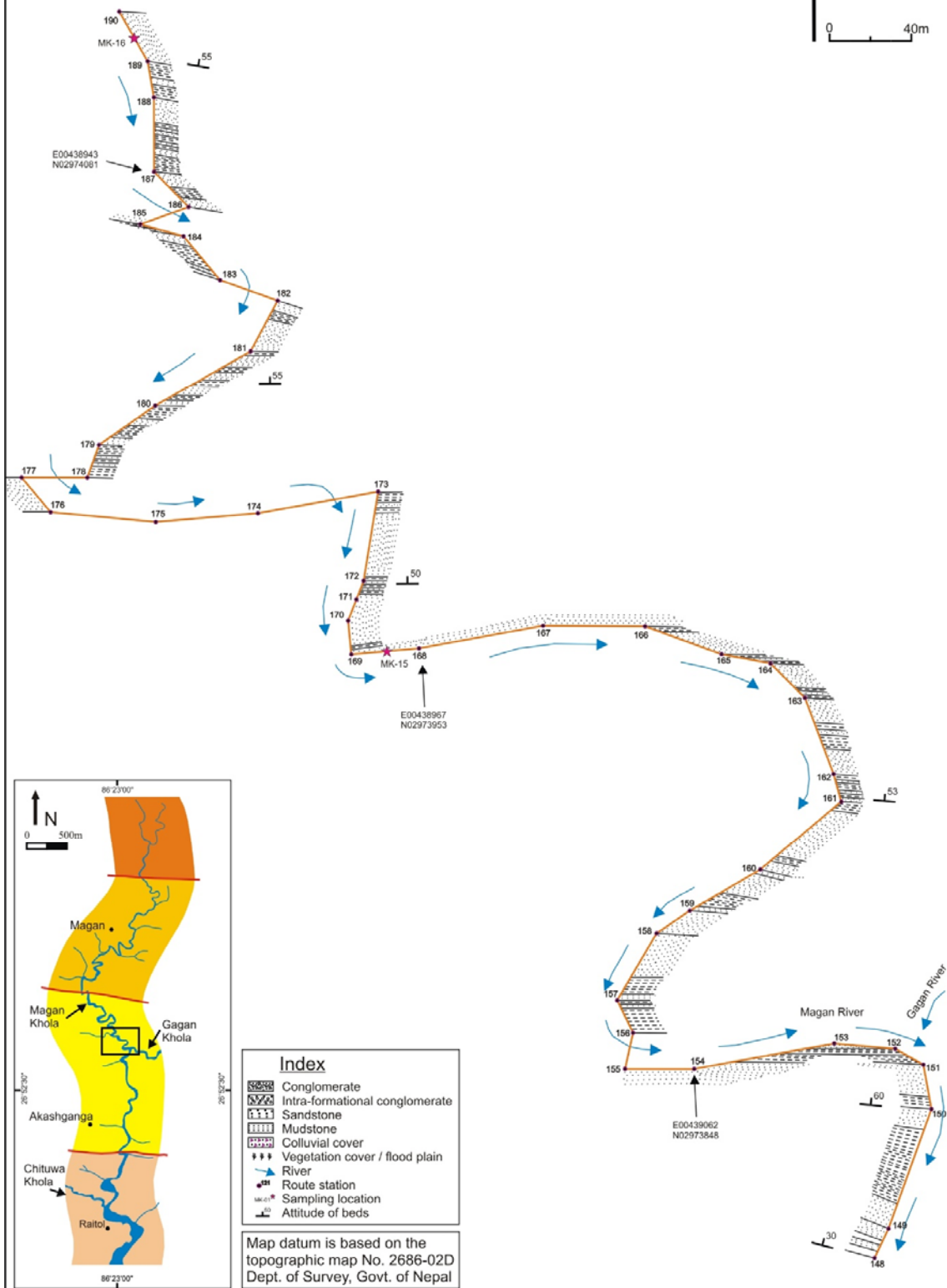
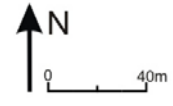
Map datum is based on the topographic map No. 2686-02D Dept. of Survey, Govt. of Nepal



**Index**

	Conglomerate
	Intra-formational conglomerate
	Sandstone
	Mudstone
	Colluvial cover
	Vegetation cover / flood plain
	River
	Route station
	Sampling location
	Attitude of beds

Map datum is based on the topographic map No. 2686-02D Dept. of Survey, Govt. of Nepal

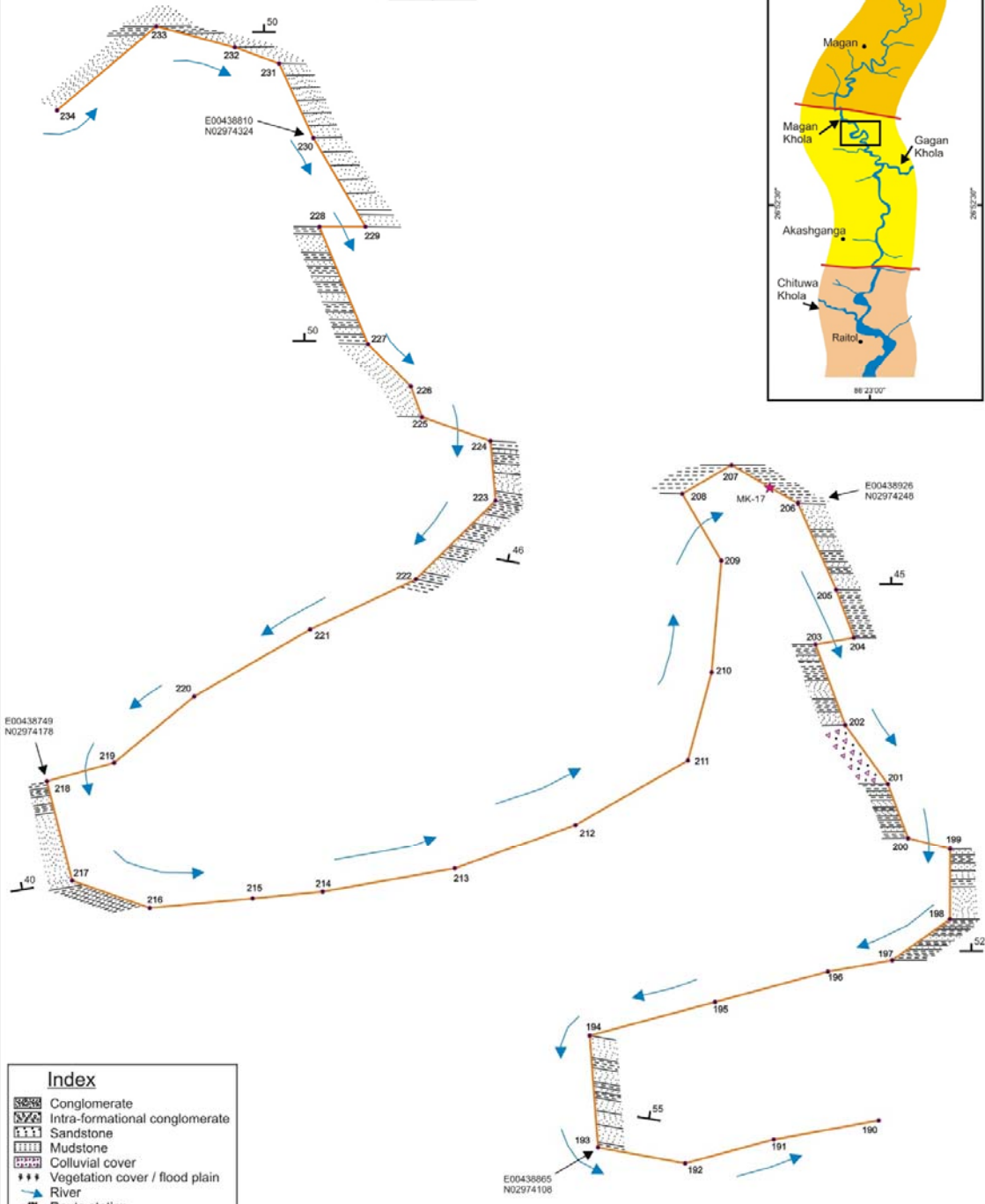
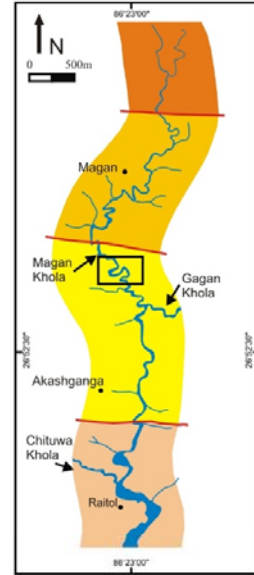
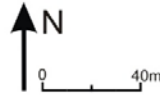


**Index**

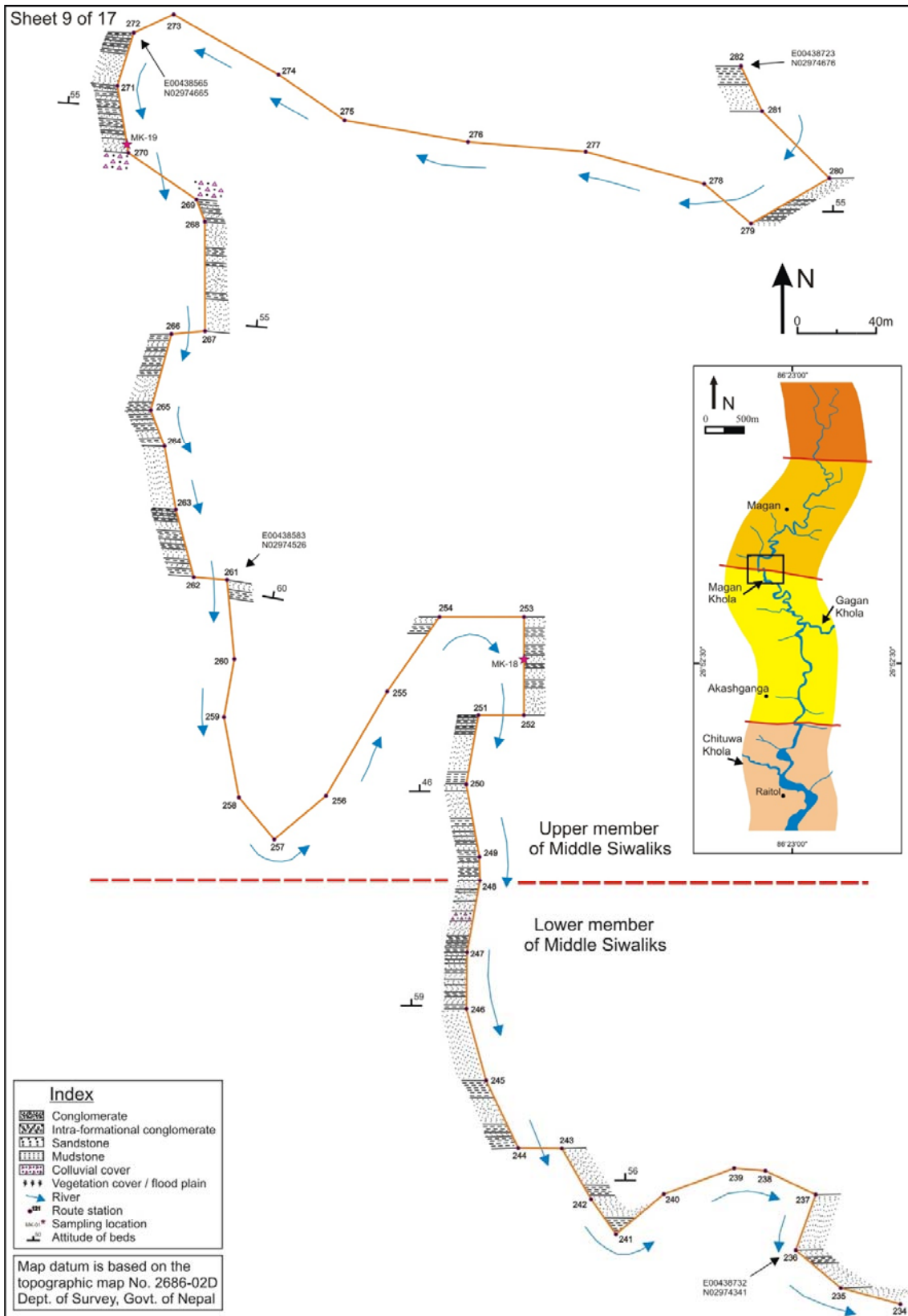
	Conglomerate
	Intra-formational conglomerate
	Sandstone
	Mudstone
	Colluvial cover
	Vegetation cover / flood plain
	River
	Route station
	Sampling location
	Attitude of beds

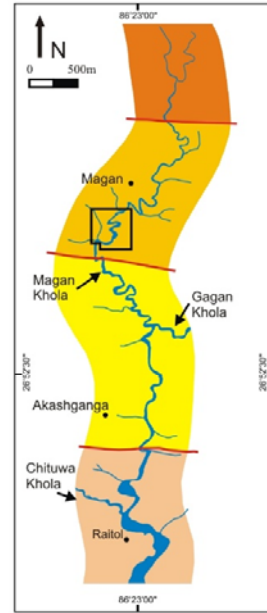
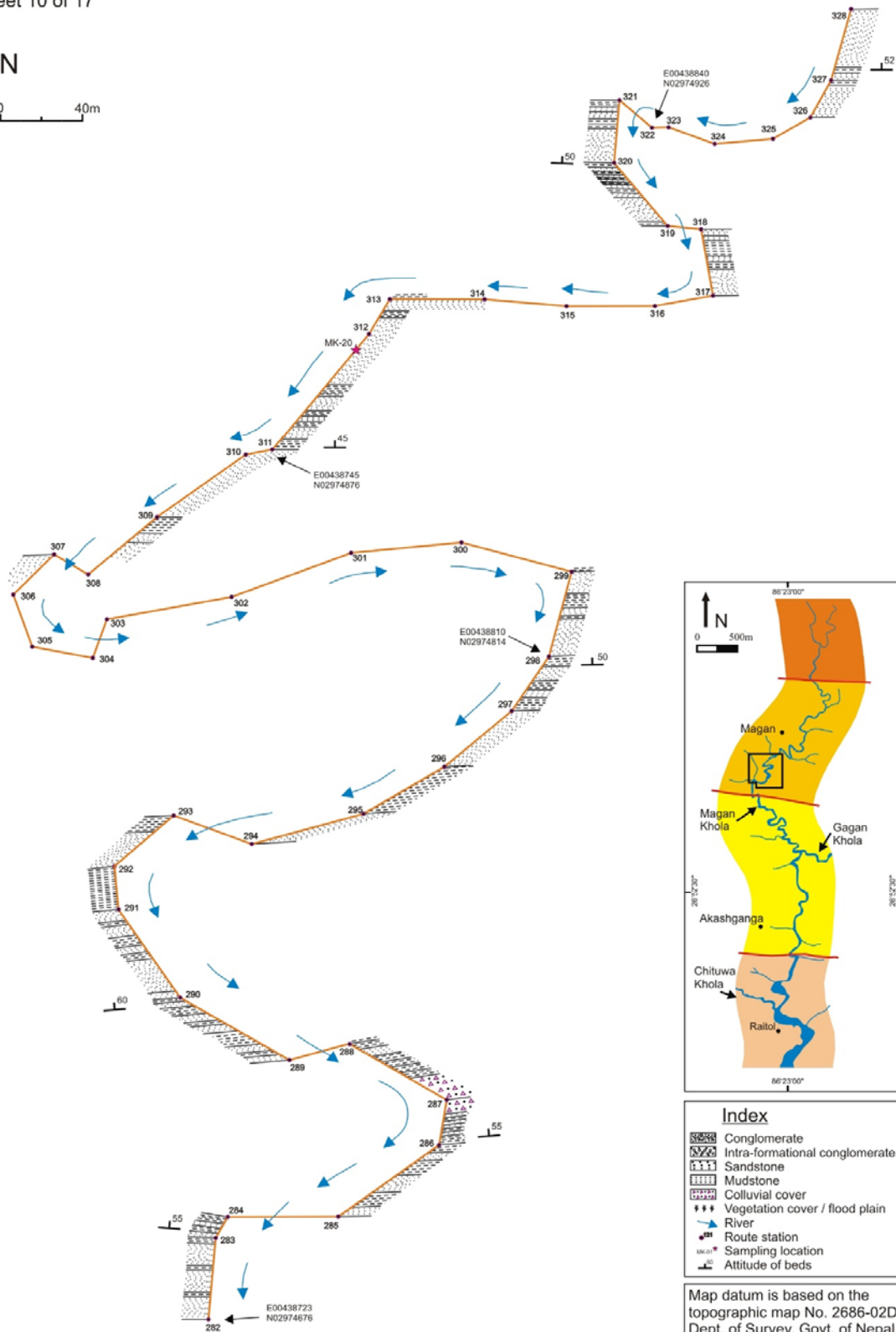
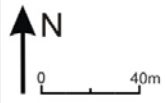
Map datum is based on the topographic map No. 2686-02D Dept. of Survey, Govt. of Nepal





Map datum is based on the topographic map No. 2686-02D Dept. of Survey, Govt. of Nepal

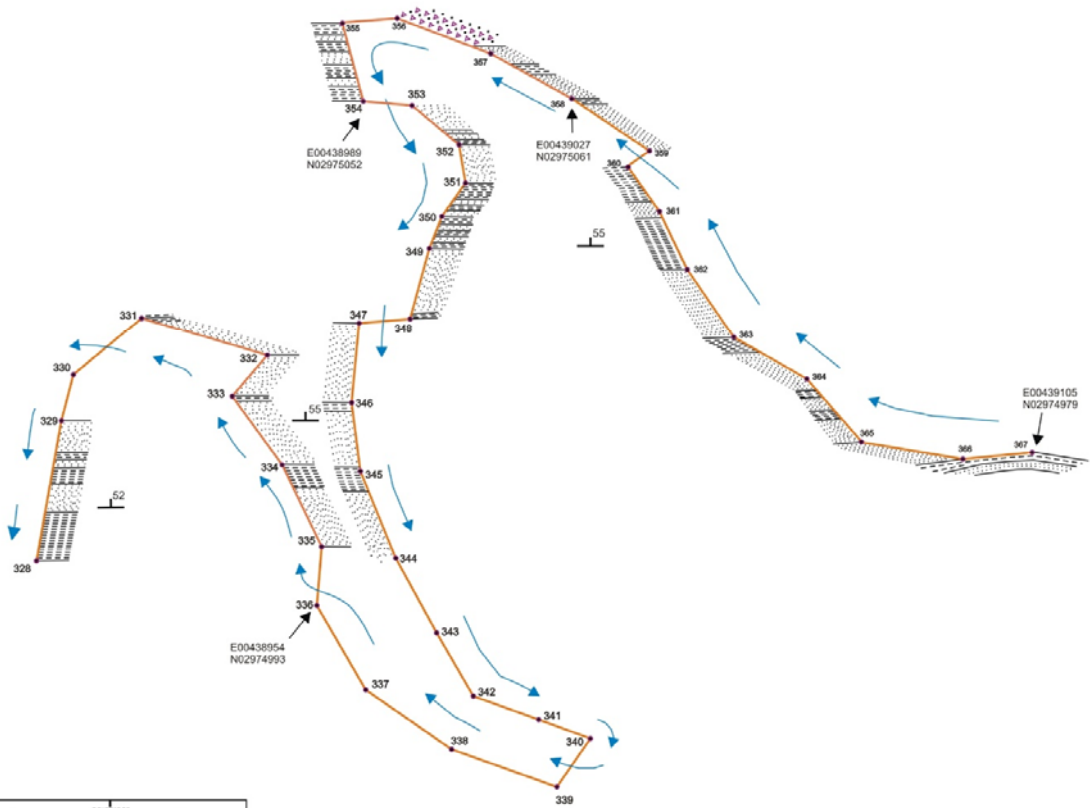
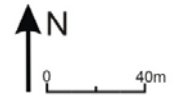




**Index**

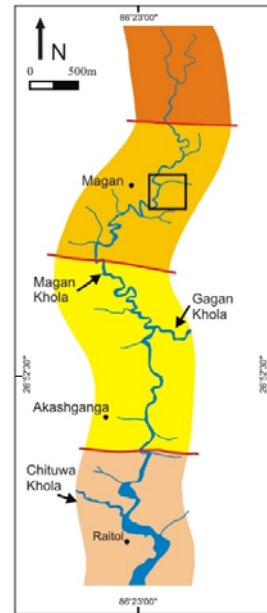
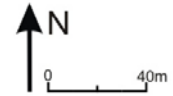
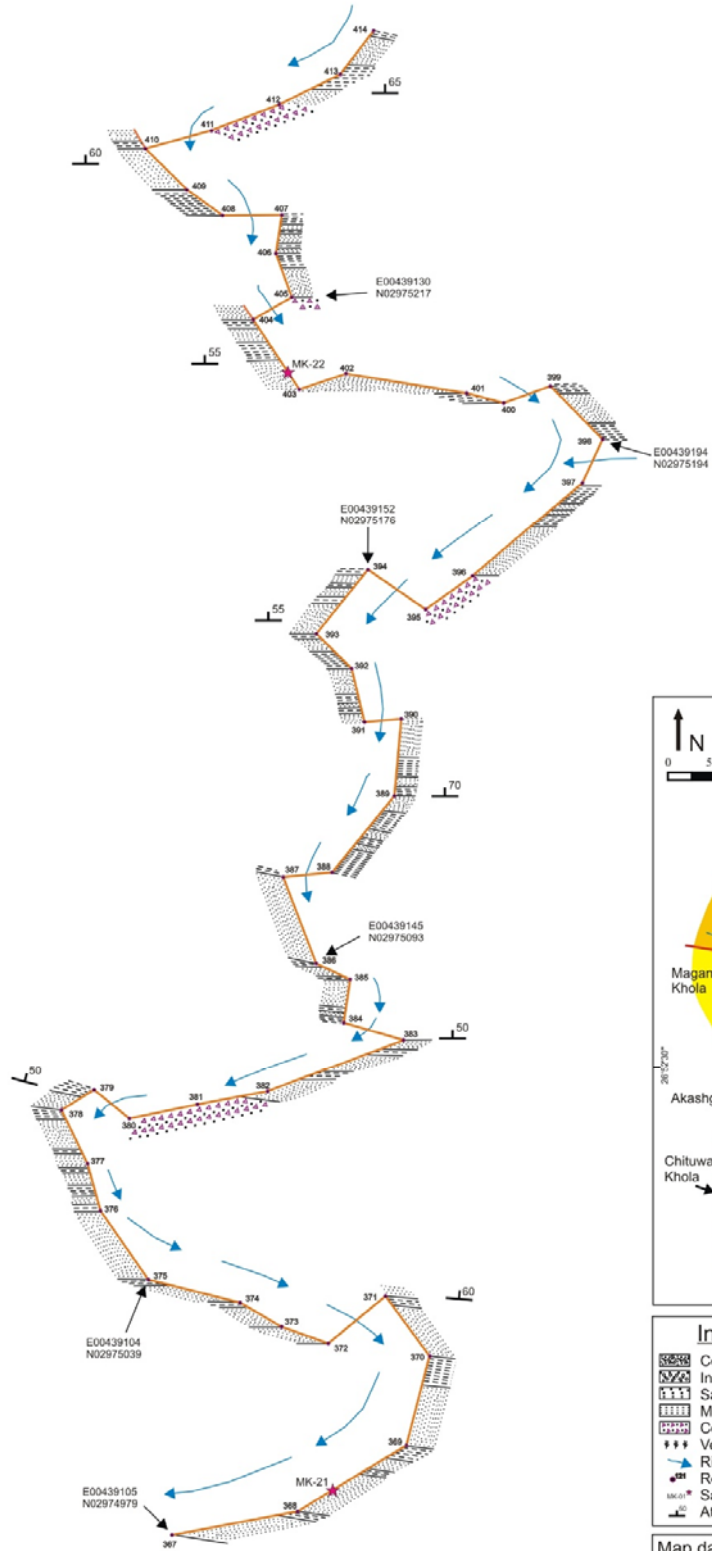
	Conglomerate
	Intra-formational conglomerate
	Sandstone
	Mudstone
	Colluvial cover
	Vegetation cover / flood plain
	River
	Route station
	Sampling location
	Attitude of beds

Map datum is based on the topographic map No. 2686-02D Dept. of Survey, Govt. of Nepal



Index	
	Conglomerate
	Intra-formational conglomerate
	Sandstone
	Mudstone
	Colluvial cover
	Vegetation cover / flood plain
	River
	Route station
	Sampling location
	Attitude of beds

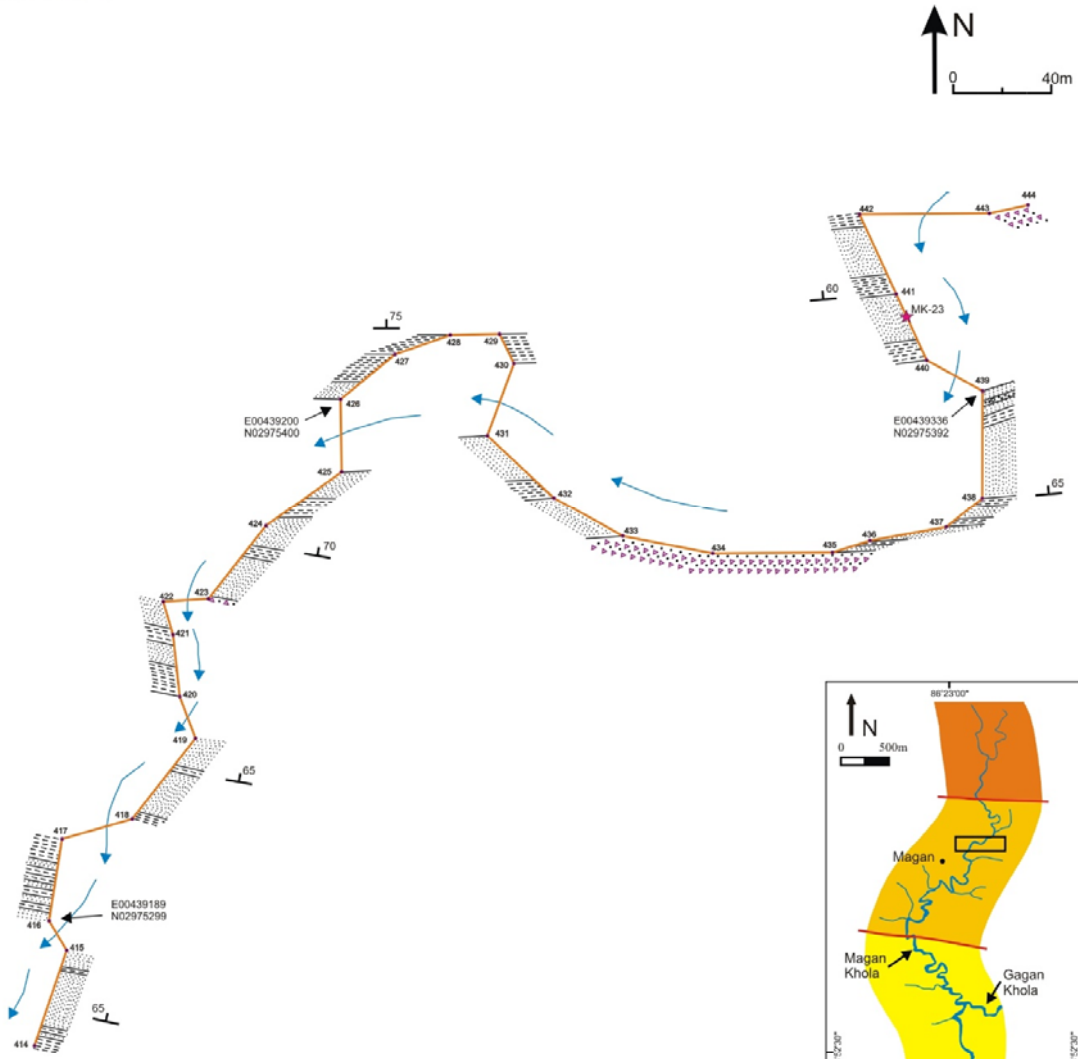
Map datum is based on the topographic map No. 2686-02D Dept. of Survey, Govt. of Nepal



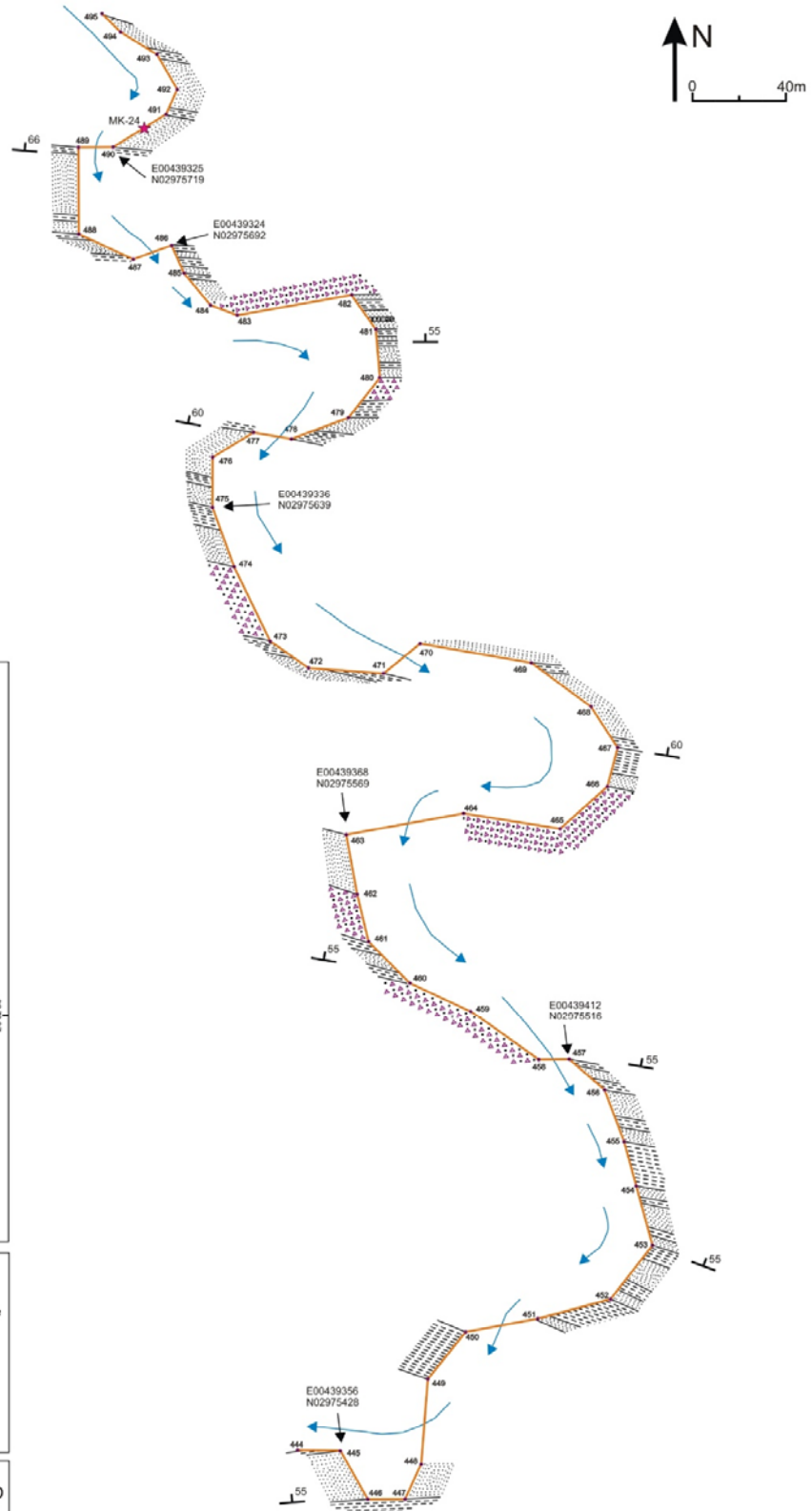
**Index**

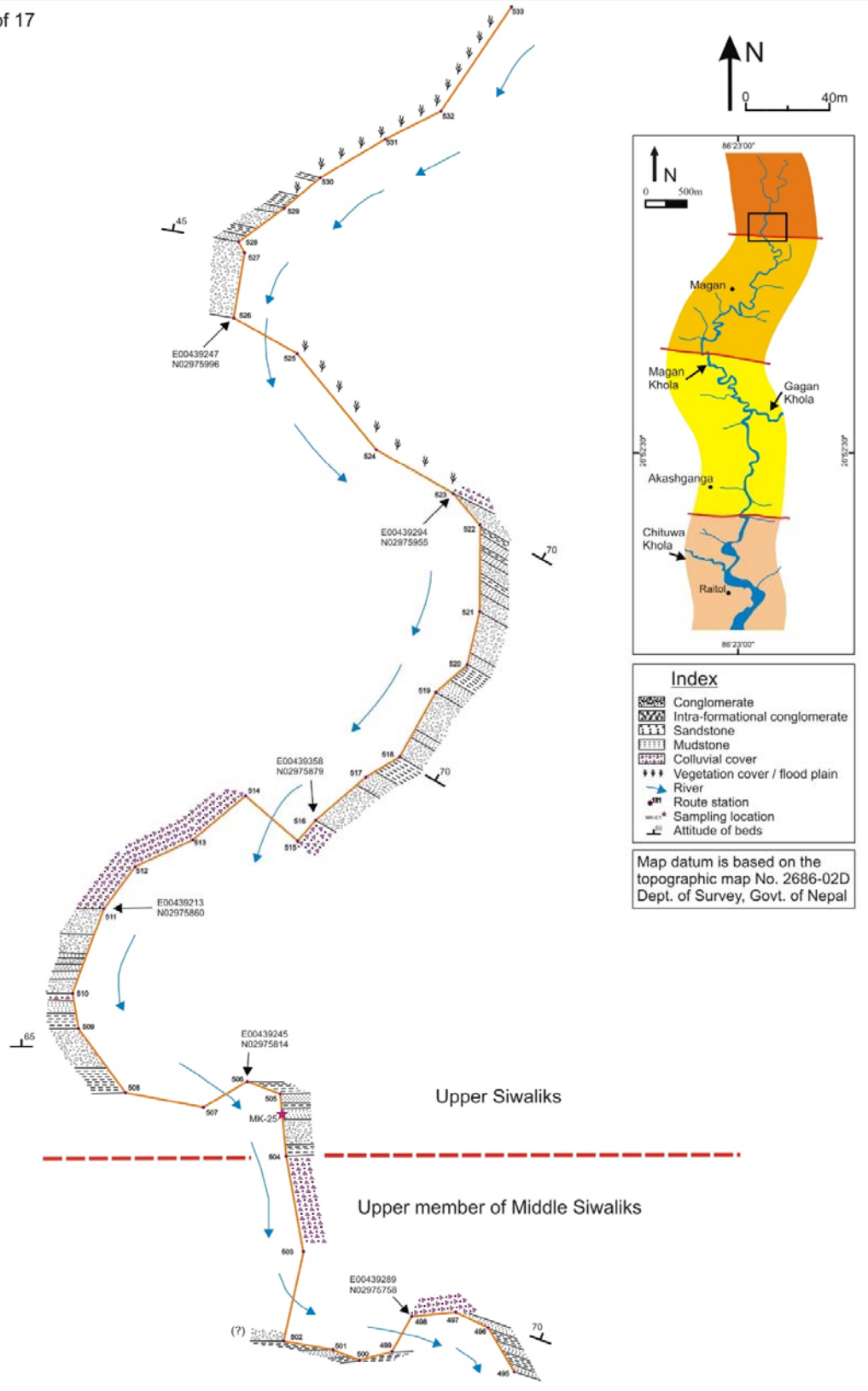
	Conglomerate
	Intra-formational conglomerate
	Sandstone
	Mudstone
	Colluvial cover
	Vegetation cover / flood plain
	River
	Route station
	Sampling location
	Attitude of beds

Map datum is based on the topographic map No. 2686-02D Dept. of Survey, Govt. of Nepal

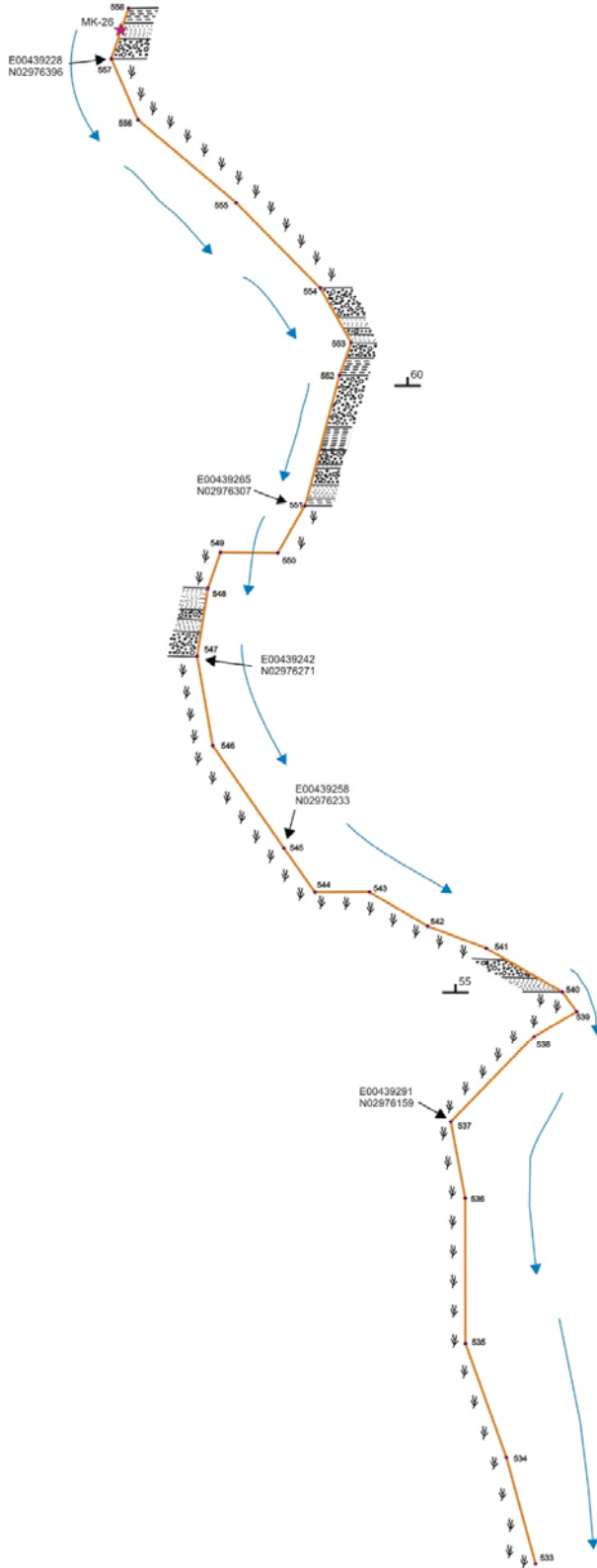
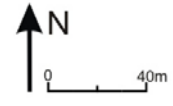


Map datum is based on the topographic map No. 2686-02D Dept. of Survey, Govt. of Nepal





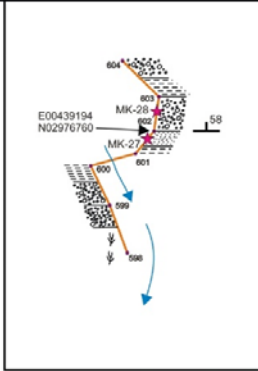
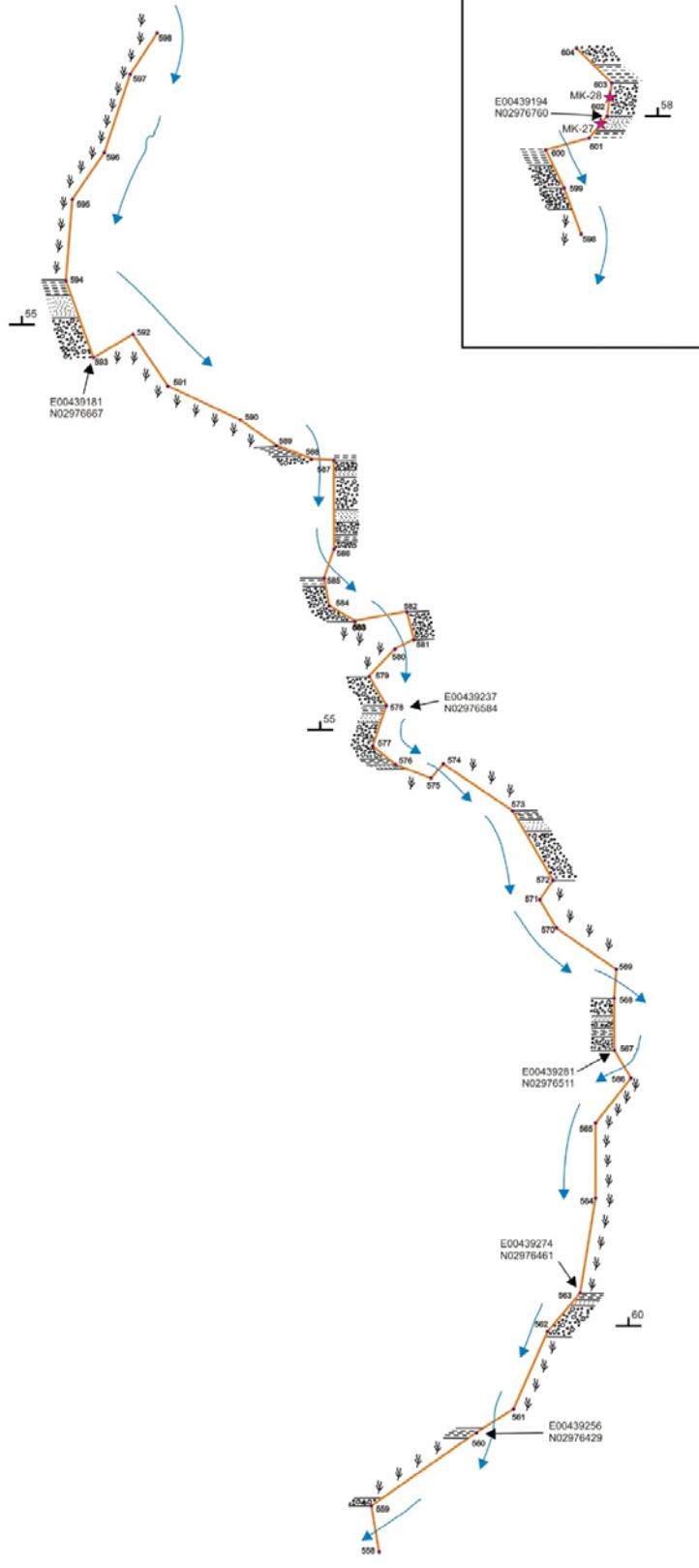
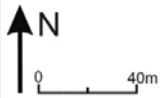




**Index**

	Conglomerate
	Intra-formational conglomerate
	Sandstone
	Mudstone
	Colluvial cover
	Vegetation cover / flood plain
	River
	Route station
	Sampling location
	Attitude of beds

Map datum is based on the topographic map No. 2686-02D Dept. of Survey, Govt. of Nepal



**Index**

	Conglomerate
	Intra-formational conglomerate
	Sandstone
	Mudstone
	Colluvial cover
	Vegetation cover / flood plain
	River
	Route station
	Sampling location
	Attitude of beds

Map datum is based on the topographic map No. 2686-02D Dept. of Survey, Govt. of Nepal